Magnetic quantum phase transitions: $1/d$ expansion, bond-operator theory, and coupled-dimer magnets

DISSERTATION
zur Erlangung des akademischen Grades
Doctor rerum naturalium
(Dr. rer. nat.)

vorgelegt
der Fakultät Mathematik und Naturwissenschaften der
Technischen Universität Dresden

von
Darshan Gajanan Joshi
geboren am 14.10.1989 in Kalyan, Indien

eingereicht am 27.11.2015

verteidigt am 19.02.2016

Die Dissertation wurde im Zeitraum von Oktober 2012 bis November 2015 am Institut für Theoretische Physik angefertigt.

Erstgutachter: Prof. Dr. Matthias Vojta
Zweitgutachter: Prof. Dr. Fabian Essler

Abstract

In the study of strongly interacting condensed-matter systems controlled microscopic theories hold a key position. Spin-wave theory, large-N expansion, and ϵ-expansion are some of the few successful cornerstones. In this doctoral thesis work, we have developed a novel large-d expansion method, d being the spatial dimension, to study model Hamiltonians hosting a quantum phase transition between a paramagnet and a magnetically ordered phase. A highlight of this technique is that it can consistently describe the entire phase diagram of the above mentioned models, including the quantum critical point. Note that most analytical techniques either efficiently describe only one of the phases or suffer from divergences near the critical point. The idea of large-d formalism is that in this limit, non-local fluctuations become unimportant and that a suitable product state delivers exact expectation values for local observables, with corrections being suppressed in powers of $1/d$. It turns out that, due to momentum summation properties of the interaction structure factor, all diagrams are suppressed in powers of $1/d$ leading to an analytic expansion. We have demonstrated this method in two important systems namely, the coupled-dimer magnets and the transverse-field Ising model.

Coupled-dimer magnets are Heisenberg spin systems with two spins, coupled by intra-dimer antiferromagnetic interaction, per crystallographic unit cell (dimer). In turn, spins from neighboring dimers interact via some inter-dimer interaction. A quantum paramagnet is realized for a dominant intra-dimer interaction, while a magnetically ordered phase exists for a dominant (or of the same order as intra-dimer interaction) inter-dimer interaction. These two phases are connected by a quantum phase transition, which is in the Heisenberg O(3) universality class. Microscopic analytical theories to study such systems have been restricted to either only one of the phases or involve uncontrolled approximations. Using a non-linear bond-operator theory for spins with S=1/2, we have calculated the $1/d$ expansion of static and dynamic observables for coupled dimers on a hypercubic lattice at zero temperature. Analyticity of the $1/d$ expansion, even at the critical point, is ensured by correctly identifying suitable observables using the mean-field critical exponents. This method yields gapless excitation modes in the continuous symmetry broken phase, as required by Goldstone's theorem. In appropriate limits, our results match with perturbation expansion in small ratio of inter-dimer and intra-dimer coupling, performed using continuous unitary transformations, as well as the spin-wave theory for spin-1/2 in arbitrary dimensions. We also discuss the Brueckner approach, which relies on small quasiparticle density, and derive the same $1/d$ expansion for the dispersion relation in the disordered phase. Another success of our work is in describing the amplitude (Higgs) mode in coupled-dimer magnets. Our novel method establishes the popular bond-operator theory as a controlled

approach.

In $d = 2$, the results from our calculations are in qualitative agreement with the quantum Monte Carlo study of the square-lattice bilayer Heisenberg AF spin-1/2 model. In particular, our results are useful to identify the amplitude (Higgs) mode in the QMC data. The ideas of large-d are also successfully applied to the transverse-field Ising model on a hypercubic lattice. Similar to bond operators, we have introduced auxiliary Bosonsic operators to set up our method in this case.

We have also discussed briefly the bilayer Kitaev model, constructed by antiferromagnetically coupling two layers of the Kitaev model on a honeycomb lattice. In this case, we investigate the dimer quantum paramagnetic phase, realized in the strong inter-layer coupling limit. Using bond-operator theory, we calculate the mode dispersion in this phase, within the harmonic approximation. We also conjecture a zero-temperature phase diagram for this model.

Contents

Chapter 1

Introduction

In a many-particle system, each individual particle follows the same basic fundamental laws of nature. But the collective behavior of a large group of particles is difficult to understand by just knowing the properties of a few particles. This is one of the most fascinating aspects of nature! With a large number of entities comes complexity and emergent phenomena. In the words of P. W. Anderson, "More is different" [1]. In condensed-matter physics we are familiar with several exciting phenomena resulting from strong interactions. Superconductivity and Bose-Einstein condensation are two of the most popular examples which have been discovered only in the last century. On the other hand, magnetism is one of the oldest disciplines of science, and it still presents a lot of surprises! It is a breeding ground of several exotic states of matter. In particular, magnetism in Mott insulators, where only electronic spin degree of freedom is relevant leading to local moments, displays rich physics especially when competing exchange interactions lead to frustration [2]. One of the celebrated examples is the prediction and discovery of magnetic monopoles in spin ice [3]. Even the physics of high-T_c superconductors, one of the most enigmatic phases, in many ways is thought to be linked to the magnetism in their parent Mott insulator compound. In many interesting cases, by tuning some non-thermal parameter such as pressure, external field or doping (electron or hole) one realizes phase transitions between different phases. In cuprates, for instance, electron (or hole) doping in the parent antiferromagnetic Mott insulator leads to superconductivity. There are several other examples and we will encounter one such in this work. It turns out that the theory of quantum phase transitions, i.e. phase transitions occuring at absolute zero temperature, provides a good understanding of these phase transitions.

The renormalization group approach [4, 5] pioneered by Kadanoff, Wilson and Fisher as well as various classical and quantum field theory approaches have provided invaluable insights into the physics of classical and quantum phase transitions [5, 6, 7]. Through these approaches we have learned the universal properties of critical phenomena and understood the power-law behavior of observables near a critical point. The Landau theory, one of the widely used tools, can remarkably predict its own breakdown. Within the Landau theory we can use the Ginzburg criterion, which uses the condition that the theory is valid when the fluctuations in the order parameter are smaller than its own value, to derive the upper critical dimension below which it is invalid. However, in order to understand the non-universal properties in a given phase

we require microscopic theories, especially when it comes to calculating observables to quantitatively match laboratory or computer experiments.

As theorists, usually our aim is then to write down a minimal model (ideally simple) to understand a given physical phenomenon and solve it. But very often it turns out that even the simplest models are analytically unsolvable! At this point we have to make clever and justified assumptions in order to make any progress in approximately solving our model. There are many strategies depending on the problem at hand. One approach is to identify and neglect irrelevant terms in our model so that our problem becomes technically simpler. But how does one identify these irrelevant terms? This is dictated by the fact that the neglected terms have much smaller contribution to observables than the terms that we have retained. Thus we need a small parameter to monitor and decide which terms are important in our calculation to a given accuracy. It is an art of systematically throwing away unimportant terms. There are several magnetic systems, where due to lack of a small parameter consistent description of their entire phase diagram using a single microscopic approach is not possible. The prime goal of this work is to identify a suitable small parameter and perform controlled calculation across a magnetic quantum phase transition. At the end of this work we will see that we have succeeded in achieving our target.

1.1 Outline

The thesis is organized in the following way. In the present chapter, we proceed by first recalling some of the important ideas of quantum phase transitions, which are relevant in the study of magnetic Mott insulators. Then we briefly discuss the phenomenon of spontaneous symmetry breaking, which will help us to set the terminology for various types of excitations in the system and identifying ordered and disordered phases. Next, we will discuss a few spin models used to study local moment magnetism and which will be relevant in later chapters. We will close this chapter by reviewing some important ideas of magnetic quantum phase transitions and series expansion technique.

After the introduction chapter, the thesis is divided into two parts. Part I of this thesis deals with coupled-dimer magnets, which is an important system in the study of magnetic quantum phase transitions, and consists of chapters 2 to 6. In chapter 2, we introduce the model of coupled-dimer magnets. We will discuss some examples from real materials and their experimental study. Next, within chapter 2, we will review various theoretical approaches to study coupled-dimer systems prior to our work and discuss their success and shortcomings. This will further motivate the relevance of our work. The main philosophy of our work, which relies on the limit of large spatial dimension, will be discussed in chapter 3. Then in chapter 4 and 5 we present explicit calculations demonstrating our novel method in the quantum paramagnetic and antiferromagnetic phases respectively. These two chapters form the main part of our work and expressions for various static as well as dynamic observables can be found here. The main success here is consistent description of the entire phase diagram of coupled-dimer magnets including the quantum critical point. Later, in chapter 6 we will see the application of our technique in explaining the quantum Monte Carlo results for the widely studied square-lattice bilayer Heisenberg antiferromagnet.

Part II of the thesis deals with magnetic quantum phase transitions in various other

interesting models, such as the transverse-field Ising model and the bilayer Kitaev model. In chapter 7 we will see that using our new method entire phase diagram of the transverse-field Ising model can be studied consistently. Here, most of the ideas are borrowed from those developed for the case of coupled-dimer magnets, and again we calculate $1/d$ expansion for various observables. Then in chapter 8 we explore the quantum paramagnetic phase of the bilayer Kitaev model. The ambitious idea here is to look for signatures of phases in a single layer by studying the quantum paramagnetic phase resulting due to strong inter-layer coupling. We will also briefly mention some other relevant models.

We will then conclude this thesis by summarizing our work and discussing potential future projects arising from this work. Various technical details which are not immediately relevant in the main text are relegated to respective appendices.

1.2 Classical phase transitions

Before we discuss quantum phase transitions in the next section, let us quickly recall some of the ideas from classical phase transitions. A more detailed account can be found in several excellent textbooks such as ref. [5]. Classical phase transitions like that of water to ice or water to vapor occur upon tuning the temperature and hence are driven by thermal fluctuations. In this case the thermodynamic free energy becomes non-analytic at the point where the phase transition occurs. Many familiar examples of phase transitions fall into one of the two classes: (i) First-order and (ii) Continuous[1]. When one phase transforms into another at a fixed temperature with either absorption or release of a *latent heat* then it is said to have undergone a first order phase transition. This is accompanied by a jump in the entropy of the system as the first derivative of the free energy becomes discontinuous. Common examples of melting of ice and boiling of water comes under this category. The most important characteristic of first order phase transition is that both the phases coexist at the phase transition.

A continuous phase transition on the other hand does not involve a latent heat since the first derivative of the free energy is continuous. In this case the second derivative of the free energy becomes non-analytic and the corresponding phase transition point is known as the critical point. A characteristic feature of such phase transitions is an infinite correlation length, which is the characteristic length scale of decay of correlations in the system, at the critical point and power-law decay of observables near the criticality. A textbook example is the phase transition between a paramagnet and a ferromagnet at the Curie temperature. Another interesting example is that of a superconductor to a normal metal phase transition. The physics of these phase transitions is well captured by the phenomenological Landau theory[2], wherein exploiting the symmetry of the system the free energy density is expanded in powers of the order parameter. Continuous phase transitions show universal behavior which depends only on the dimensionality, the symmetry of the system and the range of the interaction.

[1] According to Ehrenfest classification a phase transition is of nth order if the nth derivative of the free energy is discontinuous [5]. This classification is however inadequate to account for phase transitions where a derivative of the free energy diverges and hence the modern classification is required.

[2] When the order parameter has spatial variation, a gradient term appears in the free energy expansion and we then have the Ginzburg-Landau theory.

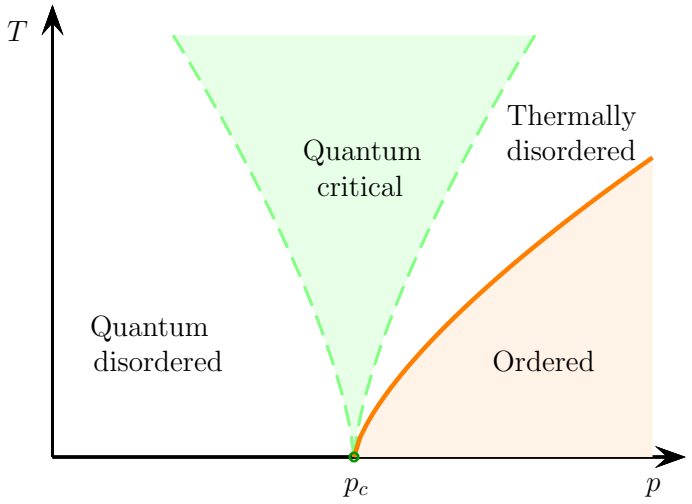

Figure 1.1: Phase diagram involving temperature T and a non-thermal parameter p, with a quantum critical point at p_c. For non-zero temperatures there is a quantum critical region (green), as explained in the text. Systems where ordering at $T > 0$ is allowed can undergo a thermal phase transition (orange curve) into a thermally disordered phase.

We will be interested in such phase transitions in this work.

Most phase transitions involve symmetry breaking. For instance when a liquid cools into a solid it breaks the translation symmetry, while in the case when a paramagnet turns into a ferromagnet the spin rotation symmetry is broken. But there are exotic phase transitions which can not be described in terms of symmetry breaking and the local order-parameter theory. Berezinsky-Kosterlitz-Thouless (BKT) transition is one such example where no symmetry breaking is involved. However, we will not be dealing with such phase transitions in this work.

1.3 Quantum phase transitions

Quantum phase transitions [6, 8, 9] occur at absolute zero temperature and involve a non-thermal tuning parameter such as pressure or an external field. Now instead of the free energy the non-analyticity of just the ground-state energy defines a quantum phase transition. We thus have a phase transition in the many-body ground state of the system. It is also often stated that quantum phase transitions are driven by *quantum fluctuations*[3]. Just as in the case of classical phase transitions we also have first order and continuous quantum phase transitions. Here on we shall focus our attention only on continuous phase transitions as these will be relevant to our work.

At a first glance it may seem that the study of quantum phase transitions is interesting for theorists only, since absolute zero temperature can not be achieved in a laboratory. However it turns out that in many cases finite temperature properties

[3]Note that strictly speaking the ground state of a system is a stationary state and so quantum fluctuations can not take the system away from it. It is more instructive to think of the behavior of observables in the ground state as function of the tuning parameter.

of a system are linked to the underlying quantum phase transition. A generic phase diagram involving temperature and some other tuning parameter p is shown in fig. 1.1. Consider a simple case where we have two stable phases at zero temperature connected by a quantum critical point at p_c. One is a disordered phase, whose ground state has the same symmetry as the underlying Hamiltonian, and the other is an ordered phase, whose ground state breaks certain symmetry of the Hamiltonian. Upon switching on the temperature we can have a classical phase transition which takes the ordered phase into a thermally disordered phase[4]. However what is more interesting is the *quantum critical* region, which is bounded by two crossover lines defined by the relation $k_B T \propto |p-p_c|^{\nu z}$, where ν and z are the critical exponents which will be discussed soon. Unlike the stable phases which have well-defined quasiparticle excitations, this region hosts thermal excitations of the critical continuum of excitations present at the quantum critical point. This has dramatic effects such as unconventional thermodynamic and transport properties which can be directly probed in experiments. Some of the examples include the non-Fermi liquid behavior [11], unconventional superconductors, and strange metals [6, 11]. In fact in this region there is a complicated interplay of thermal and quantum fluctuations. However, recently in the context of quantum magnets, it has been shown that near a quantum critical point thermal and quantum fluctuations can behave largely independent of each other [12]. Understanding of this rich physics thus requires the knowledge of quantum phase transitions.

1.3.1 Critical exponents

For the sake of future use let us briefly recall some of the critical exponents. As a consequence of scale invariance near a critical point, observables follow a universal power-law behavior as a function of parameters such as the distance to criticality $|t|$, an external field h and the real-space co-ordinate r. The corresponding exponents are termed as the critical exponents. Let $t \equiv p_c - p$, where p is our tuning parameter and p_c is the quantum critical point, such that $t > 0$ and $t < 0$ corresponds to the disordered and the ordered phase respectively. In the limit $|t| \to 0$ and $h = 0$ the specific heat $\mathcal{C}$, order parameter Ψ, correlation length ξ and correlation time τ_c have a power-law behavior which defines the respective critical exponents as follows:

$$\mathcal{C} \propto |t|^{-\alpha}\,, \tag{1.1}$$

$$\Psi \propto (-t)^{\beta}\,, \tag{1.2}$$

$$\xi \propto |t|^{-\nu}\,, \tag{1.3}$$

$$\tau_c \propto \xi^{z}\,. \tag{1.4}$$

Similarly, other critical exponents are defined. For a detailed discussion on universal behavior and critical exponents we refer to ref. [5, 6, 8, 9]. Critical exponents depend only on the dimensionality and the symmetry of the system, and the range of the interaction. However, the constants of proportionality are not universal and may differ for systems within the same universality class.

[4]This aspect depends on the dimension of the system (and also the number of order parameter components). For instance, in many classical magnets in two dimensions, ordering at finite temperatures is forbidden by the Mermin-Wagner theorem [10] and so there won't be any classical phase transition line in the phase diagram (fig. 1.1).

Recall that for any given model, phase transition occurs only above its lower critical dimension[5] d_c^-. While above the upper critical dimension d_c^+ mean field behavior is recovered.

1.3.2 Quantum to classical mapping

In many cases a striking correspondence exists between the quantum and classical phase transitions via the so called quantum to classical mapping [6, 8, 9]. It says that a d dimensional quantum phase transition is analogous to a $d+z$ dimensional classical phase transition[6] with z being the dynamical critical exponent (1.4).

However note that there are many counter examples where this correspondence is not obeyed [9]. Notable exceptions include quantum spin systems with Berry-phase dynamics [6] and quantum phase transitions in metallic or semi-metallic systems [11]. More recently, the quantum to classical correspondence was found to be violated in a spin-Boson model [13].

1.4 Spontaneous symmetry breaking

Many phenomena in condensed matter physics occur due to spontaneous breaking of certain symmetry. Given a Hamiltonian (or Lagrangian in quantum field theory) which is invariant under certain symmetry (say symmetry group $\mathcal{G}$), for a certain range of parameters the system can choose to be in a ground state which has lower symmetry (say symmetry group $\mathcal{H}$ such that $\mathcal{H} \subset \mathcal{G}$) thus breaking some symmetry spontaneously. Popular examples of phases with spontaneously broken symmetry include a superconductor ($U(1)$ is broken), an Ising ferromagnet ($\mathbb{Z}_2$ is broken), the nematic phase in the vicinity of a high-T_c superconductor ($\mathcal{C}_4$ is broken down to $\mathcal{C}_2$), a Heisenberg antiferromagnet ($SU(2)$ is broken) and a valence bond solid (lattice translation is broken).

1.4.1 Goldstone modes

If a continuous symmetry (i.e. the underlying symmetry group is continuous) is spontaneously broken then according to the *Goldstone's theorem* [14] there are corresponding massless Bosons. In other words, in this case there are gapless excitations. These Goldstone Bosons are long-wavelength fluctuations of the corresponding order parameter. The number of Goldstone modes is given by the dimension of $\mathcal{G}/\mathcal{H}$ [7]. In many situations, counting of Goldstone modes is non-trivial, and for the related discussion we refer to ref. [15]. Note that in the case of spontaneous breaking of a discrete symmetry there is no such theorem.

[5]Note that in many cases, the Ginzburg criterion can be used to determine the upper critical dimension but often there is no straightforward way to get d_c^-. However, for many spin models, Mermin-Wagner theorem [10] can be used to determine d_c^-.

[6]This is one way to see why in $1d$ a quantum Heisenberg ferromagnet orders at $T = 0K$ while a quantum Heisenberg antiferromagnet does not. From Mermin-Wagner theorem [10], for classical Heisenberg model long range order is possible only for $d \geq 3$ but for antiferromagnets $z = 1$ while for ferromagnets $z = 2$.

1.4.2 Ψ^4 theory

Let us quickly review the idea of spontaneous symmetry breaking by considering a Ψ^4 field theory with U(1) symmetry in the absence of any external field. Many phenomena can be understood via this simple model. We start with the Lagrangian

$$\mathcal{L} = (\partial_\mu \Psi)(\partial^\mu \Psi^*) - \alpha \Psi^* \phi - \beta (\Psi^* \Psi)^2 \equiv (\partial_\mu \Psi)(\partial^\mu \Psi^*) - V(\Psi, \Psi^*) \tag{1.5}$$

where $\Psi \equiv |\Psi| e^{\imath\phi}$ corresponds to the complex order-parameter field, while α and β are phenomenological constants such that $\beta > 0$. This Lagrangian is invariant under a global $U(1)$ rotation, i.e. $\Psi \to e^{\imath\lambda}\Psi$ (λ is a constant) does not change the form of the above Lagrangian. Minimizing $V(\Psi, \Psi^*)$ leads to two possible solutions for the ground state:

$$\Psi = \Psi^* = 0\,; \quad \alpha > 0 \tag{1.6}$$

corresponding to the disordered phase and

$$|\Psi|^2 = -\frac{\alpha}{2\beta} \equiv a^2\,; \quad \alpha < 0 \tag{1.7}$$

corresponding to the symmetry broken ordered phase where the potential V realizes a Mexican-hat shape as shown in fig. 1.2. Thus we have a phase transition at $\alpha = 0$. To further understand the ordered phase let us study the excitations over the ground state by introducing

$$\Psi = (a + \rho) e^{\imath\phi} \tag{1.8}$$

such that ρ represents the oscillation of amplitude of Ψ around its ground-state value a. Substituting the above ansatz in the expression for V we obtain

$$V = -\beta a^4 + 4\beta a^2 \rho^2 + \mathcal{O}(\rho^3)\,. \tag{1.9}$$

Thus we see that in the symmetry broken phase ρ field, which corresponds to the amplitude fluctuation, is massive with mass $m_\rho = 2a\sqrt{\beta}$. While the ϕ field, which corresponds to the phase fluctuation, is massless. Physically this means that amplitude (longitudinal) mode excitation costs finite energy and hence are gapped while the phase (transverse) mode excitation is gapless as it does not require any excitation energy. This gapless excitation takes the system from one ground state to another since it does not change the condition $|\Psi| = a$. This gapless transverse mode is the *Goldstone mode* discussed earlier.

It is easy to perform similar analysis for spontaneous breaking of a discrete symmetry such as the $\mathbb{Z}_2$. In this case the order parameter field is not complex but a real scalar. So in terms of the Ψ^4 theory we see that the symmetry broken phase will have two minima at $\Psi = \pm a$ and there will be no zero energy mode connecting these two distinct ground states. The textbook example of an Ising ferromagnet where $\mathbb{Z}_2$ symmetry is broken spontaneously falls under this category.

Higgs mechanism

We can perform a similar analysis in the case of a *local* $U(1)$ symmetry. This requires the introduction of massless gauge field via minimal coupling for the Lagrangian to be

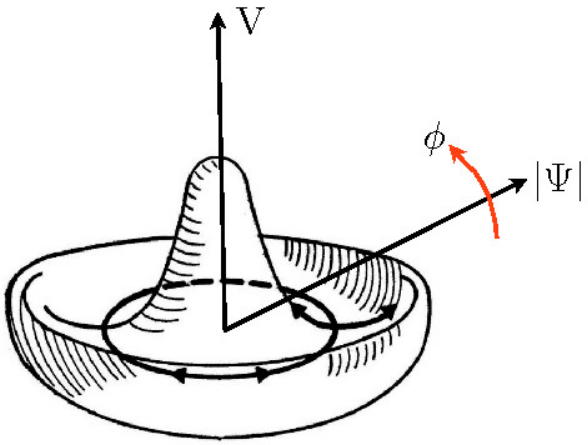

Figure 1.2: Mexican-hat potential corresponding to Ψ^4 theory. This figure is taken from the ref. [16].

invariant under local gauge transformation. This scenario corresponds to, for instance, conventional superconductors. Here again the order parameter field is complex i.e. two real scalar fields. In the disordered phase we thus have two massive scalar fields and one massless gauge field (or photon). Spontaneously breaking the $U(1)$ (global) symmetry results into one massive scalar field and one massive gauge field (or photon)[7]. Thus there are no Goldstone Bosons in this case. This mechanism wherein upon spontaneous breaking of a continuous symmetry[8] leads to massive gauge field instead of massless Goldstone Bosons is known as the *Higgs mechanism*[9].

Heisenberg antiferromagnets

The system we will be most interested in is the Heisenberg antiferromagnet. In this case the spin rotation symmetry is spontaneously broken. In terms of the above discussion, here the order-parameter field is a vector field with three scalar components and it can be described by the O(3) model. In the disordered phase, we thus have three massive scalar fields, while in the ordered phase there is one massive scalar field and two massless scalar fields. In other words, in the disordered phase there are triply degenerate gapped excitation modes, while in the ordered phase there is one gapped amplitude mode and two gapless transverse (Goldstone) modes. Often these days in the literature the gapped amplitude mode is called the *Higgs* mode, although there is no Higgs mechanism involved in this case. There are several other instances of Higgs mode in condensed matter where also there is no Higgs mechanism (see ref. [16] and

[7]The number of components of field is same on both side. A massless gauge field has 2 components while a massive gauge field has 3 components.

[8]Note that in this case there is no gauge symmetry breaking and importantly all the equations for superconductor are gauge invariant. We refer to an article [17] by Martin Greiter which clarifies this confusion.

[9]To be precise this is one of the examples of Higgs mechanism where Abelian gauge field is involved. This was first proposed by Anderson [18] in the context of superconductors. There are other examples of Higgs mechanism especially in the high-energy physics.

references therein). This usage of the term Higgs mode is motivated from the fact that the symmetry broken phase has a gapped (massive) mode.

1.5 Local-moment magnetism

Almost every substance in nature has magnetic properties. It could be in one of the familiar forms: diamagnetism, paramagnetism, ferromagnetism or antiferromagnetism. Unless other form of magnetism dominates almost every material has weak diamagnetism[10]. The most spectacular example of diamagnetism is a superconductor, where one can clearly see the magnetic levitation. A less known but a daily life example is graphite, which (for a thin layer) also shows magnetic levitation! In the present work however we will not encounter diamagnetism.

Both metals and insulators can have magnetic properties. Metals are itinerant magnets[11] when the magnetism is predominantly caused by mobile electrons. On the contrary, magnetism in Mott insulators arises from static local moments. In this work we will be interested in magnetism occurring in Mott insulators only and we will not discuss magnetism in metals here. Throughout this text whenever we refer to magnetic systems it is to be understood as magnetic Mott insulators.

In Mott insulators, due to strong local electron-electron interaction, charge degrees of freedom can be neglected, and at low energies we have an effective model of interacting localized spins (local moments). A formal way to see this aspect is to start from the Hubbard model[12]

$$\mathcal{H}_{Hubbard} = -\sum_{\langle ij\rangle\sigma}\left[t_{ij}c^{\dagger}_{i\sigma}c_{j\sigma} + h.c.\right] - \mu\sum_{i\sigma} n_{i\sigma} + U\sum_{i} n_{i\uparrow}n_{i\downarrow} \tag{1.10}$$

where $\langle ij\rangle$ represents sum over nearest neighbor sites, σ is the spin index, c ($c^{\dagger}$) is electron annihilation (creation) operator, $n_{i\sigma} = c^{\dagger}_{i\sigma}c_{i\sigma}$ ($n_i = \sum_\sigma n_{i\sigma}$), t_{ij} is the hopping strength, μ is the chemical potential and U is the on-site interaction strength. At half filling (in our notation $\langle n\rangle = 1$) and in the limit $t_{ij} \to 0$ there is exactly one electron per site. For small values of t_{ij} but $U \gg t_{ij}$, virtual hopping (second order process in t_{ij}) is allowed if the neighboring electrons have anti-parallel spins, and we thus have an effective interaction[13]. Single hopping is not present in the low energy sector because double occupancy costs energy of the order of U. After appropriate canonical transformation, it can be shown that the low energy sector of the above Hamiltonian is governed by the Heisenberg model (upto an additive constant), which is a spin model

[10]For instance, wood and water. Magnetic levitation of frog is another example.

[11]Magnetism in metals is more complicated [11]. In some cases, for instance due to Kondo screening in heavy Fermion compounds, magnetism in metals could arise from local moments.

[12]Apart from deriving the Heisenberg model or the $t-J$ model for high T_c superconductors, one of the main successes of Hubbard model is in the study of metal-Mott insulator phase transition.

[13]For localized moments, one natural interaction is magnetic dipole interaction. However it turns out that in many cases, it is small compared to the quantum-mechanical exchange interaction.

whose Hamiltonian is given by

$$\mathcal{H}_{Heisenberg} = \sum_{\langle ij \rangle} J_{ij} \vec{S}_i \cdot \vec{S}_j \,, \tag{1.11}$$

$$J_{ij} = \frac{4t_{ij}^2}{U} \,. \tag{1.12}$$

Starting from a (single band) Hubbard model we thus obtain only an antiferromagnetic interaction, though ironically the original motivation of the Hubbard model was to study ferromagnetism. But nevertheless the Heisenberg model can be studied independently as a spin model with either antiferromagnetic ($J_{ij} > 0$) or ferromagnetic ($J_{ij} < 0$) interaction. We will be dealing with this model for the most part of our work. This model has been investigated on various lattices with or without further neighbor interactions as well. Just for completeness we also mention here that if we consider further neighbor hoppings in the Hubbard model, then the resultant spin model has biquadratic spin interaction terms of the form $(\vec{S}_i \times \vec{S}_j) \cdot (\vec{S}_k \times \vec{S}_l)$ along with further neighbor Heisenberg interaction terms. Such interactions often play important role, especially in frustrated magnetic systems.

Often in real insulator materials certain ions contribute to an effective spin which may be even larger than $S = 1/2$. If these ions form a regular arrangement then effectively we realize a lattice of spins which can be studied using various spin models such as the Heisenberg model mentioned earlier. In terms of our discussion on spontaneous symmetry breaking, a paramagnetic insulator is a disordered phase where individual spins can fluctuate in any direction and hence respect the full spin rotation symmetry. On the other hand a magnetically ordered phase such as an antiferromagnet, a ferromagnet, or other exotic magnetic phase break certain symmetry.

In many cases due to constraints from other atoms in the material or spin anisotropy, we may have different coupling strengths for (say) the interaction between $\hat{z}$ component of the spins and the $\hat{x}, \hat{y}$ component of the spins. Thereby instead of the isotropic Heisenberg model we may realize a XXZ model. Further, if the spins can orient only along a particular axis then it is best studied using an Ising model

$$\mathcal{H}_{Ising} = -J \sum_{\langle ij \rangle} S_i^z S_j^z \,. \tag{1.13}$$

This is a classical model since in the absence of any other component of spin one can treat S^z as simply vectors with unit length. In other words, there are no non-commuting operators. The quantum version of this model namely the quantum Ising model or the transverse-field Ising model given by

$$\mathcal{H}_{trans-Ising} = -J \sum_{\langle ij \rangle} S_i^z S_j^z - h \sum_i S_i^x \,, \tag{1.14}$$

will be considered in chapter 7. Great deal of theoretical study has been devoted to this model on different lattice geometries. The Ising model on a triangular lattice is one of the standard examples to explain magnetic frustration.

Among the very few exactly solvable spin models the Kitaev model on a honeycomb lattice has recently attracted enormous interest. One of the reasons being that

its ground state hosts a quantum spin liquid, an exotic state of matter which has characteristic features such as no symmetry breaking down to absolute zero temperature, fractionalized excitations, and non-trivial topology. It is a compass model [19] where nearest neighbor spin interaction involves only a specific spin component depending on the bond direction and its Hamiltonian is given by

$$\mathcal{H}_{kitaev} = 2\sum_{\langle ij\rangle_\alpha} K^\alpha S_i^\alpha S_j^\alpha \,. \tag{1.15}$$

This model was first proposed and solved using Majorana representation by Alexei Kitaev [20]. Initially it was thought to be of theoretical interest only, but it has been argued that due to strong spin-orbit coupling certain Iridate compounds may actually realize Kitaev type interaction [21]. This has attracted many theoretical [22, 23] as well as experimental investigations [24, 25]. Consequently, several modifications such as the Kitaev-Heisenberg model [21] and Kitaev model with second nearest neighbor interaction have emerged [26]. It has been challenging to find *smoking gun* evidence for quantum spin liquids in general and Kitaev spin liquid in particular. In this direction some recent work motivated from Graphene physics has appeared [27]. In chapter 8 we consider one such modification wherein a bilayer of Kitaev model on a honeycomb lattice is considered.

Apart from the models discussed above there are other important and interesting spin models which are widely studied in the context of local-moment magnetism. However we do not attempt to survey them here. We also note that apart from just spins, the orbital degree of freedom may also play an important role for magnetism in Mott insulators.

1.6 Magnetic quantum phase transitions

Depending on the lattice geometry, the dimensionality of the system and the number of further nearest neighbors involved, a particular spin model, such as those discussed above, can host a variety of spin orderings. An antiferromagnet, fully polarized ferromagnet, canted states and commensurate as well as incommensurate spiral orderings are some of the familiar examples. Apart from long-range magnetic ordering there could also be non-magnetic phases such as a trivial quantum paramagnet, a valence bond solid, a plaquette valence bond solid or even a spin liquid. In general due to competition between different couplings involved a given model can host multiple phases, and so there could be magnetic quantum phase transitions. For instance, it is easy to see that in the transverse field Ising model (1.14) there is a quantum paramagnetic phase in the limit $J \to 0$ while a ferromagnetic state exits in the limit $h \to 0$. Thus there must be a quantum phase transition. We will encounter more such examples in this work.

In fact, in many real solids one or more magnetic (non-magnetic) phases are realized by tuning a non-thermal parameter such as pressure or an external magnetic field at a fixed low temperature. One of the well studied materials is $TlCuCl_3$ [28, 29]. Upon tuning pressure, this system undergoes a phase transition from a quantum paramagnet to an antiferromagnetically ordered phase. Interestingly, this compound also undergoes

a phase transition under the application of an external magnetic field [30]. Another beautiful example is MnSi, a B−20 compound, which realizes a skyrmion crystal [31] in the presence of an applied magnetic field. In order to understand such systems and their corresponding phase transitions, knowledge of quantum phase transitions is indispensable. Over the years theorist have studied many spin models and their underlying magnetic quantum phase transitions. Apart from the general understanding of experiments on real materials, study of magnetic quantum phase transitions have resulted in the discovery of fundamentally new theoretical ideas such as the deconfined criticality [32]. In this thesis, however, we will be dealing with more conventional magnetic quantum phase transitions which fall within the Landau-Ginzburg-Wilson paradigm.

A magnetically ordered phase is typically characterized by two quantities namely the ordering wavevector $\vec{Q}$ and a local order parameter Ψ defined via the thermodynamic average of a local operator $\hat{O}$ as follows:

$$\langle \hat{O}(\vec{r}_i) \rangle = \Re(e^{\imath \vec{Q}\cdot\vec{r}_i} \Psi(\vec{r}_i)) \,. \tag{1.16}$$

We are familiar with textbook examples of a ferromagnet and an antiferromagnet whose order parameters are total magnetization and staggered magnetization respectively. In these cases the relevant local operator is simply the total spin operator[14]. Although the above relation looks very simple, finding a correct order parameter may be a non-trivial task. It is worth mentioning here that near a critical point the local order parameter is a slowly varying quantity which allows to promote it as a continuum field and write down the corresponding field theory. In general, quantum fluctuations tend to destabilize magnetically ordered phases, such that the corresponding order parameter decreases continuously until it vanishes at the critical point. As mentioned earlier, it has a power-law behavior with the corresponding critical exponent β, as sketched in fig. 1.3(a). It can be determined in a scattering experiment like the magnetic neutron scattering.

Apart from the order parameter, the dynamic structure factor $S(\vec{k}, \omega)$ is an important observable in the study of magnetic quantum phase transitions. It can be measured in a magnetic neutron scattering experiment. It is related to the imaginary part of the two-point correlation function $\chi(\vec{k}, \omega)$ by the fluctuation-dissipation theorem [33]. Typically, the dynamic structure factor in the quantum paramagnetic phase, at a momentum $\vec{k}$ away from the dispersion minimum, looks as shown in fig. 1.3(b). We see that it yields the information about the energy of the quasiparticle (location of the peak), its lifetime (which is related to the width of the peak) and also the quasiparticle continua. However, at the $\vec{k}$ where the dispersion is minimum, there is no damping at $T = 0$K and we will instead have a sharp peak [6, 8]. This is simply because there are no states available for a decay. Similar picture also holds in the continuous symmetry broken phase, at a momentum $\vec{k}$ away from the ordering wavevector $\vec{Q}$. Here, at the ordering wavevector, the mode is gapless and so there is no peak at a finite energy. We also point out that at finite temperatures there will be damping at all momenta. Moreover disorder in the system may also add to the damping.

From our earlier discussion we also know that the energy gap has a power-law behavior and picture is similar to that of the order parameter. In the case of interacting

[14]This is in general true for any spiral state.

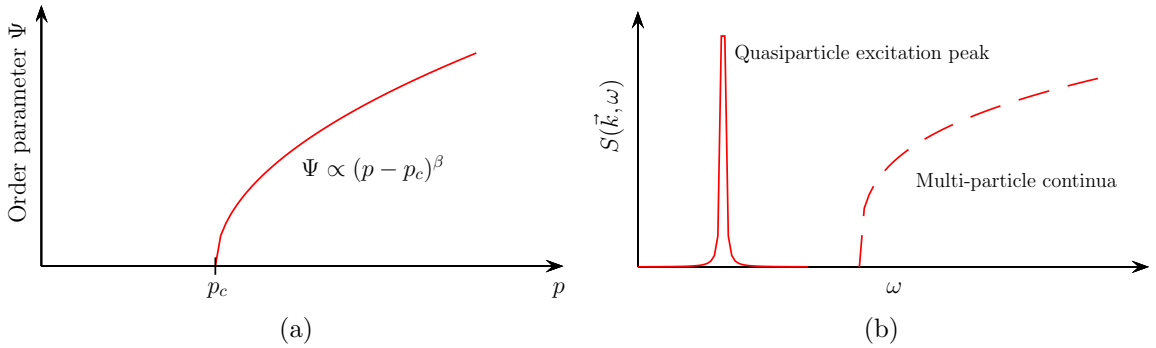

Figure 1.3: (a) Power-law behavior of the order parameter Ψ as a function of the tuning parameter p near the quantum critical point p_c. (b) Dynamic structure factor $S(\vec{k}, \omega)$ in the quantum paramagnetic phase, at a momentum $\vec{k}$ away from the dispersion minimum, and in the magnetically ordered phase, at a momentum $\vec{k}$ away from the ordering wavevector $\vec{Q}$. The peak shows the quasiparticle energy along with the corresponding broadening due to possible damping. Also shown is the multi-particle continua.

systems, in this case spin systems, it is important to keep in mind that the effect of interactions is efficiently captured by calculating self-energy. The real part of these self energies shifts (or renormalizes) the pole in $\chi(\vec{k}, \omega)$ thus shifting the quasiparticle energy and the imaginary part of the self-energy determines the lifetime of these quasiparticle excitations. In the magnetically ordered phase, one can define $\chi(\vec{k}, \omega)$ as the correlation function of the order parameter. While in the disordered phase (i.e. symmetry unbroken phase), we can define $\chi(\vec{k}, \omega)$ using a local operator (which defines the order parameter in the symmetry broken phase). We briefly also mention that at the quantum critical point $\chi(\vec{k}, \omega)$ does not have a sharp pole but instead branch cuts [6, 8]. Therefore at the quantum critical point there are no quasiparticles but only a critical continuum of excitations [15].

In the present work we will frequently make contact with the observables discussed above and their respective critical exponents. Concrete definitions and expressions will be presented in due course.

1.7 Perturbation theory and series expansions

In the field of strongly interacting condensed-matter systems, and especially in the study of interacting spin systems it is important to have a systematic way to take into account interactions. The reason is that only very few systems are exactly solvable. Thus on top of the exactly solvable piece of the Hamiltonian we have to resort to a perturbation theory which is controlled by some small parameter. Now, spins being

[15] This is related to the non-zero value of the critical exponent η which appears in the correlation function. If $\eta = 0$ or very small then one expects peaks even at the quantum critical point. For instance, in case of $TlCuCl_3$ no critical continuum has been detected owing to the fact that $\eta = 0$, since the system is at the upper critical dimension. In this case, logarithmic corrections are expected, which are usually hard to detect.

neither Bosons nor Fermions, we have to map them either to Bosons, or to Fermions, and sometimes to Majoranas, in order to use the machinery of many-body theory. In this case the exactly solvable part is usually the non-interacting particle problem. In some cases we readily have a small parameter in the theory. For instance, the ratio $p = J/h$ is small in the quantum paramagnetic phase of the transverse field Ising model (1.14) and so a perturbation theory can be set up such that an observable can be calculated to a given order in p. Another popular example is the spin-wave theory, widely used for Heisenberg model (1.11) on various lattices, which is controlled in the limit of large spin S i.e. small $1/S$. But in many situations we do not have any small parameter in the theory. In such cases theorist often come up with clever tricks to introduce a small control parameter. One of the well known examples is the large-N expansion where a $SU(2)$ spin problem is generalized to a $SU(N)$ problem such that the observables have an analytic $1/N$ expansion. Similarly, the ϵ-expansion treats $\epsilon = d_c^+ - d$, d and d_c^+ being the spatial dimension and upper critical dimension respectively, as a small parameter and is extremely successful in calculating critical exponents.

In order to construct a perturbation theory we also need a suitable reference state using which we can formally perform a series expansion in our small parameter. It has the property that the value of an observable calculated with respect to this reference state is the zeroth order result in the corresponding series expansion. In principle, the choice of reference state depends on the small parameter. In case of the spin-wave theory, a suitable reference state is the classical ground state, such that in the limit $S \to \infty$, corrections to all observables beyond their classical values vanish.

If we can express an observable as a power series of some small control parameter then it means the observable can be treated perturbatively. In other words we can systematically improve the value of an observable which is perturbative in nature by calculating higher order coefficients in the power series. However, in certain cases some or all observables may be non-perturbative in nature i.e. they may not have an analytic expansion in the chosen small parameter. This might mean that either the choice of the small parameter is incorrect or the problem is generically non-perturbative in nature. Some of the well known examples where non-perturbative behavior is observed includes the superconducting gap Δ and the Kondo resistivity, which is not analytic in the coupling constant. However even in these cases, systematic controlled calculations helped to realize that the perturbation theory breaks down. Thus a small control parameter and related series expansion plays an important role in microscopic calculations.

In the context of magnetic quantum phase transitions an additional challenge is to find a small parameter which can be used in multiple phases across the quantum critical point. Mostly a parameter which is small in one phase becomes large in the other. Consider, for instance, the transverse-field Ising model (1.14), wherein the parameter $p = J/h$ is small in the quantum paramagnetic phase. It is no more the case in the ferromagnetic phase. There are several such instances and many attempts to perform controlled calculations across the critical point by introducing artificial small parameter have failed. In this work we have addressed this challenge by identifying a suitable small control parameter and by presenting an explicit demonstration in the following chapters.

Part I

Coupled-dimer magnets

Chapter 2

Coupled-dimer magnets

In the wide landscape of interesting spin systems coupled-dimer magnets hold a special position. As we will see these are a paradigm of magnetic quantum phase transitions. Coupled-dimer magnets have two spins per crystallographic unit cell i.e. a dimer unit cell[1]. The spins within a dimer are coupled antiferromagnetically and in turn the spins from neighboring dimers interact via some inter-dimer interaction (see fig. 2.1). In general the Hamiltonian describing coupled-dimer magnets can be written as follows:

$$\mathcal{H} = J \sum_{\langle ij \rangle \in \mathcal{D}} \vec{S}_i \cdot \vec{S}_j + K \sum_{\langle ij \rangle \notin \mathcal{D}} \vec{S}_i \cdot \vec{S}_j \,, \tag{2.1}$$

where $\vec{S}_i$ is the spin at lattice site i, $\mathcal{D}$ denotes the dimer forming pair and $\langle ij \rangle$

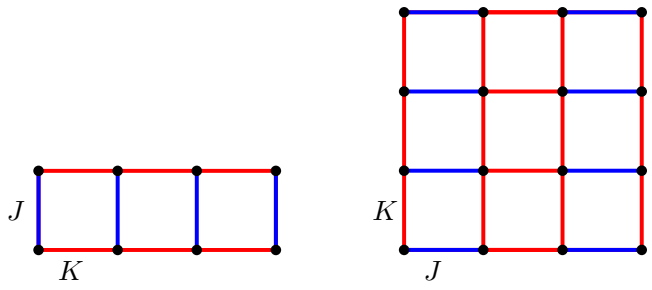

Figure 2.1: Examples of coupled-dimer magnets: (a) A spin ladder; (b) Staggered pattern on a square lattice.

represents sum over nearest neighbors. For Heisenberg spins with $S = 1/2$ and antiferromagnetic intra-dimer interaction ($J > 0$), the ground state is simply a product-state of singlets in the limit $K \to 0$. While in the limit $|K| \gtrsim J$, the system can have magnetic long-range order ($d \geq 2$). Thus there is a magnetic quantum phase transition at some critical value of $|K|/J$.

[1]Note that in many frustrated magnetic systems spontaneous dimerization can occur in a certain region of the parameter space. This is driven by magnetic interactions and will not be discussed here.

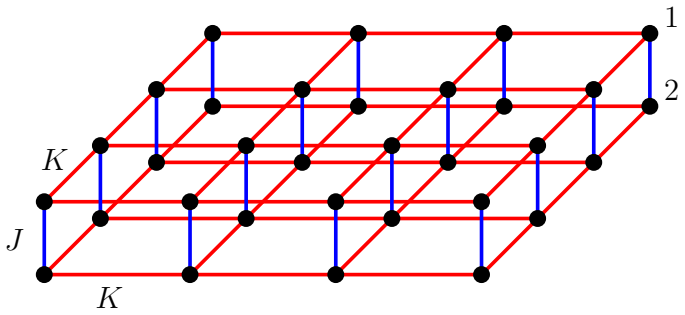

Figure 2.2: Square-lattice bilayer Heisenberg model; an example of a coupled-dimer magnet in $2d$.

2.1 Square-lattice bilayer Heisenberg model

To better understand the phase diagram and physics of coupled-dimer magnets let us consider a concrete model with Heisenberg spins on a square-lattice bilayer (see fig.2.2):

$$\mathcal{H} = J \sum_i \vec{S}_{1,i} \cdot \vec{S}_{2,i} + K \sum_{\langle ij \rangle} (\vec{S}_{1,i} \cdot \vec{S}_{1,j} + \vec{S}_{2,i} \cdot \vec{S}_{2,j}) \,, \tag{2.2}$$

where $\vec{S}_{1,i}$ ($\vec{S}_{2,i}$) is the spin operator in layer 1 (2) such that $\vec{S}_{1,i}$ and $\vec{S}_{2,i}$ form a dimer unit at site i. The sum over $\langle ij \rangle$ represents a sum over nearest neighbor dimers. Instead of looking at individual spin sites it is helpful to view this as a square lattice of dimers. This picture will aid better visualization later on. Thus the couplings $J > 0$ and K are the intra-dimer and the inter-dimer interactions respectively. For clarity, we will consider the inter-dimer interaction K to be positive i.e. antiferromagnetic. Note that the above Hamiltonian is invariant under rotation in the spin space. In other words the Hamiltonian has SU(2) symmetry.

Let us first construct the zero-temperature phase diagram for the above model. It is helpful to first understand the extreme limits. We see that if the inter-dimer interaction vanishes, i.e. $K = 0$ in the above equation, then we simply have an arrangement of isolated dimers with the spins within the dimers coupled antiferromagnetically. Thus the ground-state wavefunction is simply a product-state of singlet states

$$|\Psi_0\rangle = \prod_i |\Psi\rangle_i \,, \tag{2.3}$$

$$|\Psi\rangle_i = \frac{1}{\sqrt{2}} [|\uparrow\downarrow\rangle_i - |\downarrow\uparrow\rangle_i] \,. \tag{2.4}$$

It is easy to see that this state has the same symmetry as the underlying Hamiltonian.

On the other hand, if the intra-dimer interaction J vanishes then we are in the limit of decoupled layers, and we simply have two copies of Heisenberg AF model on a square lattice. The system thus has a Néel antiferromagnetic order. Loosely speaking neighboring spins are pointing in opposite direction[2]. In terms of the symmetry, this phase is completely distinct from the singlet phase in the other extreme limit. Here the

[2]It is important to note that a Heisenberg antiferromagnet has quantum fluctuations and this orientation does not represent the true ground state.

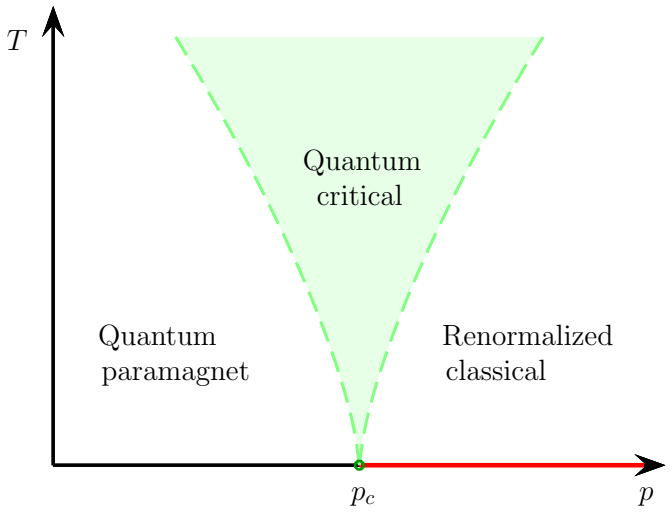

Figure 2.3: Phase diagram of the square-lattice bilayer model (2.2), with quantum critical region (green) and the corresponding quantum critical point (p_c). In this case, the Mermin-Wagner theorem forbids ordering at non-zero temperature and so the Néel AF phase (red) is restricted to $T = 0$K. The renormalized classical phase [34] has correlations which diverge exponentially as $T \to 0$.

continuous SU(2) symmetry present in the singlet phase is broken. Thus starting from the singlet product-state, and tuning the ratio of interaction strengths $p \equiv K/J$, one ends up in a completely different ground state, which a has magnetic order (in this case antiferromagnet). This indicates that at some intermediate value of tuning parameter the system undergoes a quantum phase transition and the two characteristically distinct phases are connected by a quantum critical point at $p_c \equiv (K/J)_c$.

In the light of the discussion in chapter 1, we thus have a disordered phase for $p < p_c$, where no symmetry of the Hamiltonian is broken. An ordered phase with spontaneously broken SU(2) symmetry exists for $p > p_c$. The excitations in the disordered phase are the three spin-1 excitations, popularly known as *triplons*, which cost a finite energy. In the ordered phase, according to the Goldstone's theorem, we have two gapless Goldstone modes, which are spin-wave excitations. In addition a gapped amplitude mode is also present. In the limit of decoupled layers, the amplitude mode corresponds to a simultaneous spin-flip in the two layers. In this case, the magnetically ordered state has staggered magnetization as the order-parameter, which spontaneously acquires a non-zero value in the ordered phase upon crossing the quantum critical point. The temperature T versus p phase diagram for this model is shown in fig. 2.3. This model does not have a long-range order at any non-zero temperature according to the Mermin-Wagner theorem [10]. At non-zero temperatures above the ordered phase, a *renormalized classical* regime [34] exists. In this regime, the correlation length diverges as $T \to 0$.

This model attracted a lot of attention in the last decades, because the parent compounds of some of the high-T_c superconductors are square lattice bilayer with Heisenberg spins [35, 36]. We can perform a similar analysis as above in the presence of a field or in the case of a ferromagnetic inter-dimer interaction as well. The $1d$

version of the above model is the well studied spin ladder [37]. A simple extension of this $2d$ model of dimers to $3d$ will be a cubic lattice of dimers. In this case, magnetic ordering exists for $T \geq 0$K and the system undergoes a classical phase transition into a classical paramagnet at the Néel temperature. Apart from this one can also consider the above model on other lattice geometries such as a bilayer triangular lattice or a bilayer honeycomb lattice.

2.2 Experimental studies

One of the reasons why coupled-dimer models are so interesting is that there are many real materials which realize this model. The square-lattice bilayer model with antiferromagnetic couplings, introduced above, is realized in the compound $BaCuSi_2O_6$ [38]. In this case, Cu ions form a dimer unit and these dimers are arranged on a square lattice. At ambient pressure this material is in the quantum paramagnetic phase. However, the critical pressure beyond which this material could be in an antiferromagnetically ordered phase is too high, and so no phase transition has been observed.

One of the most interesting and well studied materials realizing a coupled-dimer system is $TlCuCl_3$. In this material, a pair of Cu^{2+} ions forms a dimer unit, and these dimers are arranged on a $3d$ lattice. Each Cu^{2+} ion acts as an effective spin with $S = 1/2$. At low temperature and ambient pressure this material is in the quantum paramagnetic phase. At high pressure the inter-dimer coupling, which is antiferromagnetic in this case, becomes more enhanced and the system goes to an antiferromagnetically ordered state. It is one of the best known experiments [28, 29] to illustrate a magnetic quantum phase transition. Using the inelastic neutron scattering, the experiment [28] measured the quasiparticle excitation energy in the quantum paramagnetic phase as well as that in the magnetically ordered phase. The experimental plot is shown in fig. 2.4(a). We see that as one increases the pressure the triplon gap in the quantum paramagnetic phase becomes soft and vanishes at the critical point. Upon increasing the pressure further, gapless spin-wave excitation is seen, corresponding to the spontaneous breaking of the SU(2) symmetry. Also, the gapped longitudinal (amplitude or Higgs) mode is identified. In this material, due to anisotropy in the spin-space, one of the triplon remains gapped even at the critical point and further in the ordered phase it corresponds to a gapped excitation.

Interestingly, $TlCuCl_3$ also exhibits a phase transition upon tuning an external magnetic field (see fig. 2.4(b)). In this case, upon increasing the field from zero the system first goes into a XY-antiferromagnetic (XY-AFM) phase at a critical field H_{c1}, and then at a higher critical field H_{c2} it becomes a ferromagnet. The XY-AFM is often referred to as the Bose-Einstein condensate of triplons [30], due to the possibility of defining a $U(1)$ order parameter $\langle S_i^x + \imath S_i^y \rangle$ in this phase. There are some other spin-1 and spin-1/2 dimerized antiferromagnets which realizes the same physics.

Apart from this, recently a very interesting investigation has been performed on the same compound $TlCuCl_3$, where it was shown that near a quantum critical point classical and quantum fluctuations behave independent of each other [12]. Interestingly, reminiscent of the amplitude mode present at $T = 0K$ was studied at finite temperature, where it is usually expected to be thermally damped.

All these experiments provide a good playground to apply theory of magnetic quan-

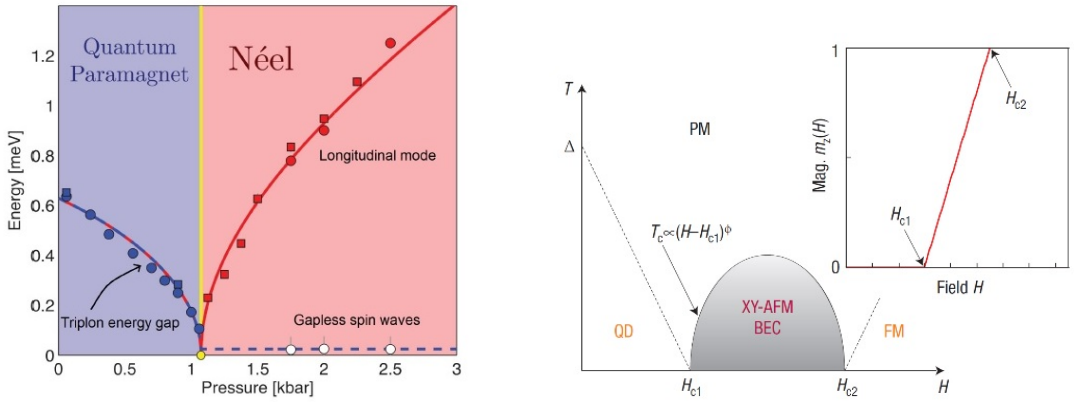

(a) (b)

Figure 2.4: (a) Inelastic neutron scattering data of $TlCuCl_3$ showing the triplon energy as well as the gapless spin waves, and the gapped longitudinal mode. Here the phase transition is driven by an external pressure. Figure is taken from ref. [28]. (b) Schematic phase diagram of a magnetic field driven phase transition in $TlCuCl_3$. Figure is taken from ref. [30].

tum phase transitions. This further motivates a detailed and systematic theoretical investigation of coupled-dimer magnets.

2.3 Theoretical methods

Let us now turn our attention to theoretically solving the model of coupled-dimer magnets. Solving any spin system analytically is always challenging and often one has to employ approximation techniques to get reasonable results. There are very few instances of exactly solvable spin models and even in those cases one arrives at the solution using non-trivial mathematical tools. The problem is more serious near a critical point where inevitably one has to face divergences. In this context low energy field theory is an extremely useful tool [6, 7]. Exploiting the symmetry of problem it provides a good description of different phases and related phase transitions. Although one must bear in mind that often identifying a suitable order parameter to write down the field theory is a non-trivial task. But once the field theory is constructed it offers us a heap of information about the critical phenomena. Importantly it helps us to understand the universal properties of the system. Same can be said regarding the renormalization group approach. However, one has to keep in mind that these methods are suitable near the critical point, and to get a handle on observables and non-universal properties in individual phases one has to resort to a microscopic description of the phenomenon.

Microscopic theories to tackle spin systems typically consist of two important steps. Firstly, the spin Hamiltonian is transformed into a Hamiltonian in terms of either Bosons, Fermions, or Majoranas, so as to facilitate the use of our familiar many-particle theory. If this transformation leads to a solvable problem like that of free fermion theory (eg. The $1d-$XY model via Jordan-Wigner transformation or the Kitaev compass

model on a honeycomb lattice via Majoranas [20]) then one has essentially solved the problem. All the relevant observables can be then computed. However, most often this is not the case, and one has to face an interacting Hamiltonian. Then as a second step, we have to come up with an efficient way to handle the interaction terms in the Hamiltonian. One choice is to perform a mean-field approximation, or in some cases apply dynamical mean-field theory (DMFT). In many cases mean-field theory works reasonably well. However, it is important to realize that mean-field description of an interacting problem is often uncontrolled and can not consistently describe the entire phase diagram. More technically speaking, in the absence of a small control parameter a mean-field description need not satisfy the Goldstone's theorem in magnetically ordered phases. Actually it has been recently noticed that application of DMFT to spin systems indeed violates the Goldstone's theorem [39]. We shall comment on this issue later when we introduce our systematic $1/d$ expansion.

One has to then resort to a perturbation theory. There are many schemes and techniques of solving a model using perturbation theory. Each one has its own control parameter and/or perturbation scheme to tackle the interacting piece in the Hamiltonian. As discussed earlier in chapter 1, one can then calculate observables as a series expansion in the respective small parameter. Each method has its own merit and has proven to be successful in one or the other problems. We shall point out some of these methods in the context of coupled-dimer magnets in the following discussion.

Before we dive into details of some of the analytical methods used to solve the system of coupled-dimer magnets, let us quickly survey some of the numerical methods. As noted above often spin systems are unsolvable analytically and in this regards exact numerics provides an efficient way to study such systems. There is a whole array of sophisticated numerical techniques like exact diagonalization, classical and quantum Monte Carlo, DMRG etc. The most sever limitation to numerical methods may come from the fact that often these techniques are restricted to small system sizes. Some of them are also restricted to $d = 1$ and 2, or suffer from a sign problem in frustrated systems. But nevertheless these are often benchmark methods for solving spin systems. We shall not go into any further details of numerical methods used to solve system of coupled-dimer magnets and concentrate only on analytical methods. In chapter 6, we shall present a comparison of our method with recent QMC results.

Let us now briefly review some of the standard analytical methods available in the literature to study coupled-dimer magnets.

2.3.1 Bond-operator theory

As discussed in the previous section, a coupled-dimer magnet is in a quantum paramagnetic phase for strong antiferromagnetic intra-dimer interaction. This means for spins with $S = 1/2$, there are predominantly spin-0 singlet bonds on dimer sites. It is then clear that the excitation on every dimer site is a spin-1 triplet. To capture this picture, for spins with $S = 1/2$, Sachdev and Bhatt [40] introduced bond operators which create either a singlet or triplet out of a fictitious vacuum. Later it was realized [41, 42] that it is more convenient to introduce bond operators which creat a triplet excitation over a singlet background. We shall stick to this convention throughout this

work. Bond operators are thus defined as follows:

$$|t_0\rangle = \frac{1}{\sqrt{2}}[|\uparrow\downarrow\rangle - |\downarrow\uparrow\rangle]\,, \tag{2.5}$$

$$t_1^\dagger|t_0\rangle = |t_1\rangle = -\frac{1}{\sqrt{2}}[|\uparrow\uparrow\rangle - |\downarrow\downarrow\rangle]\,, \tag{2.6}$$

$$t_2^\dagger|t_0\rangle = |t_2\rangle = \frac{\iota}{\sqrt{2}}[|\uparrow\uparrow\rangle + |\downarrow\downarrow\rangle]\,, \tag{2.7}$$

$$t_3^\dagger|t_0\rangle = |t_3\rangle = \frac{1}{\sqrt{2}}[|\uparrow\downarrow\rangle + |\downarrow\uparrow\rangle]\,, \tag{2.8}$$

where $|t_0\rangle$ is the spin-0 singlet state and $t_\alpha^\dagger$ ($\alpha = 1, 2, 3$) creates a spin-1 triplet state $|t_\alpha\rangle$ out of the singlet state. We can then express our spin operators in terms of these states as follows:

$$S_{i1,2}^\alpha = \frac{1}{2}\left(\pm|t_\alpha\rangle\langle t_0| \pm |t_0\rangle\langle t_\alpha| - \iota\epsilon_{\alpha\beta\gamma}|t_\beta\rangle\langle t_\gamma|\right)\,. \tag{2.9}$$

Note that $t_\alpha^\dagger$ (t_α) is a Bosonic creation (annihilation) operator satisfying the usual Bosonic commutation rules,

$$\left[t_{i\alpha}, t_{j\beta}^\dagger\right] = \delta_{i,j}\delta_{\alpha,\beta}\,;\ \left[t_{i\alpha}, t_{j\beta}\right] = \left[t_{i\alpha}^\dagger, t_{j\beta}^\dagger\right] = 0\,. \tag{2.10}$$

The resulting quasiparticle excitations are popularly known as *triplons*.

So far what we have found is a suitable Bosonic representation of our original spin operators. But this transformation brings along a complication namely the constraint from the physical Hilbert space. For spins with $S = 1/2$ only four states are possible per dimer site - one singlet and three triplets. However we know that on a given site Bosons can be in any number, because there is no exclusion principle for Bosons. This means that out of infinitely many states per dimer, our physical Hilbert space consists of only those states where we have no more than one Boson per site. This is the hard-core constraint which can be phrased as follows:

$$\sum_{\alpha=1}^{3} t_{i\alpha}^\dagger t_{i\alpha} \leq 1\,. \tag{2.11}$$

Tackling this constraint is challenging, and over the past decades, sophisticated techniques have been developed to address this issue. We will discuss some of them soon.

2.3.2 Generalized bond-operator theory

Although the original formulation of bond-operator theory was designed for quantum paramagnetic phase, it has been generalized to magnetically ordered phases as well [43]. This involves a suitable rotation in the Hilbert space, which is also equivalent to condensing one or more triplons. We will discuss this procedure in some detail in the following. Apart from this, generalization of bond operators for larger spins has been studied as well [44].

The paramagnetic phase of a coupled-dimer model can be conveniently described using a state which involves a product of singlets, $|\psi_0\rangle = \prod_i |t_0\rangle_i$. But the magnetically

ordered phases require a reference state with broken SU(2) spin symmetry. For a consistent description of excitations, it is convenient to perform a SU(4) basis rotation in the Hilbert space of each dimer [43]. The most general form reads

$$|\tilde{t}_k\rangle_i = U^{(i)}_{kk'}|t_{k'}\rangle_i, \qquad (k,k'=0,\ldots,3). \tag{2.12}$$

The rotation should be chosen such that $|\tilde{\psi}_0\rangle = \prod_i |\tilde{t}_0\rangle_i$ is a suitable reference state in the magnetically ordered phase. For instance, a local Néel state polarized along $\hat{z}$ is obtained from $|\tilde{t}_0\rangle = (|t_0\rangle + |t_3\rangle)/\sqrt{2} = |\uparrow\downarrow\rangle$.

In general, the spin operators $\vec{S}_{im}$ can be then represented in terms of transitions between the states $|t_k\rangle_i$ of a dimer,

$$S^\alpha_{im} = \sum_{kk'} s^{\alpha m}_{kk'} |t_k\rangle_i \, {}_i\langle t_{k'}|, \tag{2.13}$$

with 4×4 matrices $s^{\alpha m}$ for the spin components S^α ($\alpha = x,y,z \equiv 1,2,3$) of the $m=1,2$ spins:

$$\begin{aligned}
s^{x1,2} &= \frac{1}{2}\begin{pmatrix} 0 & \pm 1 & 0 & 0 \\ \pm 1 & 0 & 0 & 0 \\ 0 & 0 & 0 & -\imath \\ 0 & 0 & \imath & 0 \end{pmatrix}, \\
s^{y1,2} &= \frac{1}{2}\begin{pmatrix} 0 & 0 & \pm 1 & 0 \\ 0 & 0 & 0 & \imath \\ \pm 1 & 0 & 0 & 0 \\ 0 & -\imath & 0 & 0 \end{pmatrix}, \\
s^{z1,2} &= \frac{1}{2}\begin{pmatrix} 0 & 0 & 0 & \pm 1 \\ 0 & 0 & -\imath & 0 \\ 0 & \imath & 0 & 0 \\ \pm 1 & 0 & 0 & 0 \end{pmatrix}.
\end{aligned} \tag{2.14}$$

This is of course equivalent to the bond-operator representation of Sachdev and Bhatt [40], written in terms of transition operators:

$$S^\alpha_{i1,2} = \frac{1}{2}\left(\pm|t_0\rangle_i \, {}_i\langle t_\alpha| \pm |t_\alpha\rangle_i \, {}_i\langle t_0| - \imath\epsilon_{\alpha\beta\gamma}|t_\beta\rangle_i \, {}_i\langle t_\gamma|\right).$$

After the basis rotation (2.12), eq. (2.13) becomes

$$S^\alpha_{im} = \sum_{kk'} \tilde{s}^{\alpha m}_{i,kk'} |\tilde{t}_k\rangle_i \, {}_i\langle \tilde{t}_{k'}|, \tag{2.15}$$

with the transformed spin matrices now being in general site-dependent:

$$\tilde{s}^{\alpha m}_{i,kk'} = \sum_{ll'} (U^\dagger)^{(i)}_{lk} s^{\alpha m}_{ll'} U^{(i)}_{k'l'}. \tag{2.16}$$

Now as before, we can introduce Bosonic operators $\tilde{t}_{i\alpha}$ ($\alpha = 1,2,3$) for local excitations w.r.t. the reference state $|\tilde{t}_0\rangle_i$,

$$|\tilde{t}_\alpha\rangle_i = \tilde{t}^\dagger_{i\alpha}|\tilde{t}_0\rangle_i. \tag{2.17}$$

In the untransformed case, the $\tilde{t}^\dagger_{i\alpha}$ are the triplon bond operators introduced earlier, and we will continue to refer to them as (generalized) triplons. Again, these operators obey the hard-core constraint

$$\sum_{\alpha=1}^{3} \tilde{t}^\dagger_{i\alpha}\tilde{t}_{i\alpha} \leq 1. \tag{2.18}$$

Next we discuss a couple of approaches to tackle this hard-core constraint.

Hard-core constraint: mean-field treatment

The initial bond-operator approach of Sachdev and Bhatt [40] introduced four bosonic operators $t^\dagger_{ik}$ which creates the singlet and triplet states out of a fictituous vacuum, $|t_k\rangle_i = t^\dagger_{ik}|vac\rangle_i$. This leads to the following representation of the original spin operators in terms of bond bosons:

$$S^\alpha_{i1,2} = \frac{1}{2}\left(\pm t^\dagger_{i\alpha}t_{i0} \pm t^\dagger_{i0}t_{i\alpha} - \imath\epsilon_{\alpha\beta\gamma}t^\dagger_{i\beta}t_{i\gamma}\right), \tag{2.19}$$

where $\alpha = 1, 2, 3 \equiv x, y, z$, and the upper (lower) sign corresponds to spin 1 (2) of each dimer. In terms of these operators, the hard-core constraint is

$$\sum_{k=0}^{3} t^\dagger_{ik}t_{ik} = 1\,. \tag{2.20}$$

In the original formulation by Sachdev and Bhatt [40], the singlet operator was condensed, $t_{i0} \to \langle t_{i0}\rangle = s$. The constraint was then treated in a mean-field fashion via a Lagrange multiplier μ, such that $\sum_{\alpha=1}^{3}\langle t^\dagger_{i\alpha}t_{i\alpha}\rangle + s^2 = 1$. In the Hamiltonian, only bilinear terms in the t_α operators were kept. The mean-field parameters s and μ were determined variationally. However this approach is uncontrolled, and later on controlled methods were developed. We shall discuss a couple of alternatives in the following.

Brueckner theory

As pointed out above, dealing with the hard-core constraint of Bosons is non-trivial. One way to think about this constraint is to introduce hard-core (infinite) on-site repulsion between the triplons:

$$\mathcal{H}_U = U\sum_{i\alpha\beta} t^\dagger_{i\alpha}t^\dagger_{i\beta}t_{i\alpha}t_{i\beta}\,, \quad U \to \infty\,. \tag{2.21}$$

In ref. [41], Kotov et al. treated this interaction term using the so-called *Brueckner theory* of dilute Bose gas. In this approach, solving the Bethe-Salpeter equation amounts to summing an infinite number of diagrams to obtain the interaction vertex. Such a re-summation is controlled by the presence of small triplon density (hence the analogy to dilute Bose gas). Further it is used to calculate the self-energy, and therefore the Green's function. Location of the pole in the Green's function then gives the dispersion relation. This entire procedure is implemented in a self-consistent fashion to obtain

the gap and the quasiparticle weight. This is a very successful method as it yields very accurate results for the critical point. Apart from the coupled-dimer magnets, this procedure has been implemented successfully in other models as well. For instance, it has been used to calculate the stability region of the valence-bond solid phase in the case of spin-1/2 J_1 -J_2 Heisenberg antiferromagnet on a square lattice [45].

However, it is important to note here that the extension of this method to magnetically ordered phase does not work. It has been observed [46] that implementing Brueckner theory in magnetically ordered phase leads to violation of Goldstone's theorem, and/or the quantum phase transition is erroneously rendered to be of first order. The reason for this failure is simple to understand. As mentioned above, the Brueckner theory relies on triplon density being small. But in the magnetically ordered phase this is not the case. In fact, it is clear from the fact that since bond operator rotation involves condensing at least one of the triplons the density is not going to be small. Later, in chapter 4 we will make connection of our method to the Brueckner theory.

Projection operator

Another interesting way to tackle the hard-core constraint was proposed by Collins et al. [42] by introducing the so-called projection operator

$$P_i = 1 - \sum_{\gamma=1}^{3} t_{i\gamma}^{\dagger} t_{i\gamma} \,. \tag{2.22}$$

This is unlike the usual quantum mechanical projection operator whose squared value is unity. But what this operators does is that it suppresses the matrix elements between the physical and unphysical states of the Hilbert space for any observable. One can easily motivate the usage of this operator. In terms of the singlet and triplet states, the hard-core constraint reads as

$$|t_0\rangle\langle t_0| + \sum_{\alpha=1}^{3} |t_\alpha\rangle\langle t_\alpha| = 1 \,. \tag{2.23}$$

It means that in eq. (2.9) one can replace $|t_0\rangle\langle t_0| = 1 - \sum_{\alpha=1}^{3} |t_\alpha\rangle\langle t_\alpha|$. Now in the physical Hilbert space consisting of only singlet and triplet states, $|t_\alpha\rangle\langle t_\alpha| = t_\alpha^{\dagger} t_\alpha$. With the help of the P_i the transitions between the dimer states can now be written in terms of the bond operators as follows:

$$\begin{aligned}
|t_0\rangle_{i\ i}\langle t_0| &= P_i, \\
|t_\alpha\rangle_{i\ i}\langle t_0| &= t_{i\alpha}^{\dagger} P_i, \\
|t_0\rangle_{i\ i}\langle t_\alpha| &= P_i t_{i\alpha}, \\
|t_\alpha\rangle_{i\ i}\langle t_\beta| &= t_{i\alpha}^{\dagger} t_{i\beta}.
\end{aligned} \tag{2.24}$$

Hence using projection operators we obtain the following expression for the spin operators in terms of triplon operators

$$S_{i1,2}^{\alpha} = \frac{1}{2}\left(\pm t_{i\alpha}^{\dagger} P_i \pm P_i t_{i\alpha} - i\epsilon_{\alpha\beta\gamma} t_{i\beta}^{\dagger} t_{i\gamma}\right) . \tag{2.25}$$

It is easy to verify that all the spin commutation relations are satisfied *within* the physical Hilbert space. Actually it turns out that this is a very convenient way to handle the constraint and we will be using this approach in this work. The hard-core constraint, using the projection technique, will be implemented on similar lines in the magnetically ordered phase, using the generalized triplons.

We point out that instead of P_i we could have used a projection operator involving a square root such as $\sqrt{1-\sum_{\gamma=1}^{3} t_{i\gamma}^{\dagger} t_{i\gamma}}$. In fact it turns out that the square root choice delivers correct spin commutation relations everywhere in the Hilbert space. However, it can not be used for two reasons: (i) For calculations we need to expand the square root and formally there is no small parameter controlling this expansion, although it can be justified that $\langle \sum_{\gamma=1}^{3} t_{i\gamma}^{\dagger} t_{i\gamma} \rangle$ is small (see later chapters); (ii) A more serious issue is that even if we expand the square root then we face the problem that coefficients of higher order terms in the expansion diverge. In the appendix B we present a more general discussion on other choices of projection operators.

2.3.3 Spin-wave theory

When it comes to describing the magnetically ordered phases of Heisenberg spin systems, the spin-wave theory[3] surely counts among the most successful theories. It was first studied in ferromagnets where it was realized that the excitations are collective spin waves which are gapless in the long wavelength limit. Similar gapless excitations (Goldstone modes) are realized in other ordered magnets (with spontaneously broken continuous symmetry) as well. Bloch first treated these excitations as independent spin waves and due to its analogy to quanta of lattice vibrations, phonon, the term magnon was coined.

However, it was soon realized that these magnons can interact. In order to take into account the interaction among the magnons, it is convenient to work in second quantization wherein the spins are mapped onto Bosons. There are two popular ways to accomplish this task; one is the Holstein-Primarkoff transformation and the other is the Dyson-Maleev transformation. In most cases, both descriptions are known to yield same results. The main difference between these approaches is that while the Holstein-Primarkoff transformation gives a Hermitian Hamiltonian, the Dyson-Maleev transformation results in a non-Hermitian Hamiltonian. This is clear from the respective transformations. Let us write down the two transformations for Néel antiferromagnets. In this case the reference state consists of adjacent spins with opposite orientation. Let us label the up-spins with site index i, and those with the down-spins with site index l. We will then introduce two types of Boson operators: a_i and b_l on the respective

[3]There are several textbooks and research articles dealing with the spin-wave theory. We refer to two textbooks, one by Ashcroft and Mermin [47] and the other by K. Yosida [48], for more elaborate discussion.

sites[4]. Within the Holstein-Primarkoff transformation, spins transform as follows

$$S_i^z = S - a_i^\dagger a_i\,, \quad S_i^+ = \sqrt{2S}\sqrt{1-\frac{a_i^\dagger a_i}{2S}}a_i\,, \quad S_i^- = \sqrt{2S}a_i^\dagger\sqrt{1-\frac{a_i^\dagger a_i}{2S}}\,, \tag{2.26}$$

$$S_l^z = b_l^\dagger b_l - S\,, \quad S_l^+ = \sqrt{2S}b_l^\dagger\sqrt{1-\frac{b_l^\dagger b_l}{2S}}\,, \quad S_l^- = \sqrt{2S}\sqrt{1-\frac{b_l^\dagger b_l}{2S}}b_l\,. \tag{2.27}$$

On the other hand the Dyson-Maleev transformation reads

$$S_i^z = S - a_i^\dagger a_i\,, \quad S_i^+ = \sqrt{2S}\left(1-\frac{a_i^\dagger a_i}{2S}\right)a_i\,, \quad S_i^- = \sqrt{2S}a_i^\dagger\,, \tag{2.28}$$

$$S_l^z = b_l^\dagger b_l - S\,, \quad S_l^+ = \sqrt{2S}b_l^\dagger\left(1-\frac{b_l^\dagger b_l}{2S}\right)\,, \quad S_i^- = \sqrt{2S}b_l\,. \tag{2.29}$$

Even in this case, there is a constraint from the physical Hilbert space namely that $a_i^\dagger a_i, b_l^\dagger b_l \leq 2S$. However it turns out that the matrix elements of S^+ and S^- between the $2S$ and $2S+1$ states vanishes, thus ensuring no mixing of states from the physical and unphysical sector.

Philosophically, the spin-wave theory relies on the large-S limit which allows for the square-root expansion in the transformation. In the limit $S \to \infty$ the problem reduces to that of classical spins. Hence the classical ground state is taken as the reference state and perturbative corrections to the observables are arranged in a power series in $1/S$. It is therefore clear that this method can not be used in the quantum paramagnetic case where no semi-classical approximation is possible. Moreoever, since this theory is designed to capture only the collective spin-wave excitations, the analysis of the amplitude mode, which is present in the coupled-dimer magnets for any non-zero inter-dimer coupling, is beyond its scope.

2.3.4 Some other proposals

So far we have discussed approaches based on the bond-operator theory. There are also a few other methods which do not formally use the bond operators introduced above. One such notable work is by Chubukov and Morr [49]. In this work, Bosonic operators are introduced to describe the spin-1 triplet excitations in the quantum paramagnetic phase. The hard-core constraint is implemented via the operator

$$U_i = \sqrt{1 - a_i^\dagger a_i - b_i^\dagger b_i - c_i^\dagger c_i} \tag{2.30}$$

where the operators a, b and c are the Boson annihilation operators corresponding to the triplet excitations. This is similar to the square-root projection operator discussed earlier. In principle, there is no small parameter which allows the expansion of this

[4]Alternatively, it is possible to work in a rotating frame where all spins are ferromagnetically aligned and then only one kind of Boson needs to be introduced. In fact this approach is inevitable when working with spirals with a large wavelength.

square-root and so Chubukov and Morr [49] introduced an artificial small parameter $\lambda \ll 1$ such that

$$U_i = \sqrt{1 - \lambda(a_i^\dagger a_i + b_i^\dagger b_i + c_i^\dagger c_i)}\,. \tag{2.31}$$

Calculations are then performed by formally treating λ as a small parameter, such that the physical scenario corresponds to $\lambda \to 1$. This method can be generalized to the ordered phase as well. However, it was found that the expansion for the critical coupling ratio has a log-divergence at second-order. We believe that the reason for this divergence is rooted in the fact that for $\lambda \to 1$ higher order coefficients in the square-root expansion diverge.

Apart from this, many series expansion methods exists in the literature. For instance, using the bond operators one can formulate a series expansion in the ratio of K/J in the quantum paramagnetic phase. Of course, this cannot be used in the magnetically ordered phase, since K/J will not be a small parameter. Some other prominent examples include the dimer series expansion [50], Ising expansion [51] etc. All these excellent expansion techniques are, however, either limited to only one of the phases, or breakdown near the critical point. For a detailed overview of these methods and its applications we refer to ref. [52].

2.4 Discussion

In this chapter we have introduced the system of coupled-dimer magnets and specifically discussed the square-lattice bilayer model for Heisenberg spin-1/2. Focusing on the analytical approaches we discussed several well known techniques. We argued that although these methods have their own merit, none of them can consistently describe both the disordered and the magnetically ordered phases. As seen from the above discussion, the problem is rooted in the fact that there is no known small control parameter in the problem. In this context, we propose that $1/d$, where d is the spatial dimension of the system, is a suitable control parameter. In the following chapters we will explicitly demonstrate that using $1/d$ as a small parameter we can consistently describe the entire phase diagram of coupled-dimer magnets.

Chapter 3

Limit $d \to \infty$

There is a scarcity of analytic methods which can consistently describe a magnetic quantum phase transition, and the corresponding phases connected to it. In the last chapter, we discussed a few methods and their limitations in the context of coupled-dimer magnets. It is clear that a lack of small control parameter has halted systematic calculations. Series expansions, as the name suggests, is an expansion in a small parameter. Often this is chosen as one of the parameters in the model Hamiltonian. But, as we have already seen, in many cases one has to introduce artificial small parameters as well. The basic necessity for a series expansion to be valid is analyticity. If the series is analytic, then one can argue that any pre-factor multiplying the small parameter still results in a small term, and hence one can assume convergence as well. Once the existence of a small parameter is ensured, then the task is to express observables as a series expansion in the chosen small parameter. Depending on the desired accuracy one can compute observables to a particular order in the small parameter. It is clear that there are infinite terms in any series expansion, and by restricting to a particular order we essentially neglect all higher order contributions. Usually finding a small parameter is a non-trivial task, as we have repeatedly emphasized, and in the context of coupled-dimer magnets (in general for magnetic quantum phase transitions) there is no small parameter known in the literature.

This brings us to the present work where we propose a novel expansion method using the inverse spatial dimension of the system, $1/d$, as a small control parameter. Technical details regarding the calculation of observables will follow in the next chapters. What we plan to discuss here are the general aspects of the large-d limit, in the context of quantum phase transitions. Although most of the arguments which will follow are model independent, we will make precise statements for the model of coupled-dimer magnets on a d-dimensional hypercubic lattice.

3.1 Large-d generalization

The first step to setup or motivate the use of $1/d$ as a small parameter is to *generalize* the underlying lattice of a given model, in a fixed dimension, to an arbitrary dimension d. In general there could be several ways of generalizing a given $2d$ or $3d$ lattice. One straightforward way is to generalize the primitive vectors of a given lattice, such that the generalized set of d primitive vectors results in the d dimensional lattice.

Another way could be to generalize the lattice in such a way that the coordination number remains the same. One can think of many more alternatives and each type of generalization would in principle give a different expansion in $1/d$. In this work, we will stick to the idea of generalizing a given set of primitive vectors, since we find it to be both convenient and consistent, as will be shown in the later chapters. It is certainly an interesting task to compare $1/d$ expansions resulting from different kinds of generalization but this goes beyond the scope of present work. We note that sometimes a d-dimensional generalization of a lattice might be dictated by the model under consideration. For instance, generalizing *compass models* might involve certain constraints on the coordination number; for eg., it has to be a multiple of 3 in the case of generalizing the *Kitaev model* on a honeycomb lattice to d dimensions. However, for Heisenberg or Ising type spin exchanges there is more freedom in terms of a d dimensional generalization.

Our main focus is on Heisenberg spin-1/2 coupled-dimer magnets, whose material realizations have either a square or a cubic arrangement of dimer unit cells. Hence we will be interested in a d-dimensional generalization of these lattices. The set of primitive vectors for a square and a cubic lattice simply consists of the unit vectors along their respective coordinates[1]: $\{\hat{e}_1, \hat{e}_2\}$ for the square lattice, while $\{\hat{e}_1, \hat{e}_2, \hat{e}_3\}$ for the cubic lattice[2]. So the straightforward generalization to d dimensions means going from $\mathbb{R}^2$, or $\mathbb{R}^3$ to $\mathbb{R}^d$. Thus the unit vectors along the d directions are our primitive vectors: $\{\hat{e}_1, \hat{e}_2, \ldots \hat{e}_d\}$. The resulting lattice is nothing but a d-dimensional hypercube.

We also note that for frustrated systems, where further neighbor interactions are involved, a large-d generalization could be achieved by generalizing the further neighbor interactions along with the lattice. For instance, the $J_1 - J_2$ Heisenberg model on a square lattice could be generalized in such a way, that in d dimensions it involves d further neighbor interactions on a d dimensional hypercubic lattice.

3.2 Reference state in the large-d limit

Any series expansion is formally performed around a suitable choice of reference state. For instance, in case of perturbation theory for Hamiltonians with discrete non-degenerate spectra, we expand around the ground-state of the exactly solvable part. To give another example, classical magnetically ordered ground-state is used as a reference state to perform a large-S (where S is spin) expansion in the spin-wave theory. In the spin-wave theory, the choice of classical state as a reference state is motivated by the fact that in the limit $S \to \infty$ we can treat the spins classically, i.e. just vectors instead of operators. This is most easily seen by realizing that the local ground-state expectation values correspond to their classical values in the limit $S \to \infty$.

Here we want to deal with quantum spins (specifically with $S = 1/2$), such that no semi-classical approximation is possible. To be precise, we will be dealing with the model (2.2) on a hypercubic lattice. But we have a simplification if we work in the large-d limit, where the number of nearest neighbors increases with d. Due to large coordination number fluctuations tend to average out, such that the non-

[1] Here and throughout the text we will set the lattice constant $a = 1$.

[2] $\hat{e}_1 \equiv \hat{x}$, $\hat{e}_2 \equiv \hat{y}$ and $\hat{e}_3 \equiv \hat{z}$.

local fluctuations become irrelevant, and we can assume a product-state ansatz for our reference state:

$$|\psi_0\rangle = \prod_i |\psi_i\rangle \tag{3.1}$$

where i is the dimer site and $|\psi_i\rangle$ is an arbitrary normalized state at the corresponding dimer site. A suitable choice of $|\psi_0\rangle$ can be made by variationally minimizing $\langle\psi_0|\mathcal{H}|\psi_0\rangle$, for a given Hamiltonian $\mathcal{H}$. For the case of Heisenberg spin-1/2 coupled-dimer magnets (2.2) on a hypercubic lattice, it turns out[3] that in the quantum paramagnetic phase a singlet product-state is a good reference state i.e.

$$|\psi_0\rangle = \prod_i \frac{|\uparrow\downarrow\rangle_i - |\downarrow\uparrow\rangle_i}{\sqrt{2}}\,. \tag{3.2}$$

If we now calculate local observables with respect to this state, then we find[4] that these vanish in the limit $d \to \infty$, i.e. the product-state delivers exact ground-state expectation values. This justifies our earlier statement about non-local fluctuations being irrelevant in the large-d limit. We must caution that, unlike the spin-wave theory, $|\psi_0\rangle$ is *not* an exact ground state of eq. (2.2) on a hypercubic lattice (except at the isolated point $K = 0$) in the limit $d \to \infty$, and we will see this in the next chapter. To complete the discussion, we mention here that in the magnetically ordered phase of coupled-dimer magnets on a hypercubic lattice, a suitable reference state is a linear combination of the singlet and one, or more triplet states. Even in this phase we will see that the local observables calculated with respect to the reference state are suppressed in powers of $1/d$, such that in the limit $d \to \infty$ they correspond to exact ground-state expectation values. The discussion about the precise choice of this state is postponed to chapter 5.

3.3 Geometric properties of a hypercubic lattice

Let us now discuss the geometric properties arising in the large-d limit, which will play an important role in our formalism of $1/d$ expansion. We will discuss general ideas, but as mentioned before, we will give specific details only for the hypercubic lattice. To start with, let us define the nearest neighbor interaction structure factor

$$\gamma_{\vec{k}} \equiv \gamma^1_{\vec{k}} = \frac{1}{z_1/2}\frac{1}{2}\sum_{\vec{\Delta}_1} e^{\imath\vec{k}\cdot\vec{\Delta}_1} \tag{3.3}$$

where z_1 is the number of nearest neighbors, $\vec{\Delta}_1$ is the vector joining a given site to its nearest neighbors, and $\vec{k}$ is the crystal momentum in the first Brillioun zone. Similarly, we can define the structure factor for further nearest neighbor interactions as

$$\gamma^n_{\vec{k}} = \frac{1}{z_n/2}\frac{1}{2}\sum_{\vec{\Delta}_n} e^{\imath\vec{k}\cdot\vec{\Delta}_n} \tag{3.4}$$

[3]It is easy to see this by simply considering $|\psi_0\rangle$ as a linear combination of the singlet and the triplet states. Minimizing $\langle\psi_0|\mathcal{H}|\psi_0\rangle$ gives the desired result.

[4]Concrete expressions will be presented in the next chapter.

where z_n is the number of nth nearest neighbors, $\vec{\Delta}_n$ is the vector joining a given site to its nth nearest neighbors, and again $\vec{k}$ is the crystal momentum in the first Brillioun zone. Observe that for lattices with symmetrically located nearest neighbors[5] around every lattice site, we have a purely real $\gamma_{n\vec{k}}$. Essentially, these are sum over some cosine functions depending on the primitive vectors. Furthermore, these structure factors are all normalized such that $\gamma^n_{\vec{k}} \in [-1, 1]$.

For the hypercubic lattice, $z_1 = 2d$ and $\vec{\Delta}_1$s are just the primitive vectors. Thus $\gamma_{\vec{k}}$ takes a simple form as follows:

$$\gamma_{\vec{k}} = \frac{1}{d} \sum_{i=1}^{d} \cos k_i \,. \tag{3.5}$$

In case of a hypercube, the first Brillioun zone is a hypercube with 2^d corners located at each of these momenta $\{\pm\pi, \pm\pi, \ldots \pm \pi\}$, and has a volume of $(2\pi)^d$. In our work, we will be considering only nearest neighbor interaction and so we focus our discussion on $\gamma_{\vec{k}}$ only. This interaction structure factor has the following momentum summation properties when summed over all the momenta in the first Brillioun zone:

$$\frac{1}{N} \sum_{\vec{k}} \gamma^{2n+1}_{\vec{k}} \overset{N\to\infty}{\longrightarrow} \frac{1}{(2\pi)^d} \int_{-\pi}^{\pi} \ldots \int_{-\pi}^{\pi} d\vec{k} \gamma^{2n+1}_{\vec{k}} = 0 \,, \quad n \in \mathbb{Z} \,, \tag{3.6}$$

$$\frac{1}{N} \sum_{\vec{k}} \gamma^{2}_{\vec{k}} \overset{N\to\infty}{\longrightarrow} \frac{1}{(2\pi)^d} \int_{-\pi}^{\pi} \ldots \int_{-\pi}^{\pi} d\vec{k} \gamma^{2}_{\vec{k}} = \frac{1}{2d} \,, \tag{3.7}$$

$$\frac{1}{N} \sum_{\vec{k}} \gamma^{4}_{\vec{k}} \overset{N\to\infty}{\longrightarrow} \frac{1}{(2\pi)^d} \int_{-\pi}^{\pi} \ldots \int_{-\pi}^{\pi} d\vec{k} \gamma^{4}_{\vec{k}} = \frac{3}{4d^2} - \frac{3}{8d^3} \,, \tag{3.8}$$

$$\frac{1}{N} \sum_{\vec{k}} \gamma_{\vec{k}+\vec{k}'} \gamma_{\vec{k}+\vec{k}''} \overset{N\to\infty}{\longrightarrow} \frac{1}{(2\pi)^d} \int_{-\pi}^{\pi} \ldots \int_{-\pi}^{\pi} d\vec{k} \gamma_{\vec{k}+\vec{k}'} \gamma_{\vec{k}+\vec{k}''} = \frac{\gamma_{\vec{k}'+\vec{k}''}}{2d} \tag{3.9}$$

and so on, with $d\vec{k} \equiv dk_1 dk_2 \ldots dk_d$. We have also taken the thermodynamic limit by sending the number of lattice sites $N \to \infty$. These properties have important consequences. Consider an analytic function in $\gamma_{\vec{k}}$: $f(\gamma_{\vec{k}})$. This function has a Taylor expansion in $\gamma_{\vec{k}}$ which is an infinite series. Since $\gamma_{\vec{k}}$ itself is not a small parameter, we can not truncate this series at any arbitrary power in $\gamma_{\vec{k}}$. However due to the above momentum summation properties, we can Taylor expand $f(\gamma_{\vec{k}})$ *inside a momentum integral* to obtain a power series in $1/d$. We see that while the Taylor expansion of $f(\gamma_{\vec{k}})$ itself is not a controlled expansion, momentum integration of Taylor expansion of $f(\gamma_{\vec{k}})$ is a controlled expansion in $1/d$ in the limit of large-d. This means that in the large-d limit, we can safely truncate the Taylor series of $f(\gamma_{\vec{k}})$ inside the momentum integration, and obtain a series up to a particular order in $1/d$.

Another view point is to consider $\gamma_{\vec{k}}$ as a sum of random variables lying between -1 and 1. Thus $\gamma_{\vec{k}}$ has some probability distribution in finite dimension. However, by the central limit theorem [53, 54], in the limit $d \to \infty$, the probability distribution of $\gamma_{\vec{k}}$ will be a Gaussian distribution which is strongly peaked at $\gamma_{\vec{k}} = 0$. This means that for most $\vec{k}$ value of $\gamma_{\vec{k}}$ is zero. For a given $\vec{k}$ we can not assume $\gamma_{\vec{k}}$ to be small.

[5]Here on we will make statements about such lattices only.

But in the limit of large-d and inside a momentum integral, $\gamma_{\vec{k}}$ will take typical values around zero.

In the later chapters, above properties will play a central role in *generating* $1/d$ expansion for observables. We will be treating our problem perturbatively and will use diagrammatic perturbation theory. It will turn out that the vertex functions in the Hamiltonian will have a momentum dependence only through factors of $\gamma_{\vec{k}}$. Evaluation of diagrams would mean performing a momentum integral over some combination of vertex functions. In the light of above properties it is then clear that each diagram will result in an expansion in powers of $1/d$. We will see this aspect in detail in the next chapter.

We note that for any $\gamma_{\vec{k}}^n$ (3.4), there are similar properties as discussed above for $\gamma_{\vec{k}}$, which can be worked out easily. This also suggests the applicability of our large-d ideas to systems with geometric frustration, arising from competing further neighbor interactions.

3.4 Quantum criticality and the large-d limit

Taking the limit $d \to \infty$ involves subtleties in the context of quantum phase transition, and we discuss them in this section. In the last section, we generalized the square and the cubic lattices to a d-dimensional hypercubic lattice. We saw that in this case the number of nearest neighbors is given by $2d$. It means that in the limit of large-d, nearest neighbor interaction term in the Hamiltonian will always dominate. Consider the coupled-dimer Hamiltonian (2.2) introduced in the last chapter. Simply taking the limit $d \to \infty$ will result in the ordered phase, due to dominant inter-dimer term (which is the nearest neighbor term in this case). Hence there will be no quantum phase transition.

To ensure a non-trivial competition between the inter-dimer and the intra-dimer terms in the Hamiltonian, we must rescale our coupling constants with d. For this purpose, in case of our model (2.2) on the hypercubic lattice, we define the tuning parameter

$$q = \frac{Kd}{J} \tag{3.10}$$

such that it takes a finite value even in the limit $d \to \infty$. In other words, in the limit of large-d we must crank up the intra-dimer interaction appropriately, such that q is finite for any non-zero J, and there is a quantum phase transition. This is similar in spirit to rescaling of interaction constant in the case of the dynamical mean-field theory (DMFT) [53, 54]. After this proper rescaling we see that even in the limit of $d \to \infty$, for small q there is a quantum paramagnetic phase, while for large q we have a magnetically ordered phase. In the later chapters we will precisely determine the phase boundary between these phases in the $1/d$ formalism. In general, for other models and their large-d generalizations one needs to do similar rescaling between on-site interaction and nearest (or further) neighbor interaction[6]. For frustrated systems,

[6]This is also the reason why, systems where spontaneous dimerization happens are not considered. In such cases usually the inter-dimer and intra-dimer interaction is the same, which makes it difficult to introduce a suitable tuning parameter in the large-d limit.

we will have to rescale all the competing interactions appropriately to ensure phase transition.

For the case of coupled-dimers (and other models we are interested in), the quantum phase transition is continuous, as discussed earlier. Since we work in the limit of large-d, we are always above the upper critical dimension (for coupled-dimer magnets considered here, $d_c^+ = 3$). Consequently, we will always obtain mean-field critical exponents. However, we must point out that although the nature of the quantum phase transition itself is mean-field, our treatment of interaction terms in a $1/d$ expansion is perturbative, and goes beyond mean-field. Quantum critical points are also accompanied by singular behavior, whereas we have proposed an analytic expansion in $1/d$ across the quantum phase transition. At first sight it seems like a contradiction, but it turns out that if we look at the *correct* observables then analytic expansion in $1/d$, even at the critical point, is possible. We will see in the following that the mean-field nature of the quantum phase transition plays an important role in determining these correct observables.

3.5 Observables in the large-d limit

The central idea of this work is that $1/d$ is a suitable small parameter, using which we can write analytic expansion for observables. But as stated above, we have to choose the observables correctly so as to ensure that we can go from one phase to the other smoothly[7]. In this section we will discuss what we mean by an appropriate observable and how to identify it.

As we discussed in chapter 1, observables have a universal power-law behavior near the quantum critical point. These power-laws are typically not a simply polynomial (i.e. the power-law exponent need not be an integer). Hence, observables are non-analytic at the critical point. For instance, consider the quantum paramagnetic phase of the coupled-dimers on a hypercubic lattice, which is realized for $q < q_c$. The excitation energy gap varies as

$$\Delta \propto (q_c - q)^{\nu z} \tag{3.11}$$

where q is our tuning parameter, q_c is the quantum critical point, ν is correlation length critical exponent and z is the dynamical critical exponent. For Heisenberg spins above the upper critical dimension, the mean-field values of these exponents are $\nu = 1/2$ and $z = 1$. So clearly, $\Delta \propto \sqrt{q_c - q}$ is not analytic. However, Δ^2 being analytic, we can expect it to have an analytic $1/d$ expansion everywhere, including the critical point. Indeed we will see this in chapter 4 and chapter 5. However we must mention that above arguments do not mean that Δ can not admit analytic $1/d$ expansion at all. It has a well-defined $1/d$ expansion everywhere except the critical point. But since we want to analytically connect the two phases, we are interested in observables which remain analytic even at the critical point.

Now for the model of coupled-dimers on the hypercubic lattice, one can also look at the order parameter M_{st} (staggered magnetization) in the antiferromagnetic phase. In this case the mean-field critical exponent $\beta = 1/2$, and so $M_{st} \propto \sqrt{q - q_c}$. So, on

[7]It means that our expansion does not break down at the quantum critical point.

the lines of above argument M_{st}^2 will have an analytic $1/d$ expansion, and we will see in chapter 5 that this is indeed the case.

So we see that using the mean-field critical exponents we can identify the observables which will have an analytic expansion. Although most observables can be calculated perturbatively using $1/d$ as a small parameter, we know from previous discussions that some observables may be non-perturbative in nature. In our case, we find that the quasiparticle decay rate is non-perturbative in large-d formalism and hence does not admit an analytic $1/d$ expansion.

3.6 Dynamical mean-field theory (DMFT)

Our approach relies on taking the limit $d \to \infty$, and a natural question arises whether there is any connection to the DMFT. Dynamical mean-field theory is a mean-field theory, where fluctuations do not have any spatial dependence but are allowed to have a finite lifetime [53, 54]. Consequently the self-energy arising from the interactions is independent of momentum, but has a frequency dependence: $\Sigma_{int} \equiv \Sigma_{int}(\omega)$. Recall that in the Hartree-Fock mean-field theory, the self-energy due to interactions is just a constant. In the DMFT, the approximation that the self-energy is only frequency dependent becomes exact in the limit $d \to \infty$ [53]. However, in finite dimensions this is an approximation. In the $1/d$ expansion, we systematically calculate observables in powers of $1/d$, such that in the limit $d \to \infty$ we obtain exact local expectation values. The DMFT is a self-consistent method. Whereas, in our approach, we do not need self-consistency at any order in $1/d$. Application of the DMFT to spin systems is not trivial due to the residual entropy of $\ln 2$, in the Mott insulating phase. We note that one of the DMFT theories applied to the magnetically ordered phase *could not* obtain gapless modes [39], as otherwise required by the Goldstone's theorem for spontaneously broken continuous symmetry. On the other hand, we will see in chapter 5 that in our formalism we correctly obtain the gapless modes in the magnetically ordered phase to all orders in $1/d$.

Nevertheless, we must point out that the DMFT has been the most successful theory to study the metal-Mott insulator transition. In this case the Hubbard model is the relevant model, and the problem in the limit $d \to \infty$ is locally non-trivial due to an on-site interaction term. Typically this local problem is mapped onto some known impurity problem to obtain the large-d solution in a self-consistent way. However the coupled-dimer model (2.2) on the hypercubic lattice, and other spin systems that are amenable to $1/d$ expansion boils down to a problem of non-interacting Bosons in the large-d limit. So the local problem in the large-d limit in our case is simple, as opposed to that addressed by the DMFT.

3.7 Thermodynamic limit and finite systems

The hypercubic-lattice model with linear size L has $N = L^d$ dimer sites. While discussing the geometric properties of hypercubic lattice in relation to the interaction structure factor we first used the limit $N \to \infty$ and then the large-d limit. We said that we have taken the thermodynamic limit before. Actually, to be more precise the

thermodynamic limit corresponds to the limit $L \to \infty$. However, since our discussion above (as well as those in the following chapters) relies only on the limit $N \to \infty$, we could as well take the limit $d \to \infty$ at a finite L, provided that L is even, as eq. (3.6)-(3.9) and other identities are still valid.

3.8 Discussion

In this chapter we have discussed the aspects of the large-d limit. Although we have considered the model of coupled-dimer magnets on a hypercubic lattice, it is clear that the general ideas can be applied to other systems as well. In particular, we will see the application of these ideas to the transverse-field Ising model in chapter 7. As we have seen, the central idea of using $1/d$ as a small parameter stems from the momentum summation properties of the interaction structure factor. It is important to note that unlike many other cases, we do not have to worry about the UV or IR cutoff. All momentum summations can be performed analytically in the entire first Brillioun zone in the large-d limit. Now we are ready with the idea, and we will demonstrate the technique by performing concrete calculations for coupled-dimer magnets on a hypercubic lattice. We start with the quantum paramagnetic phase in chapter 4 and consider the antiferromagnetic phase in chapter 5.

Chapter 4

Quantum paramagnetic phase

In the previous chapter we discussed the large-d generalization of coupled-dimer magnets to the model of coupled-dimers on a hypercubic lattice. We argued that after appropriate rescaling of the interaction strengths, one can still have a quantum phase transition in arbitrarily large dimensions. In fact, the problem in large-d is essentially that of non-interacting Bosons, such that the *harmonic* approximation corresponds to the leading result in a systematic $1/d$ expansion. Based on the philosophy of large-d introduced in the previous chapter, we now present explicit calculations to obtain a systematic $1/d$ expansion for physical observables in the quantum paramagnetic (disordered) phase. The following discussion is largely based on ref. [55].

4.1 Model Hamiltonian

As pointed out earlier we shall be focusing on a model of coupled dimers on a hypercubic lattice in spatial dimension d with the Hamiltonian

$$\mathcal{H} = \sum_i J_i \vec{S}_{i1} \cdot \vec{S}_{i2} + \sum_{ii'mm'} K_{ii'}^{mm'} \vec{S}_{im} \cdot \vec{S}_{i'm'} \,, \tag{4.1}$$

where i, i' are sites on the lattice formed by dimers and index $m, m' = 1, 2$ refer to individual spins within the dimer. In what follows, we will consider isotropic nearest neighbor inter-dimer interactions, i.e. $K_{ii'}^{mm'} \equiv K^{mm'}$. Moreover, the nearest neighbor interaction between $\vec{S}_{i1}$ and $\vec{S}_{i2}$ is absent, meaning $K^{12} = K^{21} = 0$, but we allow K^{11} and K^{22} to be different (see fig.4.1). So we have

$$\mathcal{H} = J \sum_i \vec{S}_{i1} \cdot \vec{S}_{i2} + \sum_{\langle ii' \rangle} (K^{11} \vec{S}_{i1} \cdot \vec{S}_{i'1} + K^{22} \vec{S}_{i2} \cdot \vec{S}_{i'2}) \tag{4.2}$$

such that $\langle ii' \rangle$ refers to nearest neighbor sum on the dimer lattice. It is convenient to define the coupling constant K and the asymmetry parameter κ as follows:

$$K = \frac{K^{11} + K^{22}}{2} \,, \quad \kappa K = \frac{K^{11} - K^{22}}{2} \,. \tag{4.3}$$

The model considered in eq. (4.2) on hypercubic lattice corresponds to the widely studied two-leg ladder and the square-lattice bilayer magnets in $d = 1$ and 2 respectively.

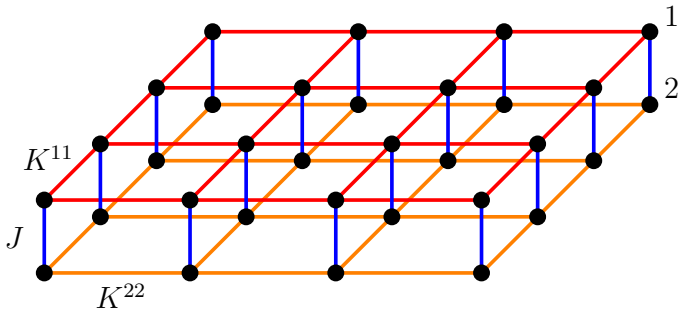

Figure 4.1: Coupled-dimer magnet corresponding to eq. (4.2) in $2d$.

In the case of hypercubic lattice in spatial dimension d, number of nearest neighbors is $2d$. So as discussed in the previous chapter, to ensure a non-trivial competition between the inter-dimer and intra-dimer coupling we must appropriately rescale our coupling constants. So

$$q = \frac{Kd}{J} \tag{4.4}$$

is a suitable tuning parameter such that even in the limit $d \to \infty$ we have a quantum phase transition at a finite value of q.

4.2 Reference state

To remind us again, in order to perform perturbation theory we need a suitable starting point or a reference state. As explained in the previous chapter we can use a product state ansatz as follows:

$$|\Psi_0\rangle = \prod_i |\Psi\rangle_i \,. \tag{4.5}$$

A good choice of $|\Psi\rangle_i$ is dictated by minimizing $\langle\Psi_0|\mathcal{H}|\Psi_0\rangle$. In the quantum paramagnetic phase we obtain

$$|\Psi\rangle_i = \frac{1}{\sqrt{2}}[|\uparrow\downarrow\rangle_i - |\downarrow\uparrow\rangle_i] \,. \tag{4.6}$$

4.3 Bond operators and projection

As explained in chapter 2, bond-operator theory employs a slave-particle description of the states of each dimer. Recall that we defined Bosonic operators $t^\dagger_{i\alpha}$ $(\alpha = 1, 2, 3)$ to treat spin-1 triplet excitations, $|t_\alpha\rangle$ $(\alpha = 1, 2, 3)$ over the spin-0 singlet state $|t_0\rangle$.

For convenience we quote them here again:

$$|t_0\rangle = \frac{1}{\sqrt{2}}[|\uparrow\downarrow\rangle - |\downarrow\uparrow\rangle]\,, \tag{4.7}$$

$$t_1^\dagger|t_0\rangle = |t_1\rangle = -\frac{1}{\sqrt{2}}[|\uparrow\uparrow\rangle - |\downarrow\downarrow\rangle]\,, \tag{4.8}$$

$$t_2^\dagger|t_0\rangle = |t_2\rangle = \frac{\imath}{\sqrt{2}}[|\uparrow\uparrow\rangle + |\downarrow\downarrow\rangle]\,, \tag{4.9}$$

$$t_3^\dagger|t_0\rangle = |t_3\rangle = \frac{1}{\sqrt{2}}[|\uparrow\downarrow\rangle + |\downarrow\uparrow\rangle]\,. \tag{4.10}$$

In terms of this notation our reference state is

$$|\Psi_0\rangle = \prod_i |t_0\rangle_i\,. \tag{4.11}$$

Recall that we have to deal with the hard-core constraint for Bosons

$$\sum_{\alpha=1}^{3} t_{i\alpha}^\dagger t_{i\alpha} \leq 1\,, \tag{4.12}$$

to restrict ourselves to the physical part of the Hilbert space. In chapter 2, we discussed ways to deal with this, and argued that we shall implement it using the projection operator introduced by Collins *et al.* [42]. We saw that using this we can express the spin operators in the following way:

$$S_{i1,2}^\alpha = \frac{1}{2}\left(\pm t_{i\alpha}^\dagger P_i \pm P_i t_{i\alpha} - \imath\epsilon_{\alpha\beta\gamma} t_{i\beta}^\dagger t_{i\gamma}\right) \tag{4.13}$$

where P_i prevents the creation of more than one triplet excitation on site i and is defined as

$$P_i = 1 - \sum_\gamma t_{i\gamma}^\dagger t_{i\gamma}. \tag{4.14}$$

As noted before, $\vec{S}_{im}$ (4.13) obeys the standard spin commutation relations within the physical Hilbert space.

4.4 Hamiltonian and perturbation theory

In this section, we will discuss in detail how to *generate* the perturbative expansion in $1/d$, for the coupled-dimer magnets on a hypercubic lattice. We will start with the triplon Hamiltonian in real-space and then discuss in detail how to set-up the perturbation theory.

4.4.1 Real-space bond-operator Hamiltonian

Let us now express our spin Hamiltonian in eq. (4.2) in terms of triplons. Using the relation in eq. (4.13) we get

$$\begin{aligned}\mathcal{H} = J\sum_{i\alpha}\left(t^\dagger_{i\alpha}t_{i\alpha} - \frac{3}{4}\right) + \frac{K}{2}\sum_{\langle ii'\rangle\alpha}\left(t^\dagger_{i\alpha}P_iP_{i'}t_{i'\alpha} + t^\dagger_{i\alpha}P_it^\dagger_{i'\alpha}P_{i'} + h.c.\right)\\ - \frac{\kappa K}{2}\sum_{\langle ii'\rangle\alpha\beta\gamma}\epsilon_{\alpha\beta\gamma}\left[\left(\imath t^\dagger_{i\alpha}P_it^\dagger_{i'\beta}t_{i'\gamma} + h.c.\right) + (i\leftrightarrow i')\right]\\ + \frac{K}{2}\sum_{\langle ii'\rangle\alpha\beta}\left(t^\dagger_{i\alpha}t^\dagger_{i'\beta}t_{i\beta}t_{i'\alpha} - t^\dagger_{i\alpha}t^\dagger_{i'\alpha}t_{i\beta}t_{i'\beta}\right)\,. \end{aligned} \tag{4.15}$$

Inserting the explicit expression for the projection operator (4.14) in the above equation, we obtain the Hamiltonian for interacting Bosons with upto 6th order terms in triplon operator,

$$\mathcal{H} = \mathcal{H}_0 + \mathcal{H}_2 + \mathcal{H}_3 + \mathcal{H}_4 + \mathcal{H}_5 + \mathcal{H}_6\,. \tag{4.16}$$

Here, $\mathcal{H}_n$ contains n triplon operators. $\mathcal{H}_0 = -\frac{3}{4}JN$ is the energy of the product state $|\psi_0\rangle$, with N being the number of dimer sites. The remaining even-n terms read:

$$\mathcal{H}_2 = J\sum_{i,\alpha}t^\dagger_{i\alpha}t_{i\alpha} + \frac{K}{2}\sum_{\langle ii'\rangle\alpha}\left(t^\dagger_{i\alpha}t_{i'\alpha} + t^\dagger_{i\alpha}t^\dagger_{i'\alpha} + h.c.\right)\,, \tag{4.17}$$

$$\begin{aligned}\mathcal{H}_4 = \frac{K}{2}\sum_{\langle ii'\rangle\alpha\beta}\left(t^\dagger_{i\alpha}t^\dagger_{i'\beta}t_{i\beta}t_{i'\alpha} - t^\dagger_{i\alpha}t^\dagger_{i'\alpha}t_{i\beta}t_{i'\beta}\right)\\ - \frac{K}{2}\sum_{\langle ii'\rangle\alpha\beta}\left(t^\dagger_{i\alpha}t^\dagger_{i\beta}t_{i\beta}t_{i'\alpha} + t^\dagger_{i\alpha}t^\dagger_{i'\beta}t_{i'\beta}t_{i'\alpha} + t^\dagger_{i\alpha}t^\dagger_{i'\alpha}t^\dagger_{i\beta}t_{i\beta} + t^\dagger_{i\alpha}t^\dagger_{i'\alpha}t^\dagger_{i'\beta}t_{i'\beta} + h.c.\right)\,,\end{aligned} \tag{4.18}$$

and

$$\mathcal{H}_6 = \frac{K}{2}\sum_{\langle ii'\rangle}\sum_{\alpha,\beta,\gamma}\left(t^\dagger_{i\alpha}t^\dagger_{i\beta}t^\dagger_{i'\alpha}t^\dagger_{i'\gamma}t_{i\beta}t_{i'\gamma} + t^\dagger_{i\alpha}t^\dagger_{i\beta}t^\dagger_{i'\gamma}t_{i\beta}t_{i'\gamma}t_{i'\alpha} + h.c.\right)\,. \tag{4.19}$$

For asymmetric couplings, $K^{11} \neq K^{22}$, we also have odd-n terms in addition:

$$\mathcal{H}_3 = -\frac{\kappa K}{2}\sum_{\langle ii'\rangle}\sum_{\alpha\beta\gamma}\epsilon_{\alpha\beta\gamma}\left[\left(\imath t^\dagger_{i\alpha}t^\dagger_{i'\beta}t_{i'\gamma} + h.c.\right) + (i\leftrightarrow i')\right] \tag{4.20}$$

and

$$\mathcal{H}_5 = \frac{\kappa K}{2}\sum_{\langle ii'\rangle}\sum_{\alpha\beta\gamma\kappa}\epsilon_{\alpha\beta\gamma}\left[\left(\imath t^\dagger_{i\alpha}t^\dagger_{i\kappa}t^\dagger_{i'\beta}t_{i'\gamma}t_{i\kappa} + h.c.\right) + (i\leftrightarrow i')\right]\,. \tag{4.21}$$

In the context of two-particle decay of triplons, the cubic terms play an important role and have been discussed previously in ref. [56, 57].

4.4.2 Harmonic approximation

Let us first focus on the bilinear part (4.17) of the Hamiltonian. This represents non-interacting Bosons and can be solved exactly. Often in the literature, this is referred to as the *harmonic* approximation. As a first step to solve $\mathcal{H}_2$, using the lattice translation symmetry, we will go to Fourier space by introducing

$$t_{i\alpha} = \frac{1}{\sqrt{N}} \sum_{\vec{k}} t_{\vec{k}\alpha} e^{-\imath \vec{k}\cdot\vec{r}_i} \tag{4.22}$$

where $\vec{k}$ is the crystal momentum in the first Brillioun zone. It is easy to see that the Fourier transformed triplon operators satisfy the usual Bosonic commutation relations

$$\left[t_{\vec{k}\alpha}, t^\dagger_{\vec{k}'\beta}\right] = \delta_{\vec{k},\vec{k}'}\delta_{\alpha,\beta}\,;\ \left[t_{\vec{k}\alpha}, t_{\vec{k}'\beta}\right] = \left[t^\dagger_{\vec{k}\alpha}, t^\dagger_{\vec{k}'\beta}\right] = 0\,. \tag{4.23}$$

Using the above transformation and orthogonality relations in the Fourier space, we obtain the following expression for the Hamiltonian:

$$\mathcal{H}_2 = \sum_{\vec{k}\alpha} \left[A_{\vec{k}} t^\dagger_{\vec{k}\alpha} t_{\vec{k}\alpha} + \frac{B_{\vec{k}}}{2}(t^\dagger_{\vec{k}\alpha} t^\dagger_{-\vec{k}\alpha} + h.c.) \right]. \tag{4.24}$$

In the above equation we have introduced

$$A_{\vec{k}} = J + B_{\vec{k}}\,,\ B_{\vec{k}} = qJ\gamma_{\vec{k}} \tag{4.25}$$

and the interaction structure factor, introduced in chapter 3,

$$\gamma_{\vec{k}} = \frac{1}{d}\sum_{n=1}^{d} \cos k_n \tag{4.26}$$

which is normalized such that $-1 \leq \gamma_{\vec{k}} \leq 1$.

The bilinear Hamiltonian (4.24) is not diagonal in the basis of triplons because it contains anomalous terms. For brevity let us express eq. (4.24) in the following way:

$$\mathcal{H}_2 = \frac{1}{2}\sum_{\vec{k}\alpha} \left[T^\dagger_{\vec{k}\alpha} h_{2\vec{k}} T_{\vec{k}\alpha} - A_{\vec{k}} \right] \tag{4.27}$$

where

$$T_{\vec{k}\alpha} = \left[\ t_{\vec{k}} \quad t^\dagger_{-\vec{k}}\ \right]^T, \tag{4.28}$$

$$h_{2\vec{k}} = \begin{pmatrix} A_{\vec{k}} & B_{\vec{k}} \\ B_{\vec{k}} & A_{\vec{k}} \end{pmatrix}. \tag{4.29}$$

So to solve $\mathcal{H}_2$ we need to diagonalize $h_{2\vec{k}}$. This is a subtle issue. If one diagonalizes the Hermitian matrix $h_{2\vec{k}}$, then in the diagonal basis one does not obtain Bosonic quasiparticles. To preserve the Bosonic description, instead one needs to diagonalize the non-Hermitian matrix[1]

$$\tilde{h}_{2\vec{k}} = \Sigma h_{2\vec{k}} \tag{4.30}$$

[1]For a detailed discussion on this aspect we refer to ref. [58] and [59]. A numerical application of this procedure to systems with disorder can be found in ref. [60].

where

$$\Sigma = \begin{pmatrix} 1 & 0 \\ 0 & -1 \end{pmatrix}. \tag{4.31}$$

This procedure leads to Bogoliubov transformation for Bosons,

$$t_{\vec{k}\alpha} = u_{\vec{k}}\tau_{\vec{k}\alpha} + v_{\vec{k}}\tau^{\dagger}_{-\vec{k}\alpha} \tag{4.32}$$

with the property

$$u^2_{\vec{k}} - v^2_{\vec{k}} = 1\,. \tag{4.33}$$

Note that for Fermions $u^2_{\vec{k}} + v^2_{\vec{k}} = 1$ and this is what one obtains if we diagonalize simply $h_{2\vec{k}}$ instead. However now using eq. (4.32) with the property (4.33), we see that τ-particles obeys the correct Bosonic commutation relations

$$\left[\tau_{\vec{k}\alpha}, \tau^{\dagger}_{\vec{k}'\beta}\right] = \delta_{\vec{k},\vec{k}'}\delta_{\alpha,\beta}\,;\ \left[\tau_{\vec{k}\alpha}, \tau_{\vec{k}'\beta}\right] = \left[\tau^{\dagger}_{\vec{k}\alpha}, \tau^{\dagger}_{\vec{k}'\beta}\right] = 0\,. \tag{4.34}$$

Now using the Bogoliubov transformation (4.32), $\mathcal{H}_2$ is transformed into a diagonal form

$$\mathcal{H}_2 = \sum_{\vec{k}\alpha} \omega_{\vec{k}}\tau^{\dagger}_{\vec{k}\alpha}\tau_{\vec{k}\alpha} + \frac{3}{2}\sum_{\vec{k}}(\omega_{\vec{k}} - A_{\vec{k}}) \tag{4.35}$$

with the mode energy given by

$$\omega_{\vec{k}} = \sqrt{A^2_{\vec{k}} - B^2_{\vec{k}}} = J\sqrt{1 + 2\gamma_{\vec{k}}q}\,. \tag{4.36}$$

We see that the triplon dispersion is minimum when $\gamma_{\vec{k}} = -1$, which corresponds to $\vec{k} = \vec{Q} \equiv \{\pi, \pi, \ldots\}$. Thus at the harmonic level, the triplon excitation energy gap is given by

$$\Delta = \omega_{\vec{Q}} = J\sqrt{1 - 2q}\,. \tag{4.37}$$

Physically, Δ is the minimum amount of energy required to create a single triplon excitation. The gap decreases upon increasing q and goes to zero when $q = q_c = 1/2$. For $q > q_c$ the gap becomes an imaginary quantity which essentially means that the phase ceases to exist. Hence at the harmonic level $q_c = 1/2$ is the quantum critical point. At this level, for $q > 1/2$ we have a magnetically ordered phase which will be discussed in detail in the next chapter. We shall see later that the interaction terms add corrections to the harmonic level expression of the triplon dispersion. These corrections will be shown to be positive due to the repulsive nature of the interactions, thereby shifting the quantum critical point to a value $q_c > 1/2$.

Lastly, we quote here the expressions for the Bogoliubov coefficients in terms of $A_{\vec{k}}$ and $B_{\vec{k}}$:

$$u^2_{\vec{k}}, v^2_{\vec{k}} = \pm\frac{1}{2} + \frac{A_{\vec{k}}}{2\omega_{\vec{k}}}\,,\quad u_{\vec{k}}v_{\vec{k}} = -\frac{B_{\vec{k}}}{2\omega_{\vec{k}}}. \tag{4.38}$$

4.4.3 Expectation values of local observables

The physics of the bilinear Hamiltonian $\mathcal{H}_2$ can be already used to motivate the usage of $1/d$ as a small parameter. The anomalous piece in the eq. (4.24) creates a pair of triplets at the momenta $\pm\vec{k}$. This is similar to the scenario in the case of BCS

superconductivity, where a Cooper pair consisting of two electrons with opposite spins is created at the momenta $\pm\vec{k}$ near the Fermi momentum. Therefore, the wavefunction in the harmonic approximation takes a form similar to that of the BCS wavefunction, and can be written as

$$|\psi\rangle \propto \exp\left(\sum_{\vec{k}\alpha} \frac{v_{\vec{k}}}{u_{\vec{k}}}\, t^{\dagger}_{\vec{k}\alpha}\, t^{\dagger}_{-\vec{k}\alpha}\right)|\psi_0\rangle\,. \tag{4.39}$$

The *local* triplet density in the harmonic approximation is

$$\langle\psi|t^{\dagger}_{i\gamma}t_{i\gamma}|\psi\rangle = \frac{1}{N}\sum_{\vec{k}} v^2_{\vec{k}} \overset{d\to\infty}{=} \frac{q^2}{8d}\,, \tag{4.40}$$

see Appendix C.1. Similarly, expectation values like $\langle t_{i\gamma}t_{j\gamma}\rangle$, with i, j being neighboring sites, vanish as $d \to \infty$. This implies, as mentioned in chapter 3, that the product state $|\psi_0\rangle$ yields exact ground-state expectation values in the limit $d \to \infty$. All corrections can be then systematically evaluated in a power series in $1/d$ as will be shown in the following. We caution again that the above statements do not mean that the product-state considered above is the exact ground state of the paramagnetic phase.

4.4.4 Normal-ordered Hamiltonian

In this section, we will discuss the strategy to go beyond the harmonic approximation. To achieve this objective we have to resort to diagrammatic perturbation theory. As pointed out several times earlier, a priori there is no small parameter controlling the perturbation theory. However we will show that once we start evaluating diagrams for required observables, perturbative corrections can be arranged in a systematic $1/d$ expansion. In order to carry out the diagrammatic treatment, we first need to normal-order the Hamiltonian in the basis which diagonalizes the non-interacting piece. In this case the non-interacting piece is $\mathcal{H}_2$ (4.24) and we have seen that it is diagonal in τ basis. It is easy to see that normal ordering with respect to τ operators will generate additional bilinear terms coming from $\mathcal{H}_4$ and $\mathcal{H}_6$. This opens up two possibilities namely; (i) Leading order Bogoliubov transformation: treat only $\mathcal{H}_2$ as non-interacting piece and all other contributions including the additional bilinear terms as perturbation; (ii) Global Bogoliubov transformation: perform another Bogoliubov transformation so as to diagonalize all the bilinear terms upto a given order. It is clear that the option (ii) will lead to a self-consistent equation for the Bogoliubov coefficients. Though it is technically possible to handle (ii), we find the option (i) more convenient. Appraoch (ii) will require a $1/d$ expansion of $\omega_{\vec{k}}$, which is ill-defined at the critical point for reasons discussed in chapter 3, and so we will stick with approach (i). Thus using the leading-order Bogoliubov transformation according to eqs. (4.32), (4.38), and (4.25), we generate a normal-ordered Hamiltonian in terms of the $\tau_{\vec{k}\alpha}$. The normal-ordered Hamiltonian takes the form

$$\mathcal{H} = \mathcal{H}'_0 + \mathcal{H}'_2 + \mathcal{H}'_3 + \mathcal{H}'_4 + \mathcal{H}'_5 + \mathcal{H}'_6 \tag{4.41}$$

where the $\mathcal{H}'_n$ contains n transformed τ operators and can be obtained after a few tedious but easy steps of algebra. In the following discussion we will need terms only

up to 4th order in t operators to obtain all the corrections to order $1/d$ to the mode dispersion, and all corrections to order $1/d^2$ to the ground state energy.

We can use the explicit form of $A_{\vec{k}}$ and $B_{\vec{k}}$ in eq. (4.25) to obtain the constant term. Additionally note that we have $u_{\vec{k}} = u^*_{\vec{k}} = u_{-\vec{k}}$ and $v_{\vec{k}} = v^*_{\vec{k}} = v_{-\vec{k}}$. Thus we have

$$\mathcal{H}'_0 = 3JN\Big[-\frac{1}{4} + R_2 + q(R_3+R_4) - 2q(R_1+4R_2)(R_3+R_4) \\ - \frac{q}{N}\big[\sum_{\vec{k}} u_{\vec{k}}v_{\vec{k}}R'_3(\vec{k}) - \sum_{\vec{k}} v^2_{\vec{k}}R'_4(\vec{k})\big]\Big] \tag{4.42}$$

which involves the abbreviations

$$R_1 = \frac{1}{N}\sum_{\vec{k}} u_{\vec{k}}v_{\vec{k}}\,, \qquad R_2 = \frac{1}{N}\sum_{\vec{k}} v^2_{\vec{k}} \\ R_3 = \frac{1}{N}\sum_{\vec{k}} \gamma_{\vec{k}}u_{\vec{k}}v_{\vec{k}}\,, \quad R_4 = \frac{1}{N}\sum_{\vec{k}} \gamma_{\vec{k}}v^2_{\vec{k}} \tag{4.43}$$

and

$$R'_3(\vec{k'}) = \frac{1}{N}\sum_{\vec{k}} \gamma_{\vec{k'}-\vec{k}}u_{\vec{k}}v_{\vec{k}}\,, \quad R'_4(\vec{k'}) = \frac{1}{N}\sum_{\vec{k}} \gamma_{\vec{k'}-\vec{k}}v^2_{\vec{k}}. \tag{4.44}$$

Note that using the summation properties of $\gamma_{\vec{k}}$ (discussed in chapter 3) we see that the $R_{1\ldots4}$ are suppressed in the large-d limit at least as $1/d$ (see appendix C.1).

As argued earlier, normal ordering of $\mathcal{H}_4$ in terms of τ operators will generate additional bilinear terms apart from the one appearing in (4.35) at harmonic level. Thus the bilinear part in terms of τ can be written as $\mathcal{H}'_2 = \mathcal{H}'_{2a} + \mathcal{H}'_{2b}$ where

$$\mathcal{H}'_{2a} = \sum_{\vec{k}\alpha} \omega_{\vec{k}}\tau^\dagger_{\vec{k}\alpha}\tau_{\vec{k}\alpha} \tag{4.45}$$

is the leading-order piece from $\mathcal{H}_2$, and

$$\mathcal{H}'_{2b} = \sum_{\vec{k}\alpha}\left[C_{\vec{k}}\tau^\dagger_{\vec{k}\alpha}\tau_{\vec{k}\alpha} + \frac{D_{\vec{k}}}{2}(\tau^\dagger_{\vec{k}\alpha}\tau^\dagger_{-\vec{k}\alpha} + h.c.)\right] \tag{4.46}$$

contains the bilinear terms generated from normal-ordering of $\mathcal{H}_4$, with

$$C_{\vec{k}} = qJ\big[2(u^2_{\vec{k}}+v^2_{\vec{k}})R'_4 - 4u_{\vec{k}}v_{\vec{k}}R'_3 - (2\gamma_{\vec{k}}R_1 + 8\gamma_{\vec{k}}R_2)(u_{\vec{k}}+v_{\vec{k}})^2 \\ -4(R_3+R_4)(2u^2_{\vec{k}}+2v^2_{\vec{k}}+u_{\vec{k}}v_{\vec{k}})\big]\,, \tag{4.47}$$

$$D_{\vec{k}} = qJ\big[4u_{\vec{k}}v_{\vec{k}}R'_4 - 2(u^2_{\vec{k}}+v^2_{\vec{k}})R'_3 - (2\gamma_{\vec{k}}R_1 + 8\gamma_{\vec{k}}R_2)(u_{\vec{k}}+v_{\vec{k}})^2 \\ -2(R_3+R_4)(u^2_{\vec{k}}+v^2_{\vec{k}}+8u_{\vec{k}}v_{\vec{k}})\big]\,. \tag{4.48}$$

It is important to note here that all terms in both $C_{\vec{k}}$ and $D_{\vec{k}}$ are of order $1/d$ or smaller owing to the large-d limit behavior of $R_{1\ldots4}$ discussed earlier. Consequently the contribution of $\mathcal{H}'_{2b}$ is suppressed relative to $\mathcal{H}'_{2a}$ in the large-d limit. In the following

sections we will see that in fact perturbative corrections from all the interaction terms are suppressed in increasing powers of $1/d$ in the this limit.

Next we consider the quartic term which reads as

$$\begin{aligned}\mathcal{H}_4' = \frac{1}{N}\sum_{1234}\big[&\delta_{1+2+3+4}\Phi_{41}(\tau_{1\alpha}^\dagger\tau_{2\alpha}^\dagger\tau_{3\beta}^\dagger\tau_{4\beta}^\dagger + \tau_{1\alpha}\tau_{2\alpha}\tau_{3\beta}\tau_{4\beta}) \\ &+ \delta_{1+2-3-4}(\Phi_{42}\tau_{1\alpha}^\dagger\tau_{2\alpha}^\dagger\tau_{3\beta}\tau_{4\beta} + \Phi_{43}\tau_{1\alpha}^\dagger\tau_{2\beta}^\dagger\tau_{3\alpha}\tau_{4\beta}) \\ &+ \delta_{1+2+3-4}\Phi_{44}(\tau_{1\alpha}^\dagger\tau_{2\alpha}^\dagger\tau_{3\beta}^\dagger\tau_{4\beta} + \tau_{4\beta}^\dagger\tau_{3\beta}\tau_{2\alpha}\tau_{1\alpha})\big]\end{aligned} \tag{4.49}$$

where the momenta have been abbreviated according to $\vec{k}_1 \equiv 1$ etc., and the vertex functions $\Phi_{41}\ldots\Phi_{44}$ are given in Appendix C.2. As a quick cross check of the terms in the Hamiltonian, we note that for $d = 2$ our expressions (4.42)–(4.49) agree with those given in ref. [61].

In the asymmetric case, $\kappa \neq 0$, the cubic term is also present and relevant for order $1/d$ calculation. It reads:

$$\begin{aligned}\mathcal{H}_3' = \frac{1}{\sqrt{N}}\sum_{123}\epsilon_{\alpha\beta\gamma}\big[&\delta_{1+2+3}\Phi_{31}(\tau_{1\alpha}^\dagger\tau_{2\beta}^\dagger\tau_{3\gamma}^\dagger - \tau_{1\alpha}\tau_{2\beta}\tau_{3\gamma}) \qquad (4.50)\\ &+\delta_{1+2-3}\Phi_{32}(\tau_{1\alpha}^\dagger\tau_{2\beta}^\dagger\tau_{3\gamma} - \tau_{3\gamma}^\dagger\tau_{2\beta}\tau_{1\alpha}) \\ &+\delta_{2+3-1}\Phi_{33}(\tau_{3\gamma}^\dagger\tau_{2\beta}^\dagger\tau_{1\alpha} - \tau_{1\alpha}^\dagger\tau_{2\beta}\tau_{3\gamma}) \qquad (4.51)\\ &+\delta_{1-2+3}\Phi_{34}(\tau_{1\alpha}^\dagger\tau_{3\gamma}^\dagger\tau_{2\beta} - \tau_{2\beta}^\dagger\tau_{3\gamma}\tau_{1\alpha})\big]\,,\end{aligned}$$

with its vertex functions $\Phi_{31}\ldots\Phi_{34}$ listed in appendix C.2.

4.4.5 Evaluation of diagrams in the large-d limit

As shown in the last section, in the large-d limit, the $1/d$ suppression of expectation values at harmonic level, and the structure of normal-ordered terms hints towards the usefulness of $1/d$ as a small parameter. In this case, the calculation of observables involves diagrammatic perturbation theory, due to the presence of interaction terms. To clearly demonstrate our procedure of *generating* a systematic $1/d$ expansion, we consider here a sample diagram and evaluate the self energy in the large-d limit.

Let us consider a sample self-energy diagram involving two cubic vertices, with the full structure of the cubic Hamiltonian piece given in eq. (4.50). To be precise, we focus on a normal self-energy diagram involving two Φ_{31} vertices, which furthermore have τ_x as external legs with frequency ω and momentum $\vec{k}$, fig. 4.2. Its explicit expression reads:

$$\begin{aligned}\Sigma_\Gamma = \frac{i}{2\pi}\int d\omega_1 d\omega_2 \frac{1}{N}\sum_{\vec{k}_1\vec{k}_2}\Gamma(\vec{k},\vec{k}_1,\vec{k}_2)\mathcal{G}_{0N}(\vec{k}_1,\omega_1) \\ \times\,\mathcal{G}_{0N}(\vec{k}_2,\omega_2)\delta(\omega+\omega_1+\omega_2)\delta_{\vec{k}+\vec{k}_1+\vec{k}_2}\end{aligned} \tag{4.52}$$

where $\mathcal{G}_{0N}$ is the normal τ Green's function for the unperturbed Hamiltonian,

$$\mathcal{G}_{0N}(\vec{k},\omega) = \frac{1}{\omega-\omega_k} \tag{4.53}$$

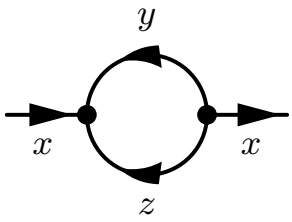

Figure 4.2: Sample self-energy diagram with two cubic Φ_{31} vertices. The external momentum and frequency are $\vec{k}$ and ω respectively. This figure is taken from ref. [55].

and $\Gamma(\vec{k},\vec{k}_1,\vec{k}_2)$ represents product of vertex functions and respective permutations of the legs of the cubic vertex corresponding to this diagram ($\vec{k}_y \equiv \vec{k}_1$, $\vec{k}_z \equiv \vec{k}_2, \omega_{\vec{k}_y} \equiv \omega_1, \omega_{\vec{k}_z} \equiv \omega_2$).

More precisely,

$$\Gamma(\vec{k},\vec{k}_1,\vec{k}_2) = \Gamma_1(\vec{k},\vec{k}_1,\vec{k}_2) + \Gamma_2(\vec{k},\vec{k}_1,\vec{k}_2) + \Gamma_3(\vec{k},\vec{k}_1,\vec{k}_2) \tag{4.54}$$

with

$$\begin{aligned}
\Gamma_1(\vec{k},\vec{k}_1,\vec{k}_2) =& 2\Big[\Phi_{31}(\vec{k}\vec{k}_1\vec{k}_2)\Phi_{31}(\vec{k}\vec{k}_1\vec{k}_2) - \Phi_{31}(\vec{k}\vec{k}_1\vec{k}_2)\Phi_{31}(\vec{k}\vec{k}_2\vec{k}_1) \\
&+ \Phi_{31}(\vec{k}\vec{k}_1\vec{k}_2)\Phi_{31}(\vec{k}_2\vec{k}\vec{k}_1) - \Phi_{31}(\vec{k}\vec{k}_1\vec{k}_2)\Phi_{31}(\vec{k}_1\vec{k}\vec{k}_2) \\
&+\Phi_{31}(\vec{k}\vec{k}_1\vec{k}_2)\Phi_{31}(\vec{k}_1\vec{k}_2\vec{k}) - \Phi_{31}(\vec{k}\vec{k}_1\vec{k}_2)\Phi_{31}(\vec{k}_2\vec{k}_1\vec{k})\Big], \qquad (4.55)\\
\Gamma_2(\vec{k},\vec{k}_1,\vec{k}_2) =& 2\Big[\Phi_{31}(\vec{k}_2\vec{k}\vec{k}_1)\Phi_{31}(\vec{k}\vec{k}_1\vec{k}_2) - \Phi_{31}(\vec{k}_2\vec{k}\vec{k}_1)\Phi_{31}(\vec{k}\vec{k}_2\vec{k}_1) \\
&+ \Phi_{31}(\vec{k}_2\vec{k}\vec{k}_1)\Phi_{31}(\vec{k}_2\vec{k}\vec{k}_1) - \Phi_{31}(\vec{k}_2\vec{k}\vec{k}_1)\Phi_{31}(\vec{k}_1\vec{k}\vec{k}_2) \\
&+\Phi_{31}(\vec{k}_2\vec{k}\vec{k}_1)\Phi_{31}(\vec{k}_1\vec{k}_2\vec{k}) - \Phi_{31}(\vec{k}_2\vec{k}\vec{k}_1)\Phi_{31}(\vec{k}_2\vec{k}_1\vec{k})\Big], \qquad (4.56)\\
\Gamma_3(\vec{k},\vec{k}_1,\vec{k}_2) =& 2\Big[\Phi_{31}(\vec{k}_1\vec{k}_2\vec{k})\Phi_{31}(\vec{k}\vec{k}_1\vec{k}_2) - \Phi_{31}(\vec{k}_1\vec{k}_2\vec{k})\Phi_{31}(\vec{k}\vec{k}_2\vec{k}_1) \\
&+ \Phi_{31}(\vec{k}_1\vec{k}_2\vec{k})\Phi_{31}(\vec{k}_2\vec{k}\vec{k}_1) - \Phi_{31}(\vec{k}_1\vec{k}_2\vec{k})\Phi_{31}(\vec{k}_1\vec{k}\vec{k}_2) \\
&+\Phi_{31}(\vec{k}_1\vec{k}_2\vec{k})\Phi_{31}(\vec{k}_1\vec{k}_2\vec{k}) - \Phi_{31}(\vec{k}_1\vec{k}_2\vec{k})\Phi_{31}(\vec{k}_2\vec{k}_1\vec{k})\Big]. \qquad (4.57)
\end{aligned}$$

The factors of 2 arise from permutations that yield identical contributions as the ones that appear above, e.g., $\Phi_{31}(\vec{k}\vec{k}_2\vec{k}_1)\Phi_{31}(\vec{k}\vec{k}_2\vec{k}_1)\hat{=}\Phi_{31}(\vec{k}\vec{k}_1\vec{k}_2)\Phi_{31}(\vec{k}\vec{k}_1\vec{k}_2)$.

For the purpose of illustration we will now show the explicit calculation using Γ_1 as the vertex function. We first perform the frequency integral in (4.52) which yields

$$\Sigma_{\Gamma_1} = \frac{1}{N}\sum_{\vec{k}_1\vec{k}_2} \frac{\Gamma_1(\vec{k},\vec{k}_1,\vec{k}_2)}{-\omega-\omega_1-\omega_2}\,\delta_{\vec{k}+\vec{k}_1+\vec{k}_2}\,. \tag{4.58}$$

The remaining momentum integration is the backbone of the $1/d$ expansion. We recall that momentum sums of powers of $\gamma_{\vec{k}}$ scale as powers of $1/d$, see equations (3.6)–(3.9). In particular, a momentum sum of $\gamma_{\vec{k}}^{2n+1}$ is zero and that of $\gamma_{\vec{k}}^{2n}$ scales as $1/d^n$ (plus possible higher-order terms). As a consequence, as discussed in detail in chapter 3, any analytic function $f(\gamma_{\vec{k}})$ can be Taylor-expanded in $\gamma_{\vec{k}}$ under a momentum integral.

This will generate an expansion in $1/d$ *after* the momentum integration. Recall that our small parameter is $1/d$ and not $\gamma_{\vec{k}}$.

The actual calculation requires the $\gamma_{\vec{k}}$ expansions of the mode energy and the Bogoliubov coefficients, eq. (C.1), as input. As we restrict our attention to order $1/d$ of the self-energy, we can approximate $u_{\vec{k}}^2 \approx 1$ and $\omega_{\vec{k}} \approx J$, since Γ_1 involves factors of $\gamma_{\vec{k}}$ and $v_{\vec{k}}$ which will generate at least one factor of $1/d$. Obtaining higher orders is straightforward, but tedious, and requires the inclusion of higher orders for $u_{\vec{k}}^2$ and $\omega_{\vec{k}}$. Hence, to order $1/d$ eq. (4.58) reduces to

$$\Sigma_{\Gamma_1} = -\frac{1}{\omega + 2J}\frac{1}{N}\sum_{\vec{k}_1}\Gamma_1(\vec{k},\vec{k}_1,-\vec{k}_1-\vec{k})\,. \tag{4.59}$$

Here we now need to collect only those terms which are $\mathcal{O}(\gamma_{\vec{k}}^2)$, as $\sum\gamma_{\vec{k}}^2 \propto 1/d$. For instance, we need terms like $u_{\vec{k}}^2 u_{\vec{k}_1}^2 v_{-\vec{k}-\vec{k}_1}^2$ etc. This yields

$$\begin{aligned}\Sigma_{\Gamma_1} = -\frac{2\gamma_{\vec{k}}\kappa^2K^2}{\omega+2J}\frac{1}{N}\sum_{\vec{k}_1}\big[&\gamma_{\vec{k}}u_{\vec{k}}^2u_{\vec{k}_1}^2v_{-\vec{k}-\vec{k}_1}^2 - 2\gamma_{\vec{k}}u_{\vec{k}}v_{\vec{k}}u_{\vec{k}_1}v_{\vec{k}_1}u_{-\vec{k}-\vec{k}_1}v_{-\vec{k}-\vec{k}_1}\\
&+\gamma_{\vec{k}}v_{\vec{k}}^2v_{\vec{k}_1}^2u_{-\vec{k}-\vec{k}_1}^2 - \gamma_{\vec{k}}u_{\vec{k}}^2u_{\vec{k}_1}v_{\vec{k}_1}u_{-\vec{k}-\vec{k}_1}v_{-\vec{k}-\vec{k}_1} + 2\gamma_{\vec{k}}u_{\vec{k}}v_{\vec{k}}u_{\vec{k}_1}^2v_{-\vec{k}-\vec{k}_1}^2\\
&-\gamma_{\vec{k}}v_{\vec{k}}^2u_{\vec{k}_1}v_{\vec{k}_1}u_{-\vec{k}-\vec{k}_1}v_{-\vec{k}-\vec{k}_1} + u_{\vec{k}}v_{\vec{k}}\gamma_{\vec{k}_1}u_{\vec{k}_1}^2u_{-\vec{k}-\vec{k}_1}v_{-\vec{k}-\vec{k}_1} - v_{\vec{k}}^2\gamma_{\vec{k}_1}u_{\vec{k}_1}v_{\vec{k}_1}v_{-\vec{k}-\vec{k}_1}^2\\
&-u_{\vec{k}}v_{\vec{k}}u_{\vec{k}_1}^2\gamma_{\vec{k}_2}u_{-\vec{k}-\vec{k}_1}v_{-\vec{k}-\vec{k}_1} + v_{\vec{k}}^2u_{\vec{k}_1}v_{\vec{k}_1}\gamma_{\vec{k}_2}u_{-\vec{k}-\vec{k}_1}^2\big]\,.\end{aligned} \tag{4.60}$$

Using the definitions of $R_{1\ldots5}$ in Eqs. (4.43) and (4.44), this can be converted into

$$\begin{aligned}\Sigma_{\Gamma_1} = -\frac{2\gamma_{\vec{k}}\kappa^2K^2}{\omega+2J}\Big\{&\gamma_{\vec{k}}u_{\vec{k}}^2\big[R_2 - R_5'(\vec{k})\big] + v_{\vec{k}}^2\big[\gamma_{\vec{k}}R_2 - \gamma_{\vec{k}}R_5'(\vec{k}) - R_3 + R_3'(\vec{k})\big]\\
&+u_{\vec{k}}v_{\vec{k}}\big[2\gamma_{\vec{k}}R_2 - 2\gamma_{\vec{k}}R_5'(\vec{k}) - R_3 + R_3'(\vec{k})\big]\Big\}\,.\end{aligned} \tag{4.61}$$

A similar calculation for the Γ_2 and Γ_3 combination of vertices results in:

$$\Sigma_{\Gamma_2} = \mathcal{O}(1/d^2), \tag{4.62}$$

$$\Sigma_{\Gamma_3} = -\frac{2\kappa^2K^2}{\omega+2J}\left\{v_{\vec{k}}^2\left[\gamma_{\vec{k}}R_3'(\vec{k}) - \gamma_{\vec{k}}R_3 + \frac{1}{2d} - \frac{\gamma_{\vec{k}}}{2d}\right] + \gamma_{\vec{k}}u_{\vec{k}}v_{\vec{k}}\left[R_3'(\vec{k}) - R_3\right]\right\}. \tag{4.63}$$

Finally, summing all the contributions gives the total self energy to order $1/d$ for the diagram under consideration

$$\Sigma_\Gamma = \Sigma_{\Gamma_1} + \Sigma_{\Gamma_2} + \Sigma_{\Gamma_3}\,, \tag{4.64}$$

$$\begin{aligned}\Sigma_\Gamma(\vec{k},\omega) = -\frac{2\kappa^2q^2J^2}{\omega+2J}\Big\{&\frac{v_{\vec{k}}^2(1-\gamma_{\vec{k}})}{2d} + 2\gamma_{\vec{k}}(v_{\vec{k}}^2 + u_{\vec{k}}v_{\vec{k}})\left[R_3'(\vec{k}) - R_3\right]\\
&+\gamma_{\vec{k}}^2(u_{\vec{k}}+v_{\vec{k}})^2\left[R_2 - R_5'(\vec{k})\right]\Big\} + \mathcal{O}\left(\frac{1}{d^2}\right).\end{aligned} \tag{4.65}$$

We see here that the self energy is suppressed at least as $1/d$. In fact this holds for all the diagrams arising from the interaction part of the Hamiltonian. This then means

that in the limit $d \to \infty$, the harmonic approximation becomes exact! From the above procedure it is also clear how to systematically go to higher orders in $1/d$. In a nutshell, the recipe to generate a systematic $1/d$-expansion to order $1/d^n$ is: identify the power m of $\gamma_{\vec{k}}$ which under momentum summation yields $\mathcal{O}(1/d^n)$, and then retain all the terms up to $\mathcal{O}(\gamma_{\vec{k}}^m)$ inside the momentum integral to get the final expression.

Note that any given diagram in the large-d limit has a power series expansion in $1/d$ which starts at a particular order in $1/d$. So at a given order n, we just have to collect those diagrams whose expansion starts at $\mathcal{O}(1/d^n)$ or below. Thus we need only a finite number of diagrams to a given order in $1/d$. Also, it is clear from the above discussion that these diagrams do not have a simple loop expansion.

The calculation for other diagrams used to evaluate observables in the later sections follows the same strategy as outlined here. Typically only a small fraction of possible vertex contributions of a given diagram eventually contributes to order $\mathcal{O}(1/d)$. For higher orders, the use of computer algebra is indispensable.

4.5 $1/d$ expansion for observables

Having established the diagrammatic procedure in the last section, we are now ready to calculate observables with the perturbative contributions being arranged in an expansion in $1/d$. For the Hamiltonian in eq. (4.41) we have,

$$\mathcal{H} = \underbrace{\mathcal{H}'_0 + \mathcal{H}'_{2a}}_{\text{exactly solvable}} + \underbrace{\mathcal{H}'_{2b} + \mathcal{H}'_3 + \mathcal{H}'_4 + \mathcal{H}'_5 + \mathcal{H}'_6}_{\text{perturbation}} \tag{4.66}$$

where the unperturbed piece $\mathcal{H}'_{2a}$ is defined in eq. (4.45) and the relevant perturbation terms are given by eq. (4.50) and (4.49). In this work we will calculate leading corrections beyond the harmonic approximation, i.e. we will go one order higher in $1/d$ than that obtained at the harmonic level. As will become clear below, these corrections will enter at different orders in $1/d$ for different observables.

We will exclusively work at zero absolute temperature. This greatly reduces the number of contributing diagrams as all closed (unidirectional) loops of τ particles vanish in the vacuum state. Evaluating individual diagrams involving cubic or quartic vertices typically leads to a large number of terms, most of which turn out to *not* contribute to the leading $1/d$ corrections. Since we have already discussed the diagrammatic scheme in previous section we will mostly quote the relevant results only.

4.5.1 Ground-state energy

In general, for phase transitions one has to consider the free energy but at $T = 0$ we only need to consider the ground-state energy. Since we are working in terms of dimer lattice sites it is convenient to consider the ground-state energy per dimer. The harmonic-approximation result easily follows from $\mathcal{H}_0$ and $\mathcal{H}_2$ (4.35):

$$\frac{E_0^{\text{harm}}}{JN} = -\frac{3}{4} + \frac{3}{2JN}\sum_{\vec{k}}(\omega_{\vec{k}} - A_{\vec{k}}) \overset{d\to\infty}{=} -\frac{3}{4} - \frac{3}{8}\frac{q^2}{d}\,. \tag{4.67}$$

(a) (b) (c)

Figure 4.3: Feynman diagrams for the ground-state energy which contribute to order $1/d^2$. This figure is taken from ref. [55].

The last expression involves to a leading order in $1/d$, an expansion of the square-root in the expression of $\omega_{\vec{k}}$ (4.36) to order $\gamma_{\vec{k}}^2$. Subsequently, momentum summation properties of $\gamma_{\vec{k}}$ are used.

At the harmonic level, the ground-state energy involves the zero-point energy contribution apart from the trivial product-state energy part. We see that the zero-point energy contribution starts at order $1/d$ (and has higher order contributions). Now the higher-order perturbative terms contribute to ground-state energy in two ways: (i) normal-ordering in τ basis generates constant terms; (ii) diagrammatic contributions. Since we aim to go beyond the harmonic-approximation, we shall calculate all contributions to the ground-state energy to order $1/d^2$. It turns out that normal ordering of $\mathcal{H}_5$ and $\mathcal{H}_6$ contribute only at order $1/d^3$ and higher since it involves momentum summation over factors of $\gamma_{\vec{k}}^5$ or higher. Similarly, all the diagrams for the ground-state energy involving vertex from $\mathcal{H}_5'$ or $\mathcal{H}_6'$ are suppressed by factor of $1/d^3$ or higher. Hence to order $1/d^2$ we only have to calculate contributions from $\mathcal{H}_4$. We have already expressed the contribution from normal ordering of $\mathcal{H}_4$ in the expression for $\mathcal{H}_0'$ (4.42). Using the expressions for Rs to order $1/d^2$ we get

$$\frac{\mathcal{H}_0'}{JN} = -\frac{3}{4} - \frac{3q^2}{8d} - \frac{3q^3}{16d^2} + \frac{27q^4}{64d^2}\,. \tag{4.68}$$

We will now calculate the diagrammatic contributions from the cubic and quartic vertices (see appendix C.2 for explicit expressions). Up to order $1/d^2$ there are two diagrams contributing in the $\kappa = 0$ case, figs. 4.3(a,b), and one further diagram involving cubic vertices which are non-zero only for $\kappa \neq 0$, fig. 4.3(c). The ground-state energy is then sum of all these contributions, $E_0 = \mathcal{H}_0' + E_0^{4.3(a)} + E_0^{4.3(b)} + E_0^{4.3(c)}$. The diagram in Fig. 4.3(a), being of second order in $\mathcal{H}_{2b}'$, evaluates to

$$E_0^{4.3(a)} = -3\sum_{\vec{k}} \frac{D_{\vec{k}}^2}{4\omega_{\vec{k}}}\,. \tag{4.69}$$

The vertex $D_{\vec{k}}$ (4.48) is of order $1/d$, and so only those terms in $E_0^{4.3(a)}$ will contribute to order $1/d^2$ which are not further suppressed by the momentum summation. This implies to approximate $\omega_{\vec{k}}$ (4.36) by its zeroth-order term in $\gamma_{\vec{k}}$, $\omega_{\vec{k}} \approx J$, and leads to

$$\frac{E_0^{4.3(a)}}{JN} = -3q^2(R_3 + R_4)^2 = -\frac{3}{16}\frac{q^4}{d^2} \tag{4.70}$$

to order $1/d^2$.

Let us now turn to the second-order $\mathcal{H}'_4$ diagram, shown in Fig. 4.3(b). We observe that this has vertices Φ_{41} of order $1/d^0$, but will be suppressed at least down to $1/d^2$ by internal momentum summations involving $\gamma_{\vec{k}}$ or $v_{\vec{k}}$ factors from the vertices. Hence, the energies of the internal particle lines can again be approximated by $\omega_{\vec{k}} \approx J$. Enumerating all possible contractions (in this case 4!) of internal lines and using the explicit form of Φ_{41} we find to order $1/d^2$:

$$\frac{E_0^{4.3(b)}}{JN} = -\frac{3}{8}\frac{q^4}{d^2}\,. \tag{4.71}$$

Similarly, we find the contribution from the cubic diagram to order $1/d^2$:

$$\frac{E_0^{4.3(c)}}{JN} = -\frac{\kappa^2 q^2}{3J^2}\left(\frac{R_2}{2d} - R_3^2\right) = 0\,. \tag{4.72}$$

Note that this is an accidental cancellation, leading to a κ-independent ground-state energy to order $1/d^2$. We do not expect such cancellations at higher orders, see also eq. (4.137) below.

Collecting all terms gives our result for E_0:

$$\frac{E_0}{JN} = -\frac{3}{4} - \frac{3}{8}\frac{q^2}{d} - \frac{3}{16}\frac{q^3}{d^2} - \frac{9}{64}\frac{q^4}{d^2} + \mathcal{O}\left(\frac{1}{d^3}\right)\,. \tag{4.73}$$

The ground-state energy being analytic up to the critical point is consistent with the mean-field value[5] $\alpha = 0$ for the specific-heat critical exponent α.

4.5.2 Triplon dynamics

As discussed in the introductory part, in the quantum paramagnetic phase we have triply degenerate spin-1 triplon excitations and we calculated the corresponding dispersion relation in the harmonic approximation in sec. 4.4.2. We see that the result at the harmonic approximation corresponds to the zeroth order in a $1/d$ expansion and in the following we shall calculate corrections to order $1/d$. As in the case of ground-state energy, even in this case the interaction terms only up to quartic order in t are relevant. It is worth mentioning that the degeneracy of triplons remains intact since the Hamiltonian, including the interaction pieces, is symmetric with respect to the three triplon modes.

To systematically account for corrections coming from the interaction terms we need to evaluate self-energy diagrams, and solve the coupled Dyson equation (see appendix A) to obtain the full Green's function. Triplon dispersion is then given by the pole of the Green's function. As we have seen in section 4.4.5, every self-energy diagram has an expansion in powers of $1/d$ and hence it is clear that the dispersion[2] will also have a systematic $1/d$ expansion. More importantly, in the large-d limit all self-energies are suppressed at least as $1/d$, which means that the perturbative corrections to the

[2]It will be shown below that actually square of the dispersion has an analytic expansion in powers of $1/d$ everywhere in the phase diagram including the critical point, while that for dispersion is ill-defined at the critical point.

dispersion start only at order $1/d$. Taking into account both the normal and anomalous τ diagrams, and solving the Dyson equation (A.1) we obtain the following expression for the normal and anomalous Green's functions:

$$\mathcal{G}^N(\vec{k},\omega) = \frac{\omega + \omega_{\vec{k}} + \Sigma_N(\vec{k},-\omega)}{\Xi(\omega,\vec{k})}\,, \tag{4.74}$$

$$\mathcal{G}^A(\vec{k},\omega) = \frac{-\Sigma_A(\vec{k},\omega)}{\Xi(\omega,\vec{k})} \tag{4.75}$$

with

$$\begin{aligned}\Xi(\omega,\vec{k}) = &\left[\omega + \omega_{\vec{k}} + \Sigma_N(\vec{k},-\omega)\right]\left[\omega - \omega_{\vec{k}} - \Sigma_N(\vec{k},\omega)\right] \\ &+ \Sigma_A(\vec{k},\omega)\Sigma_A(\vec{k},-\omega)\,.\end{aligned} \tag{4.76}$$

Consequently, the equation for the renormalized pole energies $\Omega_{\vec{k}}$ is

$$\Xi(\Omega_{\vec{k}},\vec{k}) = 0\,. \tag{4.77}$$

In general solving the above equation would require evaluating the self-energies $\Sigma_{N,A}$ at $\omega = \Omega_{\vec{k}}$. This will, in general, lead to a complicated polynomial equation in $\Omega_{\vec{k}}$. However in the large-d formalism things become somewhat simpler. In the large-d limit, we anticipate a $1/d$ expansion for the dispersion that is

$$\Omega_{\vec{k}} = \omega_{\vec{k}} + \frac{\omega^{(1)}}{d} + \mathcal{O}\left(\frac{1}{d^2}\right)\,. \tag{4.78}$$

Also, for the $1/d$ expansion this means that the energy argument of $\Sigma_{N,A}$ itself needs to be expanded in $1/d$. For the analysis of positive-energy pole we expand the self-energy according to:

$$\Sigma_N(\vec{k},\pm\Omega_{\vec{k}}) = \Sigma_{N\pm} + (\Omega_{\vec{k}} - \omega_{\vec{k}})\Sigma'_{N\pm}\,, \tag{4.79}$$

with the abbreviations

$$\Sigma_{N\pm} = \Sigma_N(\vec{k},\pm\omega_{\vec{k}}), \quad \Sigma'_{N\pm} = \left.\frac{\partial\Sigma_N(\vec{k},\pm\omega)}{\partial\omega}\right|_{\omega=\omega_{\vec{k}}}\,. \tag{4.80}$$

In the following, we calculate $\Omega_{\vec{k}}$ up to order $1/d$ only. We observe that self-energies are suppressed at least as $1/d$ and $(\Omega_{\vec{k}} - \omega_{\vec{k}}) \propto 1/d$. This means that we can neglect $\Sigma_A(\vec{k},\omega)\Sigma_A(\vec{k},-\omega)$ term in eq. (4.76) since it is of order $1/d^2$. Similarly we can neglect $(\Omega_{\vec{k}} - \omega_{\vec{k}})\Sigma'_{N\pm}$ term in eq. (4.79) and approximate $\Sigma_N(\vec{k},\pm\Omega_{\vec{k}}) \approx \Sigma_{N\pm}$. Thus from eq. (4.76) the positive-energy pole equation reduces to

$$\Omega_{\vec{k}} - \omega_{\vec{k}} - \Sigma_{N+} = 0\,. \tag{4.81}$$

Note that for the analysis of negative-energy pole the prescription is same as above, with the only difference being that now the self-energy is to be expanded around $-\omega_{\vec{k}}$.

As discussed earlier in chapter 3, expansions have to be used with care in the vicinity of the quantum critical point. We have to be careful in identifying observables which

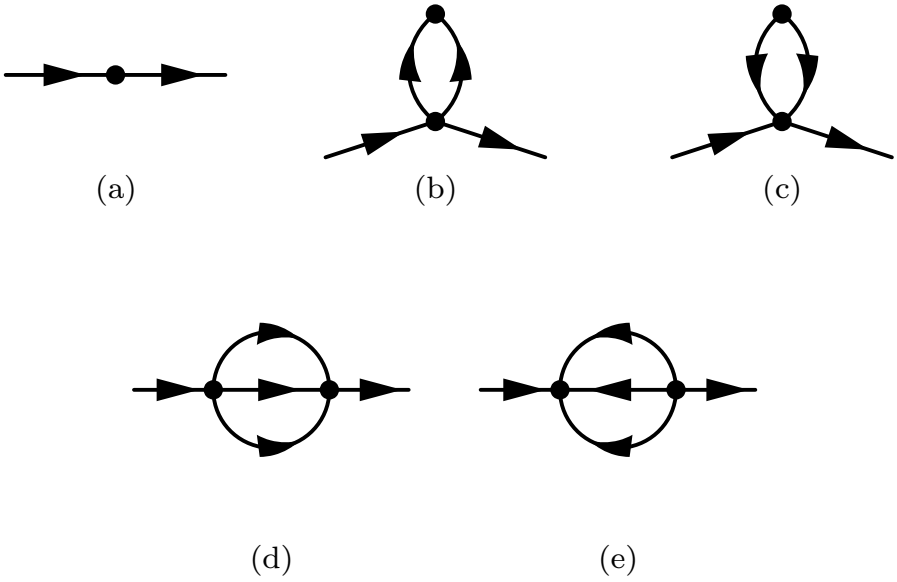

Figure 4.4: Feynman diagrams for the normal τ self-energy up to order $1/d$, with vertices from $\mathcal{H}'_{2b}$ and $\mathcal{H}'_4$. This figure is taken from ref. [55].

will have an analytic expansion even at the critical point. In particular, in this case $\Omega_{\vec{k}}$ will not have a well-defined $1/d$ expansion near $\vec{k} = \vec{Q}$ when the gap closes. However, $\Omega^2_{\vec{k}}$ can be expected to be analytic for the same reason as $\Delta^2 \propto (q_c - q)^{2\nu z} = q_c - q$ is analytic. Consequently, we shall square eq. (4.81) and thus work with the following dispersion expression, valid to order $1/d$:

$$\Omega^2_{\vec{k}} = \omega^2_{\vec{k}} + 2\omega_{\vec{k}}\Sigma_{N+}\,. \tag{4.82}$$

For calculations to higher order in $1/d$, we would require to incorporate the anomalous self-energy part, self-energy derivatives as well as the square of self-energies, thus modifying the above equation.

Let us now turn our attention to calculate the normal self-energy in the symmetric case, i.e. $\kappa = 0$. In fig. 4.4 we have sketched the Feynman diagrams contributing to order $1/d$. The evaluation of these diagrams is on the same lines as discussed in section 4.4.5 namely perform the frequency integral and then approximating the energies of the internal particle lines by $\omega_{\vec{k}} \approx J$ perform the large-d momentum integration. According to these guidelines we get the following contributions from these diagrams to order $1/d$:

$$\Sigma^{4.4(a)}(\vec{k},\omega) = C_{\vec{k}}\,, \tag{4.83}$$

$$\Sigma^{4.4(b)}(\vec{k},\omega) = \Sigma^{4.4(c)}(\vec{k},\omega) = -\gamma_{\vec{k}} q^2 J (R_3 + R_4)(u_{\vec{k}} + v_{\vec{k}})^2\,, \tag{4.84}$$

$$\Sigma^{4.4(d)}(\vec{k},\omega) = \frac{q^2J^2}{\omega - 3J}\left[4\gamma^2_{\vec{k}}(u_{\vec{k}} + v_{\vec{k}})^2 R_2 + 8\gamma_{\vec{k}}(u^2_{\vec{k}} + u_{\vec{k}}v_{\vec{k}})R_3 + \frac{2u^2_{\vec{k}}}{d}\right]\,, \tag{4.85}$$

$$\Sigma^{4.4(e)}(\vec{k},\omega) = \frac{-q^2J^2}{\omega + 3J}\left[4\gamma^2_{\vec{k}}(u_{\vec{k}} + v_{\vec{k}})^2 R_2 + 8\gamma_{\vec{k}}(v^2_{\vec{k}} + u_{\vec{k}}v_{\vec{k}})R_3 + \frac{2v^2_{\vec{k}}}{d}\right]\,. \tag{4.86}$$

The frequency integrals in these diagrams is straightforward and so we briefly mention the way to go on with the momentum integrations. Evaluating $\Sigma^{4.4(a)}$ is trivial. For

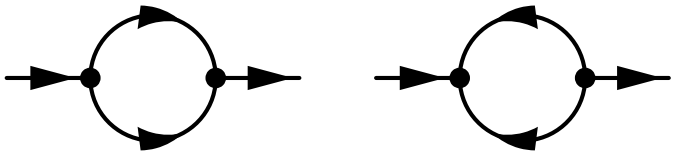

(a) (b)

Figure 4.5: Feynman diagrams for the contribution of cubic ($\mathcal{H}_3'$) terms to the normal τ self-energy up to order $1/d$. This figure is taken from ref. [55].

$\Sigma^{4.4(b)}$ and $\Sigma^{4.4(c)}$ we need the bilinear vertex $D_{\vec{k}}/2$ (4.48) and the quartic vertex Φ_{44}. In each case, there are 3 combinations corresponding to the choice of external leg from one of the three $\tau^\dagger$ (or τ) and on top of this a factor of 2! arising from internal permutations. So in total there are 6 permutations involved[3]. Now the diagram for $\Sigma^{4.4(d)}$ involves two quartic vertices, both Φ_{44}, and it is easy to see that the total number of permutations involved is $3! = 6$. The diagram for $\Sigma^{4.4(e)}$ is again composed of two quartic vertices, both Φ_{41}, thus giving rise to a total number of permutations equal to $4 \times 4! = 96$. Moreover, in each of these diagrams we have to be careful with the spin labels in the τ operators since the propagator involving two different types of τs is zero.

Using the explicit expressions for the Bogoliubov coefficients (4.38), the $R_{1\ldots4}$ (appendix C.1), and then inserting all the explicit expressions in eq. (7.50), we obtain the $1/d$ expansion for the triplon dispersion in the symmetric case $\kappa = 0$:

$$\frac{\Omega_{\vec{k}}^2}{J^2} = 1 + 2\gamma_{\vec{k}} q + \frac{1}{d}(2q^2 - \gamma_{\vec{k}}^2 q^3) + \mathcal{O}\left(\frac{1}{d^2}\right) . \tag{4.87}$$

We see that interactions generically increase the triplon energy (for $q < 2$ which holds everywhere in the disordered phase treated here) – this is of course expected for dominantly repulsive quartic interactions. We can now try to write a $1/d$ expansion for $\Omega_{\vec{k}}/J$ from the above expression. It means that we have to perform a square-root expansion of eq. (4.87). It is then immediately clear that this is a well defined procedure only if the leading order term $\omega_{\vec{k}} = \sqrt{1 + 2\gamma_{\vec{k}} q}$ is non zero. Hence an expansion for $\Omega_{\vec{k}}/J$ is valid everywhere except for $\vec{k} = \vec{Q}$ at criticality. Although the above expression gives an impression that a $1/d$ expansion is simply an expansion in powers of q or $\gamma_{\vec{k}}$, it will become clear in the following that this is not the case. It is a particular property of the symmetric case that the non-trivial factors of q and $\gamma_{\vec{k}}$ vanish.

In the asymmetric case, $\kappa \neq 0$, additional self-energy diagrams involving cubic vertices contribute to order $1/d$ and these are sketched in fig. 4.5. As explained earlier, fifth order terms in τ are irrelevant at this level. These diagrams are evaluated using the same prescription as discussed above for the quartic terms. To order $1/d$, these

[3]One can also see this as simply a permutation of three $\tau^\dagger$ (or τ) giving rise to $3! = 6$ permutations.

diagrams have following contributions:

$$\Sigma^{4.5(a)}(\vec{k},\omega) = \frac{2\kappa^2 q^2 J^2}{\omega - 2J}\Bigg\{ \frac{u_{\vec{k}}^2(1-\gamma_{\vec{k}})}{2d} + 2\gamma_{\vec{k}}(u_{\vec{k}}^2 + u_{\vec{k}}v_{\vec{k}})\left[R_3'(\vec{k}) - R_3\right] + \gamma_{\vec{k}}^2(u_{\vec{k}} + v_{\vec{k}})^2\left[R_2 - R_5'(\vec{k})\right]\Bigg\} \tag{4.88}$$

$$\Sigma^{4.5(b)}(\vec{k},\omega) = \frac{-2\kappa^2 q^2 J^2}{\omega + 2J}\Bigg\{ \frac{v_{\vec{k}}^2(1-\gamma_{\vec{k}})}{2d} + 2\gamma_{\vec{k}}(v_{\vec{k}}^2 + u_{\vec{k}}v_{\vec{k}})\left[R_3'(\vec{k}) - R_3\right] + \gamma_{\vec{k}}^2(u_{\vec{k}} + v_{\vec{k}})^2\left[R_2 - R_5'(\vec{k})\right]\Bigg\}, \tag{4.89}$$

see appendix C.1 for R_5'. Here, the momentum integration in $\Sigma^{4.5(a)}$ involves different combinations of two out of the three cubic vertices, Φ_{32}, Φ_{33} and Φ_{34}, which gives 9 permutations. Here internal permutation is not required due to $\epsilon_{\alpha\beta\gamma}$. Similarly, $\Sigma^{4.5(b)}$ involves only Φ_{31} and gives rise to 3 permutations. Taking into account these additional contributions from the cubic-vertex self-energy diagrams the triplon dispersion is as follows:

$$\frac{\Omega_{\vec{k}}^2}{J^2} = 1 + 2\gamma_{\vec{k}}q + \frac{1}{d}(2q^2 - \gamma_{\vec{k}}^2 q^3) + \frac{\kappa^2 q^2(1-\gamma_{\vec{k}})(6 + 14\gamma_{\vec{k}}q + 6\gamma_{\vec{k}}^2 q^2)}{(2\gamma_{\vec{k}}q - 3)d} + \mathcal{O}\left(\frac{1}{d^2}\right). \tag{4.90}$$

We see that in the above expression, unlike the symmetric case, there are terms which are not simply powers of q or $\gamma_{\vec{k}}$. This explicitly shows that the $1/d$ expansion is not a simple an expansion in powers of q or $\gamma_{\vec{k}}$. The non-trival denominator in the κ^2/d correction of eq. (4.90) arises as a product of the denominators in the self-energies (4.88) and (4.89), evaluated at $\omega = \omega_{\vec{k}}$, and unlike the symmetric case this is not canceled by identical factors in numerator. Later on we will make a comparison with a small-q expansion and in that case we need to perform a double expansion: expansion in $1/d$ (which is shown above) and on top of this an expansion in small q which involves expanding the non-trivial denominator. After doing this we will see that our results are in agreement with the small-q expansion result and thus reconfirming the correctness of our result.

It is clear that to all orders any momentum dependence can arise only via interaction structure factor $\gamma_{\vec{k}}$. However it need not be just $\gamma_{\vec{k}}$. At higher orders, $\gamma_{2\vec{k}}$, $\gamma_{3\vec{k}}$ etc. may appear as well. The dispersion results, for concrete values of d, are illustrated in fig. 4.6. We can clearly see that quantum fluctuations increase the energy as compared to the harmonic level result.

4.5.3 Triplon decay

We can see from their explicit expressions that the self-energies are purely real for all the relevant frequencies. Thus there is no triplon damping. In fact, this result is not restricted to order $1/d$ but present at all orders. The triplon density of states is strongly peaked at $\omega = J$ in the large-d limit, since the typical $\gamma_{\vec{k}}$ is small. To be precise, the density of states for $\omega \neq J$ is exponentially small [53] as $d \to \infty$. Consequently, the same applies to the density of states of multi-triplon continua which are responsible

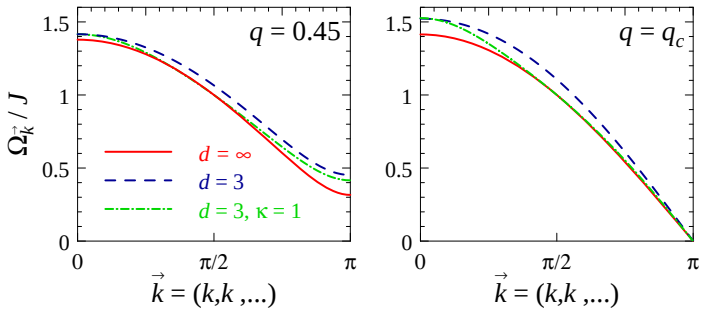

Figure 4.6: Triplon dispersion (4.90) derived from the $1/d$ expansion for the coupled-dimer model (4.2). Results shown for $d = \infty$ (solid), $d = 3$ with $\kappa = 0$ (dashed), and $d = 3$ with $\kappa = 1$ (dash-dot), where κ is the asymmetry parameter (4.3). Left: results for a fixed $q = Kd/J = 0.45$. Right: results at criticality, $q = q_c$, where here q_c is defined by $\Omega_{\vec{Q}} = 0$ with $\Omega_{\vec{k}}$ from eq. (4.90) at *fixed* d; the value of this q_c is distinct from the expansion result (4.94) evaluated at fixed d. Figure taken from ref. [55].

for damping, such that all damping rates (inverse lifetimes) are exponentially small in $1/d$ and thus vanish to all orders in a $1/d$ expansion.

Note that the poles in the self-energies, located at $\pm 2J$ and $\pm 3J$ at order $1/d$, produce additional spectral weight in the triplon propagators near these frequencies. This weight takes the form of poles with strengths of order $1/d$. This mimics the incoherent continuum present at a finite d.

4.5.4 Gap, mode velocity, and phase boundary

The minimum of the triplon dispersion gives the excitation gap, Δ, of the paramagnetic phase. We saw in the harmonic approximation that the minimum of triplon dispersion occurs at $\vec{k} = \vec{Q} \equiv \{\pi, \pi, \ldots\}$. Now with $1/d$ corrections the minimum of triplon dispersion is still located at $\vec{Q}$ and so $\Delta = \Omega_{\vec{Q}}$. This yields

$$\frac{\Delta^2}{J^2} = 1 - 2q + \frac{1}{d}(2q^2 - q^3) - \frac{2\kappa^2 q^2(6 - 14q + 6q^2)}{(2q+3)d} + \mathcal{O}\left(\frac{1}{d^2}\right) \tag{4.91}$$

and is graphically shown in Fig. 4.7. As in the case of the triplon dispersion, we find that an expansion for Δ^2 is well-behaved even at criticality. An expansion for Δ is well-defined everywhere apart from the the quantum critical point.

Another physical quantity of interest is the mode velocity. This is nothing but the slope of triplon dispersion close to $\vec{Q}$. Near $\vec{Q}$ we can expand $\gamma_{\vec{k}} \approx -1 + \sum_n (k_n - \pi)^2/(2d)$. This yields the parametrization

$$\Omega_{\vec{k}}^2 = \Delta^2 + \frac{c^2}{d}(\vec{k} - \vec{Q})^2 \,, \tag{4.92}$$

with the mode velocity c given by

$$\frac{c}{J} = \sqrt{q} + \frac{q^{5/2}}{2d} - \frac{\kappa^2 q^{3/2}}{2(2q+3)d}\left[\frac{(6 - 14q + 6q^2)(2q-3)}{2(2q+3)} + 14q - 12q^2\right] + \mathcal{O}\Big(\frac{1}{d^2}\Big). \tag{4.93}$$

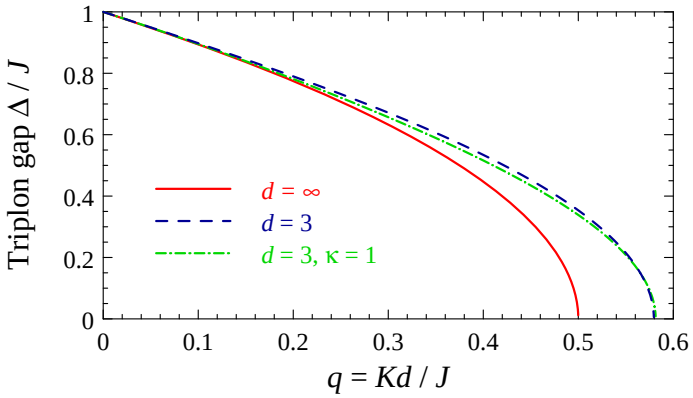

Figure 4.7: Triplon gap (4.91) is plotted for $d = \infty$ (solid), $d = 3$ with $\kappa = 0$ (dashed), and $d = 3$ with $\kappa = 1$ (dash-dot). Figure taken from ref. [55].

Here we see that c/J has a regular expansion everywhere in the paramagnetic phase including the quantum critical point, since the velocity at the leading order does not vanish at the criticality. In a situation where phase transition is driven by vanishing of velocity[4] we would expect that c^2 would be the correct observable to write a $1/d$ expansion.

As argued earlier, vanishing of the excitation gap locates the phase boundary, q_c, to the magnetically ordered phase. In order to obtain the phase boundary in a $1/d$ formalism, we need to solve the equation[5] $\Delta^2(q_c) = 0$ using the ansatz $q_c = 1/2 + q_{c1}/d$. Thus, to order $1/d$ we obtain the phase boundary:

$$q_c = \frac{1}{2} + \left(\frac{3}{16} + \frac{\kappa^2}{32}\right)\frac{1}{d} + \mathcal{O}\left(\frac{1}{d^2}\right) . \tag{4.94}$$

In $d = 2$ and for $\kappa = 0$, above result for the critical coupling of the Heisenberg bilayer model is significantly smaller than the value known from QMC calculations [62], see fig. 4.8. This indicates sizeable contributions from higher orders in the $1/d$ expansion, which we do not evaluate in the present work. However, notably for $d = 3$ and $\kappa = 0$, which is a relevant model corresponding to experimentally well-studied material $TlCuCl_3$, the agreement between our result at order $1/d$ and the recent QMC calculation [63] is satisfactory.

Also note that solving the equation $\Delta^2(q_c) = 0$ using the truncated series (4.91) for finite d yields a value for q_c which is distinct from q_c as given by the truncated series (4.94) for the same finite d. The reason is simply that Δ^2 from eq. (4.91) evaluated at q_c from eq. (4.94) contains $1/d^2$ terms which do not vanish.

Apart from the regular $1/d$ expansion we can also study the behavior of triplon excitation gap near the quantum critical point. As discussed earlier, since we work in the large-d limit, we can access only mean-field critical exponents. This means that $\Delta \propto \sqrt{q_c - q}$ corresponding to $\nu = 1/2$ and $z = 1$. We can precisely calculate the

[4]Such phase transitions are possible out of a magnetically ordered phase where the gap is always zero.

[5]Note that one cannot use any other power of Δ^2 to obtain q_c. This is because it leads to a mixing of terms from different orders in $1/d$, which is not a consistent way to deal with systematic expansions.

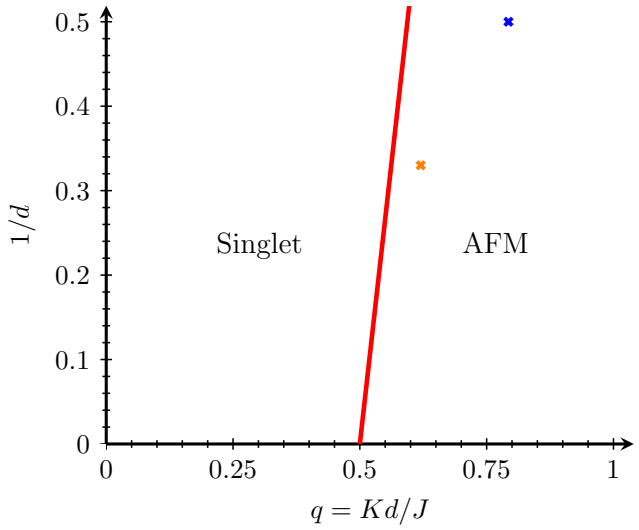

Figure 4.8: Phase diagram of the coupled-dimer model (4.2) on a hypercubic lattice as function of the control parameter $q = Kd/J$ and the inverse spatial dimension $1/d$. The solid red line shows our result (4.94) for the phase boundary q_c to order $1/d$ for the symmetric case $\kappa = 0$ (4.3). The blue cross marks QMC result for $d = 2$ obtained in ref. [62]. The orange cross marks the QMC result for $d = 3$ as obtained in ref. [63].

pre-factor, which is related to the mass of the triplon excitation in the corresponding ϕ^4 field theory, for this relation in a $1/d$ fashion. A few steps of simple algebra leads us to the following desired relation:

$$\frac{\Delta}{J} = \left[\sqrt{2} - \frac{5}{8\sqrt{2}d} + \mathcal{O}\left(\frac{1}{d^2}\right)\right]\sqrt{q_c - q}\,. \tag{4.95}$$

Later in the next chapter we shall make connection to the analogous expression in the magnetically ordered phase. Finally to complete this discussion we also quote the $1/d$ expansion for the mode velocity at the quantum critical point:

$$\frac{c}{J} = \frac{1}{\sqrt{2}} + \frac{5}{16\sqrt{2}d} + \mathcal{O}\left(\frac{1}{d^2}\right)\,. \tag{4.96}$$

4.5.5 Triplet density

We continue by calculating additional local static observables. For this purpose we will need expectation values of certain bilinear combination of τ particles which can be calculated easily from the full Green's function as follows:

$$\langle \tau_{\vec{k}} \tau^\dagger_{\vec{k}} \rangle = \imath \lim_{t\to 0^+} \int d\omega \frac{e^{-\imath\omega t}}{2\pi} \mathcal{G}_N(\vec{k},\omega) = 1 + \Sigma'_{N+}\,, \tag{4.97}$$

$$\langle \tau_{\vec{k}} \tau_{-\vec{k}} \rangle = \imath \lim_{t\to 0} \int d\omega \frac{e^{-\imath\omega t}}{2\pi} \mathcal{G}_A(\vec{k},\omega) = -\frac{\Sigma_{A+}}{\Omega_{\vec{k}} + \Omega^-_{\vec{k}}}\,. \tag{4.98}$$

The second equality in above equations is obtained using the expression (4.74) and expanding the self-energy around $\Omega_{\vec{k}}$, and we have defined

$$\Omega^-_{\vec{k}} = \omega_{\vec{k}}(1 - 2\Sigma'_{N-}) + \Sigma_{N-}. \tag{4.99}$$

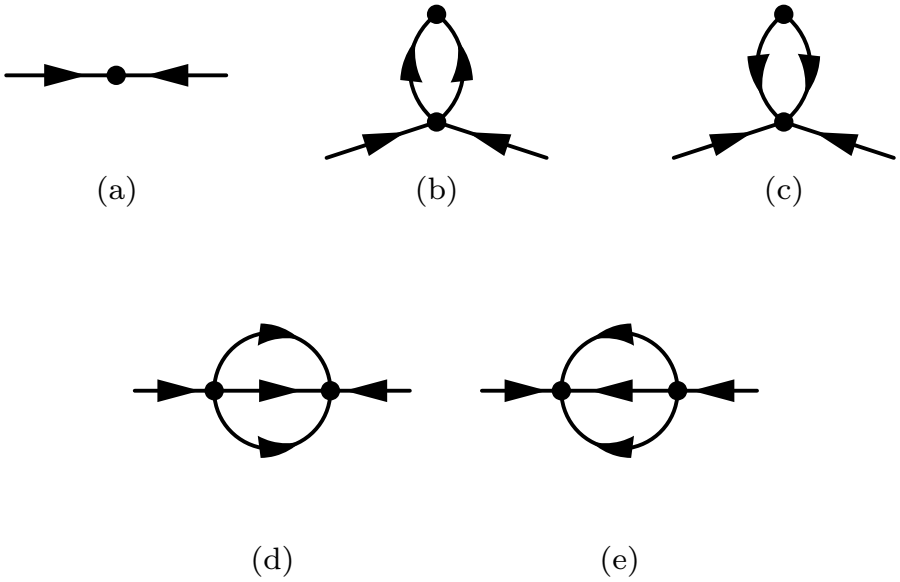

Figure 4.9: Feynman diagrams for anomalous self-energies contributing to order $1/d$ in the symmetric case, $\kappa = 0$ (4.3). Figure taken from ref. [55].

As we see we also need the contributions from the anomalous self-energies. The relevant diagrams in the symmetric case, $\kappa = 0$, to order $1/d$ are shown in fig. 4.9. Their evaluation is on the same lines as discussed in the previous subsections. We thus have the following expressions for the anomalous self-energies:

$$\Sigma^{4.9(a)}(\vec{k},\omega) = D_{\vec{k}}, \tag{4.100}$$

$$\Sigma^{4.9(b)}(\vec{k},\omega) = -2\gamma_{\vec{k}} q^2 J R_3 (u_{\vec{k}}^2 + u_{\vec{k}} v_{\vec{k}}), \tag{4.101}$$

$$\Sigma^{4.9(c)}(\vec{k},\omega) = -2\gamma_{\vec{k}} q^2 J R_3 (v_{\vec{k}}^2 + u_{\vec{k}} v_{\vec{k}}), \tag{4.102}$$

$$\Sigma^{4.9(d)}(\vec{k},\omega) = \frac{q^2 J^2}{\omega - 3J}\left[4\gamma_{\vec{k}}(u_{\vec{k}} + v_{\vec{k}})^2(\gamma_{\vec{k}} R_2 + R_3) + \frac{2u_{\vec{k}} v_{\vec{k}}}{d}\right], \tag{4.103}$$

$$\Sigma^{4.9(e)}(\vec{k},\omega) = \frac{-q^2 J^2}{\omega + 3J}\left[4\gamma_{\vec{k}}(u_{\vec{k}} + v_{\vec{k}})^2(\gamma_{\vec{k}} R_2 + R_3) + \frac{2u_{\vec{k}} v_{\vec{k}}}{d}\right]. \tag{4.104}$$

The local triplet density $\langle t_{i\alpha}^\dagger t_{i\alpha}\rangle$ per site vanishes as $d \to \infty$ as well as $q \to 0$ for any d as stated above. In the harmonic approximation we have $\sum_i \langle t_{i\alpha}^\dagger t_{i\alpha}\rangle/N = R_2$, see Appendix C.1. Perturbative corrections, which can be calculated based on the τ-particle self-energies, start only at order $1/d^2$, such that we have:

$$\frac{1}{N}\sum_i \langle t_{i\alpha}^\dagger t_{i\alpha}\rangle = \frac{q^2}{8d} + \mathcal{O}\left(\frac{1}{d^2}\right). \tag{4.105}$$

Notably, obtaining the complete $1/d^2$ contribution would require self-energies at next-to-leading order (i.e. $1/d^2$) which are beyond the scope of present work. This expression is valid even in the asymmetric case.

It is instructive to consider the expectation value of site-pair creation operator, $\langle t_{i\alpha}^\dagger t_{i\alpha}^\dagger\rangle$ – this quantity must vanish as a result of the constraint (4.12). In the harmonic

approximation we have $\sum_i \langle t^\dagger_{i\alpha} t^\dagger_{i\alpha}\rangle/N = R_1$. We can take into account the perturbative corrections arising from the self-energies by substituting the relevant expressions for the τ expectation values in the following expression:

$$\frac{1}{N}\sum_i \langle t^\dagger_{i\alpha} t^\dagger_{i\alpha}\rangle = \frac{1}{N}\sum_{\vec{k}} \langle u^2_{\vec{k}} \tau^\dagger_{\vec{k}} \tau^\dagger_{-\vec{k}} + v^2_{\vec{k}} \tau_{\vec{k}} \tau_{-\vec{k}} + u_{\vec{k}} v_{\vec{k}} \left(\tau^\dagger_{\vec{k}} \tau_{\vec{k}} + \tau_{\vec{k}} \tau^\dagger_{\vec{k}}\right)\rangle \,. \tag{4.106}$$

To order $1/d$ this gives us

$$\frac{1}{N}\sum_i \langle t^\dagger_{i\alpha} t^\dagger_{i\alpha}\rangle = \frac{1}{N}\sum_{\vec{k}} \langle u^2_{\vec{k}} \tau^\dagger_{\vec{k}} \tau^\dagger_{-\vec{k}}\rangle + \frac{1}{N}\sum_k u_{\vec{k}} v_{\vec{k}} \,. \tag{4.107}$$

We must now use only $\gamma_{\vec{k}}$ independent terms in $\langle \tau^\dagger_{\vec{k}} \tau^\dagger_{-\vec{k}}\rangle$ to obtain the result to order $1/d$. This amounts to taking into account the momentum independent part of the anomalous self-energy which then results in

$$\frac{1}{N}\sum_i \langle t^\dagger_{i\alpha} t^\dagger_{i\alpha}\rangle = qR_3 + R_1 = 0 \,. \tag{4.108}$$

This is in accord with the hardcore constraint. We expect this to hold order by order in the $1/d$ expansion [6]. As in the case of the triplet density, we need the self-energies to order $1/d^2$ to calculate the expectation value of site-pair creation operator at order $1/d^2$. Note that the above expression is also valid for the asymmetric case because here we required only the momentum independent part of anomalous self-energy and this comes from κ independent $D_{\vec{k}}$. It is easy to see that the additional anomalous diagrams arising from the cubic vertices in the $\kappa \neq 0$ case are momentum dependent.

However, the expectation value of the bond-pair creation operator, $\sum_{\langle ij\rangle} \langle t^\dagger_{i\alpha} t^\dagger_{j\alpha}\rangle$, involves two different sites and hence an additional factor of $\gamma_{\vec{k}}$. As a result, following the above recipe we can obtain the full $1/d^2$ correction in the symmetric case $\kappa = 0$, with the following result:

$$\frac{1}{Nd}\sum_{\langle ij\rangle} \langle t^\dagger_{i\alpha} t^\dagger_{j\alpha}\rangle = -\frac{q}{4d} - \frac{(2q^2+q^3)}{16d^2} + \mathcal{O}\left(\frac{1}{d^3}\right) . \tag{4.109}$$

Here a division by Nd appears because of the corresponding number of bonds involved.

4.5.6 Triplon weight in dynamic susceptibility

So far we discussed only the static observables. We will now turn our attention to dynamic spin susceptibility and determine the weight of the triplon mode. Dynamic spin susceptibility is an experimentally measurable quantity as mentioned in chapter 1. As in the case of previous observables we will write down a $1/d$ expansion for the

[6] The anomalous expectation value $Q(d) = \sum_i \langle t^\dagger_{i\alpha} t^\dagger_{i\alpha}\rangle/N$ must vanish for any physical eigenstate of $\mathcal{H}$ in any dimension d. The $1/d$ expansion calculates $\bar{Q}(x) = Q(1/x)$ in a Taylor series in x. According to our explicit results, the first two coefficients of this expansion vanish. Together with $\bar{Q}(x) = 0$ for any non-zero x this implies that $\bar{Q}(x) = 0$ order by order.

mode weight as well. Here we shall only consider the symmetric case $\kappa = 0$. Let us first define the dynamic spin susceptibility

$$\chi_\alpha(\vec{k},\omega) = -\imath \int_{-\infty}^{\infty} dt e^{\imath\omega t} \langle T_t S_\alpha(\vec{k},t) S_\alpha(-\vec{k},0)\rangle \,, \tag{4.110}$$

where T_t is the time-ordering operator and the spin operators are written in the interaction-picture. In the coupled-dimer system under consideration, the Fourier-transformed spin operator $S_\alpha(\vec{k})$ has two contributions with different form factors, namely even (e) and odd (o) ones:

$$S^e_\alpha = S^1_\alpha + S^2_\alpha = -\imath\epsilon_{\alpha\beta\gamma} t^\dagger_\beta t_\gamma \tag{4.111}$$

$$S^o_\alpha = S^1_\alpha - S^2_\alpha = t^\dagger_\alpha P + P t_\alpha \,, \tag{4.112}$$

with P the projector defined in eq. (4.14). In general the dynamic spin susceptibility will have contributions from single-mode and multi-particle continua. But we will focus only on extracting the single-mode contribution that is only the share from single quasiparticle excitation. Technically this means retaining only those terms (in product of spin operators) in (4.110) which are at most bilinear in τ operator. So henceforth we will not consider the even channel which results only in continuum. We note, however, that although the P in S^o_α generates a cubic term in τ, its normal-ordering leads to a linear term in τ with a pre-factor proportional to $1/d$ as a consequence of momentum summation. So it influences the pole weight at order $1/d$ and cannot be approximated by unity.

Using the definition of Green's function,

$$\mathcal{G}_N(\vec{k},\omega) = -\imath \int_{-\infty}^{\infty} dt e^{\imath\omega t} \langle T_t \tau_{\vec{k}\alpha}(t) \tau^\dagger_{\vec{k}\alpha}(0)\rangle \,; \tag{4.113}$$

$$\mathcal{G}_A(\vec{k},\omega) = -\imath \int_{-\infty}^{\infty} dt e^{\imath\omega t} \langle T_t \tau_{\vec{k}\alpha}(t) \tau_{-\vec{k}\alpha}(0)\rangle \tag{4.114}$$

and Bogoliubov transformation (4.32) one can write the spin susceptibility for S^o_α to order $1/d$ in terms of the τ-Green's functions as follows:

$$\begin{aligned}\tilde{\chi}_\alpha(\vec{k},\omega) = (u_{\vec{k}} + v_{\vec{k}})^2 (1 - 2R_1 - 8R_2) \times \\ \Big[\mathcal{G}^N(\vec{k},\omega) + \mathcal{G}^N(\vec{k},-\omega) + \mathcal{G}^A(\vec{k},\omega) + \mathcal{G}^A(\vec{k},-\omega)\Big] \,.\end{aligned} \tag{4.115}$$

We are interested in the pole weight and so we need to analyze $\tilde{\chi}$ in the vicinity of the pole at $\Omega_{\vec{k}}$. Expanding the self-energies in the vicinity of $\omega_{\vec{k}}$ and using the relations (4.79) and (7.50) we can cast the Green's functions into the following form:

$$\mathcal{G}^N(\vec{k},\omega) = \frac{(1 - \Sigma'_{N+})^{-1}}{\omega - \Omega_{\vec{k}}}, \tag{4.116}$$

$$\mathcal{G}^N(\vec{k},-\omega) = -\frac{(1 - \Sigma'_{N-})^{-1}}{\omega + \Omega^-_{\vec{k}}}, \tag{4.117}$$

$$\mathcal{G}^A(\vec{k},\omega) = -\frac{\Sigma_{A+} + (\omega - \omega_{\vec{k}})\Sigma'_{A+}}{(\omega - \Omega_{\vec{k}})(\omega - \Omega^-_{\vec{k}})}, \tag{4.118}$$

$$\mathcal{G}^A(\vec{k},-\omega) = -\frac{\Sigma_{A-} + (\omega - \omega_{\vec{k}})\Sigma'_{A-}}{(\omega - \Omega_{\vec{k}})(\omega - \Omega^-_{\vec{k}})}, \tag{4.119}$$

valid to order $1/d$. Here we have used the abbreviations $\Omega^-_{\vec{k}}$, $\Sigma_{N\pm}$ and $\Sigma'_{N\pm}$ introduced in eq. (4.99) and (4.80) and similar ones for the anomalous self-energy. Additionally, to order $1/d$ we see that the anomalous self-energy have the property: $\Sigma_{A+} = \Sigma_{A-}$ and $\Sigma'_{A+} = \Sigma'_{A-}$. Putting together all the above information in (4.115) we have the susceptibility in the vicinity of $\omega = \omega_{\vec{k}}$

$$\begin{aligned}\tilde{\chi}_\alpha(\vec{k},\omega) = (u_{\vec{k}} + v_{\vec{k}})^2(1 - 2R_1 - 8R_2)\times \\ \left\{ \frac{1}{\omega - \Omega_{\vec{k}}} \left[(1 - \Sigma'_{N+})^{-1} - 2\frac{\Sigma_{A+} - \omega_{\vec{k}}\Sigma'_{A+} + \Omega_{\vec{k}}\Sigma'_{A+}}{\Omega_{\vec{k}} + \Omega^-_{\vec{k}}} \right] \right. \\ \left. - \frac{1}{\omega + \Omega^-_{\vec{k}}} \left[(1 + \Sigma'_{N-})^{-1} - 2\frac{\Sigma_{A+} - \omega_{\vec{k}}\Sigma'_{A+} - \Omega^-_{\vec{k}}\Sigma'_{A+}}{\Omega_{\vec{k}} + \Omega^-_{\vec{k}}} \right] \right\}. \end{aligned} \tag{4.120}$$

From the above expression we can easily identify the pole weight corresponding to $\Omega_{\vec{k}}$ as

$$\mathcal{Z}_{\vec{k}} = (u_{\vec{k}} + v_{\vec{k}})^2 \left[1 + \Sigma'_{N+} - \frac{\Sigma_{A+}}{\omega_{\vec{k}}} - 2R_1 - 8R_2 \right]. \tag{4.121}$$

We can perform a similar analysis in the vicinity of the negative-energy pole $-\Omega_{\vec{k}}$. This will require expanding the self-energies in the vicinity of $-\omega_{\vec{k}}$ and eventually we will be lead to an expression similar as that of above with Σ'_{N-} and Σ_{A-} instead.

Inserting the expressions of the self-energies evaluated in eqs. (4.100)–(4.104) and eqs. (4.83)–(4.86), we obtain the explicit expression for the pole weight:

$$\mathcal{Z}_{\vec{k}} = \frac{J}{\omega_{\vec{k}}} \left\{ 1 - \frac{q^2}{2d} \left[7 + \frac{1 + \gamma_{\vec{k}} - 2\gamma_{\vec{k}}q + \gamma^2_{\vec{k}}q}{1 + 2\gamma_{\vec{k}}q} \right] \right\}. \tag{4.122}$$

This expression is singular at the bare critical point, i.e., $q = 1/2$ and $\gamma_{\vec{k}} = -1$. However the physical pole weight must diverge for $\Omega_{\vec{k}} \to 0$ (instead of $\omega_{\vec{k}} \to 0$). We thus expect

$$\mathcal{Z}_{\vec{k}} = \frac{J}{\Omega_{\vec{k}}} \mathcal{W}_{\vec{k}}, \tag{4.123}$$

such that $\mathcal{W}_{\vec{k}}$ has a regular $1/d$ expansion. Using this form of expression and after a few steps of algebra we find:

$$\mathcal{W}_{\vec{k}} = 1 - \frac{q^2}{2d}(6 + \gamma_{\vec{k}}) + \mathcal{O}\left(\frac{1}{d^2}\right). \tag{4.124}$$

This expression is analytic everywhere including the quantum critical point such that we have the pole weight diverging only at criticality at $\vec{Q}$. The imaginary part of the dynamic spin susceptibility (4.120) gives the dynamic structure factor:

$$S_S(\omega, \vec{k}) = 3\mathcal{Z}_{\vec{k}}\delta(\omega - \Omega_{\vec{k}}) + 3\mathcal{Z}^-_{\vec{k}}\delta(\omega + \Omega^-_{\vec{k}}) \tag{4.125}$$

where $\mathcal{Z}^-_{\vec{k}}$ is the pole weight of $\Omega^-_{\vec{k}}$ and the factor of 3 corresponds to the three degenerate modes. We have plotted the dynamic structure factor in fig. 4.10. We can see that the maximum spectral weight corresponding to $\Omega_{\vec{k}}$ occurs at $\vec{Q}$ upon approaching the critical point, which is related to the antiferromagnetic ordering for $q > q_c$. In the limit $q \to 0$, the spectral weight is equally distributed at all momenta, which is expected because in this limit the triplon dispersion becomes dispersionless.

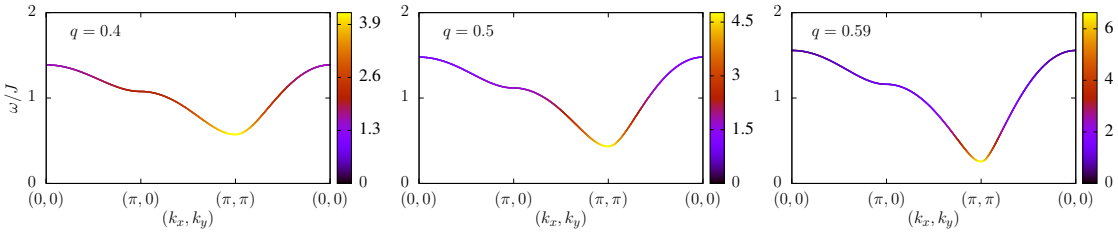

Figure 4.10: Dynamic structure factor (4.125) is plotted for different values of q in the symmetric case, $\kappa = 0$. The curve traces the triplon dispersion (4.87) and the corresponding single-mode spectral weight (4.123) is color-coded on top. There is no broadening in this approximation and the width of the curves is just for better visualization. Notice that the spectral weight is maximum near $\vec{Q}$ as we go close to the critical point.

4.5.7 Bond-bond correlation

Another dynamical quantity of interest is the bond-bond correlation. This observable will be of particular interest in the ordered phase. It could be observed in a scattering experiment. However its signal might be difficult to extract, since it represents a correlation between the square of spin operators. But nevertheless, we as theorist can calculate it. Analogous to the spin-spin correlation, at $T = 0K$ bond-bond correlation is defined as

$$\chi_{\mathcal{B}}(\vec{k},\omega) = -i\int_{-\infty}^{\infty} dt e^{i\omega t}\langle T_t \mathcal{B}_{\vec{k}}(t)\mathcal{B}_{-\vec{k}}(0)\rangle\,, \tag{4.126}$$

where T_t is time-ordering operator and

$$\mathcal{B}_i = \vec{S}_i \cdot \vec{S}_{i+d}\,, \tag{4.127}$$

$$\mathcal{B}_{\vec{k}} = \frac{1}{\sqrt{N}}\sum_i \mathcal{B}_i e^{-i\vec{k}\cdot\vec{r}_i}\,, \tag{4.128}$$

such that $\mathcal{B}_i$ represents the bond between adjacent sites i and $i+d$.

Let us first consider the inter-planar case, i.e. intra-dimer bonds. In this case, $\vec{S}_i$ and $\vec{S}_{i+d}$ correspond to $\vec{S}_{1i}$ and $\vec{S}_{2i}$ respectively. So,

$$\mathcal{B}_i = \vec{S}_{1i}\cdot\vec{S}_{2i} = \sum_{\alpha=x,y,z} t^{\dagger}_{i\alpha}t_{i\alpha} - \frac{3}{4}\,. \tag{4.129}$$

We will again work in the single-mode approximation i.e. we will not consider contributions due to continua. This technically means that in the product $\mathcal{B}_{\vec{k}}\mathcal{B}_{-\vec{k}}$ we will neglect all those terms which have more than two triplon operators. Following the steps involved in the calculation of the dynamic spin susceptibility, we are then lead to the following expression for the inter-layer bond-bond correlation in the disordered phase:

$$\chi^{dis}_{inter}(\vec{k},\omega) = N\left[\frac{9}{16} - \frac{9}{2}R_2 + \mathcal{O}(1/d^2)\right]\delta_{\vec{k},0}\delta(\omega)\,. \tag{4.130}$$

We do not see any single-mode weight in this sector apart from the Bragg peak at $\omega = 0$.

Let us now turn our attention to the intra-planar case where we consider correlation between bonds formed by nearest neighbor $\vec{S}_1$ (or $\vec{S}_2$) spins. Just as in the case of dynamical spin susceptibility here as well we have two scenarios: even channel and odd channel. In the even channel,

$$\mathcal{B}_i^d = \vec{S}_i \cdot \vec{S}_{i+d} = \vec{S}_{1,i} \cdot \vec{S}_{1,i+d} + \vec{S}_{2,i} \cdot \vec{S}_{2,i+d} \,. \tag{4.131}$$

Here, in the disordered phase, in the even channel we thus have:

$$\begin{aligned} \mathcal{B}_i^d = \frac{1}{2} \Bigg[& \sum_{\alpha} (t_{i,\alpha}^\dagger P_i P_{i+d} t_{i+d,\alpha} + t_{i,\alpha}^\dagger P_i t_{i+d,\alpha}^\dagger P_{i+d} + h.c.) \\ & + \sum_{\alpha,\beta} (t_{i,\alpha}^\dagger t_{i+d,\beta}^\dagger t_{i,\beta} t_{i+d,\alpha} - t_{i,\alpha}^\dagger t_{i+d,\alpha}^\dagger t_{i,\beta} t_{i+d,\beta}) \Bigg] \,. \end{aligned} \tag{4.132}$$

Note that in the above expression all the terms are at least bilinear in t and hence these will give only a continuum.

In the odd sector,

$$\mathcal{B}_i^d = \vec{S}_{1,i} \cdot \vec{S}_{1,i+d} - \vec{S}_{2,i} \cdot \vec{S}_{2,i+d} \,. \tag{4.133}$$

Here again we observe that $\mathcal{B}_i^d$ is at least bilinear in t. Hence to leading order in $1/d$ there is no single particle contribution but only a continuum.

4.6 Connection to perturbation theory in small K/J

As an important cross-check for our $1/d$ expansion, we compare our results with those obtained from a series expansion in small $k = K/J$. In the combined limit $d \to \infty$ and $q \to 0$ the two approaches should give same results. To accomplish this task, we first need to perform an expansion of our results in small q on top of the obtained $1/d$ expansion. Also, the series expansion in small k must be performed at an arbitrary dimension d.

In the following we quote the series expansion in small k for the triplon dispersion and the ground-state energy obtained by K. Coester and K. P. Schmidt (TU-Dortmund) using the perturbative continuous unitary transformations (pCUTs) [64, 65]. Starting

with the triplon dispersion, we have

$$\begin{aligned}
\frac{\Omega_{\vec{k}}}{J} &= 1 + d\gamma_{\vec{k}}\, k + \left\{ \left[1 + (-1+\gamma_{\vec{k}})\kappa^2\right] d - \frac{{\gamma_{\vec{k}}}^2}{2} d^2 \right\} k^2 + \left\{ \left[\frac{3\,\gamma_{\vec{k}}}{8} + \frac{5}{8} + \big(-1+\gamma_{\vec{k}}\big)\kappa^2 \right] d \right. \\
&+ \left. \left[-\gamma_{\vec{k}} - \frac{{\gamma_{\vec{k}}}^2}{2} + \big(2\,{\gamma_{\vec{k}}}^2 - 2\,\gamma_{\vec{k}}\big)\kappa^2 \right] d^2 + \frac{{\gamma_{\vec{k}}}^3}{2} d^3 \right\} k^3 \\
&+ \left\{ \left[\frac{11\,\gamma_{\vec{k}}}{16} - \frac{9}{16} + \big(-\frac{3\,\gamma_{2\vec{k}}}{8} + \frac{3\,\gamma_{\vec{k}}}{8}\big)\kappa^2 + \big(\frac{3}{4} - \frac{3\,\gamma_{\vec{k}}}{4}\big)\kappa^4 \right] d \right. \\
&+ \left[-\frac{15\,{\gamma_{\vec{k}}}^2}{16} - \frac{11\,\gamma_{\vec{k}}}{8} + \frac{5}{16} + \big(-\frac{17}{8} + \frac{39\,{\gamma_{\vec{k}}}^2}{8} - \frac{11\,\gamma_{\vec{k}}}{4}\big)\kappa^2 + \big(-\frac{1}{4} - \frac{\gamma_{\vec{k}}}{2} + \frac{3\,{\gamma_{\vec{k}}}^2}{4}\big)\kappa^4 \right] d^2 \\
&+ \left. \left[\frac{3\,{\gamma_{\vec{k}}}^2}{2} + \frac{{\gamma_{\vec{k}}}^3}{2} + \big(-\frac{3\,{\gamma_{\vec{k}}}^2}{2} + \frac{3\,{\gamma_{\vec{k}}}^3}{2}\big)\kappa^2 \right] d^3 - \frac{5\,{\gamma_{\vec{k}}}^4}{8} d^4 \right\} k^4 \\
&+ \left\{ \left[-\frac{125\,\gamma_{\vec{k}}}{128} - \frac{3\,\gamma_{2\vec{k}}}{64} - \frac{45}{64} + \big(1 - \frac{17\,\gamma_{\vec{k}}}{16} + \frac{\gamma_{2\vec{k}}}{16}\big)\kappa^2 + \big(\frac{5}{4} - \frac{9\,\gamma_{\vec{k}}}{16} - \frac{11\,\gamma_{2\vec{k}}}{16}\big)\kappa^4 \right] d \right. \\
&+ \left[\frac{83\,\gamma_{\vec{k}}}{64} - \frac{15\,{\gamma_{\vec{k}}}^2}{16} - \frac{17}{64} + \big(-\frac{21}{8} - \frac{3\,\gamma_{\vec{k}}\,\gamma_{2\vec{k}}}{2} + \frac{33\,{\gamma_{\vec{k}}}^2}{8}\big)\kappa^2 + \big(-\frac{3}{4} + \frac{7\,{\gamma_{\vec{k}}}^2}{8} - \frac{\gamma_{\vec{k}}}{8}\big)\kappa^4 \right] d^2 \\
&+ \left[\frac{\gamma_{\vec{k}}}{32} + \frac{35\,{\gamma_{\vec{k}}}^2}{16} + \frac{33\,{\gamma_{\vec{k}}}^3}{32} + \big(\frac{81\,{\gamma_{\vec{k}}}^3}{8} - \frac{45\,\gamma_{\vec{k}}}{8} - \frac{9\,{\gamma_{\vec{k}}}^2}{2}\big)\kappa^2 \right. \\
&+ \left. \big(-\frac{19\,{\gamma_{\vec{k}}}^2}{4} + \frac{5\,\gamma_{\vec{k}}}{8} + \frac{33\,{\gamma_{\vec{k}}}^3}{8}\big)\kappa^4 \right] d^3 \\
&+ \left. \left[-\frac{5\,{\gamma_{\vec{k}}}^3}{2} - \frac{3\,{\gamma_{\vec{k}}}^4}{4} + \big({\gamma_{\vec{k}}}^4 - {\gamma_{\vec{k}}}^3\big)\kappa^2 \right] d^4 + \frac{7\,{\gamma_{\vec{k}}}^5}{8} d^5 \right\} k^5 + \mathcal{O}(k^6)\,. \qquad (4.134)
\end{aligned}$$

Now rewriting the square of the above expression in terms of q we obtain

$$\begin{aligned}
\frac{\Omega_{\vec{k}}^2}{J^2} &= 1 + 2\,\gamma_{\vec{k}}\, q + \frac{1}{d}\Big\{ \Big(2\,\gamma_{\vec{k}}\,\lambda^2 - 2\,\lambda^2 + 2\Big) q^2 + \Big(6\,\lambda^2 {\gamma_{\vec{k}}}^2 - 6\,\gamma_{\vec{k}}\,\lambda^2 - {\gamma_{\vec{k}}}^2\Big) q^3 \\
&+ \Big(6\,\lambda^2 {\gamma_{\vec{k}}}^3 - 6\,\lambda^2 {\gamma_{\vec{k}}}^2\Big) q^4 + \Big(4\,\lambda^2 {\gamma_{\vec{k}}}^4 - 4\,\lambda^2 {\gamma_{\vec{k}}}^3\Big) q^5 + \mathcal{O}(q^6) \Big\} + \mathcal{O}\left(\frac{1}{d^2}\right). \qquad (4.135)
\end{aligned}$$

We get exactly the same result after performing the double expansion in q in eq. (4.90).

Now let us consider the following expression for the ground-state energy obtained from pCUT:

$$\begin{aligned}
\frac{E_0}{JN} &= -\frac{3}{4} - \frac{3}{8} d\, k^2 - \frac{3}{16} d\, k^3 + \Big(\frac{21}{128} d - \frac{9}{64} d^2\Big) k^4 + \Big(\frac{57}{256} d - \frac{3}{64} d^2\Big) k^5 \\
&+ \Big(-\frac{2781}{1024} d - \frac{7}{256} \kappa^2 d + \frac{273}{64} d^2 + \frac{7}{128} \kappa^2 d^2 - \frac{357}{256} d^3 - \frac{1}{32} \kappa^2 d^3\Big) k^6 \\
&+ \Big(-\frac{73293}{16384} d - \frac{353}{1024} d\kappa^2 + \frac{53205}{8192} d^2 + \frac{899}{1536} d^2 \kappa^2 - \frac{8499}{4096} d^3 - \frac{97}{384} d^3 \kappa^2\Big) k^7 + \mathcal{O}(k^8)\,. \qquad (4.136)
\end{aligned}$$

Again, converting the above expression in terms of q we get

$$\begin{aligned}
\frac{E_0}{JN} &= -\frac{3}{4} - \frac{3}{8}\frac{q^2}{d} + \left(-\frac{3}{16}\, q^3 + \frac{9}{64}\, q^4\right) \frac{1}{d^2} \\
&+ \left(\frac{21}{128}\, q^4 - \frac{3}{64}\, q^5 - \frac{357}{256}\, q^6 - \frac{1}{32}\, \lambda^2 q^6\right) \frac{1}{d^3} + \mathcal{O}\left(\frac{1}{d^4}\right). \qquad (4.137)
\end{aligned}$$

A comparison to eq. (4.73) again shows the agreement. In fact the ground-state energy obtained in $1/d$ expansion already has a structure of a small q expansion. However this is not a generic feature and is a property of the model-dependent selection rules. The model-dependent selection rules can be used to prove [66] that only terms up to order q^{2m} contribute to the $1/d^m$ term in E_0, such that the above expression represents the complete expansion up to $1/d^3$ of E_0.

We have thus seen that the two different methods are consistent in their combined regime of validity which provides an independent check for our $1/d$ expansion results.

4.7 Connection to Brueckner approach

In chapter 2 we discussed a few approaches to take into account the hard-core constraint. We argued that using projection operator we can conveniently generate $1/d$ expansion and in fact we have already seen this in the present chapter. In section 4.5.5 we calculated the triplon density and found that it scales as $1/d$. This means that in the large-d limit, the triplet density can be treated as a small parameter. We know one successful method in the literature, namely the Brueckner approach [41], which relies on small triplet density. So an interesting question arises whether there is any relation with our $1/d$ expansion. In the following, we will show that one can extract our $1/d$ expansion for triplon dispersion from Brueckner approach. We will explicitly demonstrate the calculation for the symmetric case, $\kappa = 0$, only. Furthermore, we will also discuss the differences between the two approaches.

The Brueckner approach, as proposed in ref. [41], treats the hard-core constraint by introducing an infinite onsite repulsion term,

$$\mathcal{H}_U = U \sum_{i\alpha\beta} t^\dagger_{i\alpha} t^\dagger_{i\beta} t_{i\alpha} t_{i\beta}, \quad U \to \infty \,, \tag{4.138}$$

in the triplon Hamiltonian (without projectors). A renormalized quartic vertex is obtained in the limit of large-U after a self-consistent ladder summation [41]. The vertex function is then given by

$$\Gamma(\vec{k}, \omega) = -\left(\frac{1}{N} \sum_{\vec{p}} \frac{u^2_{\vec{p}} u^2_{\vec{k}-\vec{p}}}{\omega - \omega_{\vec{p}} - \omega_{\vec{k}-\vec{p}}} \right)^{-1} . \tag{4.139}$$

Apart from this there would be some anomalous scattering vertices which have been neglected. A simple justification is that all these contributions will be small compared to the above vertex in the small-density limit. In the language of large-d, the additional vertices have factors of v^2_k which means that upon momentum summation these diagrams would be suppressed by one order higher in $1/d$ compared to the above vertex.

Let us calculate the triplon dispersion using the self-energy obtained from the above vertex, as well as that from the quartic terms in the triplon Hamiltonian. Note that these are only the terms in the first line of eq. (4.18), while those in the other lines arise from the projectors and are absent here. An important methodological difference here

is that all the diagrammatics is done for the t particles, i.e., the following self-energies and propagators are those of t particles as opposed to τ particles.

To leading order, the normal self-energy from $\mathcal{H}_U$ is given by the sum of Hartree and Fock diagrams:

$$\begin{aligned}\Sigma^U_\alpha(\vec{k},\omega) &= \Sigma_{\alpha\alpha}(\vec{k},\omega) + \sum_\beta \Sigma_{\alpha\beta}(\vec{k},\omega)\,,\\ \Sigma_{\alpha\beta}(\vec{k},\omega) &= \frac{1}{N}\sum_{\vec{q}} v^2_{\vec{q}\beta}\Gamma_{\alpha\beta,\alpha\beta}(\vec{k}+\vec{q},\omega-\omega_{\vec{q}\beta}).\end{aligned} \tag{4.140}$$

Spin indices α,β are written here for book-keeping purposes only; both the Γ vertex and the self-energies do not depend on α,β in the paramagnetic phase.

We see that the self-energy expression involves a factor of v^2_k under the momentum summation. This is already a source for a factor of $1/d$ (recall that $v^2_k \propto \gamma^2_{\vec{k}}$) and so to obtain the self-energy to order $1/d$ we have to evaluate the vertex function Γ only to order $1/d^0$. For this purpose we can approximate $u^2_{\vec{k}} = 1$, $v^2_{\vec{k}} = 0$, and the mode energy $\omega_{\vec{p}} = J$, such that eq. (4.139) immediately gives

$$\Gamma(\vec{k},\omega) = -(\omega - 2J) + \mathcal{O}\left(\frac{1}{d}\right)\,. \tag{4.141}$$

The normal self-energy in eq. (4.140) is

$$\Sigma^U_N(\vec{k},\omega) = -\frac{q^2(\omega-3J)}{2d} \tag{4.142}$$

up to order $1/d$, where we have again set the mode energy to J and used the momentum-summation result (D.4). Apart from this there is also an anomalous self-energy contribution from the Γ vertex [67] which contributes to order $1/d$. This is given by:

$$\Sigma^U_A(\vec{k},\omega) = \frac{1}{N}\sum_{\vec{p}} u_{\vec{p}} v_{\vec{p}} \Gamma(0,0)\,. \tag{4.143}$$

Again, evaluating this in the large-d and using eq. (D.3), we find:

$$\Sigma^K_A(\vec{k},\omega) = \frac{1}{N}\sum_{\vec{p}} u_{\vec{p}} v_{\vec{p}} 2J = J\frac{q^2}{2d}\,. \tag{4.144}$$

Along with the above diagrammatic contributions coming from the hard-core repulsion term, we need to consider the quartic terms in the triplon Hamiltonian (those which do not arise from projectors). These are treated at Hartree-Fock level [41]. This is equivalent to drawing one-loop diagrams for each of these quartic vertex, or normal-ordering in the τ basis. Summing all self-energy contributions we then have:

$$\Sigma_N(\vec{k},\omega) = -\frac{q^2(\omega-3J)}{2d} + 2\gamma_{\vec{k}} J R_4\,, \tag{4.145}$$

$$\Sigma_A(\vec{k},\omega) = J\frac{q^2}{2d} - 2\gamma_{\vec{k}} J R_3\,. \tag{4.146}$$

Solving the Dyson equation for the t particles and retaining the coherent part we obtain

$$\mathcal{G}(\vec{k},\omega) = \frac{\omega Z^{-1} + A_{\vec{k}} + \Sigma_N(\vec{k},0)}{\omega^2\big(Z^{-2} - \Sigma_A'^2(\vec{k},0)\big) - \big(A_{\vec{k}} + \Sigma_N(\vec{k},0)\big)^2 + \big(B_k + \Sigma_A(\vec{k},0)\big)^2} \tag{4.147}$$

where

$$Z^{-1} = 1 - \frac{\partial\Sigma_N(\vec{k},\omega)}{\partial\omega}|_{\omega=0} = 1 + \frac{q^2}{2d}\,, \tag{4.148}$$

$$\Sigma_A'(\vec{k},0) = \frac{\partial\Sigma_A(\vec{k},\omega)}{\partial\omega}|_{\omega=0} = 0\,. \tag{4.149}$$

Note that unlike the treatment in section 4.5.2 in this case we have to consider the anomalous self-energy to evaluate the renormalized pole. This is because B_k is of order one and hence the last term involving the anomalous self-energy in the denominator of eq. (4.147) would contribute to order $1/d$. Therefore the pole equation from the t Green's function (4.147) is

$$\Omega_k^2 = \frac{\big(A_k + \Sigma_N(\vec{k},0)\big)^2 - \big(B_k + \Sigma_A(\vec{k},0)\big)^2}{Z^{-2} - \Sigma_A'^2(\vec{k},0)}\,. \tag{4.150}$$

Inserting the explicit expressions of self-energy in the above equation we obtain the expansion of the dispersion relation to order $1/d$,

$$\frac{\Omega_k^2}{J^2} = 1 + 2\gamma_{\vec{k}}q + \frac{1}{d}(2q^2 - \gamma_{\vec{k}}^2 q^3)\,. \tag{4.151}$$

This is the same result (4.87) (for $\kappa = 0$) derived in section 4.5.2.

Thus we have shown that indeed the Brueckner approximation is controlled in the large-d limit. However we do not see a transparent way to use it for generating a systematic $1/d$ expansion beyond the above result. This is because the Γ vertex becomes extremely complicated beyond the leading order. Moreover, as noted above this mode of calculation uses t particles for diagrammatics whereas to ensure Wick's theorem we must formulate the diagrammatics in terms of τ particles. For the same reason, this is not an appropriate way to calculate the ground-state energy.

4.8 Discussion

We have seen the recipe of generating $1/d$ expansion for a given observable. We also successfully calculated various static and dynamic observables for a coupled-dimer magnet on a hypercubic lattice with nearest neighbor interaction. We note that more complicated models with frustration can be treated in a similar way. To get an idea consider again the general Hamiltonian in eq. (4.1). Upon re-writing it in terms of bond operators, the coeffcients of the non-local bilinear, cubic, and quartic terms in the real-space bond-operator Hamiltonian (4.16) are related to the $K^{mm'}$ in eq. (4.1)

according to

$$\begin{aligned} K_2 &= (K^{11} + K^{22} - K^{12} - K^{21})/2, \\ K_3 &= (K^{11} - K^{22} + K^{12} - K^{21})/2, \\ K_4 &= (K^{11} + K^{22} + K^{12} + K^{21})/2. \end{aligned} \tag{4.152}$$

The model treated in this chapter corresponds to $K_2 = K_4 = K$ and $K_3 = \kappa K$.

Eq. (4.152) shows that the prefactor K_3 of the cubic piece vanishes provided that the model remains invariant if in every dimer the spins 1 and 2 are inter-changed (together with all their couplings). A non-vanishing cubic term occurs if this symmetry is broken, which applies, in addition to the asymmetric bilayer model [41], also, e.g., to the staggered dimer model [68, 69] and to the alternating chain model [56, 57].

Eq. (4.152) also shows that frustration, introduced by antiferromagnetic K^{12} and K^{21}, can induce large quartic couplings which consequently also produce large $1/d$ corrections.

As discussed in chapter 3, for exchange interactions beyond nearest-neighbor dimers one needs to define a large-d rescaling scheme for every interaction such that a non-trivial large-d limit is obtained. Also we then have to use the corresponding interaction structure factors introduced in chapter 3.

Chapter 5

Antiferromagnetic phase

In the last chapter, we introduced our new series expansion method using $1/d$, d being the spatial dimension, as a small parameter. Using the large-d formalism together with bond-operator theory we presented explicit calculations in the quantum paramagnetic (disordered) phase, which occurs for $q < q_c$ in the model of coupled-dimer magnets on a hypercubic lattice. Recall that $q = Kd/J$ where J is the intra-dimer interaction strength and K is the interaction strength between nearest neighbor dimers. In this chapter we will continue our quest to describe the entire zero-temperature phase diagram of coupled-dimers on a hypercubic lattice. To be precise, we will calculate observables in the antiferromagnetic (ordered) phase ($q > q_c$) using $1/d$ expansion and show that we can smoothly connect to the disordered phase at the critical point. Most importantly, we will show that using different criteria (for instance vanishing of gap and order-parameter) we obtain the same phase boundary (4.94) as derived in the last chapter and thus establish $1/d$ expansion as a consistent technique. In the limit of vanishing intra-dimer interaction strength J, our model reduces to nearest neighbor Heisenberg spin model (in this case for spin-1/2) on a hypercubic lattice, and spin-wave theory is an efficient description. We will show that our results reproduce the spin-wave theory results in the large-d limit. This also serves as another crosscheck for our method.

Our model Hamiltonian (4.2) introduced in the last chapter is invariant under continuous spin rotations. In the quantum paramagnetic phase this symmetry is preserved. However, for $q > q_c$ this symmetry ($SU(2)$) is spontaneously broken and the system develops a long-range order. Consequently, the system now has gapless excitations (magnons) as expected from the Goldstone's theorem (see chapter 1). In fact there are two degenerate transverse gapless modes as well as a gapped longitudinal/amplitude mode. We have already discussed these kinds of excitations within the Mexican-hat picture in chapter 1. We point out that the amplitude mode is often refered to as the 'Higgs mode'[1] in condensed matter physics. We will characterize these modes and calculate their dispersion and spectral weights within the $1/d$ formalism. The gapped amplitude mode goes soft at the critical point, and using this criterion we will derive the phase boundary as in the last chapter. Apart from this, we note that in this case the order parameter of the phase is staggered magnetization. It is zero in the param-

[1]There is no Higgs mechanism at work here but the name has stuck because this mode is also gapped in the ordered phase just as the Higgs mode.

agnetic phase and spontaneously attains non-zero value in the ordered phase owing to symmetry breaking according to the Landau theory of continuous phase transitions. Again we will write a $1/d$ expansion for the staggered magnetization. We will show that we obtain the same phase boundary from the condition that the order parameter goes to zero at the critical point. The following discussion in this chapter is largely based on ref. [70].

5.1 Model Hamiltonian

In this chapter we will consider only the symmetric case[2] of our Hamiltonian (4.2). We shall introduce a staggered field[3], which couples to the operator corresponding to our order parameter. We will thus work with the following Hamiltonian:

$$\begin{aligned}\mathcal{H} = J\sum_i \vec{S}_{i1}\cdot\vec{S}_{i2} + K\sum_{\langle ii'\rangle}(\vec{S}_{i1}\cdot\vec{S}_{i'1} + \vec{S}_{i2}\cdot\vec{S}_{i'2}) \\ + h^z\sum_i e^{i\vec{Q}\cdot R_i}(S^z_{i1} - S^z_{i2})\,. \end{aligned} \tag{5.1}$$

Here, $\sum_{\langle ii'\rangle}$ denotes a summation over pairs of nearest-neighbor dimer sites and h^z denotes the staggered field which couples to the collinear AF order parameter at $\vec{Q} = (\pi, \pi, \ldots)$. It is important to note that there is a non-trivial quantum phase transition to the disordered phase only in the limit of vanishing staggered field. Therefore throughout this chapter all the quantities relevant in the context of quantum phase transition will be evaluated for $h^z = 0$. Nevertheless, we shall quote the general results for non-zero h^z wherever possible. We will see in the following that now the appropriate reference state is given by a linear combination of singlet and one of the triplet states. Thus the above spin Hamiltonian will not be transformed into the same triplon Hamiltonian as in the last chapter, but we will have to work with *generalized triplons*. These generalized triplons will be the excitations on top of the reference state in the ordered phase.

5.2 Reference state and bond operators

For antiferromagnetic inter-dimer interaction K we have a collinear antiferromagnetic phase with ordering wavevector $\vec{Q} = (\pi, \pi, \ldots)$ when $q > q_c$. Now the description in terms of spin-1 excitations, triplons, on top of singlet background is not correct since as noted in the last chapter the triplon excitation energy is imaginary in the ordered phase. Instead we have to choose another suitable reference state. When K is dominant interaction (i.e. $q \to \infty$), a Néel state is realized in both the layers[4] with

[2]The asymmetric case is not very different but we do not consider it in order to avoid lengthy algebra. Also qualitatively it does not add anything interesting.

[3]We are interested in the zero field case, but to facilitate calculations we have introduced this field, which will be set to zero in the end. Often this trick is called the method of sources [5].

[4]Here the word layer is used to denote the network of $\vec{S}_1$ or $\vec{S}_2$ spins. Its usage is motivated from $2d$ where our model is that of square-lattice bilayer, and in that case we have a square lattice layer of $\vec{S}_1$ spins and $\vec{S}_2$ spins. Wherever we use the word layer it is in the general sense in d dimensions.

opposite spin orientation in the two layers. If we assume the staggered magnetization to be in the $\hat{z}$ direction then we have $|\uparrow\downarrow\rangle$ and $|\downarrow\uparrow\rangle$ states on alternating dimer sites, i.e. the reference state would be proportional to $(|t_0\rangle \pm |t_3\rangle)$ on alternating sites. It is therefore clear that for any q in the ordered phase we require a q dependent linear combination of $|t_0\rangle$ and $|t_3\rangle$. In other words we will have a condensation[5] of t_3 triplon in this phase. Moreover, since this is a collinear state we can express the spin orientation as (assuming the staggered magnetization is in the $\hat{z}$ direction):

$$\langle \vec{S}_{1,i} \rangle = -\langle \vec{S}_{2,i} \rangle \propto \cos \vec{Q} \cdot \vec{r}_i \hat{z} = e^{\vec{Q}\cdot\vec{r}_i} \hat{z} \tag{5.2}$$

where the last equality holds because of the fact that $\vec{Q} \cdot \vec{r}_i = \pm 1$ on alternating sites, and the proportionality constant is given by the staggered magnetization. Using all this information we can now write down a Hilbert-space rotation involving a single real-condensate parameter λ:

$$|\tilde{t}_0\rangle_i = (|t_0\rangle_i + \lambda_i |t_3\rangle_i)/\sqrt{1+\lambda^2}\,, \tag{5.3}$$

$$|\tilde{t}_3\rangle_i = (|t_3\rangle_i - \lambda_i |t_0\rangle_i)/\sqrt{1+\lambda^2}\,, \tag{5.4}$$

$$|\tilde{t}_1\rangle_i = |t_1\rangle_i,\ |\tilde{t}_2\rangle_i = |t_2\rangle_i\,, \tag{5.5}$$

with $\lambda_i = \lambda e^{i\vec{Q}\cdot\vec{r}_i} = \pm\lambda$. Thus the reference state in this phase is

$$|\tilde{\psi}_0\rangle = \prod_i |\tilde{t}_0\rangle_i\,. \tag{5.6}$$

At this point we do not know the functional form of λ and later we will define a precise way to determine it. We will see that λ acquires a $1/d$ expansion and these corrections play a crucial role in determining corrections to other observables. It is interesting to note here that this bears similarity to the reference state of a non-collinear phase in the spin-wave theory. For instance, in case of an antiferromagnet in a uniform field there is a canted state and the moment orientation receives systematic $1/S$ corrections which influences other observables. We also note that the reference state introduced here can not be used to describe the physics in a uniform field, as it yields zero net magnetization. In case of uniform field it turns out that one has to condense $|t_1\rangle + \imath|t_2\rangle$ which has been described in Ref. [43] at the level of linear bond-operator theory. We leave the corresponding $1/d$ expansion for future work.

In terms of general Hilbert-space rotation introduced in chapter 2, for the above transformation we have the rotation matrix

$$U^{(i)} = \begin{pmatrix} c\lambda_i & 0 & 0 & s\lambda_i \\ 0 & 1 & 0 & 0 \\ 0 & 0 & 1 & 0 \\ -s\lambda_i & 0 & 0 & c\lambda_i \end{pmatrix}, \tag{5.7}$$

with $s\lambda_i = \sin\tan^{-1}\lambda_i$ and $c\lambda_i = \cos\tan^{-1}\lambda_i$. Apparently, $|\tilde{t}_0\rangle_i$ smoothly interpolates between a singlet for $\lambda = 0$ and a $\hat{z}$-oriented Néel configuration for $\lambda = \pm 1$. We will consider $\lambda \in [0, 1]$.

[5]Here the word condensation is used in the sense that $\langle t_3 \rangle \neq 0$, where the expectation value is taken with respect to the reference state in this phase.

We shall call our reference state, $|\tilde{t}_0\rangle$, as *generalized singlet* state and $|\tilde{t}_\alpha\rangle$ ($\alpha = 1,2,3$) states as *generalized triplet* states. As in the case of disordered phase we can introduce Bosonic operators to create these generalized triplet states over the reference state as follows:

$$\tilde{t}_1^\dagger|\tilde{t}_0\rangle = |\tilde{t}_1\rangle\,; \quad \tilde{t}_2^\dagger|\tilde{t}_0\rangle = |\tilde{t}_2\rangle\,; \quad \tilde{t}_3^\dagger|\tilde{t}_0\rangle = |\tilde{t}_3\rangle\,. \tag{5.8}$$

These operators obey the usual Bosonic commutation relations:

$$\left[\tilde{t}_i, \tilde{t}_j^\dagger\right] = \delta_{i,j}\,; \quad \left[\tilde{t}_i, \tilde{t}_j\right] = \left[\tilde{t}_i^\dagger, \tilde{t}_j^\dagger\right] = 0\,. \tag{5.9}$$

It is easy to interpret the excitations created by these operators. Observe that $\tilde{t}_{i1,2}^\dagger \equiv \tilde{t}_{ix,y}^\dagger$ corresponds to *transverse* (or single spin-flip) excitations which will yield the Goldstone modes of the ordered phase. On the other hand $\tilde{t}_{i3}^\dagger \equiv \tilde{t}_{iz}^\dagger$ is a gapped *longitudinal/amplitude* excitation. We will see concrete results describing these excitations in following sections.

Just as in the case of triplons used in the last chapter, these operators have to obey the hard-core constraint

$$\sum_{\alpha=1}^{3} \tilde{t}_\alpha^\dagger \tilde{t}_\alpha \leq 1\,. \tag{5.10}$$

Analogous to the disordered phase we will implement this hard-core constraint via the projection operator:

$$P_i = 1 - \sum_{\gamma=1}^{3} \tilde{t}_\gamma^\dagger \tilde{t}_\gamma\,. \tag{5.11}$$

Using the projection operator we can write the transition between the states in the Hilbert-space as follows (same as explained in chapter 2):

$$\begin{aligned} |\tilde{t}_0\rangle_{i\ i}\langle\tilde{t}_0| &= P_i\,, & |\tilde{t}_\alpha\rangle_{i\ i}\langle\tilde{t}_0| &= \tilde{t}_{i\alpha}^\dagger P_i\,, \\ |\tilde{t}_0\rangle_{i\ i}\langle\tilde{t}_\alpha| &= P_i\tilde{t}_{i\alpha}\,, & |\tilde{t}_\alpha\rangle_{i\ i}\langle\tilde{t}_\beta| &= \tilde{t}_{i\alpha}^\dagger\tilde{t}_{i\beta}\,. \end{aligned} \tag{5.12}$$

With this information and the rotation matrix quoted above, it is now possible to express the spin operators in terms of the generalized triplon operators:

$$\begin{aligned} S_{i1,2}^x = \frac{1}{2\sqrt{1+\lambda^2}}\Big[&\pm \tilde{t}_{ix}^\dagger P_i \pm P_i\tilde{t}_{ix} \mp \lambda e^{-\imath\vec{Q}\cdot\vec{r}_i}\tilde{t}_{ix}^\dagger\tilde{t}_{iz} \mp \lambda e^{\imath\vec{Q}\cdot\vec{r}_i}\tilde{t}_{iz}^\dagger\tilde{t}_{ix} \\ &- \imath\lambda e^{\imath\vec{Q}\cdot\vec{r}_i}\tilde{t}_{iy}^\dagger P_i + \imath\lambda e^{-\imath\vec{Q}\cdot\vec{r}_i}P_i\tilde{t}_{iy} - \imath\tilde{t}_{iy}^\dagger\tilde{t}_{iz} + \imath\tilde{t}_{iz}^\dagger\tilde{t}_{iy}\Big]\,, \end{aligned} \tag{5.13}$$

$$\begin{aligned} S_{i1,2}^y = \frac{1}{2\sqrt{1+\lambda^2}}\Big[&\pm \tilde{t}_{iy}^\dagger P_i \pm P_i\tilde{t}_{iy} \mp \lambda e^{-\imath\vec{Q}\cdot\vec{r}_i}\tilde{t}_{iy}^\dagger\tilde{t}_{iz} \mp \lambda e^{\imath\vec{Q}\cdot\vec{r}_i}\tilde{t}_{iz}^\dagger\tilde{t}_{iy} \\ &+ \imath\lambda e^{\imath\vec{Q}\cdot\vec{r}_i}\tilde{t}_{ix}^\dagger P_i - \imath\lambda e^{-\imath\vec{Q}\cdot\vec{r}_i}P_i\tilde{t}_{ix} + \imath\tilde{t}_{ix}^\dagger\tilde{t}_{iz} - \imath\tilde{t}_{iz}^\dagger\tilde{t}_{ix}\Big]\,, \end{aligned} \tag{5.14}$$

$$\begin{aligned} S_{i1,2}^x = \frac{1}{2(1+\lambda^2)}\Big[&\pm (1-\lambda^2)\tilde{t}_{iz}^\dagger P_i \pm (1-\lambda^2)P_i\tilde{t}_{iz} \pm \lambda(e^{-\imath\vec{Q}\cdot\vec{r}_i} + e^{\imath\vec{Q}\cdot\vec{r}_i})P_i \\ &\mp \lambda(e^{-\imath\vec{Q}\cdot\vec{r}_i} + e^{\imath\vec{Q}\cdot\vec{r}_i})\tilde{t}_{iz}^\dagger\tilde{t}_{iz} + \imath(1+\lambda^2)(\tilde{t}_{iy}^\dagger\tilde{t}_{ix} - \tilde{t}_{ix}^\dagger\tilde{t}_{iy})\Big]\,. \end{aligned} \tag{5.15}$$

5.3 Hamiltonian and $1/d$ expansion strategy

Having expressed our spin operators in terms of the generalized triplon operators we are now in a position to write down the Hamiltonian in terms of $\tilde{t}$ for coupled-dimer model (5.1) on a hypercubic lattice. Even in this case we will perform a Bogoliubov transformation for leading-order bilinear part and use it as the unperturbed piece to set-up our perturbation theory. The Bogoliubov transformed operator will then be used to normal-order the rest of the Hamiltonian. An important complication in the ordered phase is that apart from the corrections arising from the interaction terms in the Hamiltonian there will be corrections as a result of λ. In this view we shall discuss our strategy to generate a $1/d$ expansion in this phase. All these aspects will be dealt with in detail in this section.

5.3.1 Real-space bond-operator Hamiltonian

The Hamiltonian of the model (5.1) in terms of the rotated bond operators $\tilde{t}_{i\alpha}$ is obtained using eq. (5.13)-(5.15). Our Hamiltonian now depends on the arbitrary condensate parameter λ. Inserting the projectors P_i (5.11), we can split the Hamiltonian with respect to number (n) of $\tilde{t}$ operators as follows:

$$\mathcal{H} = \mathcal{H}_0 + \mathcal{H}_1 + \mathcal{H}_2 + \mathcal{H}_3 + \mathcal{H}_4 + \mathcal{H}_5 + \mathcal{H}_6\,. \tag{5.16}$$

Thus $\mathcal{H}_n(\lambda)$ contains n triplon operators $\tilde{t}_{i\alpha}$ and it explicitly depends on the condensate parameter λ. While in the disordered phase only the asymmetric case contained $\mathcal{H}_n$ with odd-n, in the ordered phase we generically have $\mathcal{H}_n$ with odd-n as a consequence of Hilbert-space rotation. Most importantly unlike disordered phase there is also a linear piece in $\tilde{t}$.

It turns out that as in the case of disordered phase, terms only upto $\mathcal{H}_4$ are relevant for calculations to order $1/d$. We therefore list here the terms up to order four (recall $\lambda_i = \lambda e^{i\vec{Q}\cdot\vec{r}_i}$):

$$\mathcal{H}_0 = -\frac{NJ(3-\lambda^2)}{4(1+\lambda^2)} - \frac{2NKd\lambda^2}{(1+\lambda^2)^2} + \frac{2Nh^z\lambda}{1+\lambda^2}\,, \tag{5.17}$$

$$\mathcal{H}_1 = \sum_i e^{i\vec{Q}\cdot\vec{r}_i}\left[\frac{\lambda J}{1+\lambda^2} - \frac{2Kd\lambda(1-\lambda^2)}{(1+\lambda^2)^2} + \frac{h^z(1-\lambda^2)}{1+\lambda^2}\right](\tilde{t}^\dagger_{iz} + \tilde{t}_{iz})\,, \tag{5.18}$$

$$\begin{aligned}\mathcal{H}_2 = &\sum_{i,a}\left[\frac{J}{1+\lambda^2} - \frac{2\lambda h^z}{1+\lambda^2} + \frac{4Kd\lambda^2}{(1+\lambda^2)^2}\right]\tilde{t}^\dagger_{ia}\tilde{t}_{ia} + \sum_{\langle ii'\rangle,a}\frac{K(1-\lambda^2)}{1+\lambda^2}\tilde{t}^\dagger_{ia}\tilde{t}_{i'a}\\ &+ \sum_{\langle ii'\rangle,a}\frac{K}{2}(\tilde{t}^\dagger_{ia}\tilde{t}^\dagger_{i'a} + h.c.) + \sum_i\left[J\frac{1-\lambda^2}{1+\lambda^2} - \frac{4\lambda h^z}{1+\lambda^2} + \frac{8Kd\lambda^2}{(1+\lambda^2)^2}\right]\tilde{t}^\dagger_{iz}\tilde{t}_{iz}\\ &+ \sum_{\langle ii'\rangle}\frac{K(1-\lambda^2)^2}{2(1+\lambda^2)^2}\left(\tilde{t}^\dagger_{iz}\tilde{t}^\dagger_{i'z} + \tilde{t}^\dagger_{iz}\tilde{t}_{i'z} + h.c.\right)\,,\end{aligned} \tag{5.19}$$

$$\mathcal{H}_3 = \frac{2K}{1+\lambda^2}\sum_{\langle ii'\rangle}\lambda_i\left[\tilde{t}^\dagger_{ix}\tilde{t}^\dagger_{i'z}\tilde{t}_{i'x}+\tilde{t}^\dagger_{iy}\tilde{t}^\dagger_{i'z}\tilde{t}_{i'y}+h.c.\right]$$
$$-\frac{2K(1-\lambda^2)}{(1+\lambda^2)^2}\sum_{\langle ii'\rangle}\lambda_{i'}\left[\sum_\gamma \tilde{t}^\dagger_{iz}\tilde{t}^\dagger_{i'\gamma}\tilde{t}_{i'\gamma}+\tilde{t}^\dagger_{iz}\tilde{t}^\dagger_{i'z}\tilde{t}_{i'z}+h.c.\right]$$
$$+\left[\frac{2K\lambda(1-\lambda^2)}{(1+\lambda^2)^2}-\frac{J\lambda}{1+\lambda^2}-\frac{h^z(1-\lambda^2)}{1+\lambda^2}\right]\sum_{i,\gamma}e^{i\vec{Q}\cdot\vec{r}_i}\left[\tilde{t}^\dagger_{iz}\tilde{t}^\dagger_{i\gamma}\tilde{t}_{i\gamma}+h.c.\right], \qquad (5.20)$$

$$\mathcal{H}_4 = -\frac{K}{2(1+\lambda^2)}\sum_{\langle ii'\rangle,a}\Bigg[2\sum_\gamma\left[(1+\lambda^2)\tilde{t}^\dagger_{ia}\tilde{t}^\dagger_{i'a}\tilde{t}^\dagger_{i'\gamma}\tilde{t}_{i'\gamma}+(1-\lambda^2)\tilde{t}^\dagger_{ia}\tilde{t}^\dagger_{i'\gamma}\tilde{t}_{i'\gamma}\tilde{t}_{i'a}\right]$$
$$+(1+\lambda^2)\tilde{t}^\dagger_{ia}\tilde{t}^\dagger_{i'a}\tilde{t}_{iz}\tilde{t}_{i'z}-(1-\lambda^2)\tilde{t}^\dagger_{ia}\tilde{t}^\dagger_{i'z}\tilde{t}_{iz}\tilde{t}_{i'a}+h.c.\Bigg]$$
$$-\frac{K}{2(1+\lambda^2)^2}\sum_{\langle ii'\rangle}\Bigg[2\sum_\gamma\left[(1-\lambda^2)^2\tilde{t}^\dagger_{i'z}\tilde{t}^\dagger_{iz}\tilde{t}^\dagger_{i\gamma}\tilde{t}_{i\gamma}+(1-\lambda^2)^2\tilde{t}^\dagger_{iz}\tilde{t}^\dagger_{i\gamma}\tilde{t}_{i\gamma}\tilde{t}_{i'z}\right.$$
$$\left.+2\lambda^2\tilde{t}^\dagger_{iz}\tilde{t}^\dagger_{i'\gamma}\tilde{t}_{i'\gamma}\tilde{t}_{iz}\right]+2\sum_{\gamma,\delta}\lambda^2\tilde{t}^\dagger_{i\gamma}\tilde{t}^\dagger_{i'\delta}\tilde{t}_{i\gamma}\tilde{t}_{i'\delta}+2\lambda^2\tilde{t}^\dagger_{iz}\tilde{t}^\dagger_{i'z}\tilde{t}_{iz}\tilde{t}_{i'z}$$
$$+(1+\lambda^2)^2\tilde{t}^\dagger_{ix}\tilde{t}^\dagger_{i'x}\tilde{t}_{iy}\tilde{t}_{i'y}-(1+\lambda^2)^2\tilde{t}^\dagger_{ix}\tilde{t}^\dagger_{i'y}\tilde{t}_{iy}\tilde{t}_{i'x}+h.c.\Bigg]. \qquad (5.21)$$

Here, summations over a refer to the transverse components $a = x, y$, while $\gamma, \delta = x, y, z$. We see that the Hamiltonian is symmetric under $x \leftrightarrow y$ which means that the transverse modes (x, y) are degenerate. But at the same time these are distinct from the longitudinal (z) mode. Also note that upto $\mathcal{H}_2$ we can separate the Hamiltonian into $\mathcal{H}_{x,y}$ and $\mathcal{H}_z$. But the higher order interaction terms involve interaction between different modes such that the z mode can decay into the two transverse modes.

5.3.2 Linear part

Linear terms in $\tilde{t}$ operators would generate an additional condensate and so we must set $\mathcal{H}_1 = 0$. Since the coefficient of linear term depends on the condensate parameter λ, vanishing of $\mathcal{H}_1$ determines λ to the leading order. Setting $\mathcal{H}_1$ to zero we obtain

$$h_{1a}(\lambda, h^z) \equiv \frac{\lambda J}{1+\lambda^2} - \frac{2qJ\lambda(1-\lambda^2)}{(1+\lambda^2)^2} + \frac{h^z(1-\lambda^2)}{1+\lambda^2} = 0\,. \qquad (5.22)$$

Let us denote the solution of this equation by $\lambda_0(h^z)$. We will be most interested in the case when $h^z = 0$, and in this case the solution reads

$$\lambda_0^2(h^z{=}0) = \frac{2q-1}{2q+1}\,. \qquad (5.23)$$

Note that the same result can be obtained variationally by minimizing $\langle\tilde{\psi}_0|\mathcal{H}|\tilde{\psi}_0\rangle$.

From eq. (5.23) we see that λ_0^2 (or $|\lambda_0|$) varies between 0 and 1 as a function of q. The real-condensate parameter λ is zero in the disordered phase and takes non-zero value in the ordered phase. Hence the vanishing of λ locates the quantum critical point. From eq. (5.23) we see that to leading order the quantum critical point is given by $q_c = 1/2$.

Recall that we obtained the same critical point from the harmonic approximation in the disordered phase (section 4.4.2). Later we will see that the interaction terms give a $1/d$ correction to this leading order result λ_0. The phase boundary obtained then coincides with that calculated in the last chapter.

On the other hand, we see that $|\lambda_0| \to 1$ for $q \to \infty$ which corresponds to $J = 0$. Thus a classical Néel state emerges as the reference state in the limit of decoupled layers. Finally, we note that a dominant staggered field, $|h^z| \gg J, qJ$, also results in $|\lambda_0| \to 1$.

5.3.3 Harmonic approximation

We now proceed to solve the bilinear part $\mathcal{H}_2$ in eq. (5.19) to leading order. As a first step we will make use of the lattice translation symmetry in the system, and introduce Fourier transformed operators according to

$$\tilde{t}_i = \frac{1}{\sqrt{N}} \sum_{\vec{k}} \tilde{t}_{\vec{k}} e^{-\imath \vec{k}\cdot\vec{r}_i} \,. \tag{5.24}$$

Here $\vec{k}$ is the momentum in the *full* first Brillouin zone and we do not need to work in a reduced Brillouin zone as often practiced in magnetically ordered phases[6]. Thus the bilinear part of the $\tilde{t}$ Hamiltonian, $\mathcal{H}_2$ in eq. (5.19), takes the following form in momentum space:

$$\mathcal{H}_2(\lambda) = \sum_{\vec{k},\alpha} \left[A_{\vec{k}\alpha} \tilde{t}^\dagger_{\vec{k}\alpha} \tilde{t}_{\vec{k}\alpha} + \frac{B_{\vec{k}\alpha}}{2} (\tilde{t}^\dagger_{\vec{k}\alpha} \tilde{t}^\dagger_{-\vec{k}\alpha} + h.c.) \right] . \tag{5.25}$$

The momentum and λ dependent coefficients are as follows:

$$A_{\vec{k}a} = \frac{J}{1+\lambda^2} - \frac{2\lambda h^z}{1+\lambda^2} + \frac{4qJ\lambda^2}{(1+\lambda^2)^2} + \frac{1-\lambda^2}{1+\lambda^2} B_{\vec{k}a} \,, \tag{5.26}$$

$$B_{\vec{k}a} = qJ\gamma_{\vec{k}} \,, \tag{5.27}$$

$$A_{\vec{k}z} = J\frac{1-\lambda^2}{1+\lambda^2} - \frac{4\lambda h^z}{1+\lambda^2} + \frac{8qJ\lambda^2}{(1+\lambda^2)^2} + B_{\vec{k}z} \,, \tag{5.28}$$

$$B_{\vec{k}z} = qJ\gamma_{\vec{k}} \left(\frac{1-\lambda^2}{1+\lambda^2} \right)^2 . \tag{5.29}$$

Here again we have the convention that $a = x, y(1, 2)$ and $\gamma_{\vec{k}}$ is the normalized interaction structure factor

$$\gamma_{\vec{k}} = \frac{1}{d} \sum_{n=1}^{d} \cos k_n \,. \tag{5.30}$$

[6]For instance, in the spin-wave theory for antiferromagnets on a square lattice, one often introduces two sublattices corresponding to the up and the down spins respectively. Thus one introduces a magnetic Brillouin zone, which is reduced version of the full lattice Brillouin zone, corresponding to an individual sublattice. However this can be avoided by writing the spin-wave theory in a rotated frame wherein all spins point in the same direction.

Note that the interaction structure factor is same as that introduced in the disordered phase. This is not surprising because this is the property of the lattice and does not depend on the phases realized. Thereby we are ensured that we can use the machinery developed in the last chapter to generate $1/d$ expansion even in this phase.

As mentioned earlier in this chapter, it is possible to write the bilinear Hamiltonian piece as a sum of x, y and z part. This means there is no mixing of the three excitation modes at this level. However we must point out that this is not a generic situation. It is specific for the collinear order in this case, and moreover due to the rotation we have employed. For instance[7], we can introduce generalized bond operators for a bilayer triangular lattice, and in this case, even at the harmonic level different modes are coupled in the non-collinear phase.

Anticipating the fact that λ will acquire a $1/d$ correction on top of λ_0 we define the leading (in $1/d$) piece of this bilinear Hamiltonian as unperturbed system, i.e. $\mathcal{H}_2^{(0)} \equiv \mathcal{H}_2(\lambda_0)$. The corresponding coefficients then are $A^{(0)}_{\vec{k}\alpha} \equiv A_{\vec{k}\alpha}(\lambda_0)$ and $B^{(0)}_{\vec{k}\alpha} \equiv B_{\vec{k}\alpha}(\lambda_0)$ i.e. evaluating eq. (5.26) - (5.29) at $\lambda = \lambda_0$. Using $h^z(\lambda_0)$ from eq. (5.22) we can write $A^{(0)}_{\vec{k}\alpha}$ as

$$A^{(0)}_{\vec{k}a} = J_1 + \frac{1-\lambda_0^2}{1+\lambda_0^2} B^{(0)}_{\vec{k}a}\,, \quad A^{(0)}_{\vec{k}z} = J_2 + B^{(0)}_{\vec{k}z} \tag{5.31}$$

with the shorthands

$$J_1 = \frac{J}{1-\lambda_0^2}, \quad J_2 = J\frac{1+\lambda_0^2}{1-\lambda_0^2}\,. \tag{5.32}$$

Note that these expressions are valid for any h^z.

We can solve the above leading order bilinear Hamiltonian by a standard Bogoliubov transformation (as discussed in detail in section 4.4.2),

$$\tilde{t}_{\vec{k}\alpha} = u_{\vec{k}}\tilde{\tau}_{\vec{k}\alpha} + v_{\vec{k}}\tilde{\tau}^\dagger_{-\vec{k},\alpha}\,, \tag{5.33}$$

where the Bogoliubov coefficients obey[8]

$$u^2_{\vec{k}\alpha}, v^2_{\vec{k}\alpha} = \pm\frac{1}{2} + \frac{A^{(0)}_{\vec{k}\alpha}}{2\tilde{\omega}_{\vec{k}\alpha}}\,, \quad u_{\vec{k}\alpha}v_{\vec{k}\alpha} = -\frac{B^{(0)}_{\vec{k}\alpha}}{2\tilde{\omega}_{\vec{k}\alpha}}\,. \tag{5.34}$$

The eigenmode energies are given by

$$\tilde{\omega}_{\vec{k}\alpha} = \sqrt{{A^{(0)}_{\vec{k}\alpha}}^2 - {B^{(0)}_{\vec{k}\alpha}}^2}\,. \tag{5.35}$$

As in the disordered phase the solution of this non-interacting Boson problem is termed as the harmonic approximation.

Since we will be interested in the quantum phase transition to the disordered phase let us obtain explicit expressions for the case $h^z = 0$. Using eq. (5.23) we have

$$J_1 = \frac{(2q+1)J}{2}\,, \qquad J_2 = 2qJ\,, \tag{5.36}$$

[7] Another example would be excitations of canted states [43].

[8] We are using the same notation as in the case of disordered phase since there is no possibility of any confusion.

leading to

$$\tilde{\omega}_{\vec{k}a} = J\frac{2q+1}{2}\sqrt{1+\frac{2\gamma_{\vec{k}}}{2q+1}-\frac{2q-1}{2q+1}\gamma_{\vec{k}}^2}\,, \tag{5.37}$$

$$\tilde{\omega}_{\vec{k}z} = 2Jq\sqrt{1+\frac{\gamma_{\vec{k}}}{4q^2}}\,. \tag{5.38}$$

From the above expressions, we see that the x, y transverse modes are the Goldstone modes i.e gapless excitations since $\tilde{\omega}_{\vec{Q},a} = 0$ for any q in the ordered phase. On the other hand the dispersion of the amplitude mode $\tilde{\omega}_{\vec{k}z}$ has a minimum at $\vec{k} = \vec{Q}$ and it has a finite gap in the ordered phase. However, at the quantum critical point, $q_c = 1/2$, the amplitude mode becomes soft. The ordered phase ceases to exist for $q < q_c = 1/2$ within the harmonic approximation. This again gives us the same value of critical point obtained within the harmonic approximation in disordered phase and by the condition of vanishing λ_0. Thus so far things are consistent at leading order in $1/d$.

In the limit of decoupled layers, i.e. $q \to \infty$ ($J = 0$) the transverse mode dispersion has additional gapless point at $\vec{k} = (0, 0, \ldots)$. In this limit, $\tilde{\omega}_{\vec{k}a} = Kd\sqrt{1-\gamma_{\vec{k}}^2}$, which is the same as obtained from linear spin-wave theory for square-lattice Heisenberg antiferromagnet [48]. This further substantiates our idea of x, y transverse modes being single spin-flip excitations. The amplitude mode however becomes dispersionless in this limit. The reason being that the z mode corresponds to simultaneous spin-flip in both layers. In presence of J such an excitation can propagate. However, in absence of intra-dimer (i.e. inter-layer) coupling this is strongly localized. Later in sec. 5.4.5 we will investigate the effect of interaction terms on the mode dispersion relations.

5.3.4 Strategy for $1/d$ expansion

The basis for the $1/d$ expansion is the observation that a suitably chosen product state $|\tilde{\psi}_0\rangle$ delivers exact expectation values of local observables in the limit $d \to \infty$, with corrections vanishing as $1/d$. In the disordered phase, based on this idea, we found the leading order result for observables at the product-state level and within the harmonic approximation, while the non-trivial $1/d$ corrections originated from the higher order interaction terms. So the strategy in the paramagnetic phase was simple: normal-order the Hamiltonian in the basis of Bogoliubov quasiparticles and draw Feynman diagrams for each observable, which results in a systematic $1/d$ expansion.

The situation in the ordered phase is more complicated. Here our product state itself depends on the condensate parameter λ, which varies as a function of the coupling ratio q. More importantly, λ is subject to quantum corrections and hence it will acquire a $1/d$ expansion. Consequently, it means that now the product-state level calculation is also a source of $1/d$ corrections. Moreover, our ordered phase Hamiltonian is λ dependent. Therefore each vertex itself will have a $1/d$ expansion coming from corrections to λ. Consequently there are two sources for $1/d$ corrections for observables in the ordered phase: (i) External - those originating from the $1/d$ expansion of λ; (ii) Internal - those generated via momentum summation during diagrammatics.

Note that this distinction of external versus internal source is purely for book-keeping and is being introduced to make the calculations in the following section more

transparent. The source of $1/d$ corrections to λ itself is also via momentum summation and corresponding diagrammatics. But the important point is that $\mathcal{O}(1/d^n)$ corrections on top of λ_0 are fully determined by the interaction vertices at $\mathcal{O}(1/d^{n-1})$. Hence we can practically treat the corrections from $1/d$ expansion of λ as an independent source.

Later we will see that λ is proportional to the staggered magnetization (at small λ), such that λ is expected to vary in a non-analytic, but mean-field-like, fashion near the quantum critical point. Therefore as per our discussion in chapter 3, we expect to have an analytic $1/d$ expansion for λ^2 with the following ansatz:

$$\lambda^2 = \lambda_0^2 + \frac{\lambda_1}{d} + \frac{\lambda_2}{d^2} + \dots \tag{5.39}$$

Next using this we will arrange the vertices of our normal-ordered Hamiltonian to set the stage for diagrammatic perturbation theory.

5.3.5 Normal-ordered Hamiltonian

We will now normal-order the generalized triplon Hamiltonian (5.16) with respect to the Bogoliubov quasiparticles that diagonalizes the leading-order bilinear terms according to eqs. (5.33) and (5.34). There will be additional bilinear terms arising from normal ordering of $\mathcal{H}_4$ and $\mathcal{H}_6$, as well those from $\mathcal{H}_2$ as a result of $1/d$ corrections to λ. However, as explained in detail in the last chapter we shall not further diagonalize these terms and treat them perturbatively referring to the leading order bilinear terms only as the unperturbed Hamiltonian. So after expressing the Hamiltonian via the $\tilde{\tau}$ operators and subsequent normal ordering, it takes the form

$$\mathcal{H} = \mathcal{H}'_0 + \mathcal{H}'_1 + \mathcal{H}'_2 + \mathcal{H}'_3 + \mathcal{H}'_4 + \mathcal{H}'_5 + \mathcal{H}'_6 \,. \tag{5.40}$$

Here $\mathcal{H}'_n(\lambda)$ contains n of the Bogoliubov-transformed $\tilde{\tau}$ operators.

The $1/d$ expansion of λ (5.39) can be used to formally split each $\mathcal{H}'_n$ into pieces arising from the different orders in the λ expansion:

$$\mathcal{H}'_n(\lambda) = \mathcal{H}'^{(0)}_n + \mathcal{H}'^{(1)}_n + \mathcal{H}'^{(2)}_n + \dots \tag{5.41}$$

where $\mathcal{H}'^{(0)}_n \equiv \mathcal{H}'_n(\lambda_0)$, $\mathcal{H}'^{(1)}_n = \mathcal{H}'_n(\sqrt{\lambda_0^2 + \lambda_1/d}) - \mathcal{H}'_n(\lambda_0)$ and so on. With this prescription, all terms in a particular piece $\mathcal{H}'^{(m)}_n$ are at least suppressed as $1/d^m$. We will make frequent use of this splitting in the course of evaluating observables in the next section.

Now having introduced the notations we will present the explicit normal-ordered expressions for those terms in the Hamiltonian which are relevant for calculation to order $1/d$. Using the above procedure and the following calculations it will be clear that going to higher order is straight forward though tedious. Just as in the disordered phase, for calculation of relevant observables to order $1/d$ it is sufficient to consider the terms arising from $\mathcal{H}_{0,\dots,4}$ only. The reason is same as discussed in last chapter. In the following we will quote the normal-ordered Hamiltonian as a function of *full* λ and the splitting with respect to $1/d$ expansion of λ will be done when we calculate

observables. Starting with the constant term,

$$\mathcal{H}'_0 = -\frac{NJ(3-\lambda^2)}{4(1+\lambda^2)} - \frac{2NKd\lambda^2}{(1+\lambda^2)^2} + \frac{2Nh^z\lambda}{1+\lambda^2} + \sum_{\vec{k},\alpha}\left[A_{\vec{k}\alpha}v^2_{\vec{k}\alpha} + B_{\vec{k}\alpha}u_{\vec{k}\alpha}v_{\vec{k}\alpha}\right]. \tag{5.42}$$

Here the first line is just the product-state contribution while the second line arises from normal ordering of $\mathcal{H}_2$ and it is of order $1/d$ and smaller. Normal ordering of $\mathcal{H}_4$ results in terms which are suppressed at least to order $1/d^2$ and are *not* shown.

The linear piece of the Hamiltonian in $\tilde{\tau}$ operators reads:

$$\mathcal{H}'_1 = \mathcal{H}'_{1a} + \mathcal{H}'_{1b} = (h_{1a} + h_{1b})(u_{\vec{Q}z} + v_{\vec{Q}z})(\tilde{\tau}^\dagger_{\vec{Q}z} + \tilde{\tau}_{\vec{Q}z}) \tag{5.43}$$

with $h_{1a}(\lambda, h^z)$ from eq. (5.22) and h_{1b} arises from the normal ordering of $\mathcal{H}_3$. We do not need contributions from $\mathcal{H}_5$ since they are of higher order in $1/d$. In terms of momentum summations $R_{1\ldots4}$ (listed in Appendix D.1),

$$h_{1b} = -2J_3R_{4a} + 2J_4(R_{2a} + R_{2z} - R_{4z} - R_{3z}) - h_{1a}(2R_{2a} + 2R_{2z} + R_{1z}) \tag{5.44}$$

with the shorthands

$$J_3 = \frac{2qJ\lambda}{1+\lambda^2}; \quad J_4 = J_3\frac{1-\lambda^2}{1+\lambda^2}. \tag{5.45}$$

Since $R_{1\ldots4}$ are $\mathcal{O}(1/d)$ or higher, h_{1b} is suppressed at least as $1/d$.

The bilinear Hamiltonian in $\tilde{\tau}$ has contributions coming from $\mathcal{H}_2$ and normal ordering of $\mathcal{H}_4$. We have already encountered the leading order bilinear term in the harmonic approximation 5.3.3, which we solved using Bogoliubov transformation. This unperturbed piece is

$$\mathcal{H}'_{2a} = \sum_{\vec{k},\alpha}\tilde{\omega}_{\vec{k}\alpha}\tilde{\tau}^\dagger_{\vec{k}\alpha}\tilde{\tau}_{\vec{k}\alpha}. \tag{5.46}$$

But this is not all we have from $\mathcal{H}_2$. Since we defined our unperturbed Hamiltonian with respect to λ_0 in $\mathcal{H}_2$ there are terms left which arise from the $1/d$ expansion of λ. These are given by

$$\mathcal{H}'_{2b} = \sum_{\vec{k},\alpha}\Big\{\Big[A^{(r)}_{\vec{k}\alpha}(u^2_{\vec{k}\alpha}+v^2_{\vec{k}\alpha}) + 2B^{(r)}_{\vec{k}\alpha}u_{\vec{k}\alpha}v_{\vec{k}\alpha}\Big]\tilde{\tau}^\dagger_{\vec{k}\alpha}\tilde{\tau}_{\vec{k}\alpha} + \Big[A^{(r)}_{\vec{k}\alpha}u_{\vec{k}\alpha}v_{\vec{k}\alpha} + \frac{B^{(r)}_{\vec{k}\alpha}}{2}(u^2_{\vec{k}\alpha}+v^2_{\vec{k}\alpha})\Big](\tilde{\tau}^\dagger_{\vec{k}\alpha}\tilde{\tau}^\dagger_{-\vec{k}\alpha} + h.c.)\Big\} \tag{5.47}$$

where $A^{(r)}_{\vec{k}\alpha} = A_{\vec{k}\alpha}(\lambda) - A^{(0)}_{\vec{k}\alpha}$ and $B^{(r)}_{\vec{k}\alpha} = B_{\vec{k}\alpha}(\lambda) - B^{(0)}_{\vec{k}\alpha}$. Here we made an exception to split the terms with respect to corrections to λ in order to clearly separate our unperturbed Hamiltonian from the perturbation. So although $\mathcal{H}'_{2b}$ also arises from $\mathcal{H}_2$ it is treated as a perturbation because it is higher order in $1/d$ compared to $\mathcal{H}'_{2a}$.

Finally, the contribution from the normal ordering of $\mathcal{H}_4$ is given by

$$\mathcal{H}'_{2c} = \sum_{\vec{k}\alpha}\left[C_{\vec{k}\alpha}\tilde{\tau}^\dagger_{\vec{k}\alpha}\tilde{\tau}_{\vec{k}\alpha} + \frac{D_{\vec{k}\alpha}}{2}(\tilde{\tau}^\dagger_{\vec{k}\alpha}\tilde{\tau}^\dagger_{-\vec{k}\alpha} + h.c.)\right] \tag{5.48}$$

with the coefficients $C_{\vec{k}\alpha}$ and $D_{\vec{k}\alpha}$ listed in Appendix D.2. As with the case of linear terms coming from the normal ordering of $\mathcal{H}_3$, above contribution is also suppressed at least as $1/d$. Thus we have $\mathcal{H}'_2 = \mathcal{H}'_{2a} + \mathcal{H}'_{2b} + \mathcal{H}'_{2c}$.

In the bilinear terms we saw that all modes were decoupled. However this is not the case with the cubic terms. It involves interactions between a longitudinal and two transverse excitations as well as those of three longitudinal ones. Here we need to normal order only $\mathcal{H}_3$ since $\mathcal{H}_5$ is irrelevant for us. It is quoted below:

$$\begin{aligned}\mathcal{H}'_3 = \sum_{123,a} \big[&\Phi^a_{31}(\tilde{\tau}^\dagger_{1a}\tilde{\tau}^\dagger_{2z}\tilde{\tau}^\dagger_{3a} + \tilde{\tau}_{1a}\tilde{\tau}_{2z}\tilde{\tau}_{3a})\delta_{Q+1+2+3} \\ &+ \Phi^a_{32}(\tilde{\tau}^\dagger_{1a}\tilde{\tau}^\dagger_{3a}\tilde{\tau}_{2z} + \tilde{\tau}^\dagger_{2z}\tilde{\tau}_{3a}\tilde{\tau}_{1a})\delta_{Q+1-2+3} \\ &+ \Phi^a_{33}(\tilde{\tau}^\dagger_{1a}\tilde{\tau}^\dagger_{2z}\tilde{\tau}_{3a} + \tilde{\tau}^\dagger_{3a}\tilde{\tau}_{2z}\tilde{\tau}_{1a})\delta_{Q+1+2-3}\big] \\ + \sum_{123} \big[&\Phi^z_{31}(\tilde{\tau}^\dagger_{1z}\tilde{\tau}^\dagger_{2z}\tilde{\tau}^\dagger_{3z} + \tilde{\tau}_{1z}\tilde{\tau}_{2z}\tilde{\tau}_{3z})\delta_{Q+1+2+3} \\ &+ \Phi^z_{32}(\tilde{\tau}^\dagger_{1z}\tilde{\tau}^\dagger_{2z}\tilde{\tau}_{3z} + \tilde{\tau}^\dagger_{3z}\tilde{\tau}_{2z}\tilde{\tau}_{1z})\delta_{Q+1+2-3}\big]\,, \end{aligned} \tag{5.49}$$

where the δ functions account for momentum conservation up to reciprocal lattice vectors of the hypercubic lattice. We see that the condensate is staggered, i.e., each longitudinal ($\tilde{\tau}_z$) excitation carries an additional momentum $\vec{Q}$.

Finally, we turn to the quartic terms. Even in this case the different modes are coupled and for convenience we split it as $\mathcal{H}'_4 = \mathcal{H}'^{az}_4 + \mathcal{H}'^{z}_4 + \mathcal{H}'^{ab}_4$, with the individual pieces:

$$\begin{aligned}\mathcal{H}'^{az}_4 = \sum_{1234,a} \big[&\Phi^{az}_{41}(\tilde{\tau}^\dagger_{1a}\tilde{\tau}^\dagger_{2a}\tilde{\tau}^\dagger_{3z}\tilde{\tau}^\dagger_{4z} + \tilde{\tau}_{1a}\tilde{\tau}_{2a}\tilde{\tau}_{3z}\tilde{\tau}_{4z})\delta_{1+2+3+4} \\ &+ (\Phi^{az}_{42}\tilde{\tau}^\dagger_{1a}\tilde{\tau}^\dagger_{2a}\tilde{\tau}_{3z}\tilde{\tau}_{4z} + \Phi^{az}_{43}\tilde{\tau}^\dagger_{1a}\tilde{\tau}^\dagger_{2z}\tilde{\tau}_{3a}\tilde{\tau}_{4z} + \Phi^{az}_{44}\tilde{\tau}^\dagger_{1z}\tilde{\tau}^\dagger_{2z}\tilde{\tau}_{3a}\tilde{\tau}_{4a})\delta_{1+2-3-4} \\ &+ \Phi^{az}_{45}(\tilde{\tau}^\dagger_{1a}\tilde{\tau}^\dagger_{2a}\tilde{\tau}^\dagger_{3z}\tilde{\tau}_{4z} + \tilde{\tau}^\dagger_{4z}\tilde{\tau}_{3z}\tilde{\tau}_{2a}\tilde{\tau}_{1a})\delta_{1+2+3-4} \\ &+ \Phi^{az}_{46}(\tilde{\tau}^\dagger_{1z}\tilde{\tau}^\dagger_{2z}\tilde{\tau}^\dagger_{3a}\tilde{\tau}_{4a} + \tilde{\tau}^\dagger_{4a}\tilde{\tau}_{3a}\tilde{\tau}_{2z}\tilde{\tau}_{1z})\delta_{1+2+3-4}\big]\,, \end{aligned} \tag{5.50}$$

$$\begin{aligned}\mathcal{H}'^{z}_4 = \sum_{1234} \big[&\Phi^{z}_{41}(\tilde{\tau}^\dagger_{1z}\tilde{\tau}^\dagger_{2z}\tilde{\tau}^\dagger_{3z}\tilde{\tau}^\dagger_{4z} + \tilde{\tau}_{1z}\tilde{\tau}_{2z}\tilde{\tau}_{3z}\tilde{\tau}_{4z})\delta_{1+2+3+4} \\ &+ \Phi^{z}_{42}\tilde{\tau}^\dagger_{1z}\tilde{\tau}^\dagger_{2z}\tilde{\tau}_{3z}\tilde{\tau}_{4z}\delta_{1+2-3-4} \\ &+ \Phi^{z}_{43}(\tilde{\tau}^\dagger_{1z}\tilde{\tau}^\dagger_{2z}\tilde{\tau}^\dagger_{3z}\tilde{\tau}_{4z} + \tilde{\tau}^\dagger_{4z}\tilde{\tau}_{3z}\tilde{\tau}_{2z}\tilde{\tau}_{1z})\delta_{1+2+3-4}\big]\,, \end{aligned} \tag{5.51}$$

$$\begin{aligned}\mathcal{H}'^{ab}_4 = \sum_{1234,ab} \big[&\Phi^{ab}_{41}(\tilde{\tau}^\dagger_{1a}\tilde{\tau}^\dagger_{2a}\tilde{\tau}^\dagger_{3b}\tilde{\tau}^\dagger_{4b} + \tilde{\tau}_{1a}\tilde{\tau}_{2a}\tilde{\tau}_{3b}\tilde{\tau}_{4b})\delta_{1+2+3+4} \\ &+ (\Phi^{ab}_{42}\tilde{\tau}^\dagger_{1a}\tilde{\tau}^\dagger_{2a}\tilde{\tau}_{3b}\tilde{\tau}_{4b} + \Phi^{ab}_{43}\tilde{\tau}^\dagger_{1a}\tilde{\tau}^\dagger_{2b}\tilde{\tau}_{3a}\tilde{\tau}_{4b})\delta_{1+2-3-4} \\ &+ \Phi^{ab}_{44}(\tilde{\tau}^\dagger_{1a}\tilde{\tau}^\dagger_{2a}\tilde{\tau}^\dagger_{3b}\tilde{\tau}_{4b} + \tilde{\tau}^\dagger_{4b}\tilde{\tau}_{3b}\tilde{\tau}_{2a}\tilde{\tau}_{1a})\delta_{1+2+3-4}\big]\,. \end{aligned} \tag{5.52}$$

Explicit expressions for selected vertex functions $\Phi_{3,4}$ are given in Appendix D.2.

5.4 $1/d$ expansion for observables

We are now equipped with all the necessary expressions and strategy to calculate observables in the collinear phase of the hypercubic coupled-dimer model in an expansion

in $1/d$. As in the disordered phase, we will restrict our calculation to first correction beyond the harmonic approximation.

As discussed before we will first calculate the corrections to the condensate parameter λ, which involves vanishing of the linear piece in $\tilde{\tau}$ operators. Subsequently, using $\mathcal{H}'_{2a}$ as unperturbed piece we will perform standard diagrammatic perturbation theory with $\mathcal{H}'_{2b} + \mathcal{H}'_{2c} + \mathcal{H}'_3 + \mathcal{H}'_4 + \mathcal{H}'_5 + \mathcal{H}'_6$ as perturbation. Importantly, we will have to use the correction to λ in order to obtain all the contributions to an observable. As mentioned earlier, at this level of calculation we will not need $\mathcal{H}'_5$ and $\mathcal{H}'_6$. Moreover, since we exclusively consider zero temperature all the Hartree loops (i.e. closed loops) of $\tilde{\tau}$ particles vanish.

5.4.1 Condensate parameter and phase boundary

To satisfy the condition that no additional condensate is generated we demanded $\mathcal{H}_1$ to vanish. This led us to the leading order result λ_0 for the condensate parameter. Now to generate a $1/d$ expansion for λ we impose the condition $\mathcal{H}'_1 = 0$. But as in the disordered phase we have to be careful while writing a $1/d$ expansion near the quantum critical point. Following the arguments discussed in chapter 3 and section 5.3.4, λ^2 will have a well-defined $1/d$ expansion with the parametrization as in eq. (5.39).

The condition $\mathcal{H}'_1 = 0$ (5.43) implies that $h_{1a} + h_{1b} = 0$. Recall that $h_{1a}(\lambda_0, h^z) = 0$ followed from the condition $\mathcal{H}_1 = 0$. So in order to obtain $1/d$ correction we have to consider the expansion of $h_{1a}(\lambda, h^z)$ around λ_0 to order $1/d$. On the other hand, $h_{1b}(\lambda, h^z)$ can be evaluated at λ_0, because the $R_{1\ldots4}$ factors in eq. (5.44) are of order $1/d$ or smaller. Expanding h_{1a} around λ_0 yields to order $1/d$:

$$h_{1a} = \frac{\lambda_1}{d}\left[\frac{J(1-\lambda_0^2)}{2\lambda_0(1+\lambda_0^2)^2} - \frac{qJ(1+\lambda_0^4-6\lambda_0^2)}{\lambda_0(1+\lambda_0^2)^3} - \frac{2h^z}{(1+\lambda_0^2)^2}\right] \tag{5.53}$$

which has to equal $-h_{1b}$. Using $h^z(\lambda_0)$ from eq. (5.22) and solving for λ_1 we find

$$\frac{\lambda_1}{d} = -\frac{4J_4\lambda_0(R_{2a}+R_{2z}-R_{3z})(1-\lambda_0^2)(1+\lambda_0^2)^3}{J(1+\lambda_0^2)^3 - 2qJ(1-\lambda_0^2)^3}\,, \tag{5.54}$$

where we have used that the R_4 are of order $1/d^2$ and can be neglected. Note that this expression is valid for any value of h^z. However, we are interested in the quantum phase transition to the quantum paramagnetic phase and so focus on $h^z = 0$. In the case $h^z = 0$ using λ_0 from eq. (5.23) we can simplify the above expression to

$$\frac{\lambda_1}{d} = -\frac{8q}{(2q+1)^2}(R_{2a}+R_{2z}-R_{3z})\,. \tag{5.55}$$

Using the explicit values of $R_{2,3}$ from appendix D.1, we thus obtain the following result for the condensate parameter at $h^z = 0$:

$$\lambda^2 = \frac{2q-1}{2q+1} - \frac{1}{d}\left[\frac{4q^3}{(2q+1)^4} + \frac{16q^2+1}{64q^3(2q+1)^2}\right] + \mathcal{O}\left(\frac{1}{d^2}\right)\,. \tag{5.56}$$

The behavior of the condensate parameter for specific values of d is illustrated in fig. 5.1. An important point to note here is that for $q \to \infty$ there are no fluctuation

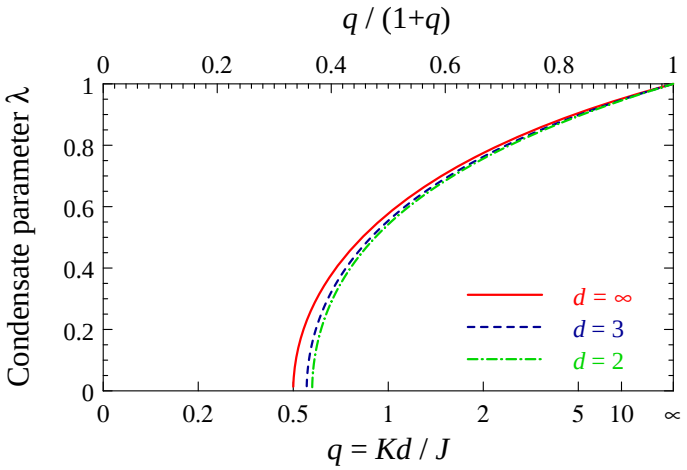

Figure 5.1: Condensate parameter (5.56) for the coupled-dimer model (5.1) is plotted in the absence of staggered field, $h^z = 0$. We have plotted the curves for $d = \infty$ (solid), $d = 3$ (dashed), and $d = 2$ (dash-dot). Note that $q/(1+q) = Kd/(J+Kd)$ varies linearly along the horizontal axis. Figure is taken from ref. [70].

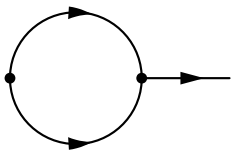

Figure 5.2: One of the additional diagrams contributing to the evaluation of condensate parameter, λ, beyond $\mathcal{O}(1/d)$.

corrections to $|\lambda| = 1$ and so all the curves in fig. 5.1 merge at $\lambda = 1$ and $q \to \infty$. On general grounds we expect this result to hold to all orders in $1/d$, as $|\lambda| \neq 1$ implies entanglement between the layers which must be absent for $J = 0$.

Since the condensate parameter is zero in the quantum paramagnetic phase the condition $\lambda^2 = 0$ can be used to determine the location of the quantum critical point. For this purpose we insert the ansatz $q_c = 1/2 + q_{1c}/d$ into eq. (5.56) and impose $\lambda^2 = 0$. This then yields the phase boundary of the ordered phase as:

$$q_c = \frac{1}{2} + \frac{3}{16d} + \mathcal{O}\left(\frac{1}{d^2}\right) . \tag{5.57}$$

Remarkably, this is the same expression as obtained in chapter 4 for the boundary of the disordered phase by using the condition of a vanishing triplon gap. A continuous onset of the order parameter upon increasing q correctly yields the second-order quantum phase transition. The quantum correction to the condensate parameter is negative and consequently tend to destabilize the ordered phase. The fluctuations are strongest in $d = 2$ which is also reflected in the fact that the phase boundary for $d = 2$ is at larger value of q compared to that in $d = 3$ or $d \to \infty$.

Note that the above depiction of just vanishing linear piece to obtain $1/d$ expansion for λ is not the complete picture. It is special only to leading order and order $1/d$

correction. In general, apart from the linear piece we must also draw appropriate Feynman diagram for the condensate parameter, and together these need to vanish. A specimen diagram relevant for the condensate parameter is shown in fig. 5.2. It turns out that all such diagrams are at least suppressed as $\mathcal{O}(1/d^2)$ and hence do not play any role in the above analysis. However at higher orders these need to be considered apart from the linear piece.

5.4.2 Ground-state energy

Let us now determine the ground-state energy E_0. It is given by $\mathcal{H}'_0$ (5.42) plus perturbative corrections coming from $\mathcal{H}'_{2b} + \mathcal{H}'_{2c} + \mathcal{H}'_3 + \mathcal{H}'_4 + \mathcal{H}'_5 + \mathcal{H}'_6$. The constant $\mathcal{H}'_0$ depends on the condensate parameter λ. So we need to expand it in $1/d$, using the $1/d$ expansion for λ itself. We have determined the expansion of λ to order $1/d$, and so we can calculate E_0 only up to this order. Calculation to $\mathcal{O}(1/d^2)$ requires the expansion of λ to the same order. Recall that in the disordered phase, in chapter 4, we were able to extract the $1/d^2$ piece as well. Importantly, the perturbative corrections are of order $1/d^2$ or smaller. The vertices in both $\mathcal{H}'_{2b}$ and $\mathcal{H}'_{2c}$ are of order $1/d$ and so all relevant diagrams are suppressed further to at least $\mathcal{O}(1/d^2)$. Similarly, the diagrams involving $\mathcal{H}'_{3,\ldots,6}$ contain at least two momentum summations each contributing at least a factor of $1/d$, and so do not contribute to $1/d$ corrections. Hence, we have

$$E_0 = \mathcal{H}'_0 + \mathcal{O}\left(\frac{1}{d^2}\right) = E_{00} + \frac{E_{01}}{d} + \mathcal{O}\left(\frac{1}{d^2}\right). \tag{5.58}$$

where we have parametrized the first two orders in the expansion.

The leading piece E_{00} is from $\mathcal{H}_0$ (5.17), evaluated at λ_0:

$$\begin{aligned}\frac{E_{00}}{N} &= -\frac{J(3-\lambda_0^2)}{4(1+\lambda_0^2)} - \frac{2qJ\lambda_0^2}{(1+\lambda_0^2)^2} + \frac{2h^z\lambda_0}{1+\lambda_0^2} \\ &= -\frac{J(3+\lambda_0^2)}{4(1-\lambda_0^2)} + \frac{2qJ\lambda_0^2}{(1+\lambda_0^2)^2},\end{aligned} \tag{5.59}$$

where $h^z(\lambda_0)$ from eq. (5.22) has entered the second equality. E_{01} receives contributions from $1/d$ corrections to λ and from the normal-ordering piece in eq. (5.42), where the latter can be evaluated at λ_0. This gives

$$\begin{aligned}\frac{E_{01}}{N} = \lambda_1 &\left[\frac{J}{(1+\lambda_0^2)^2} - 2qJ\frac{(1-\lambda_0^2)}{(1+\lambda_0^2)^3} + \frac{h^z(1-\lambda_0^2)}{\lambda_0(1+\lambda_0^2)^2}\right] \\ &+ \frac{q^2J^3}{8J_2^2}\left(\frac{1-\lambda_0^2}{1+\lambda_0^2}\right)^3 - \frac{q^2J^2}{4J_2}\left(\frac{1-\lambda_0^2}{1+\lambda_0^2}\right)^4 \\ &+ \frac{q^2J^3}{4J_1^2(1-\lambda_0^2)} - \frac{q^2J^2}{2J_1},\end{aligned} \tag{5.60}$$

with J_1 and J_2 defined in eq. (5.32). Eliminating h^z as before, using λ_1 from eq. (5.54), and using the expressions for $R_{2,3}$ from appendix D.1, we get

$$\frac{E_{01}}{JN} = -\frac{q^2}{8}\left(\frac{1-\lambda_0^2}{1+\lambda_0^2}\right)^5 - \frac{q^2}{4}(1-\lambda_0^2). \tag{5.61}$$

In the limit $h^z = 0$, the ground-state energy reads

$$\frac{E_0}{JN} = -\frac{4q^2+2q+1}{8q} - \frac{1}{2d}\left[\frac{1}{128q^3} + \frac{q^2}{2q+1}\right] + \mathcal{O}\left(\frac{1}{d^2}\right). \tag{5.62}$$

Again, this expression is analytic even at the quantum critical point. This is corresponding to the mean-field value [5] $\alpha = 0$ of the specific-heat exponent α.

At the critical point, the above calculation matches the ground-state energy obtained in chapter 4 for the paramagnetic phase. This is easily seen by inserting $\lambda = 0$ directly into $\mathcal{H}_0'$ from eq. (5.42). This yields the leading two terms of the $1/d$ expansion of E_0 in the corresponding equation (4.73) in chapter 4. Alternatively, the same result can be obtained by setting $\lambda_0 = 0$ in eqs. (5.59) and (5.61). We will discuss the connection of our results, in the decoupled-layer limit $q \to \infty$, to the spin-wave theory in section 5.5.

5.4.3 Triplet density

Let us now calculate the triplet densities, expressed as $\langle t_{i\alpha}^\dagger t_{i\alpha}\rangle$ via the triplon operators t, (4.7)–(4.10), defined in chapter 4. In terms of $\tilde{t}$ operators we have,

$$t_{ia}^\dagger t_{ia} = \tilde{t}_{ia}^\dagger \tilde{t}_{ia} \quad (a = x, y)\,, \tag{5.63}$$

$$t_{iz}^\dagger t_{iz} = \frac{\tilde{t}_{iz}^\dagger \tilde{t}_{iz} + \lambda^2 P_i + \lambda_i(\tilde{t}_{iz}^\dagger + \tilde{t}_{iz})}{1+\lambda^2}\,. \tag{5.64}$$

Here we have used the basis rotation eqs. (5.3-5.5). So the expectation values to order $1/d$ are

$$\frac{1}{N}\sum_i \langle t_{ia}^\dagger t_{ia}\rangle = \frac{1}{N}\sum_i \langle \tilde{t}_{ia}^\dagger \tilde{t}_{ia}\rangle = R_{2a}\,, \tag{5.65}$$

$$\frac{1}{N}\sum_i \langle t_{iz}^\dagger t_{iz}\rangle = \frac{\lambda_0^2}{1+\lambda_0^2} + \frac{\lambda_1}{d}\frac{1}{(1+\lambda_0^2)^2} - \frac{2\lambda_0^2}{1+\lambda_0^2}R_{2a} + \frac{1-\lambda_0^2}{1+\lambda_0^2}R_{2z}\,. \tag{5.66}$$

In these expressions, $\sum_i \langle \tilde{t}_{i\alpha}^\dagger \tilde{t}_{i\alpha}\rangle/N = R_{2\alpha}$ represents the result at the harmonic level. Just as in chapter 4, here as well the perturbative corrections start at order $1/d^2$ only. For $h^z = 0$, we can write the triplet densities as a function of q:

$$\frac{1}{N}\sum_i \langle t_{ia}^\dagger t_{ia}\rangle = \frac{1}{d}\frac{q^2}{2(2q+1)^2} + \mathcal{O}\left(\frac{1}{d^2}\right), \tag{5.67}$$

$$\frac{1}{N}\sum_i \langle t_{iz}^\dagger t_{iz}\rangle = \frac{2q-1}{4q} - \frac{1}{d}\left(\frac{q^2}{2(2q+1)^2} + \frac{1}{64q^3}\right) + \mathcal{O}\left(\frac{1}{d^2}\right). \tag{5.68}$$

These results are shown in fig. 5.3. We see a kink in the z triplet density at the quantum phase transition. Also, it is no more small in the ordered phase. The local spin correlator can be expressed in terms of the triplet densities according to $\vec{S}_{i1}\cdot\vec{S}_{i2} = \sum_\alpha t_{i\alpha}^\dagger t_{i\alpha} - \frac{3}{4}$. From this it is easy to see that in the limit of decoupled layers ($q \to \infty$), $\langle \sum_\alpha t_{i\alpha}^\dagger t_{i\alpha}\rangle = 1/2$ and we also see it in fig. 5.3.

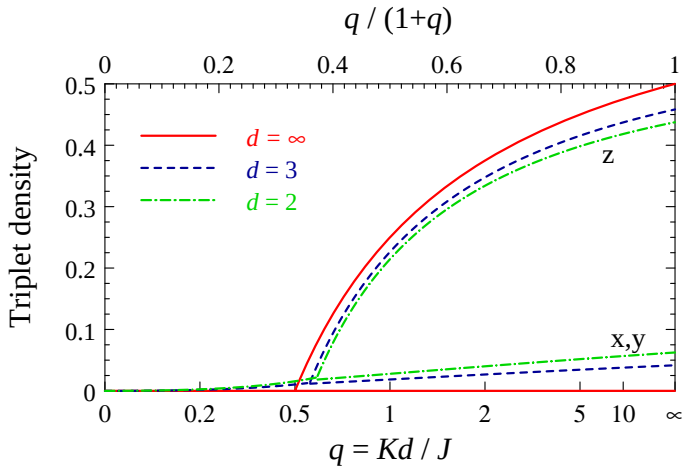

Figure 5.3: Triplet densities $\langle t^\dagger_{i\alpha} t_{i\alpha}\rangle$ (eq. (4.105) and eq. (5.67)–(5.68)) for $\alpha = x, y$ and $\alpha = z$ are plotted for the hypercubic-lattice dimer model at $h^z = 0$. Results are shown for $d = \infty$ (solid), $d = 3$ (dashed), and $d = 2$ (dash-dot). Figure is taken from ref. [70].

5.4.4 Staggered magnetization

The staggered magnetization is given by

$$M_{\rm st} = \frac{1}{N}\sum_i e^{i\vec{Q}\cdot R_i}\langle S^z_{i1} - S^z_{i2}\rangle\,. \tag{5.69}$$

As mentioned earlier, it represents the order parameter of the collinear antiferromagnet. Now our strategy of introducing h^z comes handy. The derivative of the ground-state energy w.r.t. h^z gives us the staggered magnetization,

$$M_{\rm st} = \frac{\partial E_0}{N\partial h^z} = \frac{\partial E_{00}}{N\partial h^z} + \frac{1}{d}\frac{\partial E_{01}}{N\partial h^z} + \mathcal{O}\left(\frac{1}{d^2}\right). \tag{5.70}$$

The order-parameter exponent takes the mean-field value $\beta = 1/2$. We therefore expect $M^2_{\rm st}$ to vary analytically near the QPT. So we parameterize

$$M^2_{\rm st} = M^2_{\rm st0} + \frac{M_{\rm st1}}{d} + \frac{M_{\rm st2}}{d^2} + \ldots \tag{5.71}$$

Using eq. (5.59) we find the leading piece as

$$M_{\rm st0} = \frac{2\lambda_0}{1+\lambda_0^2} + \frac{2h_{1a}(\lambda_0, h^z)}{1+\lambda_0^2}\frac{\partial\lambda_0}{\partial h^z} = \frac{2\lambda_0}{1+\lambda_0^2}\,. \tag{5.72}$$

with $h_{1a}(\lambda, h^z)$ in eq. (5.22). Given that $h_{1a}(\lambda_0, h^z) = 0$, the second term vanishes. This also applies to the limit $\lambda_0 \to 0$ where $\partial\lambda_0/\partial h^z$ diverges. From eq. (5.61) we have

$$\begin{aligned}\frac{\partial E_{01}}{N\partial h^z} &= \frac{5Jq^2\lambda_0}{2}\frac{(1-\lambda_0^2)^4}{(1+\lambda_0^2)^6}\frac{\partial\lambda_0}{\partial h^z} + \frac{Jq^2\lambda_0}{2}\frac{\partial\lambda_0}{\partial h^z}\\ &= -\left[5\frac{(1-\lambda_0^2)^4}{(1+\lambda_0^2)^6} + 1\right]\frac{Jq^2\lambda_0(1-\lambda_0^4)}{2\left[J(1-2q) + 3\lambda_0^2 J(1+2q) - 4h^z\lambda_0^3\right]}\,.\end{aligned} \tag{5.73}$$

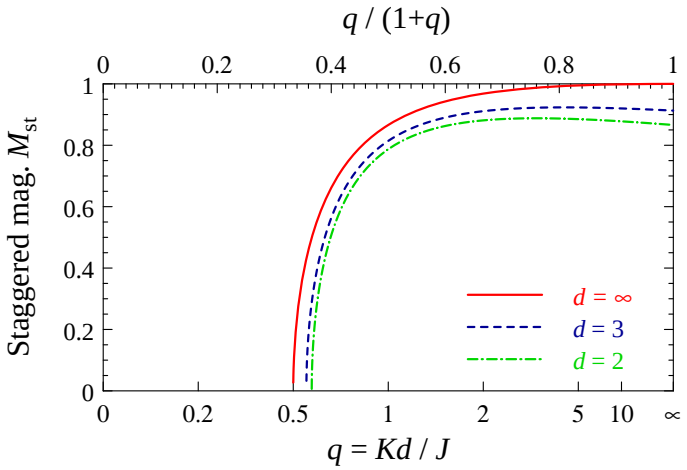

Figure 5.4: Staggered magnetization per dimer (5.75) is plotted for $h^z = 0$. Results are shown for $d = \infty$ (solid), $d = 3$ (dashed), and $d = 2$ (dash-dot). As mentioned in the text, fluctuation corrections lead to a maximum of $M_{\rm st}$ at some $q < \infty$. Note that, here as well, $q/(1+q) = Kd/(J+Kd)$ varies linearly along the horizontal axis. The figure is taken from ref. [70].

Let us now focus on the limit $h^z = 0$ where the above equation can be converted into

$$M_{\rm st1} = -\frac{(1+\lambda_0^2)^2}{8}\left[5\frac{(1-\lambda_0^2)^4}{(1+\lambda_0^2)^6}+1\right]. \tag{5.74}$$

From eq. (5.70) and (5.71) we can write our final result for the staggered magnetization:

$$M_{\rm st}^2 = \frac{4q^2-1}{4q^2} - \frac{1}{d}\frac{2q^2}{(2q+1)^2}\left[\frac{5(2q+1)^2}{256q^6}+1\right] + \mathcal{O}\left(\frac{1}{d^2}\right). \tag{5.75}$$

This is plotted in fig. 5.4. In infinite dimensions, the magnetization reaches its saturation value in the limit of decoupled layers, $q \to \infty$. Fluctuation corrections generically lead to a reduction of $M_{\rm st}$. Interestingly, there is a maximum in the $M_{\rm st}$ curve at a finite value of q, which indicates that interlayer and intralayer fluctuations compete. This is qualitatively consistent with results for the bilayer square-lattice magnet [71, 50]. We will see in section 5.5 below that our fluctuation corrections obtained in the limit $q \to \infty$ match those obtained from spin-wave theory in this limit.

The vanishing of the order parameter $M_{\rm st}$ upon decreasing q can be used to define the boundary q_c of the ordered phase. Upon solving for q_c we find the same expression as in eq. (5.57). This shows internal consistency of our method. Note that just as mentioned in chapter 4, solving the truncated series $M_{\rm st}^2 = 0$ at a fixed d will yield a phase boundary different from eq. (5.57). This is because such a procedure involves incomplete contributions from higher order corrections.

Note that the staggered magnetization can be directly calculated as the expectation value (5.69), with identical results as required by thermodynamic consistency. We have seen that the corrections to λ influence the corrections to the staggered magnetization. However, these corrections were overlooked in ref. [43]. Similar problems have appeared in the literature on frustrated hard-core boson systems and we refer to ref. [72] for a summary.

5.4.5 Mode dynamics

As already mentioned in the beginning of the chapter, in contrast to the paramagnetic phase with a triply degenerate excitations, here we have doubly degenerate gapless transverse modes (Goldstone modes) and a gapped amplitude mode. In the following, we will determine their respective mode dispersions to order $1/d$, restricting the concrete evaluation to the field-free case $h^z = 0$.

Their calculation is on the same lines as discussed in chapter 4. As in the paramagnetic phase, to order $1/d$ it is sufficient to determine only the normal self-energies Σ_N of the $\tilde{\tau}$ particles. Recall that the renormalized mode energies obey the following pole equation:

$$\tilde{\Omega}^2_{\vec{k}} = \tilde{\omega}^2_{\vec{k}} + 2\tilde{\omega}_{\vec{k}}\Sigma_N(\vec{k}, \tilde{\omega}_{\vec{k}})\,. \tag{5.76}$$

Let us first consider the $a = x, y$ modes. We will see below that these modes remain degenerate and represent the transverse Goldstone modes of the system. The relevant self-energy diagrams and the corresponding analytic expressions contributing to $\mathcal{O}(1/d)$ are listed in appendix D.3. These are similar to those appearing in chapter 4 in the context of triplon dispersion. The main difference now is that the vertices are not symmetric w.r.t. x, y and z modes. Expressing these self-energies at $h^z = 0$ in terms of q and using eq. (5.76), we obtain the dispersion of the $a = x, y$ modes:

$$\begin{aligned}
\frac{\tilde{\Omega}^2_{\vec{k}a}}{J^2} &= \frac{(2q+1)^2}{4}\left[1 + \frac{2\gamma_{\vec{k}}}{2q+1} - \gamma^2_{\vec{k}}\frac{2q-1}{2q+1}\right] \\
&\quad - \frac{1}{d}\frac{1+\gamma_{\vec{k}}}{128q^2(2q+1)^2\left(32q^2 + 4q^2\gamma^2_{\vec{k}} + 8q - 4q\gamma_{\vec{k}} - \gamma^2_{\vec{k}} - 2\gamma_{\vec{k}}\right)} \\
&\quad \times \Big[1024q^8\left(\gamma_{\vec{k}} - 1\right)\left(8 + \gamma^2_{\vec{k}}\right) + 1024q^7\left(\gamma_{\vec{k}} - 1\right)\left(10 - \gamma_{\vec{k}} + \gamma^2_{\vec{k}}\right) \\
&\quad - 256q^6\left(\gamma_{\vec{k}} + 2\right)\left(4 + 3\gamma_{\vec{k}} + \gamma^2_{\vec{k}}\right) - 256q^5\left(\gamma^3_{\vec{k}} - \gamma^2_{\vec{k}} + 20\gamma_{\vec{k}} - 4\right) \\
&\quad - 16q^4\left(\gamma^3_{\vec{k}} - 21\gamma^2_{\vec{k}} + 64\gamma_{\vec{k}} - 8\right) - 16q^3\left(\gamma^3_{\vec{k}} - 8\gamma^2_{\vec{k}} - 29\gamma_{\vec{k}} + 14\right) \\
&\quad + 8q^2\left(-18 + 25\gamma_{\vec{k}} + 9\gamma^2_{\vec{k}}\right) + 4q\left(-10 + \gamma_{\vec{k}}\left(\gamma_{\vec{k}} + 1\right)\left(\gamma_{\vec{k}} + 3\right)\right) \\
&\quad + \left(\gamma^3_{\vec{k}} + \gamma^2_{\vec{k}} - 2\gamma_{\vec{k}} - 4\right)\Big] + \mathcal{O}\left(\frac{1}{d^2}\right).
\end{aligned} \tag{5.77}$$

It is easy to see that $\tilde{\Omega}^2_{\vec{Q}a} = 0$ for all q. Therefore, both transverse modes are soft at the ordering wavevector. These are indeed our Goldstone modes. Similar to chapter 4, expanding around $\vec{k} = \vec{Q}$ we can introduce a velocity c_a of the Goldstone mode according to $\tilde{\Omega}^2_{\vec{k}a} = c_a^2(\vec{k} - \vec{Q})^2/d$, with c_a evaluating to:

$$\begin{aligned}
\frac{c_a}{J} &= \sqrt{\frac{q(2q+1)}{2}}\left[1 + \frac{1}{q(2q+1)^3(6q+1)d}\left(12q^5 + 14q^4 - 2q^3 - 4q^2\right.\right. \\
&\qquad \left.\left. - \frac{5q}{16} + \frac{13}{32} + \frac{7}{64q} + \frac{1}{128q^2}\right)\right] + \mathcal{O}\left(\frac{1}{d^2}\right).
\end{aligned} \tag{5.78}$$

The velocity is analytic at the quantum phase transition. An explicit evaluation at $q = q_c$, eq. (5.57), yields

$$\frac{c}{J} = \frac{1}{\sqrt{2}} + \frac{5}{16\sqrt{2}d} + \mathcal{O}\Big(\frac{1}{d^2}\Big)\,. \tag{5.79}$$

Importantly, this velocity equals the longitudinal-mode velocity calculated below as well as the triplon velocity (4.96) in the disordered phase. This demonstrates a smooth evolution of the excitation modes across the quantum critical point.

Let us now turn our attention to the z mode, which will be interpreted as a longitudinal/amplitude (or Higgs) mode. Again, the self-energies are listed in appendix D.3, and are similar to the previous ones. Using the pole equation (5.76) we obtain the following $1/d$ expansion for the z-mode dispersion at $h^z = 0$:

$$\begin{aligned}\frac{\tilde{\Omega}^2_{\vec{k}z}}{J^2} = \left[4q^2 + \gamma_{\vec{k}}\right] + \frac{1}{32d}\Bigg[&- \frac{1}{q^2} - \frac{16}{(2q+1)^2} + 2\gamma^2_{\vec{k}}\frac{(\gamma_{\vec{k}}-3)(\gamma_{\vec{k}}-1)^2}{4q+1-\gamma_{\vec{k}}} \\ &- 24\frac{(\gamma_{\vec{k}}-3)(\gamma_{\vec{k}}-1)}{\gamma_{\vec{k}}-12q^2} + 2(4-3\gamma_{\vec{k}}+\gamma^2_{\vec{k}})(-8-\gamma_{\vec{k}}+\gamma^2_{\vec{k}}) \\ &+ 8\frac{6-\gamma_{\vec{k}}+\gamma^2_{\vec{k}}}{2q+1} + 8q(4-\gamma^2_{\vec{k}}+\gamma^3_{\vec{k}})\Bigg] + \mathcal{O}\left(\frac{1}{d^2}\right). \end{aligned} \tag{5.80}$$

This dispersion is gapped, with a minimum energy at $\vec{k} = \vec{Q}$. Therefore the amplitude mode gap is given by

$$\frac{\Delta^2_z}{J^2} = 4q^2 - 1 + \frac{1}{32d}\left[-\frac{1}{q^2} - \frac{16}{(2q+1)^2} + \frac{48}{2q+1} + \frac{192}{12q^2+1} - 96 + 16q\right] + \mathcal{O}\left(\frac{1}{d^2}\right). \tag{5.81}$$

By setting $\Delta^2_z = 0$, we again obtain the same phase boundary (5.57) as before. This is the third observable using which we obtain the same phase boundary. As before, in the vicinity of the quantum critical point, the gap varies with a critical exponent $\nu z = 1/2$ as follows:

$$\frac{\Delta_z}{J} = \left[2 - \frac{5}{8d} + \mathcal{O}\left(\frac{1}{d^2}\right)\right]\sqrt{q - q_c}\,. \tag{5.82}$$

Utilizing the parametrization, $\tilde{\Omega}^2_{\vec{k}z} = \Delta^2_z + c^2_z(\vec{k}-\vec{Q})^2/d$, we can easily write down the z-mode velocity as

$$\begin{aligned}\frac{c_z}{J} = \frac{1}{\sqrt{2}}\Bigg[1 + \frac{1}{32d}\left(\frac{14}{2q+1} - \frac{4}{(2q+1)^2} - \frac{72}{12q^2+1} + \frac{96}{(12q^2+1)^2} + 6 + 20q\right)\Bigg] \\ + \mathcal{O}\left(\frac{1}{d^2}\right). \end{aligned} \tag{5.83}$$

This again yields eq. (5.79) if evaluated at $q = q_c$.

It is now clear that this mode can be interpreted as the amplitude (longitudinal or Higgs) mode. It is gapped in the ordered phase and becomes dispersionless in the limit of decoupled layers. In fact, in this limit, i.e. $J \to 0$, this mode corresponds to a simultaneous spin flip in the two layers. In the ordered phase, this mode corresponds to the order-parameter fluctuations (recall our discussion using Mexican-hat potential in chapter 1). At the quantum critical point, it becomes soft and merges with the Goldstone modes. This mode is always higher in energy compared to the Goldstone modes. It can decay into two magnons (transverse modes) and as a result acquire damping [73]. But we cannot calculate its decay rate in the large-d formalism, since as discussed in chapter 4 these are exponentially suppressed as $d \to \infty$.

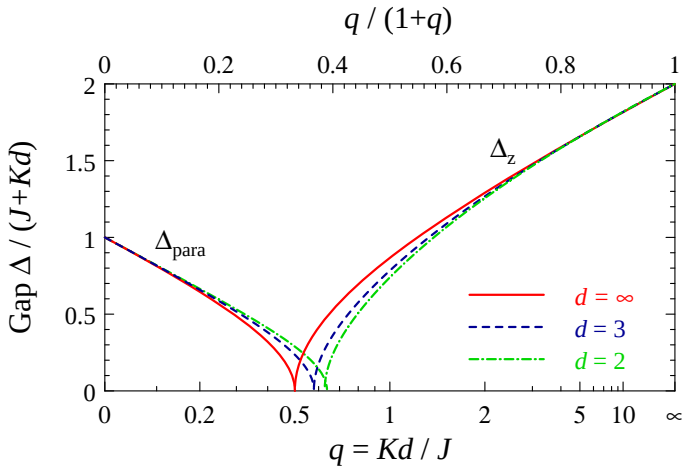

Figure 5.5: The figure shows the triplon excitation gap (4.91), Δ_{para}, for $q < q_c$ and the amplitude (Higgs) mode gap (5.81), Δ_z, for $q > q_c$. Results are plotted for $d = \infty$ (solid), $d = 3$ (dashed), and $d = 2$ (dash-dot). The two gaps become soft at the critical point. Note that $q/(1+q)$ varies linearly along the horizontal axis. Also, the gaps are plotted as $\Delta/(J + Kd)$. This figure is taken from ref. [70].

Near criticality, the ratio of the Higgs gap (5.81) and the triplon excitation gap (4.91) obeys the following relation to order $1/d$:

$$\frac{\Delta_z(q_c + \delta q)}{\Delta_{\rm para}(q_c - \delta q)} = \sqrt{2}\,. \tag{5.84}$$

This is depicted in fig. 5.5. For a ϕ^4 order-parameter field theory, which is valid for any d above the upper critical dimension d_c^+, this result has been derived before [74]. Remarkably, this relation is seen to be obeyed to a good accuracy in the neutron scattering data for $TlCuCl_3$, obtained in ref. [28]. As mentioned earlier, for this material $d = d_c^+ = 3$ such that mean-field behavior is expected up to logarithmic corrections.

5.4.6 Dynamic susceptibility

As in the case of quantum paramagnetic phase, let us connect the excitation modes to the dynamic spin susceptibility,

$$\chi_\alpha(\vec{k},\omega) = -\imath \int_{-\infty}^{\infty} dt e^{\imath\omega t} \langle T_t S_\alpha(\vec{k},t) S_\alpha(-\vec{k},0)\rangle\,. \tag{5.85}$$

Similar to chapter 4, we will restrict our calculation to the single-mode approximation and not consider excitation continua. Unlike the disordered phase, here we will calculate the distribution of mode weights to leading order $(1/d)^0$ only, since going beyond this requires the knowledge of anomalous self-energies[9].

As explained in chapter 4, there are two channels in which one can probe the dynamic spin susceptibility: even and odd. The corresponding spin operators are

[9]The calculation of anomalous self-energies is straightforward but tedious. Since the inclusion of these does not qualitatively change our results, we have not calculated them here.

given by

$$S_\alpha^{e/o} = S_\alpha^1 \pm S_\alpha^2 \,. \tag{5.86}$$

In terms of $\tilde{t}$, the leading-order single-mode expressions are

$$S_x^e(\vec{k}) = \frac{i\lambda}{\sqrt{1+\lambda^2}} \left[\tilde{t}_{(\vec{k}-\vec{Q})y} - \tilde{t}^\dagger_{(-\vec{k}-\vec{Q})y}\right] , \tag{5.87}$$

$$S_y^e(\vec{k}) = \frac{i\lambda}{\sqrt{1+\lambda^2}} \left[\tilde{t}^\dagger_{(-\vec{k}-\vec{Q})x} - \tilde{t}_{(\vec{k}-\vec{Q})x}\right] , \tag{5.88}$$

$$S_z^e(\vec{k}) = 0 \,, \tag{5.89}$$

$$S_x^o(\vec{k}) = \frac{\tilde{t}^\dagger_{-\vec{k}x} + \tilde{t}_{\vec{k}x}}{\sqrt{1+\lambda^2}} \,, \tag{5.90}$$

$$S_y^o(\vec{k}) = \frac{\tilde{t}^\dagger_{-\vec{k}y} + \tilde{t}_{\vec{k}y}}{\sqrt{1+\lambda^2}} \,, \tag{5.91}$$

$$S_z^o(\vec{k}) = \frac{(1-\lambda^2)(\tilde{t}^\dagger_{-\vec{k}z} + \tilde{t}_{\vec{k}z}) + 2\lambda\sqrt{N}\delta_{\vec{k},\vec{Q}}}{1+\lambda^2} \,. \tag{5.92}$$

S_z^e creates a two-particle continuum only and hence it vanishes in this approximation. Note that this is true at any order in $1/d$. Moreover, the contribution from the projectors is irrelevant at this level. Following the procedure explained in chapter 4 and using the Bogoliubov transformation (5.33), we can express the susceptibility in terms of the $\tilde{\tau}$-Green's functions as follows:

$$\chi_x^e(\vec{k},\omega) = \frac{\lambda^2}{1+\lambda^2}\left(u_{(\vec{k}+\vec{Q})y} - v_{(\vec{k}+\vec{Q})y}\right)^2 \Big[\mathcal{G}_y^N(\vec{k}+\vec{Q},\omega) + \mathcal{G}_y^N(\vec{k}+\vec{Q},-\omega) - \mathcal{G}_y^A(\vec{k}+\vec{Q},\omega) - \mathcal{G}_y^A(\vec{k}+\vec{Q},-\omega)\Big] , \tag{5.93}$$

$$\chi_x^o(\vec{k},\omega) = \frac{1}{1+\lambda^2}(u_{\vec{k}x} + v_{\vec{k}x})^2 \Big[\mathcal{G}_x^N(\vec{k},\omega) + \mathcal{G}_x^N(\vec{k},-\omega) + \mathcal{G}_x^A(\vec{k},\omega) + \mathcal{G}_x^A(\vec{k},-\omega)\Big] , \tag{5.94}$$

$$\chi_z^o(\vec{k},\omega) = \left(\frac{1-\lambda^2}{1+\lambda^2}\right)^2 (u_{\vec{k}z} + v_{\vec{k}z})^2 \Big[\mathcal{G}_z^N(\vec{k},\omega) + \mathcal{G}_z^N(\vec{k},-\omega) + \mathcal{G}_z^A(\vec{k},\omega) + \mathcal{G}_z^A(\vec{k},-\omega)\Big] + \frac{4\lambda^2 N}{(1+\lambda^2)^2}\delta(\omega)\delta_{\vec{k},\vec{Q}} \,. \tag{5.95}$$

In obtaining the above expressions we have used the fact that $2\vec{Q}$ is a reciprocal lattice vector. We mention that the expressions for χ_y are obtained from χ_x by replacing $x \leftrightarrow y$.

Since we work in leading order in $1/d$, we need these expressions at the harmonic level, where $\mathcal{G}^A = 0$ and $\lambda = \lambda_0$. Using the degeneracy of the transverse modes, $\tilde{\omega}_{\vec{k}x} = \tilde{\omega}_{\vec{k}y} \equiv \tilde{\omega}_{\vec{k}a}$, $u_{\vec{k}x} = u_{\vec{k}y} \equiv u_{\vec{k}a}$ etc., we obtain the susceptibilities corresponding to the transverse modes as follows:

$$\chi_a^e(\vec{k}+\vec{Q},\omega) = \frac{\lambda_0^2(u_{\vec{k}a} - v_{\vec{k}a})^2}{1+\lambda_0^2}\left[\frac{1}{\omega - \tilde{\omega}_{\vec{k}a}} - \frac{1}{\omega + \tilde{\omega}_{\vec{k}a}}\right] , \tag{5.96}$$

$$\chi_a^o(\vec{k},\omega) = \frac{(u_{\vec{k}a} + v_{\vec{k}a})^2}{1+\lambda_0^2}\left[\frac{1}{\omega - \tilde{\omega}_{\vec{k}a}} - \frac{1}{\omega + \tilde{\omega}_{\vec{k}a}}\right] . \tag{5.97}$$

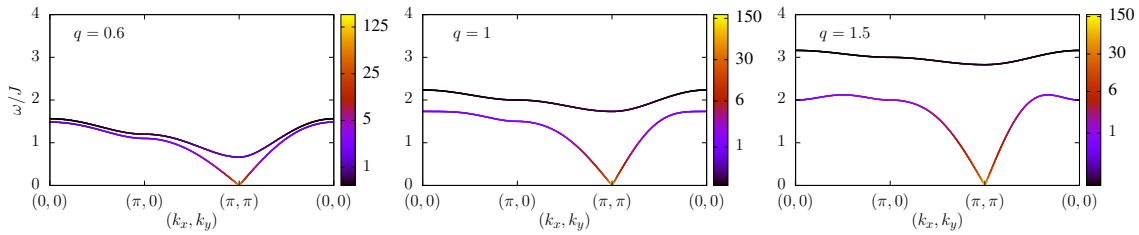

Figure 5.6: Dynamic structure factor (5.102) obtained from the imaginary part of the dynamic spin susceptibility in the odd channel is plotted for different values of q. The curves trace the transverse mode (5.37) as well as the gapped amplitude mode (5.38) dispersions in the harmonic approximation. The color coding corresponds to their respective single-mode spectral weights. There is no broadening in this approximation and the width of the curves is just for better visualization. Here, a logarithmic scale is used for color coding. The spectral weight of the Goldstone modes diverge at $\vec{Q}$. Also, note that the amplitude mode weight is very weak in comparison to the transverse mode weights.

Interestingly, the mode momentum in the even channel is shifted by $\vec{Q}$. Also, the mode weight in the even channel vanishes upon approaching the quantum critical point (since $\lambda_0 \to 0$). However, there is no shift of momentum in the odd channel. The signal from the odd channel smoothly connects to the triplon-mode response of the paramagnet, as calculated in section 4.5.6. Hence the primary signal is in the odd channel. The signal in the even channel can be interpreted as a replicated signal due to the condensate Bragg scattering, with the condensate signal itself being in the odd channel.

The longitudinal susceptibility in the odd channel is given by

$$\chi^o_z(\vec{k},\omega) = \left(\frac{1-\lambda_0^2}{1+\lambda_0^2}\right)^2 (u_{\vec{k}z}+v_{\vec{k}z})^2 \left[\frac{1}{\omega-\tilde{\omega}_{\vec{k}z}} - \frac{1}{\omega+\tilde{\omega}_{\vec{k}z}}\right] + \frac{4\lambda_0^2 N}{(1+\lambda_0^2)^2}\delta(\omega)\delta_{\vec{k},\vec{Q}}\,. \quad (5.98)$$

The last term in the above equation corresponds to the magnetic Bragg peak of the ordered state, recall $M_{\rm st} = 2\lambda_0/(1+\lambda_0^2)$ to leading order. So although the amplitude mode has no single-mode spectral weight in the even channel, it is visible in the odd channel. However, its spectral weight is much weaker than that of Goldstone modes. This can be easily understood from the fact that since the Goldstone modes are soft, they essentially have a diverging weight at the ordering wavevector $\vec{Q}$. Upon approaching the critical point, the amplitude mode signal merges with that of the Goldstone modes in this channel. As mentioned earlier, it is then connected to the triplon weight in the disordered phase. However, in the limit of decoupled layers, its weight vanishes. This is physically easy to understand. The amplitude mode describes two flipped spins w.r.t. the Néel state in this limit, so it cannot be excited by the action of a single spin operator.

As discussed in section 4.5.6, higher orders in the $1/d$ expansion for $\chi(\vec{k},\omega)$ will place the poles at the renormalized mode frequencies $\tilde{\Omega}_{\vec{k}\alpha}$, thus producing a $1/d$ correction to the weights. Therefore, it is suggestive to write the mode weights as $\mathcal{Z}^{(o)}_{\vec{k}\alpha} = (J/\tilde{\Omega}_{\vec{k}\alpha})\mathcal{W}^{(o)}_{\vec{k}\alpha}$ and $\mathcal{Z}^{(e)}_{\vec{k}+\vec{Q}\alpha} = (J/\tilde{\Omega}_{\vec{k}\alpha})\mathcal{W}^{(e)}_{\vec{k}+\vec{Q}\alpha}$. Finally, for $h^z = 0$, after a few

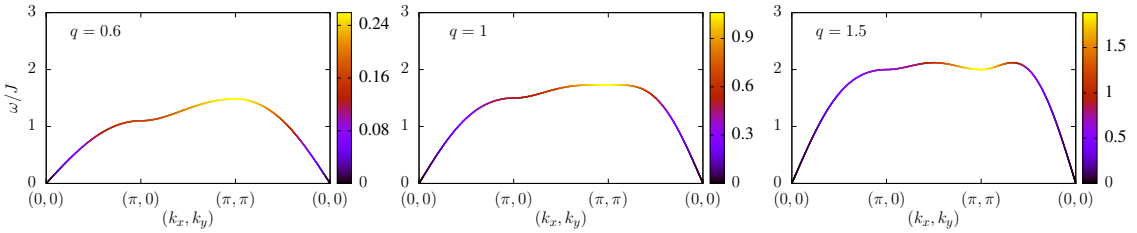

Figure 5.7: Dynamic structure factor (5.103) obtained from the imaginary part of the dynamic spin susceptibility in the even channel is plotted for different values of q. The curves trace the transverse mode dispersion (5.37) shifted by $\vec{Q}$, in the harmonic approximation. The color coding corresponds to the respective single-mode spectral weight. There is no broadening in this approximation and the width of the curves is just for better visualization. Unlike the odd channel, the spectral weight of the Goldstone modes does not diverge. Also, the amplitude mode does not have a single-mode contribution.

steps of algebra we find

$$\mathcal{W}^{(o)}_{\vec{k}a} = \frac{(2q+1)[2q(1-\gamma_{\vec{k}})+1+\gamma_{\vec{k}}]}{8q} + \mathcal{O}\left(\frac{1}{d}\right), \tag{5.99}$$

$$\mathcal{W}^{(o)}_{\vec{k}z} = \frac{1}{2q} + \mathcal{O}\left(\frac{1}{d}\right) \tag{5.100}$$

in the odd channel, and

$$\mathcal{W}^{(e)}_{\vec{k}+\vec{Q}a} = \frac{(2q-1)(2q+1)(1+\gamma_{\vec{k}})}{8q} + \mathcal{O}\left(\frac{1}{d}\right), \tag{5.101}$$

in the even channel. Here the momentum shift by $\vec{Q}$ has been made explicit. As mentioned earlier, the spectral weight of the transverse modes in the odd channel diverges as $1/\omega$ at the ordering wavevector $\vec{Q}$. Whereas, due to the factor $(1+\gamma_{\vec{k}})$ in eq. (5.101), we see that the even channel transverse mode spectral weight vanishes as ω at $\vec{Q}$. This appears qualitatively consistent with results from series expansions for the bilayer Heisenberg model [51].

As in the disordered phase, we can define the dynamic structure factor as the imaginary part of the susceptibility in each channel. At this level of calculation we will obtain

$$S^{(o)}_S(\vec{k},\omega) = \sum_{\alpha=x,y,z}\left[\mathcal{Z}^{(o)}_{\vec{k}\alpha}\delta(\omega-\tilde{\omega}_{\vec{k}\alpha}) + \mathcal{Z}^{(o)-}_{\vec{k}\alpha}\delta(\omega+\tilde{\omega}_{\vec{k}\alpha})\right], \tag{5.102}$$

$$S^{(e)}_S(\vec{k},\omega) = \sum_{\alpha=x,y,z}\left[\mathcal{Z}^{(e)}_{\vec{k}\alpha}\delta(\omega-\tilde{\omega}_{\vec{k}+\vec{Q}\alpha}) + \mathcal{Z}^{(e)-}_{\vec{k}\alpha}\delta(\omega+\tilde{\omega}_{\vec{k}+\vec{Q}\alpha})\right]. \tag{5.103}$$

Here, $\mathcal{Z}^{(e/o)-}_{\vec{k}\alpha}$ is the spectral weight of the negative pole (not calculated here). The dynamic structure factor in the odd channel and the even channel is plotted in fig.

5.6 and 5.7 respectively. In these figures, we can immediately see all the different scenarios discussed above, related to the spectral weights. Apart from that, deep in the ordered phase we notice that the longitudinal mode has a very weak dispersion, and it becomes dispersionless in the limit of decoupled layers. Also, as we approach the limit $J \to 0$, the transverse modes develop a second dispersion minimum at $\vec{k} = 0$ (seen at $\vec{k} = \vec{Q}$ in the even channel, owing to the shift), which is in accord with the spin-wave theory calculations [48]. However, in the decoupled layer limit, the single-mode spectral weight in both the channels is proportional to $\sqrt{1-\gamma_{\vec{k}}}$ and hence it is zero at $\vec{k} = 0$. Before we close this section, we mention that the contribution from the continua starts only at order $1/d$.

5.4.7 Bond-bond correlation

Let us now turn our attention to another dynamical observable namely the bond-bond correlation (4.126) introduced in the last chapter. For convenience let us write it down again,

$$\chi_{\mathcal{B}}(\vec{k},\omega) = -i\int_{-\infty}^{\infty} dt e^{i\omega t}\langle T_t \mathcal{B}_{\vec{k}}(t)\mathcal{B}_{-\vec{k}}(0)\rangle\,. \tag{5.104}$$

Even for this observable we will restrict ourselves to the leading order calculation as going beyond it requires anomalous self-energies. Also, we will be working in the zero field.

We start with the inter-layer case, i.e., correlation between intra-dimer bonds. In this case, we then have

$$\begin{aligned}\mathcal{B}_i &= \vec{S}_{i1}\cdot\vec{S}_{i2}\\ &= -\frac{3}{4} + \tilde{t}^{\dagger}_{ix}\tilde{t}_{ix} + \tilde{t}^{\dagger}_{iy}\tilde{t}_{iy} + \frac{1}{1+\lambda^2}\left[\tilde{t}^{\dagger}_{iz}\tilde{t}_{iz} + \lambda^2 P_i + \lambda e^{i\vec{Q}\cdot\vec{r}_i}(\tilde{t}^{\dagger}_{iz} + \tilde{t}_{iz})\right]\\ &= -\frac{3}{4} + \frac{\lambda^2}{1+\lambda^2} + \frac{\lambda}{1+\lambda^2}e^{i\vec{Q}\cdot\vec{r}_i}(\tilde{t}^{\dagger}_{iz} + \tilde{t}_{iz}) + \tilde{t}^{\dagger}_{iz}\tilde{t}_{iz} + \frac{\tilde{t}^{\dagger}_{ix}\tilde{t}_{ix} + \tilde{t}^{\dagger}_{iy}\tilde{t}_{iy}}{1+\lambda^2}\,,\end{aligned} \tag{5.105}$$

where $\vec{Q} = \{\pi, \pi, ...\}$ and in the last equation we have used the definition $P_i = 1 - \sum_\alpha \tilde{t}^{\dagger}_{i\alpha}\tilde{t}_{i\alpha}$ $(\alpha = x, y, z)$. This gives us

$$\begin{aligned}\mathcal{B}_{\vec{k}} = \sqrt{N}\left[-\frac{3}{4} + \frac{\lambda^2}{1+\lambda^2}\right]\delta_{\vec{k},0} + \frac{\lambda}{1+\lambda^2}(\tilde{t}^{\dagger}_{\vec{k}-\vec{Q},z} + \tilde{t}_{-\vec{k}+\vec{Q},z})\\ + \frac{1}{\sqrt{N}}\sum_{\vec{q}}\left[\tilde{t}^{\dagger}_{\vec{q},z}\tilde{t}_{\vec{q}-\vec{k},z} + \frac{\tilde{t}^{\dagger}_{\vec{q},x}\tilde{t}_{\vec{q}-\vec{k},x} + \tilde{t}^{\dagger}_{\vec{q},y}\tilde{t}_{\vec{q}-\vec{k},y}}{1+\lambda^2}\right].\end{aligned} \tag{5.106}$$

Within the single mode approximation, as explained earlier, we will ignore the last term in the above equation because it will either contribute to continuum or give a $1/d$ correction to the Bragg peak. This means that we do not have a single-mode contribution from the transverse modes in this channel. In other words the transverse modes contributes only to continua which we do not consider in the present analysis.

We thus obtain

$$\chi^{ord}_{inter}(\vec{k}+\vec{Q},\omega) = \frac{\lambda^2}{1+\lambda^2}\Big[\mathcal{G}_{N,z}(\vec{k},\omega)+\mathcal{G}_{N,z}(\vec{k},-\omega)+\mathcal{G}_{A,z}(\vec{k},\omega)+\mathcal{G}_{A,z}(\vec{k},-\omega)\Big] + N\left[-\frac{3}{4}+\frac{\lambda^2}{1+\lambda^2}\right]^2\delta_{\vec{k},0}\delta(\omega) \tag{5.107}$$

$$= \frac{\lambda^2}{1+\lambda^2}(u_{\vec{k},z}+v_{\vec{k},z})^2\left[\frac{1}{\omega-\omega_{\vec{k}z}}-\frac{1}{\omega+\omega_{\vec{k}z}}\right] + N\left[-\frac{3}{4}+\frac{\lambda^2}{1+\lambda^2}\right]^2\delta_{\vec{k},0}\delta(\omega)\,, \tag{5.108}$$

where we have used the fact that $\vec{k}$ lies in the first Brillouin zone and that $\vec{k}\pm 2\vec{Q}$ is equivalent to $\vec{k}$ (since $2\vec{Q}$ is the reciprocal lattice vector). In the above expression $\mathcal{G}_N$ and $\mathcal{G}_A$ refer to zero-temperature normal and anomalous Green's function respectively. Also, $u_{\vec{k},z}$ and $v_{\vec{k},z}$ are Bogoliubov coefficients used in diagonalizing the Hamiltonian to leading order in $1/d$ and defined in eq. (5.33). We can now read the mode weight corresponding to $\omega_{\vec{k}z}$ from the above expression,

$$\mathcal{Z}_{\vec{k}+\vec{Q}} = \frac{\lambda^2}{1+\lambda^2}(u_{\vec{k},z}+v_{\vec{k},z})^2 = \frac{2q-1}{2\sqrt{4q^2+\gamma_{\vec{k}}}}\,, \tag{5.109}$$

where, since we are working in the harmonic approximation, we have inserted $\lambda=\lambda_0$ and used the corresponding zero field value (5.23). Thus the amplitude mode has a finite signal in this channel. Moreover it is the only mode contributing to a single-mode weight. Also, its weight vanishes at the quantum critical point, $q_c = 1/2$ at this level, which correctly correlates with our earlier result in sec. 4.5.7 that the triplon excitations in the disordered phase have no single mode contribution.

As in the disordered phase, we can also look at the intra-planar case. It is again distinguished into even or odd channel. Let us first consider the even channel where

$$\mathcal{B}^d_i = \vec{S}_i\cdot\vec{S}_{i+d} = \vec{S}_{1,i}\cdot\vec{S}_{1,i+d}+\vec{S}_{2,i}\cdot\vec{S}_{2,i+d}\,. \tag{5.110}$$

At the level of single-mode approximation and to leading order in $1/d$, only relevant terms in $\mathcal{B}^d_i$ are those which are at most linear in $\tilde{t}$ because rest of the terms will either contribute to continuum or give a $1/d$ correction. We observe that $\vec{S}^x_i\cdot\vec{S}^x_{i+d}$ and $\vec{S}^y_i\cdot\vec{S}^y_{i+d}$ contain terms which are at least bilinear in $\tilde{t}$. Hence even in this case transverse modes do not carry single-mode weight but only contribute to the continuum. So relevant single-mode contribution is only from $z-$ component of the spins. At this level:

$$\vec{S}^z_{1,i} = -\vec{S}^z_{2,i} \approx \frac{1}{2(1+\lambda^2)}\left[(1-\lambda^2)(\tilde{t}^\dagger_{i,z}+\tilde{t}_{i,z})+\lambda(e^{i\vec{Q}\cdot\vec{r}_i}+e^{-i\vec{Q}\cdot\vec{r}_i})\right], \tag{5.111}$$

$$\vec{S}^z_{1,i+d} = -\vec{S}^z_{2,i+d} \approx \frac{1}{2(1+\lambda^2)}\left[(1-\lambda^2)(\tilde{t}^\dagger_{i+d,z}+\tilde{t}_{i+d,z})+\lambda(e^{i\vec{Q}\cdot\vec{r}_{i+d}}+e^{-i\vec{Q}\cdot\vec{r}_{i+d}})\right]. \tag{5.112}$$

As discussed above, retaining the relevant terms which are at most linear in $\tilde{t}$ and using the fact that $\vec{r}_{i+d} = \vec{r}_i+\vec{\Delta}$ (where $\vec{\Delta}$ is vector joining the nearest neighbor) and

$e^{2i\vec{Q}\cdot\vec{r}_i} = 1$, we have

$$\mathcal{B}_i^d = \frac{1}{2(1+\lambda^2)^2}\Big[\lambda(1-\lambda^2)\left(e^{i\vec{Q}\cdot\vec{r}_{i+d}} + e^{-i\vec{Q}\cdot\vec{r}_{i+d}}\right)\left(\tilde{t}^\dagger_{i,z} + \tilde{t}_{i,z}\right) + \lambda(1-\lambda^2)\left(e^{i\vec{Q}\cdot\vec{r}_i} + e^{-i\vec{Q}\cdot\vec{r}_i}\right)\left(\tilde{t}^\dagger_{i+d,z} + \tilde{t}_{i+d,z}\right) + 2\lambda^2\left(e^{i\vec{Q}\cdot\vec{\Delta}} + e^{-i\vec{Q}\cdot\vec{\Delta}}\right)\Big]. \quad (5.113)$$

After Fourier transformation

$$\mathcal{B}^d_{\vec{k}} = \frac{\lambda(1-\lambda^2)}{2(1+\lambda^2)^2}\Big[\left(e^{i\vec{Q}\cdot\vec{\Delta}} + e^{i(\vec{k}-\vec{Q})\cdot\vec{\Delta}}\right)\left(\tilde{t}^\dagger_{\vec{k}-\vec{Q},z} + \tilde{t}_{\vec{k}-\vec{Q},z}\right) + \left(e^{-i\vec{Q}\cdot\vec{\Delta}} + e^{i(\vec{k}+\vec{Q})\cdot\vec{\Delta}}\right)\left(\tilde{t}^\dagger_{\vec{k}+\vec{Q},z} + \tilde{t}_{\vec{k}+\vec{Q},z}\right)\Big] + \frac{\lambda^2}{(1+\lambda^2)^2}\left(e^{i\vec{Q}\cdot\vec{\Delta}} + e^{-i\vec{Q}\cdot\vec{\Delta}}\right)\delta_{\vec{k},0}\sqrt{N}\,. \quad (5.114)$$

Similarly one can write $\mathcal{B}^{d'}_{-\vec{k}}$ corresponding to a different bond within the plane by replacing $\vec{\Delta}$ with $\vec{\Delta}'$ in the above equation. However we shall concentrate on the case where $\vec{\Delta} = \vec{\Delta}'$. Now after some steps of algebra and using the fact that $e^{\pm i\vec{Q}\cdot\vec{\Delta}} = -1$, we arrive at the following expression for the susceptibility:

$$\chi^{ord}_{even}(\vec{k}+\vec{Q},\omega) = \frac{\lambda^2(1-\lambda^2)^2}{(1+\lambda^2)^4}\left(1-\cos(\vec{k}\cdot\vec{\Delta})\right)(u_{\vec{k}z} + v_{\vec{k}z})^2\left[\frac{1}{\omega-\omega_{\vec{k}z}} - \frac{1}{\omega+\omega_{\vec{k}z}}\right] + \frac{4N\lambda^4}{(1+\lambda^2)^4}\delta_{\vec{k}-\vec{Q}}\delta(\omega)\,. \quad (5.115)$$

This gives the weight corresponding to $\omega_{\vec{k}z}$ as follows:

$$\mathcal{Z}_{\vec{k}+\vec{Q}} = \frac{\lambda^2(1-\lambda^2)^2}{(1+\lambda^2)^4}\left(1-\cos(\vec{k}\cdot\vec{\Delta})\right)(u_{\vec{k}z} + v_{\vec{k}z})^2\,, \quad (5.116)$$

$$= \frac{(2q-1)(2q+1)}{16q^2}\frac{\left(1-\cos(\vec{k}\cdot\vec{\Delta})\right)}{\sqrt{4q^2+\gamma_{\vec{k}}}}\,. \quad (5.117)$$

Notice that $\mathcal{Z}_{\vec{k}+\vec{Q}}$ now depends on $\vec{k}\cdot\vec{\Delta}$. For correlation among bonds along $\hat{x}$ and for those along $\hat{y}$, $\vec{k}\cdot\vec{\Delta} = \vec{k}_x$ and $\vec{k}\cdot\vec{\Delta} = \vec{k}_y$ respectively. However due to $\mathcal{C}_4$ symmetry of the system bond-correlation in the two cases is related by a $\pi/2$ rotation in the Brillouin zone.

Now, in the intra-planar odd sector,

$$\mathcal{B}_i^d = \vec{S}_{1,i}\cdot\vec{S}_{1,i+d} - \vec{S}_{2,i}\cdot\vec{S}_{2,i+d}\,. \quad (5.118)$$

Here we observe that $\mathcal{B}_i^d$ is at least bilinear in $\tilde{t}$. Hence to leading order in $1/d$ there is no single-particle contribution, but only a continuum.

5.5 Vanishing intra-dimer coupling and spin-wave theory

As mentioned several times, for $J = 0$ our model (5.1) corresponds to two decoupled hypercubic antiferromagnets. We will therefore make connections to the spin-wave theory in this limit. We will see that the amplitude mode plays a non-trivial role in this limit.

5.5.1 Spin waves and $1/d$ expansion

As introduced in chapter 2, the spin-wave theory is an expansion around a classical ground state corresponding to the spin-S quantum magnet in the large-S limit. Here the small parameter is $1/S$. In chapter 2, we discussed two ways to formulate the spin problem in terms of interacting Bosons. One of them utilizes the Holstein-Primakoff representation [75] of spin operators. Now we apply the spin-wave theory to a spin-S Heisenberg model on a hypercubic lattice in d dimensions with nearest-neighbor interaction K and demonstrate that it can be used to generate a $1/d$ expansion. The general formalism is standard and can be found in ref. [48].

The ground-state energy per spin to order $1/S$ reads [48]

$$\frac{E_0^{\mathrm{SW}}}{N} = -\frac{KzS^2}{2}\left[1 + \frac{1}{S}\left(1 - \frac{2}{N}{\sum_{\vec{k}}}' \sqrt{1-\gamma_{\vec{k}}^2}\right)\right], \tag{5.119}$$

where $\gamma_{\vec{k}}$ is defined in eq. (5.30), $z = 2d$ the coordination number, N the number of sites, and the momentum summation is now over the reduced Brillouin zone of the antiferromagnetic state. Following our general idea of the large-d limit discussed in chapter 3, a $1/d$ expansion of this result can be generated. This is done by expanding the argument of the momentum sum in powers of $\gamma_{\vec{k}}$. Using $(2/N)\sum_{\vec{k}}' \gamma_{\vec{k}}^2 = 1/(2d)$ we arrive at the following expression

$$\frac{E_0^{\mathrm{SW}}}{N} = -KdS^2\left[1 + \frac{1}{S}\left(\frac{1}{4d} + \mathcal{O}\left(\frac{1}{d^2}\right)\right)\right]. \tag{5.120}$$

Similarly, we can obtain an expansion for the staggered magnetization per site. Firstly, to $\mathcal{O}(1/S)$ the staggered magnetization per site reads:

$$\frac{M_{\mathrm{st}}^{\mathrm{SW}}}{N} = S\left[1 - \frac{1}{2S}\left(\frac{2}{N}{\sum_{\vec{k}}}' \frac{1}{\sqrt{1-\gamma_{\vec{k}}^2}} - 1\right)\right]. \tag{5.121}$$

Expanding in powers of $\gamma_{\vec{k}}$ under the momentum sum and performing the momentum summation yields:

$$\frac{M_{\mathrm{st}}^{\mathrm{SW}}}{N} = S\left[1 - \frac{1}{S}\left(\frac{1}{8d} + \mathcal{O}\left(\frac{1}{d^2}\right)\right)\right]. \tag{5.122}$$

For both E_0 and M_{st} it can be shown that higher-order terms in the $1/S$ expansion [76] are suppressed at least as $1/d^2$ in the large-d limit. This implies that spin-wave theory to order $1/S$ is sufficient to generate the first two terms of the $1/d$ expansion for *arbitrary* value of S. We believe that similar systematics applies at higher orders as well.

5.5.2 Bond-operator theory for vanishing intra-dimer coupling

Let us now make a comparison to the results obtained from the $1/d$ expansion. The ground-state energy per dimer, eq. (5.62), reduces to $E_0/(qJN) = -1/2 - 1/(4d)$, in the limit $q \to \infty$. While in this limit, the staggered magnetization per dimer, eq. (5.75), is $M_{\rm st} = 1 - 1/(4d)$. Each dimer consists of two spins and therefore for comparison we need to send $N \to 2N$ in eq. (5.120) and (5.122). We then find the two approaches give identical results for $S = 1/2$.

Additionally, we find that the leading-order (transverse) mode dispersions in both approaches yields perfect agreement. As seen before, in this limit the Goldstone modes from $1/d$ calculation have the property $\tilde{\omega}_{\vec{k}} = \tilde{\omega}_{\vec{k}+\vec{Q}}$ and are gapless both at $\vec{k} = 0$ and $\vec{k} = \vec{Q}$. This correctly gives a total of four Goldstone modes. At any finite J, however, there are only two Goldstone modes. Moreover, we have also seen that the mode weights in the even and odd channel are identical in the $q \to \infty$ limit (recall that they are proportional to $\sqrt{1-\gamma_{\vec{k}}}$). This is expected because in the decoupled layer limit, the fluctuations in the two layers are independent and it must not matter which channel is probed.

In this limit, the amplitude mode is flat: $\tilde{\Omega}_{\vec{k}z} = 2Kd$ (5.80). Also, it carries zero spectral weight, eq. (5.92), as noted earlier. They is related to the fact that the simultaneous spin-flip is unnatural in this limit. However, the amplitude mode can not be discarded when performing bond-operator calculations for $J = 0$. It can be seen from the self-energy expressions for the transverse mode, in appendix D.3, that the diagrams involving the amplitude mode have a nonzero contribution even when $J = 0$. In particular, these are required to fulfill the Goldstone condition, $\tilde{\Omega}_{\vec{Q}a} = 0$, at order $1/d$. So it means that although the two approaches generically involve different intermediate quantities, diagrams etc., the final results are expected to match.

5.6 Discussion

Using the machinery developed in chapter 3 and 4, we have calculated observables in the antiferromagnetic phase. As we saw, the calculation in this case is more involved and we have to keep track of different sources of $1/d$. A similar analysis can be done in any given magnetically ordered phase. We also see that all the observables we have calculated here smoothly interpolate into those calculated in the disordered phase. This remarkable consistency establishes the $1/d$ expansion as a controlled and consistent approach for coupled-dimer magnets. The discussion related to generalization of the present model presented in the last chapter also applies in this phase.

Chapter 6

Comparison to QMC

There are very few spin models which can be solved analytically and this is where numerical techniques play a key role in understanding these systems. Analytic techniques and exact numerics complement each other. One of the pillars of numerical techniques is quantum Monte Carlo (QMC) simulation. In this chapter, we will compare the quantum Monte Carlo data (obtained by Maximillian Lohöfer, Stefan Wessel et al. [77]) for Heisenberg spin-1/2 antiferromagnet on a square-lattice bilayer (i.e. coupled-dimer model (2.2) in $d = 2$) with our $1/d$ expansion results. In particular we will be interested in dynamical properties especially bond-bond correlation, where we can see the signal corresponding to the amplitude (*Higgs*) mode. This chapter is based on the results in ref. [77].

6.1 Mapping

Quantum Monte Carlo being an accurate numerical method the quantum critical points obtained therein and from our $1/d$ expansion method are not the same. Recall that our result for the phase boundary from eq. (4.94) (with asymmetry parameter $\kappa = 0$) gives $q_c = 0.59375$ in $d = 2$, whereas the QMC locates the phase boundary at $(q_{QMC})_c = 0.7930(2)$ [62, 77]. We have to account for this difference while comparing the two approaches. Moreover, the QMC data has been obtained as a function of the ratio $g = J/K$ between the inter-layer and intra-layer exchange coupling and so $q_{QMC} \equiv d/g = 2/g$ in this case. In terms of the parameter g, the quantum paramagnetic phase occurs for $g > g_c$ while the magnetically ordered phase happens to be in the region $g < g_c$ with $g_c = 2.5220(1)$ [77] being the quantum critical point obtained from the QMC.

In the quantum paramagnetic phase, $g > g_c$, we choose our parameter q such that the *relative* distance to the quantum critical point is same in the two methods. The choice of q is therefore given by

$$\frac{q - q_c}{q_c} = \frac{q_{QMC} - (q_{QMC})_c}{(q_{QMC})_c} \,. \tag{6.1}$$

On the other hand, for any value of $g \leq g_c$ we choose our q such that the absolute distance to the critical point is same in the two methods. Thus in the magnetically

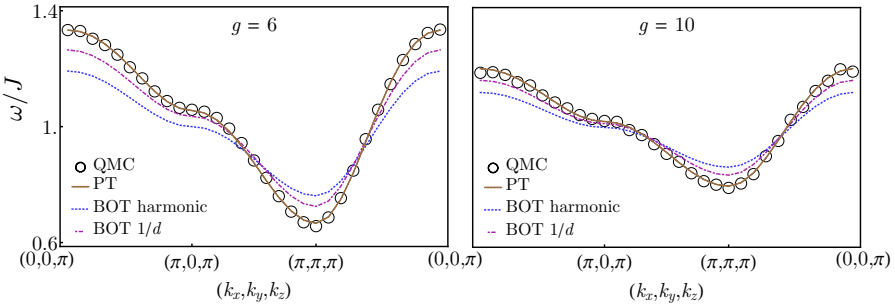

Figure 6.1: Comparison of the triplon dispersion as obtained from the dynamic spin structure factor using QMC and from our $1/d$ expansion (4.87) in the paramagnetic phase. Also shown is the dispersion obtained using perturbation theory in small K/J. The plot shows the data obtained only from the odd channel since the even channel does not yield a single-mode contribution, as seen in section 4.5.6. This figure is taken from ref. [77].

ordered phase the choice of q is made using the following relation:

$$q - q_c = q_{QMC} - (q_{QMC})_c \,. \tag{6.2}$$

The reason for these slightly different choices for comparison in the two phases is due to the fact that $g\,, q \in \big[0, \infty\big)$ but the disordered phase is realized for $g > g_c$ and $q < q_c$ while the ordered phase occurs in the region $g < g_c$ and $q > q_c$.

6.2 Observables

In this section we will compare our results from $1/d$ expansion to QMC results obtained for dynamic spin susceptibility and the bond-bond correlation.

6.2.1 Dynamic spin susceptibility

Mode dispersion from the QMC simulation is extracted from the data obtained for imaginary part of dynamic spin susceptibility (i.e. dynamic spin structure factor), after performing analytic continuation. As discussed in the last chapters, in the model under consideration we have two channels: symmetric (even) and antisymmetric (odd). Corresponding to these two channels we have plotted the triplon dispersion in the disordered phase ($g = 6, 10$) and the transverse mode dispersion in the ordered phase ($g = 1, 2$) as obtained from QMC as well as $1/d$ expansion in fig. 6.1 and fig. 6.2 respectively[1]. In the disordered and ordered phases, it is possible to use a perturbation theory (PT) in small K/J and the spin-wave theory (SWT) respectively. Whereas our large-d limit based bond-operator theory (BOT) can be used in both the phases.

[1]In these plots and other plots in this chapter, an additional component k_z is seen in the $\vec{k}$. This is relevant when probing the considered observables in a scattering experiment. In short, $k_z = 0$ ($k_z = \pi$) corresponds to the symmetric (antisymmetric), i.e. even (odd), combination of the two spins forming a dimer.

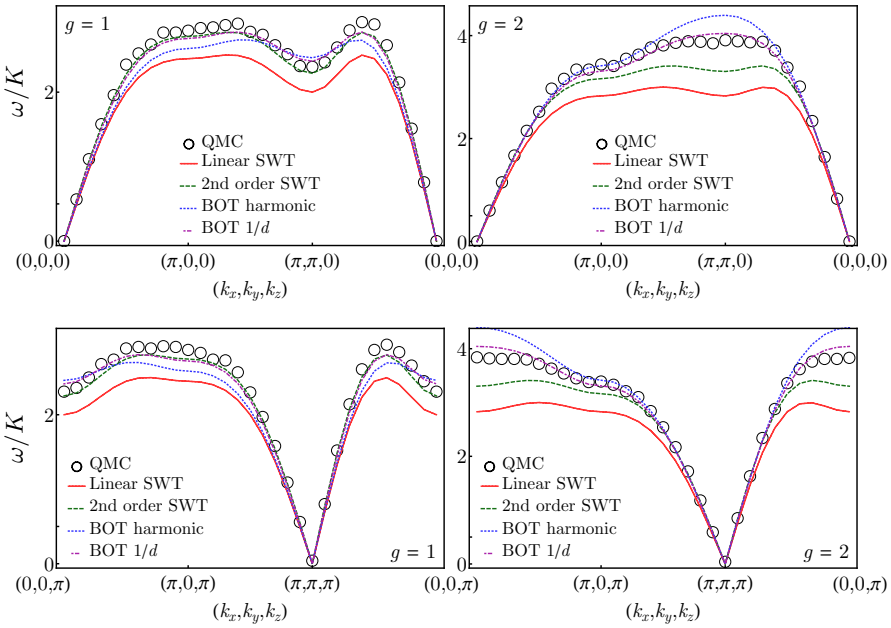

Figure 6.2: Comparison of the Goldstone mode dispersion as obtained from the dynamic spin structure factor using QMC and from our $1/d$ expansion (5.77) in the antiferromagnetic phase. Also shown is the data from the spin-wave theory. The top panel shows data corresponding to the even channel while the bottom panel shows the odd channel data. As already seen in section 5.4.6, the even channel data is shifted by $\vec{Q}$. This figure is taken from ref. [77].

Using the mapping discussed in the last section we have used the values of $q = 1.707, 0.707, 0.21, 0.126$ in the harmonic approximation, and $q = 1.846, 0.846, 0.268, 0.161$ with $1/d$ correction, corresponding to $g = 1, 2, 6, 10$ respectively. Note that there are two different sets of values of q for the harmonic level and $1/d$ corrected results because the q_c is different in the two cases. Coming back to fig. 6.1 and 6.2, we see that our $1/d$ expansion results (4.87) and (5.77) fit very well with the QMC data especially after including the $1/d$ corrections. Nevertheless even at the harmonic level we see that all the qualitative features of the QMC data are well captured. In accord with our calculation in section 4.5.6, there is no single-mode contribution to the QMC data in the symmetric channel of the disordered phase. We see that the dispersion in the symmetric channel of ordered phase is shifted by $\vec{Q}$ as predicted in section 5.4.6.

Apart from the agreement of dispersions our $1/d$ results are also in qualitative agreement with the spectral weights obtained from dynamic spin structure factor from QMC. If we consider the symmetric channel then coming from the ordered phase the single-mode spectral weight keeps diminishing until it vanishes at the quantum critical point with no single-mode contribution seen in the disordered phase. This is also seen in the QMC data (fig. 1 in ref. [77]). On the other hand, there is always a finite single-mode spectral weight in the antisymmetric channel with the maximum weight around $\vec{Q}$, and this can be verified from the QMC data as well (fig. 1 in ref. [77]). Moreover, in the last chapter we saw that the single mode contribution of the amplitude mode occurs only in the antisymmetric channel with extremely small spectral weight

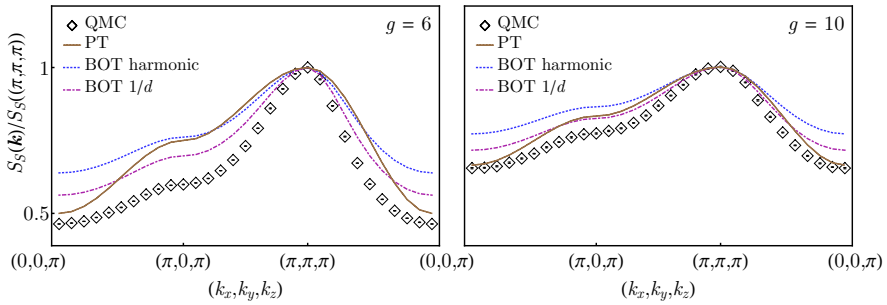

Figure 6.3: Comparison of the integrated spectral weight as obtained using QMC and from our $1/d$ expansion (4.123) in the paramagnetic phase. It is normalized using the spectral weight at $\vec{Q} = (\pi, \pi)$. Also shown is the data from perturbation theory in small K/J. The plots show data obtained only from the odd channel since the even channel does not yield a single mode contribution, as seen in section 4.5.6. This figure is taken from ref. [77].

compared to those from the Goldstone modes.This is also reflected in the QMC data[2] for dynamic spin structure factor [77].

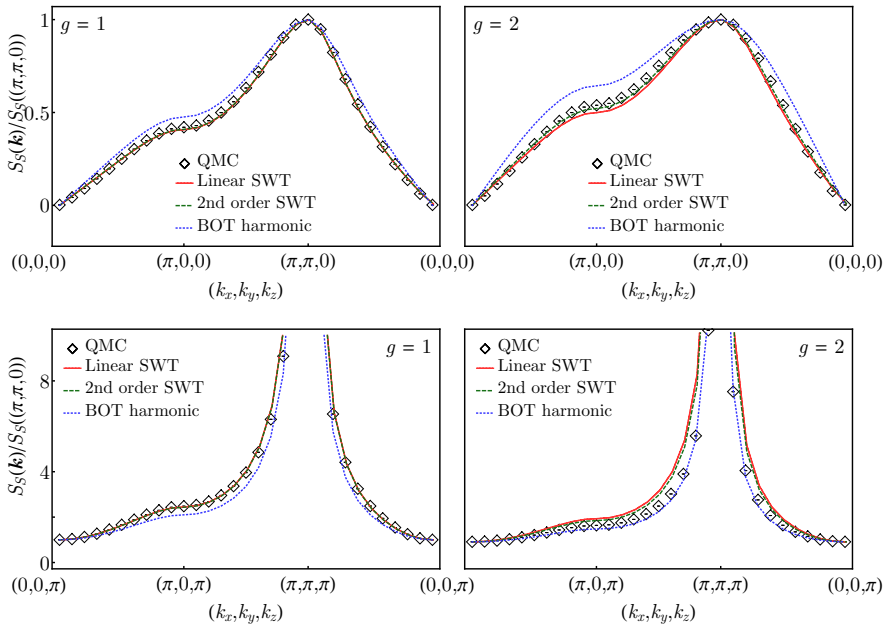

Figure 6.4: Comparison of the integrated spectral weight as obtained using QMC and from our $1/d$ expansion ((5.99),(5.101)) in the antiferromagnetic phase. It contains only the Goldstone-mode contribution. Also shown is the data from the spin-wave theory. The top panel shows the data corresponding to the even channel while the bottom panel shows the odd channel data. These are normalized by the maximum and minimum weight in these channels respectively. This figure is taken from ref. [77].

[2]In reality there is also damping which masks the amplitude mode. However this aspect is not covered in our large-d formalism.

Apart from the dispersion we can also compare the integrated spectral weight, $S_S(\vec{k}) \equiv \mathcal{Z}_{\vec{k}}$, calculated in chapter 4 and 5. This quantity can be obtained directly from QMC simulation without the need to perform analytic continuation. We see from fig. 6.3 and 6.4 that our $1/d$ expansion result agrees qualitatively with the QMC data. Here, in the ordered phase we have used the harmonic level results only, since the $1/d$ corrections to the spectral weight have not been calculated, as explained in section 5.4.6. The integrated spectral weights are appropriately normalized in the respective figures.

6.2.2 Amplitude (Higgs) mode

In the spontaneous $SU(2)$ symmetry broken phase, apart from the two degenerate gapless transverse (Goldstone) modes we also have the gapped amplitude mode. In the language of field theory with a mexican-hat potential, (see discussion in chapter 1) the tranverse modes correspond to the massless particles- Goldstone modes. While the amplitude mode corresponds to a massive particle, corresponding to the order-parameter fluctuation. As discussed in chapter 1, local gauge invariance requires a minimal coupling between a massless gauge field and a massive scalar field in the underlying filed theory. In this situation, the Higgs mechanism leads to a massive gauge field in the spontaneously broken-symmetry (continuous) phase, instead of massless Goldstone Bosons. Prominent example of this is in the case of superconductors, where the massive plasmon predicted by Anderson [18] is the Higgs mode. In the antifferromagnets under consideration, there is no local gauge invariance and hence there is no Higgs mechanism. However, being massive (gapped), the amplitude mode in this case is often referred to as the Higgs mode in the literature [16].

In the past few years, the subject of the Higgs mode in condensed matter physics has attracted enormous interest. Field-theoretic calculations in the context of antiferromagnets can be found in the literature [73, 78]. In general, it has been argued that since the Higgs mode is a massive scalar, observables which are *linear* in the order-parameter field cannot access it due to significant damping. It is therefore suggested that an observable which is quadratic in the order-parameter field might be a good choice [73, 79]. One such observable is the bond-bond correlation calculated in the previous chapters. We have found that the bond-bond correlation has single-mode contribution only from the amplitude mode, which is in accord with the above statement. It may be possible to detect the signal corresponding to this observable in a scattering experiment, for instance the Raman scattering.

In fig. 6.5 we have shown the dynamic singlet structure factor, i.e. the imaginary part of the bond-bond correlation (inter-planar), obtained from quantum Monte Carlo simulation (Maximilian Lohöfer, Stefan Wessel et al. [77]). The amplitude mode dispersion (5.38) in the harmonic approximation is shown on top. It qualitatively agrees with the QMC data. In fig. 6.6, we have shown the dynamic singlet structure factor obtained by taking the imaginary part of eq. (5.107) (leaving out the trivial Bragg peak related term). We see that the amplitude-mode dispersion is shifted by $\vec{Q}$, which is also seen in fig. 6.5. Moreover, we observe in fig. 6.6 that the single-mode spectral weight is maximum at the Γ point (i.e. $\vec{k} = (0, 0)$). This is not apparent in the QMC data shown in fig. 6.5. However, if we look at the spectral weight from the QMC

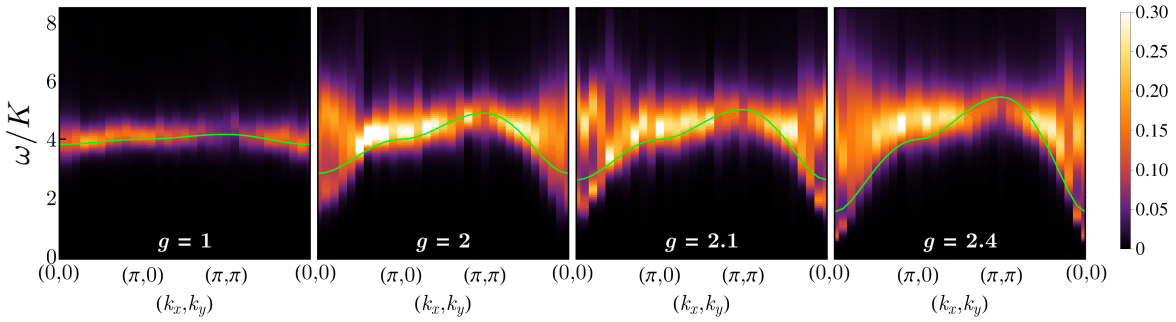

Figure 6.5: Dynamical single structure factor as obtained using QMC and on top (in green) is the amplitude mode dispersion (5.38) obtained within the harmonic approximation. This figure is taken from ref. [77].

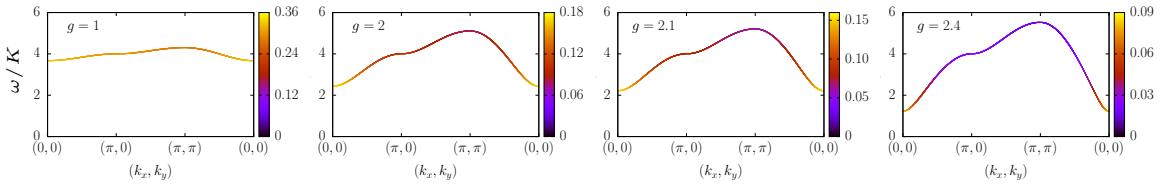

Figure 6.6: Dynamical singlet structure factor obtained within the large-d formalism. It is the imaginary part of eq. (5.107). The curve traces the amplitude-mode dispersion (5.38) and the color code is the corresponding spectral weight (5.109). This figure is taken from ref. [77].

data (fig. 7 in ref. [77]) at the Γ point (i.e. $\vec{k} = (0, 0)$) then a well-defined peak at a low energy can be identified with the Higgs mode. Upon approaching the quantum critical point, this peak is seen to be emerging out at low energy from the broad continuum, and become increasingly sharp. This is expected for the Higgs mode as the damping is small near the critical point. We can also see from our diagrammatics that the diagram corresponding to the amplitude mode decaying into two magnons (fig. D.2 (d) and (e)) vanishes upon approaching the critical point. Importantly, this low-energy peak is found to follow the universal scaling [80, 77] predicted by a $1/N$-expansion of the O(N) model, unlike the other broad peak.

Interestingly, deep inside the ordered phase, a single sharp peak seems to be emerging (see fig. 6.5) at an energy of $4K$. What remains unclear is whether it has any significant single-mode contribution from the amplitude mode or it is dominated by only the continua. At first look, it looks like it is mostly continuum because the non-universal peak seen at the Γ point is also around the energy $4K$. From our analysis, fig. 6.6, we see that the single-mode spectral weight of the amplitude mode is enhanced, deep in the ordered phase. Also, the weight is seen to get equally distributed at all momenta. But we cannot make any claim since we have not calculated the continuum. But what we can see is that the self-energy of the diagram (fig. D.2 (d) and (e)), corresponding to the scattering of amplitude mode into two magnons vanishes in the limit of decoupled layers (i.e. $\lambda = 1$ and $J = 0$). It will be an interesting task, in future, to calculate the shape of this continuum. Apparently, it seems that it should

get sharper as we go deep in the ordered phase.

6.3 Discussion

We have thus seen that our large-d formalism is a useful tool to compare with numerical data because it works in both the magnetically ordered and the paramagnetic phase. We have already seen in the previous chapters that the critical point from large-d calculation is not very far-off from the QMC result in $3d$. So, it would be interesting to have similar numerical data in $3d$, where mean-field behavior up to a logarithmic correction is expected. From our results, we can see that in $3d$ the single-mode contribution from the amplitude mode will be even more enhanced.

Part II

Other models

Chapter 7

Transverse-field Ising model

In part I, we introduced our novel expansion method using the inverse spatial dimension as a small parameter, and applied it to coupled-dimer magnets. However the technique we have developed is not restricted to dimerized systems only. To demonstrate a wider applicability of our large-d formalism, we will study the transverse-field Ising model on a hypercubic lattice ($d \geq 2$) in this chapter. We will see that most of the ideas developed in part I can be easily borrowed in this case.

The classical Ising model (1.13) was first studied by Lenz and Ising [81] to explain ferromagetism. In this model each lattice site has vectors which can point either up or down i.e. have a value $+1$ or -1. In $1d$ this was solved by Ising and it was shown that this model does not have any finite temperature phase transition. In $1d$ this model does not have long-range order at any finite temperature according to the Mermin-Wagner theorem [10]. The solution for the classical Ising model (in absence of any field) on a square lattice was first given by Lars Onsager [82] demonstrating a finite temperature phase transition.

In this chapter we are interested in the quantum version of this model namely quantum Ising model or transverse-field Ising model (1.14). This is one of the toy models frequently used by theorists to understand quantum phase transitions [6, 8]. The transverse-field Ising model is exactly solvable in $1d$. Interestingly, this model is also realized in real materials. One such example is $LiHoF_4$ [83] where the Ho ion effectively acts as an Ising spin. Another example is the compound $CoNb_2O_6$ [84]. Theoretical study of this model using series expansions has been addressed (see ref. [85] and references therein). However, for $d \geq 2$, there is no analytical method which consistently describes the entire phase diagram, including the quantum critical point. This motivates us to apply our method to this model. We will be brief in terms of calculating observables in this chapter. We will only present those observables which are essential to confirm the consistency of the method. The most important consistency check is that the phase boundary obtained from the two phase must match. Also, the phase transition must be continuous.

7.1 Model Hamiltonian

Recall that the transverse field Ising model consists of exchange interaction between the z-component of neighboring spins with $S = 1/2$ and an additional term with a

field interacting with the x-component of each spin. It is described by the following Hamiltonian[1]:

$$\mathcal{H} = -J \sum_{\langle ij \rangle} S_i^z S_j^z - h \sum_i S_i^x \tag{7.1}$$

where the J is the exchange interaction among nearest neighbor spins, h is the transverse field and the spin operators correspond to $S = 1/2$. Thus for classical spins, which can be treated as vectors, this model reduces to the usual Ising model in the absence of the transverse-field term.

We will consider the case where $J > 0$ and $h > 0$. At zero temperature, this model undergoes a quantum phase transition if we tune the ratio J/h. To see this let us as usual consider the two limiting cases: $J \gg h$ and $h \gg J$. Let us consider the first case when exchange interaction J is dominant. In the limit $h \to 0$ the ground-state energy is minimized when all the spins point along the same direction in spin space, or in other words all spins take the same value of S^z (i.e. either $1/2$ or $-1/2$). In this limit the ground-state wavefunction is thus

$$\Psi_0 = \prod_i |\uparrow\rangle_i \quad \text{or} \quad \Psi_0 = \prod_i |\downarrow\rangle_i \,. \tag{7.2}$$

This is ferromagnetic phase wherein the system spontaneously chooses one of the two possible directions by breaking the $\mathbb{Z}_2$ symmetry of the Hamiltonian. At any small finite h, the ground state will have some spins pointing in opposite direction. But in the thermodynamic limit, the system will still be in a $\mathbb{Z}_2$ symmetry broken phase [6]. In this phase the system has long-range order because the correlation between z-component of two distant spins with respect to the ground state is a constant i.e.

$$\lim_{|\vec{r}_i - \vec{r}_j| \to \infty} \langle 0 | S_i^z S_j^z | 0 \rangle = m^2 \tag{7.3}$$

where $|0\rangle$ is ground-state at any small finite h in the ferromagnetic phase and m is the magnetization.

On the other hand, if we consider the limit $h \gg J$ then we first note that for $J \to 0$ the ground state must be a product-state of eigenstate of S_i^x. The two eigenstates of S_i^x are

$$|\rightarrow\rangle_i = \frac{|\uparrow\rangle_i + |\downarrow\rangle_i}{\sqrt{2}} \,, \tag{7.4}$$

$$|\leftarrow\rangle_i = \frac{|\uparrow\rangle_i - |\downarrow\rangle_i}{\sqrt{2}} \tag{7.5}$$

with eigenvalues $\pm 1/2$ respectively. Thus in this limit the ground state is given by

$$\Psi_0 = \prod_i |\rightarrow\rangle_i \,. \tag{7.6}$$

With respect to the above state the correlation between the z-component of spins on any two different sites is strictly zero, which means this phase is characterized by

[1] Often this model is written in terms of the Pauli matrices but we find it convenient to express it as a spin Hamiltonian.

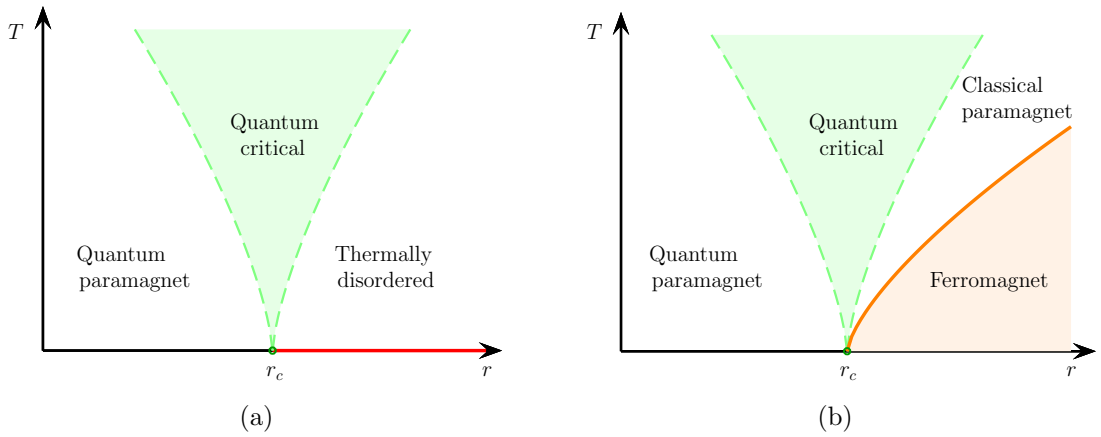

Figure 7.1: Phase diagram of the transverse-field Ising model (7.1) in $1d$, $2d$, and $3d$, as a function of temperature and the tuning parameter r. The quantum critical region (green) is shown along with the corresponding quantum critical point r_c. (a) Phase diagram in $d = 1$ and $d = 2$, where ferromagnetic ordering (red) is possible only at $T = 0$K. (b) Phase diagram in $d = 3$, where ferromagnetic ordering exists even at non-zero temperature. There is a classical phase transition (orange curve) from a ferromagnet to a paramgnet at the corresponding Curie temperature.

short-range correlation [6]. In fact even upon turning on small finite J the corrections decay exponentially with distance, and thus are short ranged. After examining the two limiting cases, we see that the corresponding phases are qualitatively different and thus there is a quantum critical point[2] separating the two phases. In the following we will see this explicitly using our $1/d$ expansion.

Before we dive into the details we would like to point out an important distinction between $d = 1$ case and $d \geq 2$ case. There is no difference in the above analysis between these two cases. The distinction arises when we consider the excitations in the ferromagnetic (ordered) phase. For $d \geq 2$ the excitation in the ordered phase is single spin-flip which can be described within a single particle picture (we will see this in the following). However, in $1d$ the excitations are domain walls, since once a spin is flipped there is no extra energy cost to be paid to flip all spins (say) to its right. Due to this different nature of excitations we leave out the $1d$ case from our analysis and concentrate on $d \geq 2$.

As we work in the limit of large-d we must ensure non-trivial competition between the nearest neighbor exchange interaction term and the transverse-field term to obtain quantum phase transition. This is done by introducing our tuning parameter r analogous to the coupled dimer case as follows:

$$r = \frac{Jd}{h}\,. \tag{7.7}$$

In the light of above analysis we expect a quantum phase transition at some critical value of the tuning parameter r_c. Thus for $r < r_c$ we have the disordered phase while the ordered phase occurs when $r > r_c$. Another consequence of working in large-d

[2]In general there could be more than one critical point and intermediate phases. But in this case it is known that there is only one quantum critical point and we will also see this in our calculation.

is that the critical exponents are locked to their mean-field values. In this case, the relevant mean-field critical exponents are $\alpha = 0\,, \beta = 1/2\,, \nu = 1/2$ and $z = 1$. As explained in chapter 3 these exponents will help us identify the *correct* observables which have analytic $1/d$ expansion throughout the phase diagram.

7.2 Quantum paramagnetic phase

Let us start our analysis with the disordered phase. As we saw in the part I, an essential ingredient to setup $1/d$ expansion is a suitable reference state. In the large-d limit, due to irrelevant non-local fluctuations, we can assume a product-state ansatz. We can find the reference state by minimizing the product-state expectation value of the Hamiltonian. In this phase it turns out that the suitable reference state is a product state of one of the eigenstates of S_i^x:

$$\Psi_0 = \prod_i |0\rangle_i\,, \tag{7.8}$$

$$|0\rangle = \frac{|\uparrow\rangle + |\downarrow\rangle}{\sqrt{2}}\,. \tag{7.9}$$

Thus on each lattice site there are only two states (since $S = 1/2$) given by

$$|0\rangle_i = \frac{|\uparrow\rangle_i + |\downarrow\rangle_i}{\sqrt{2}}\,, \tag{7.10}$$

$$|T\rangle_i = \frac{|\uparrow\rangle_i - |\downarrow\rangle_i}{\sqrt{2}}\,. \tag{7.11}$$

Analogous to bond operators defined earlier for $S = 1/2$ dimerized systems, we can introduce a Bosonic operator in this case as follows:

$$T_i^\dagger|0\rangle_i = |T\rangle_i\,; \quad T_i|0\rangle_i = 0\,, \tag{7.12}$$

such that they satisfy the usual Bosonic commutation relation

$$\left[T_i, T_j^\dagger\right] = \delta_{i,j}\,; \ \left[T_i, T_j\right] = \left[T_i^\dagger, T_j^\dagger\right] = 0\,. \tag{7.13}$$

It is then a straightforward task to work out the matrix elements of the spin operators with respect to the above mentioned states. Using this we can express our spin operators as follows:

$$S^x = \frac{1}{2}\left(|0\rangle\langle 0| - |T\rangle\langle T|\right)\,, \tag{7.14}$$

$$S^y = \frac{\imath}{2}\left(|0\rangle\langle T| - |T\rangle\langle 0|\right)\,, \tag{7.15}$$

$$S^z = \frac{1}{2}\left(|0\rangle\langle T| + |T\rangle\langle 0|\right)\,. \tag{7.16}$$

Since we have associated $|T\rangle$ to Bosonic single-particle state we have additionally the constraint (just as in the case of coupled-dimers)

$$|0\rangle\langle 0| + |T\rangle\langle T| = 1\,. \tag{7.17}$$

The mapping of spin operators to Bosons brings along additional unphysical states and thereby we have to implement the above hard-core constraint. As in the coupled-dimer case, we will implement the constraint via the projection operator

$$P_i = 1 - T_i^\dagger T_i \,. \tag{7.18}$$

Thus using the projection operator we can express the spin operators in terms of the T operators as follows:

$$S_i^x = \frac{1}{2}\left(1 - 2T_i^\dagger T_i\right) , \tag{7.19}$$

$$S_i^y = \frac{\imath}{2}\left(P_i T_i - T_i^\dagger P_i\right) , \tag{7.20}$$

$$S_i^z = \frac{1}{2}\left(P_i T_i + T_i^\dagger P_i\right) . \tag{7.21}$$

Note that using this representation the spin operators satisfy the usual spin commutation relations within the physical Hilbert space.

7.2.1 Real-space Hamiltonian

Having expressed the spin operators in terms of auxiliary Bosonic particles, we can now write our spin Hamiltonian (7.1) in terms of the T operators as follows:

$$\mathcal{H} = -\frac{J}{4}\sum_{\langle ij\rangle}\left(P_i T_i P_j T_j + T_i^\dagger P_i P_j T_j + h.c.\right) - \frac{h}{2}\sum_i \left(1 - 2T_i^\dagger T_i\right) . \tag{7.22}$$

Just as in the case of coupled-dimers, it turns out that for calculations to order $1/d$ we only need terms up to quartic order in T operators. Using the explicit form of the projector (7.18) we can write down the expressions for relevant parts of the Hamiltonian:

$$\mathcal{H}_0 = -\frac{Nh}{2}\,, \quad N \text{ is the number of lattice sites}\,, \tag{7.23}$$

$$\mathcal{H}_2 = -\frac{J}{4}\sum_{\langle ij\rangle}\left(T_i T_j + T_i^\dagger T_j + h.c.\right) + h\sum_i T_i^\dagger T_i \,, \tag{7.24}$$

$$\mathcal{H}_4 = \frac{J}{2}\sum_{\langle ij\rangle}\left[T_i^\dagger T_i T_i T_j + T_i^\dagger T_i^\dagger T_i T_j + h.c.\right] . \tag{7.25}$$

Apart from the pre-factors, above expressions are identical to those in the case of coupled-dimers. In fact the interaction term is somewhat simpler in this case because there is only one kind of excitation present, unlike the coupled-dimer case.

7.2.2 Harmonic approximation

As a first step towards $1/d$ expansion let us first solve the bilinear part (7.24). With periodic boundary condition on hypercubic lattice the crystal momentum is a good

quantum number and so it is convenient to work in the Fourier space. For this purpose we can introduce the Fourier transformed operator via

$$T_i = \frac{1}{\sqrt{N}} \sum_{\vec{k}} T_{\vec{k}} e^{-\imath \vec{k}\cdot\vec{r}_i} \,, \tag{7.26}$$

such that

$$\left[T_{\vec{k}}, T^\dagger_{\vec{k}'}\right] = \delta_{\vec{k},\vec{k}'} \,, \quad \left[T_{\vec{k}}, T_{\vec{k}'}\right] = \left[T^\dagger_{\vec{k}}, T^\dagger_{\vec{k}'}\right] = 0 \,. \tag{7.27}$$

Using the Fourier transformed T operator, the bilinear part of the Hamiltonian is given by

$$\mathcal{H}_2 = \sum_{\vec{k}} \left[A_{\vec{k}} T^\dagger_{\vec{k}} T_{\vec{k}} + \frac{B_{\vec{k}}}{2} \left(T_{\vec{k}} T_{-\vec{k}} + h.c. \right) \right] \tag{7.28}$$

where

$$A_{\vec{k}} = h + B_{\vec{k}} \,, \quad B_{\vec{k}} = -\frac{\gamma_{\vec{k}} r}{2} \,, \tag{7.29}$$

and the interaction structure factor

$$\gamma_{\vec{k}} = \frac{1}{d} \sum_{n=1}^{d} \cos k_n \tag{7.30}$$

which is normalized such that $-1 \leq \gamma_{\vec{k}} \leq 1$. Following the procedure detailed in the section 4.4.2, we can diagonalize the above Hamiltonian piece by standard Bogoliubov transformation,

$$T_{\vec{k}} = u_{\vec{k}} \tau_{\vec{k}} + v_{\vec{k}} \tau^\dagger_{-\vec{k}} \tag{7.31}$$

where $u_{\vec{k}}$ and $v_{\vec{k}}$ are the Bogoliubov coefficients and the τ operators obey the usual Bosonic commutation relations. The mode energy is then given by

$$\omega_{\vec{k}} = h\sqrt{1 - \gamma_{\vec{k}} r} \,. \tag{7.32}$$

Now unlike the coupled dimers case, here the minimum of the dispersion occurs at $\gamma_{\vec{k}} = 1$ i.e. $\vec{k} = \vec{Q} \equiv \{0, 0, \ldots\}$. We can then readily write down the energy gap which is

$$\Delta \equiv \omega_{\vec{Q}} = h\sqrt{1 - r} \,. \tag{7.33}$$

Observe that the gap becomes imaginary for $r > 1$ and hence the disordered phase at the harmonic level becomes unstable, which means we have a critical point at $r_c = 1$. For future use, we note that in terms of the mode energy and the coefficients in the bilinear Hamiltonian, the Bogoliubov coefficients are given by

$$u^2_{\vec{k}}, v^2_{\vec{k}} = \frac{1}{2} \left(\frac{A_{\vec{k}}}{\omega_{\vec{k}}} \pm 1 \right) \;; \quad u_{\vec{k}} v_{\vec{k}} = -\frac{B_{\vec{k}}}{2\omega_{\vec{k}}} \,. \tag{7.34}$$

Note that just as in the case of coupled-dimers, even here local observables evaluated with respect to the reference state are suppressed in powers of $1/d$ such that they yield exact expectation values in limit $d \to \infty$. We again caution that this does not imply that the reference state is the ground state of the Hamiltonian.

7.2.3 Perturbation theory and normal-ordered Hamiltonian

Having solved the bilinear piece of the Hamiltonian, we shall treat it as the unperturbed part and take into account the interaction terms perturbatively. A priori there is no small parameter in the theory to control our pertubative treatment. But just as in the case of coupled-dimers, we will see that the self-energy from the interaction terms is suppressed in powers of $1/d$. Hence the corrections to observables can be arranged in a power series in $1/d$. To start our diagrammtic treatment we must first normal-order our Hamiltonian with respect to the operators (τ) that diagonalize the unperturbed piece. For the same reasons as in the coupled-dimer case, we need terms only up to fourth order in T operators. Upon normal ordering, $\mathcal{H}_4$ will generate additional bilinear terms which are expressed below:

$$\mathcal{H}'_{2b} = \sum_{\vec{k}} \left[C_{\vec{k}} \tau^\dagger_{\vec{k}} \tau_{\vec{k}} + \frac{D_{\vec{k}}}{2} (\tau_{\vec{k}} \tau_{-\vec{k}} + h.c.) \right] \tag{7.35}$$

where

$$C_{\vec{k}} = rh\big[(u^2_{\vec{k}} + v^2_{\vec{k}})(\gamma_{\vec{k}} R_1 + 2\gamma_{\vec{k}} R_2 + 2R_3) + 2u_{\vec{k}} v_{\vec{k}} (\gamma_{\vec{k}} R_1 + 2\gamma_{\vec{k}} R_2 + R_3)\big] , \tag{7.36}$$

$$D_{\vec{k}} = rh\big[(u^2_{\vec{k}} + v^2_{\vec{k}})(\gamma_{\vec{k}} R_1 + 2\gamma_{\vec{k}} R_2 + R_3) + 2u_{\vec{k}} v_{\vec{k}} (\gamma_{\vec{k}} R_1 + 2\gamma_{\vec{k}} R_2 + 2R_3)\big] . \tag{7.37}$$

Following are required expressions of R's to order $1/d$ in the large-d limit:

$$R_1 = \frac{1}{N} \sum_{\vec{k}} u_{\vec{k}} v_{\vec{k}} \quad = \frac{r^2}{16d} + \mathcal{O}(d^{-2}) , \tag{7.38}$$

$$R_2 = \frac{1}{N} \sum_{\vec{k}} v^2_{\vec{k}} \quad = \frac{r^2}{32d} + \mathcal{O}(d^{-2}) , \tag{7.39}$$

$$R_3 = \frac{1}{N} \sum_{\vec{k}} \gamma_{\vec{k}} u_{\vec{k}} v_{\vec{k}} = \frac{r}{8d} + \mathcal{O}(d^{-2}) , \tag{7.40}$$

$$R_4 = \frac{1}{N} \sum_{\vec{k}} \gamma_{\vec{k}} v^2_{\vec{k}} \quad = \mathcal{O}(d^{-2}) . \tag{7.41}$$

Thus the normal ordered bilinear piece is sum of the unperturbed part and the above contribution: $\mathcal{H}'_2 = \mathcal{H}'_{2a} + \mathcal{H}'_{2b}$ where,

$$\mathcal{H}'_{2a} = \sum_{\vec{k}} \omega_{\vec{k}} \tau^\dagger_{\vec{k}} \tau_{\vec{k}} \tag{7.42}$$

is the unperturbed piece.

Now we quote the normal ordered quartic term:

$$\mathcal{H}'_4 = \frac{1}{N} \sum_{1234} \big[\delta_{1+2+3+4} \Gamma^d_{41} (\tau^\dagger_1 \tau^\dagger_2 \tau^\dagger_3 \tau^\dagger_4 + \tau_1 \tau_2 \tau_3 \tau_4) + \delta_{1+2-3-4} (\Gamma^d_{42} \tau^\dagger_1 \tau^\dagger_2 \tau_3 \tau_4 + \Gamma^d_{43} \tau^\dagger_1 \tau^\dagger_2 \tau_3 \tau_4) \tag{7.43}$$

$$+ \delta_{1+2+3-4} \Gamma^d_{44} (\tau^\dagger_1 \tau^\dagger_2 \tau^\dagger_3 \tau_4 + \tau^\dagger_4 \tau_3 \tau_2 \tau_1) \big] ,$$

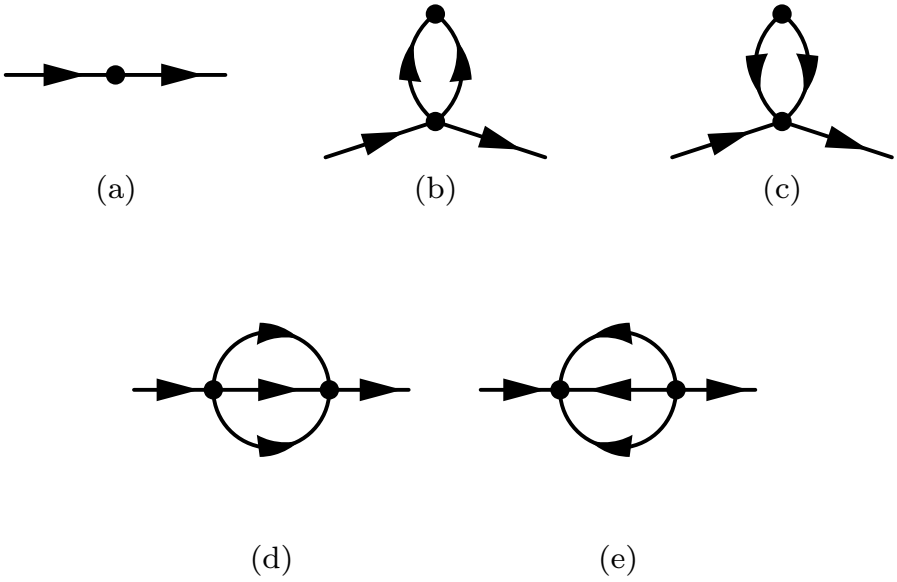

Figure 7.2: Feynman diagrams for the normal τ self-energy up to order $1/d$, with vertices from $\mathcal{H}'_{2b}$ and $\mathcal{H}'_4$.

with the relevant vertex functions given by

$$\Gamma^d_{41} = \frac{Jd}{2}\big[\gamma_4 u_1 v_2 v_3 v_4 + \gamma_4 v_1 u_2 u_3 u_4 + (\gamma_1+\gamma_4) u_1 u_2 v_3 v_4\big]\,, \tag{7.44}$$

$$\begin{aligned}\Gamma^d_{44} = \frac{Jd}{2}\big[&(2\gamma_3+\gamma_4) u_1 v_2 v_3 u_4 + (2\gamma_3+\gamma_4) v_1 u_2 u_3 v_4 + \gamma_3 v_1 v_2 v_3 v_4 \\ &+ \gamma_3 u_1 u_2 u_3 u_4 + (2\gamma_1+\gamma_3+\gamma_4) u_1 u_2 v_3 u_4 + (\gamma_1+2\gamma_3+\gamma_4) u_1 v_2 v_3 v_4\big]\,.\end{aligned} \tag{7.45}$$

7.2.4 Dispersion, energy gap, and phase boundary

In order to get the dispersion relation, including corrections from the interaction terms, we have to solve the Dyson equation. Location of the pole in the Green's function gives the dispersion. As explained in part I, we only need to calculate the normal self-energies to obtain the $1/d$ expansion for dispersion to order $1/d$. With the knowledge of calculating diagrams in large-d, we can evaluate the relevant self-energy diagrams shown in fig. 7.2. Actually in this case the diagrams involved are exactly the same as those evaluated in chapter 4. So we know all the vertex combinations and also the permutations. The resultant expressions of self-energies to order $1/d$ are quoted below:

$$\Sigma^{7.2(a)}(\vec{k},\omega) = C_{\vec{k}}\,, \tag{7.46}$$

$$\Sigma^{7.2(b)}(\vec{k},\omega) = \Sigma^{7.2(c)}(\vec{k},\omega) = -\frac{\gamma_{\vec{k}} r^2 h R_3}{4}(u_{\vec{k}}+v_{\vec{k}})^2\,, \tag{7.47}$$

$$\Sigma^{7.2(d)}(\vec{k},\omega) = \frac{r^2h^2}{4(\omega-3h)}\left[2\gamma^2_{\vec{k}}(u_{\vec{k}}+v_{\vec{k}})^2 R_2 + 4\gamma_{\vec{k}}(u^2_{\vec{k}}+u_{\vec{k}}v_{\vec{k}})R_3 + \frac{u^2_{\vec{k}}}{d}\right]\,, \tag{7.48}$$

$$\Sigma^{7.2(e)}(\vec{k},\omega) = \frac{-r^2h^2}{4(\omega+3J)}\left[2\gamma^2_{\vec{k}}(u_{\vec{k}}+v_{\vec{k}})^2 R_2 + 4\gamma_{\vec{k}}(v^2_{\vec{k}}+u_{\vec{k}}v_{\vec{k}})R_3 + \frac{v^2_{\vec{k}}}{d}\right]\,. \tag{7.49}$$

We can then insert these in the pole equation

$$\Omega_{\vec{k}}^2 = \omega_{\vec{k}}^2 + 2\omega_{\vec{k}}\Sigma_{N+}\,, \tag{7.50}$$

to obtain the $1/d$ expansion for the dispersion in the disordered phase. As noted earlier, since the mean-field critical exponent for the energy gap is $\nu z = 1/2$ we will have an analytic $1/d$ expansion for square of the dispersion and square of the gap in the entire phase diagram. We therefore have

$$\frac{\Omega_{\vec{k}}^2}{h^2} = 1 - \gamma_{\vec{k}} r + \frac{r^2}{16d}(4 + \gamma_{\vec{k}} r)\,. \tag{7.51}$$

We again point out that this is formally *not* an expansion in r and at higher orders the $1/d$ expansion need not be a simple polynomial in r. To obtain an expansion in small-r, we have to perform a double expansion, as we did in the asymmetric case of coupled-dimers in the quantum paramagnetic phase.

We can now immediately calculate the energy gap by evaluating the above expression at the Ferromagnetic ordering vector $\vec{Q}$ [3]. Thus the energy gap is given by:

$$\frac{\Delta^2}{h^2} = 1 - r + \frac{r^2}{16d}(4 + r)\,. \tag{7.52}$$

The disordered phase becomes unstable at the critical point where the energy gap vanishes. Using this criterion we can locate the phase boundary to the ordered phase. For this purpose we can make an ansatz for the critical point: $r_c = 1 + r_1/d$. Inserting this ansatz in eq. (7.52) and solving it to order $1/d$, we obtain the following result for the phase boundary:

$$r_c = 1 + \frac{5}{16d}\,. \tag{7.53}$$

7.3 Ferromagnetic phase

As explained in the beginning of the chapter, we anticipate a ferromagnetic long-range ordered phase for $r > r_c$. In the last section, we solved the quantum paramagnetic phase within our large-d formalism and determined the phase boundary to the ordered phase. Let us now calculate observables in this ordered phase. Again most of the ideas are similar to those presented in the case of coupled dimers with an important physical difference namely, here we do not have Goldstone (gapless) modes. In this case $\mathbb{Z}_2$ symmetry is broken and so Goldstone's theorem does not apply in this case. In this case we just have one kind of (gapped) excitation and so the algebra involved is less tedious.

We begin our analysis by identifying a suitable reference product state. It is clear that in this phase the T operator will be condensed meaning it will have a finite expectation value with respect to the reference product-state. It is therefore straightforward

[3] It is easy to prove that the above dispersion has minimum at $\vec{Q}$ as long as $r^2 \leq 16d$. This holds everywhere in the quantum paramagnetic phase.

to identify the correct reference state

$$\Psi_0 = \prod_i |\tilde{0}\rangle_i \,, \tag{7.54}$$

$$|\tilde{0}\rangle_i = \frac{|0\rangle_i + \lambda |T\rangle_i}{\sqrt{1+\lambda^2}} \,. \tag{7.55}$$

In the spirit of large-d, this delivers exact expectation values of local observables in the limit $d \to \infty$. In this case, λ is the condensation parameter which takes values between 0 and 1 (alternatively, -1 for the other $\mathbb{Z}_2$ symmetry related choice of reference state) as a function of the tuning parameter r. We can easily see that in the limit $\lambda \to 1$ we obtain the fully polarized ferromagnetic state as our reference state

$$\Psi_0(\lambda = 1) = \prod_i |\uparrow\rangle_i \equiv \prod_i \frac{|0\rangle + |T\rangle}{\sqrt{2}} \,. \tag{7.56}$$

In fact, later we will see that $\lambda \to 1$ limit corresponds to $h \to 0$ limit and so the above correspondence is well anticipated. On the other hand, for $\lambda = 0$ we recover the reference state for the disordered phase, where there is no condensation of T operator. In fact, later we will use this as one of the criterion to determine the phase boundary. Apart from our reference state we have one more state in the physical Hilbert space, which is orthonormal to the above state and is given by

$$|\tilde{T}\rangle_i = \frac{-\lambda |0\rangle_i + |T\rangle_i}{\sqrt{1+\lambda^2}} \,. \tag{7.57}$$

We can formulate the above scenario in terms of the generalized rotation in the Hilbert space as follows:

$$\begin{pmatrix} |0\rangle & |T\rangle \end{pmatrix} = \begin{pmatrix} |\tilde{0}\rangle & |\tilde{T}\rangle \end{pmatrix} \begin{pmatrix} 1 & \lambda \\ -\lambda & 1 \end{pmatrix} \frac{1}{\sqrt{1+\lambda^2}} \,. \tag{7.58}$$

Analogous to the disordered phase we can define Bosonic operator $\tilde{T}$ such that

$$\tilde{T}_i^\dagger |\bar{0}\rangle_i = |\tilde{T}\rangle_i \,; \quad \tilde{T}_i |\bar{0}\rangle_i = 0 \,, \tag{7.59}$$

which obey the usual Bosonic commutation relation

$$\left[\tilde{T}_i, \tilde{T}_j^\dagger\right] = \delta_{i,j} \,; \ \left[\tilde{T}_i, \tilde{T}_j\right] = \left[\tilde{T}_i^\dagger, \tilde{T}_j^\dagger\right] = 0 \,. \tag{7.60}$$

Again, due to the mapping on to Bosons, we enlarge our Hilbert space. We have to implement the hard-core constraint $|\tilde{0}\rangle\langle\tilde{0}| + |\tilde{T}\rangle\langle\tilde{T}| = 1$ in order to restrict ourselves to the physical Hilbert space. We thus introduce the projection operator

$$\tilde{P}_i = 1 - \tilde{T}_i^\dagger \tilde{T}_i \,. \tag{7.61}$$

Now using the rotation in the Hilbert space (7.58), the above definition of $\tilde{T}$ operator, and projection operator it is then straightforward to obtain the spin operators in

the $\tilde{T}$ representation:

$$S_i^x = \frac{1}{2(1+\lambda^2)} \left((1-\lambda^2)(1-2\tilde{T}_i^\dagger \tilde{T}_i) - 2\lambda(\tilde{T}_i^\dagger \tilde{P}_i + \tilde{P}_i \tilde{T}_i) \right) , \tag{7.62}$$

$$S_i^y = \frac{\imath}{2} \left(\tilde{P}_i \tilde{T}_i - \tilde{T}_i^\dagger \tilde{P}_i \right) , \tag{7.63}$$

$$S_i^z = \frac{1}{2(1+\lambda^2)} \left(2\lambda(1-2\tilde{T}_i^\dagger \tilde{T}_i) + (1-\lambda^2)(\tilde{T}_i^\dagger \tilde{P}_i + \tilde{P}_i \tilde{T}_i) \right) . \tag{7.64}$$

It is easy to verify that we obtain the correct spin commutation relations within the physical Hilbert space. Also for $\lambda = 0$ we recover the spin representation in the disordered phase.

7.3.1 Real-space Hamiltonian and perturbation theory

We are now ready to express our spin Hamiltonian (7.1) in terms of the $\tilde{T}$ operators. Using eq. (7.62), (7.63) and (7.64) the Hamiltonian in the ordered phase is

$$\begin{aligned} \mathcal{H} = & - \frac{J}{4(1+\lambda^2)^2} \sum_{\langle ij \rangle} \Big[(1-\lambda^2)^2 \left(\tilde{P}_i \tilde{T}_i \tilde{P}_j \tilde{T}_j + \tilde{T}_i^\dagger \tilde{P}_i \tilde{P}_j \tilde{T}_j + h.c. \right) \\ & + 2\lambda(1-\lambda^2) \left(\tilde{T}_i^\dagger \tilde{P}_i - 2\tilde{T}_i^\dagger \tilde{P}_i \tilde{T}_j^\dagger \tilde{T}_j + \tilde{T}_j^\dagger \tilde{P}_j - 2\tilde{T}_j^\dagger \tilde{P}_j \tilde{T}_i^\dagger \tilde{T}_i + h.c. \right) \\ & + 4\lambda^2 \left(1 - 2\tilde{T}_j^\dagger \tilde{T}_j - 2\tilde{T}_i^\dagger \tilde{T}_i + 4\tilde{T}_i^\dagger \tilde{T}_i \tilde{T}_j^\dagger \tilde{T}_j \right) \Big] \\ & - \frac{h}{2(1+\lambda^2)} \sum_i \Big[(1-\lambda^2)(1-2\tilde{T}_i^\dagger \tilde{T}_i) - 2\lambda(\tilde{T}_i^\dagger \tilde{P}_i + h.c.) \Big] . \end{aligned} \tag{7.65}$$

To order $1/d$ calculation we need only terms up to fourth order in $\tilde{T}$ operators. Inserting the explicit of the projector operator (7.61), we can write the relevant pieces in the Hamiltonian as follows:

$$\mathcal{H}_0 = -\frac{Nrh\lambda^2}{(1+\lambda^2)^2} - \frac{Nh(1-\lambda^2)}{2(1+\lambda^2)} , \tag{7.66}$$

$$\mathcal{H}_1 = \left[\frac{h\lambda}{1+\lambda^2} - \frac{hr\lambda(1-\lambda^2)}{(1+\lambda^2)^2} \right] \sum_i \left(\tilde{T}_i^\dagger + \tilde{T}_i \right) , \tag{7.67}$$

$$\begin{aligned} \mathcal{H}_2 = & -\frac{J}{4(1+\lambda^2)^2} \sum_{\langle ij \rangle} \left[(1-\lambda^2)^2 \left(\tilde{T}_i \tilde{T}_j + \tilde{T}_i^\dagger + h.c. \right) - 8\lambda^2 \left(\tilde{T}_i^\dagger \tilde{T}_i + \tilde{T}_j^\dagger \tilde{T}_j \right) \right] \\ & + \frac{h(1-\lambda^2)}{1+\lambda^2} \sum_i \tilde{T}_i^\dagger \tilde{T}_i , \end{aligned} \tag{7.68}$$

$$\mathcal{H}_3 = \frac{J\lambda(1-\lambda^2)}{(1+\lambda^2)^2} \sum_{\langle ij \rangle} \left[\tilde{T}_i^\dagger \tilde{T}_i^\dagger \tilde{T}_i + 2\tilde{T}_j^\dagger \tilde{T}_i^\dagger \tilde{T}_i + h.c. \right] - \frac{h\lambda}{1+\lambda^2} \sum_i \left[\tilde{T}_i^\dagger \tilde{T}_i^\dagger \tilde{T}_i + h.c. \right] , \tag{7.69}$$

$$\mathcal{H}_4 = \frac{J}{2(1+\lambda^2)^2} \sum_{\langle ij \rangle} \left[(1-\lambda^2)^2 \left(\tilde{T}_i^\dagger \tilde{T}_i \tilde{T}_i \tilde{T}_j + \tilde{T}_i^\dagger \tilde{T}_i^\dagger \tilde{T}_i \tilde{T}_j + h.c. \right) - 8\lambda^2 \tilde{T}_i^\dagger \tilde{T}_j^\dagger \tilde{T}_i \tilde{T}_j \right] . \tag{7.70}$$

Again note that for $\lambda = 0$ we recover the Hamiltonian in the disordered phase in terms of T operators.

As in the case of ordered phase of coupled dimers, even here we have two sources of $1/d$ corrections to observables. Firstly, we have the usual source from the interaction terms in the Hamiltonian. Secondly, the corrections arising from $1/d$ expansion of the condensate parameter λ. We will therefore follow the strategy developed in chapter 5 to perform diagrammatic perturbation theory, and we refer to section 5.3.4 for details.

7.3.2 Linear part

Within the independent-Boson approximation, we require that $\mathcal{H}_1 = 0$. This condition readily gives us $\lambda(r)$. We will denote the solution by λ_0, since later on with the interaction terms we will obtain corrections to this expression. So at this level the condensate parameter is given by

$$\lambda_0 = \sqrt{\frac{r-1}{r+1}}\,. \tag{7.71}$$

As mentioned earlier, vanishing of the condensate parameter locates the quantum critical point. So at this level, quantum critical point is located at $r_c = 1$, which was also obtained within the harmonic approximation in the disordered phase.

7.3.3 Harmonic approximation

Next, we turn our attention to the bilinear piece in the Hamiltonian, $\mathcal{H}_2$. As a first step we go the the Fourier space by introducing

$$\tilde{T}_i = \frac{1}{\sqrt{N}} \sum_{\vec{k}} \tilde{T}_{\vec{k}} e^{-\imath \vec{k}\cdot\vec{r}_i}\,, \tag{7.72}$$

such that

$$\left[\tilde{T}_{\vec{k}}, \tilde{T}^\dagger_{\vec{k}'}\right] = \delta_{\vec{k},\vec{k}'}\,;\ \left[\tilde{T}_{\vec{k}}, \tilde{T}_{\vec{k}'}\right] = \left[\tilde{T}^\dagger_{\vec{k}}, \tilde{T}^\dagger_{\vec{k}'}\right] = 0\,. \tag{7.73}$$

We then have $\mathcal{H}_2$ in the Fourier space:

$$\mathcal{H}_2(\lambda) = \sum_{\vec{k}} \left[\tilde{A}_{\vec{k}} \tilde{T}^\dagger_{\vec{k}} \tilde{T}_{\vec{k}} + \frac{\tilde{B}_{\vec{k}}}{2} \left(\tilde{T}_{\vec{k}} \tilde{T}_{-\vec{k}} + h.c. \right) \right] \tag{7.74}$$

where

$$\tilde{A}_{\vec{k}} = \frac{h(1-\lambda^2)}{1+\lambda^2} + \frac{4hr\lambda^2}{(1+\lambda^2)^2} + \tilde{B}_{\vec{k}}\,,\ \tilde{B}_{\vec{k}} = -\frac{\gamma_{\vec{k}} hr}{2} \left(\frac{1-\lambda^2}{1+\lambda^2} \right)^2\,. \tag{7.75}$$

Anticipating the $1/d$ corrections to λ we choose to treat $\mathcal{H}_2(\lambda_0) \equiv \mathcal{H}_2^{(0)}$ as the unperturbed piece, and diagonalize it (harmonic approximation). The corresponding coefficients $\tilde{A}^{(0)}_{\vec{k}} \equiv \tilde{A}_{\vec{k}}(\lambda_0)$ and $\tilde{B}^{(0)}_{\vec{k}} \equiv \tilde{B}_{\vec{k}}(\lambda_0)$ are given by

$$\tilde{A}^{(0)}_{\vec{k}} = \frac{h}{r} + \frac{h(r^2-1)}{r} + \tilde{B}_{\vec{k}}\,,\ \tilde{B}^{(0)}_{\vec{k}} = -\frac{\gamma_{\vec{k}} h}{2r} \tag{7.76}$$

where we have used the explicit expression for λ_0 (7.71).

Now using standard Bogoliubov transformation

$$\tilde{T}_{\vec{k}} = \tilde{u}_{\vec{k}}\tilde{\tau}_{\vec{k}} + \tilde{v}_{\vec{k}}\tilde{\tau}^{\dagger}_{-\vec{k}} \tag{7.77}$$

($\tilde{\tau}$ obey the usual Bosonic commutation relations) we can solve $\mathcal{H}_2^{(0)}$ to get the mode energy

$$\tilde{\omega}_{\vec{k}} = h\sqrt{r^2 - \gamma_{\vec{k}}}\,. \tag{7.78}$$

In terms of the coefficients of $\mathcal{H}_2^{(0)}$ and the mode energy, the Bogoliubov coefficients are given by

$$\tilde{u}^2_{\vec{k}}, \tilde{v}^2_{\vec{k}} = \frac{1}{2}\left(\frac{\tilde{A}_{\vec{k}}}{\tilde{\omega}_{\vec{k}}} \pm 1\right)\;; \quad \tilde{u}_{\vec{k}}\tilde{v}_{\vec{k}} = -\frac{\tilde{B}_{\vec{k}}}{2\tilde{\omega}_{\vec{k}}}\,. \tag{7.79}$$

We see that the dispersion has a minimum at $\gamma_{\vec{k}} = 1$ i.e. $\vec{k} = \vec{Q}$. Thus the energy gap is

$$\tilde{\Delta} \equiv \tilde{\omega}_{\vec{Q}} = h\sqrt{r^2 - 1}\,. \tag{7.80}$$

The ordered phase is seen to become unstable for $r < 1$ (we consider only positive r) and thereby we have a quantum phase transition to the disordered phase at $r_c = 1$. Again, the same value was obtained within the harmonic approximation in disordered phase, as well as from the linear part in the previous subsection, thus assuring consistency.

7.3.4 Normal-ordered Hamiltonian

To start calculating observables using diagrammatic perturbation theory, we first need to normal-order our Hamiltonian (7.65) with respect to $\tilde{\tau}$ operators. Moreover, we have to be careful while using the vertices in the Hamiltonian to calculate observables because these will depend on λ, which in turn has $1/d$ expansion. We again refer to sec. 5.3.4 for a detailed discussion about this issue.

In the present chapter, we are interested in calculating the corrections to condensate parameter, λ, only. So we concentrate only the linear and the cubic terms. Normal-ordered linear term comprises of $\mathcal{H}_1$ and contributions coming from normal ordering of $\mathcal{H}_3$. Together we have

$$\mathcal{H}'_1 = \sqrt{N}\big[h_1(1 - R_1 - 2R_2) + 2J_1(\gamma_{\vec{Q}}R_2 + R_3)\big](\tilde{u}_{\vec{Q}} + \tilde{v}_{\vec{Q}})(\tilde{\tau}^{\dagger}_{\vec{Q}} + \tilde{\tau}_{\vec{Q}}) \tag{7.81}$$

where

$$h_1 = \frac{h\lambda}{1+\lambda^2} - J_1\,, \quad \text{and} \quad J_1 = \frac{Jd\lambda(1-\lambda^2)}{(1+\lambda^2)^2}\,. \tag{7.82}$$

The required expressions of R's to order $1/d$ in the large-d limit are following:

$$R_1 = \frac{1}{N}\sum_{\vec{k}} \tilde{u}_{\vec{k}}\tilde{v}_{\vec{k}} \quad = \frac{1}{r^4 16d} + \mathcal{O}(d^{-2})\,, \tag{7.83}$$

$$R_2 = \frac{1}{N}\sum_{\vec{k}} \tilde{v}^2_{\vec{k}} \quad = \frac{1}{r^4 32d} + \mathcal{O}(d^{-2})\,, \tag{7.84}$$

$$R_3 = \frac{1}{N}\sum_{\vec{k}} \gamma_{\vec{k}}\tilde{u}_{\vec{k}}\tilde{v}_{\vec{k}} = \frac{1}{r^2 8d} + \mathcal{O}(d^{-2})\,, \tag{7.85}$$

$$R_4 = \frac{1}{N}\sum_{\vec{k}} \gamma_{\vec{k}}\tilde{v}^2_{\vec{k}} \quad = \mathcal{O}(d^{-2})\,. \tag{7.86}$$

Turning our attention to the cubic terms, we have the normal ordered piece:

$$\mathcal{H}'_3 = \frac{1}{\sqrt{N}}\sum_{123}\left[\delta_{1+2+3}\Gamma_{31}(\tilde{\tau}^\dagger_1\tilde{\tau}^\dagger_2\tilde{\tau}^\dagger_3 + \tilde{\tau}_1\tilde{\tau}_2\tilde{\tau}_3) + \delta_{1+2-3}\Gamma_{32}(\tilde{\tau}^\dagger_1\tilde{\tau}^\dagger_2\tilde{\tau}_3 + \tilde{\tau}^\dagger_3\tilde{\tau}_2\tilde{\tau}_1)\right]. \tag{7.87}$$

Below we quote relevant vertices useful for diagrammatics:

$$\Gamma_{31} = (2J_1\gamma_1 - h_1)(u_1u_2v_3 + v_1v_2u_3)\,, \tag{7.88}$$

$$\Gamma_{32} = 2J_1\big[\gamma_1(u_1u_2u_3 + v_1v_2v_3) + (\gamma_1+\gamma_3)(u_1v_2v_3 + v_1u_2u_3)\big]\,. \tag{7.89}$$

7.3.5 Condensate parameter

The condensate parameter λ is proportional to the order parameter, namely the magnetization. Hence from the above discussion regarding critical exponents and analytic expansion, it is clear that λ^2 will have an analytic expansion instead of λ. Now to obtain the $1/d$ corrections to λ we demand $\mathcal{H}'_1 = 0$. To order $1/d$ we need to evaluate $h_1(\lambda_0)$ and $J_1(\lambda_0)$ in eq. (7.81), where they appear as a product with R, since Rs are already suppressed in power of $1/d$. For the isolated h_1 term we must however go to order $1/d$ using the ansatz

$$\lambda^2 = \lambda_0^2 + \frac{\lambda_1}{d}\,. \tag{7.90}$$

Moreover we also know that $h_1(\lambda_0) = 0$. Using all this information and setting $\mathcal{H}'_1$ to zero we obtain the required $1/d$ expansion for λ^2:

$$\lambda^2 = \frac{r-1}{r+1} - \frac{1}{8r^3 d}\frac{1+4r^2}{(r+1)^2}\,. \tag{7.91}$$

We remind once again that in principle there are diagrammatic contributions to the condensate parameter. However, these are suppressed at least to $\mathcal{O}(1/d^2)$ and hence irrelevant to order $1/d$ calculation.

Since the condensate parameter vanishes at the critical point, we can use this condition to get the corrections to the phase-boundary result obtained from harmonic approximation. Demanding $\lambda^2 = 0$ and using the ansatz $r_c = 1 + r_1/d$ we get the following phase boundary:

$$r_c = 1 + \frac{5}{16d}\,. \tag{7.92}$$

This is exactly the same result as obtained from the disordered phase calculation (7.53). We thus correctly capture the continuous phase transition and establish internal consistency in our calculation.

7.4 Discussion

In this chapter, we have demonstrated the applicability of our $1/d$ expansion method. We have not calculated the ground-state energy in both the phases. Also, the $1/d$ expansion to the dispersion in the ordered phase has not been presented. The calculation of these observables and the dynamical observables is left as a future task. However, the basic observables required to establish consistency have been already presented.

Chapter 8

Bilayer Kitaev model

An interesting way to introduce a quantum critical point in a two-dimensional quantum spin system is to form a bilayer. By coupling two layers antiferromagnetically we naturally have at least two phases: (i) a dimer quantum paramagnet in the strong inter-layer coupling limit and (ii) usual phases of the single layer in the decoupled-layer limit. Thus we have a magnetic quantum phase transition. The coupled-dimer magnets (2.2) in two dimensions is one such example. Apart from just theoretical interest this aspect is of some practical relevance. Many real materials, specifically layered materials, often have such an inter-layer coupling. Moreover, with the success of synthesizing molecular monolayers [86] it could be possible to artificially construct bilayers in a laboratory.

Here we have a somewhat different motivation to consider a bilayer system. In many cases a two dimensional spin system may realize interesting and exotic phases, such as a quantum spin liquid. However it is difficult to characterize such a state and more so to find its experimental signatures. We can now ask the question, whether by coupling two such systems and starting from the dimer quantum paramagnetic phase, we can find any signatures of the corresponding phases in a single layer. In the following we present a short discussion on these lines in the context of the Kitaev model on a honeycomb lattice. We make a few remarks related to other interesting bilayer models.

8.1 Model Hamiltonian

Let us consider the Kitaev model on a honeycomb lattice and couple two layers of it antiferromagnetically, so that we have a bilayer (see fig. 8.1). We can write down the following Hamiltonian:

$$\mathcal{H} = J \sum_i \vec{S}_{1i} \cdot \vec{S}_{2i} + \mathcal{H}_{kitaev} \,, \tag{8.1}$$

$$\mathcal{H}_{kitaev} = 2 \sum_{\langle ij \rangle_\alpha} K^\alpha \left[S^\alpha_{1i} S^\alpha_{1j} + S^\alpha_{2i} S^\alpha_{2j} \right] \tag{8.2}$$

where i represents the dimer lattice site, $\alpha = x, y, z$ and $\langle ij \rangle_\alpha$ represents sum over nearest neighbor spins along a particular bond direction depending on the component of the spin. The first term in the Hamiltonian is just a Heisenberg exchange term

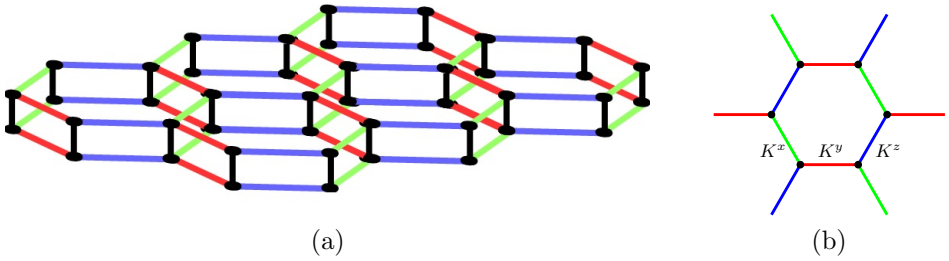

(a) (b)

Figure 8.1: (a) Bilayer Kitaev model (8.1) where the black bonds represent the inter-layer coupling J. (b) Bond directional interactions corresponding to the Kitaev model (8.2). The nearest neighbor S^x, S^y and S^z spin components in each layer interact only along the green, red and blue bonds respectively.

between the spins from layer 1 and layer 2. The second term is the Kitaev interaction term with coupling K^α, wherein different components of a spin on a lattice site interact only along a specific bond direction, as shown in fig.8.1.

The Kitaev model (8.2), introduced by Alexei Kitaev, is exactly solvable by resorting to a Majorana representation [20]. A Majorana particle is an anti-particle of itself, i.e. $m^\dagger = m$; where $m^\dagger(m)$ is Majorana creation (annihilation) operator. In this representation, each spin is replaced by four Majoranas and hence effectively enlarging the Hilbert space[1]. A string of Majorana operators along a hexagonal plaquette turns out to be a conserved quantity, which plays a crucial role in making the problem solvable. In the end the problem boils down to a Majorana hopping problem with $\mathbb{Z}_2$ gauge fields. These gauge fields represent flux through a hexagonal plaquette, which is either $+1$ or -1. It turns out that the ground state of this system is where all the fluxes take the value $+1$, and it is said to be a flux-free sector. This ground state is a quantum spin liquid, an exotic state whose characteristic features include no symmetry breaking and fractionalized excitations. Around the point of isotropic couplings, the Majorana excitations are gapless and so the phase is called the gapless quantum spin liquid. Away from this region the Majorana excitations are gapped, and so the phase is a gapped quantum spin liquid. Note that the flux sector (vison excitation) is always gapped. It is also worth mentioning that the Kitaev model (8.2) can also be solved without using the Majorana representation. This is done using a Jordan-Wigner transformation which leads to a BCS type Hamiltonian in the end [89].

In the model under consideration (8.1) we have an antiferromagnetic coupling between the two layers. For $J \gg K^\alpha$ spins within the dimer unit cell will form a singlet and a quantum paramagnetic[2] phase will be realized. On the other hand when $K^\alpha \gg J$ we expect to be in the spin liquid phase of pure Kitaev model. Hence there is an interesting possibility of a quantum phase transition from a quantum paramagnet to a spin liquid. In this case, both the phases do not break any symmetry of the Hamiltonian. However, quantum spin liquid phase is more exotic in the sense that it has fractionalized quasiparticles as excitations, and it bears non-trivial topological proper-

[1]A systematic study of finite-size effects, and the role of physical and unphysical states, can be found in ref. [87] and [88].

[2]Hereon, by quantum paramagnetic phase we mean the dimer quantum paramagnetic phase, realized in the strong inter-layer coupling limit. We will explicitly call the phases in the dominant Kitaev interaction as spin liquid, so there is no room for confusion.

ties. However, we can not rule out the possibility of some other intermediate phases and multiple quantum phase transitions as we go from a quantum paramagnet to a Kitaev spin liquid. To determine all these details is an interesting and challenging project. Our aim here will be to start from the quantum paramagnetic phase and study some of its properties. A simple question we can ask is whether it is possible to see any signs of the Kitaev model in this bilayer system. We will employ the bond-operator theory in harmonic approximation as our theoretical tool and calculate the dispersion relation in the quantum paramagnetic phase.

Another interesting route could be to start from the Kitaev limit using Majorana particle representation and investigate the effect of (small) interlayer coupling. Alternatively one could as well use the Majorana representation, to start with, in the quantum paramagnetic phase. These aspects go beyond the scope of the present work and will be addressed in near future.

8.2 Harmonic approximation

Let us now use the spin representation (2.19) in terms of the auxiliary Bosons (triplons) within the bond-operator theory. We will restrict ourselves to the harmonic approximation, i.e. only at the level of bilinear terms. Note that from our large-d formalism we know that bond-operator theory is controlled and that the harmonic approximation gives the leading order result of a systematic $1/d$ expansion. We can therefore write down our Hamiltonian (8.1) in terms of triplons as follows:

$$\mathcal{H} = \mathcal{H}_0 + \mathcal{H}_2 + \dots , \tag{8.3}$$

$$\mathcal{H}_0 = -\frac{3}{4}JN , \tag{8.4}$$

$$\mathcal{H}_2 = J\sum_{i\alpha} t^\dagger_{i\alpha}t_{i\alpha} + \sum_{\langle ij\rangle,\alpha} K^\alpha \left[t^\dagger_{i\alpha}t^\dagger_{j\alpha} + t^\dagger_{i\alpha}t_{j\alpha} + h.c.\right] . \tag{8.5}$$

Here N is the number of dimer sites. Note that at the harmonic level there is no interaction among the different modes. But beyond harmonic approximation there will be terms involving interaction among the three modes.

Honeycomb lattice has two sites per unit cell and we label them as A and B. The basis vectors for this lattice in real space are

$$\vec{a}_1 = \frac{\hat{x}}{2} + \frac{\sqrt{3}\hat{y}}{2} \quad \text{and} \quad \vec{a}_2 = -\frac{\hat{x}}{2} + \frac{\sqrt{3}\hat{y}}{2} . \tag{8.6}$$

While in the reciprocal space the basis vectors are

$$\vec{b}_1 = 2\pi\left(\hat{x} + \frac{\hat{y}}{\sqrt{3}}\right) \quad \text{and} \quad \vec{b}_2 = 2\pi\left(-\hat{x} + \frac{\hat{y}}{\sqrt{3}}\right) . \tag{8.7}$$

We will now go to the Fourier space by introducing the Fourier transformed triplon operators

$$t_{A,i\alpha} = \sqrt{\frac{2}{N}}\sum_k t_{A,\vec{k}\alpha}e^{-\imath\vec{k}\cdot\vec{r}_i} \quad \text{and} \quad t_{B,i\alpha} = \sqrt{\frac{2}{N}}\sum_k t_{B,\vec{k}\alpha}e^{-\imath\vec{k}\cdot\vec{r}_i} \tag{8.8}$$

on the two sublattices, such that $\vec{k}$ is the crystal momentum within the first Brillioun zone of a sublattice. So the bilinear Hamiltonian (8.5) takes the form

$$\begin{aligned}\mathcal{H}_{2\vec{k}} = J\sum_{\vec{k}\alpha}\left[t^{\dagger}_{A,\vec{k}\alpha}t_{A,\vec{k}\alpha} + t^{\dagger}_{B,\vec{k}\alpha}t_{B,\vec{k}\alpha}\right] + K^z\sum_{\vec{k}}\left[t^{\dagger}_{A,\vec{k}z}t^{\dagger}_{B,-\vec{k}z} + t^{\dagger}_{A,\vec{k}z}t_{B,\vec{k}z} + h.c.\right] \\ + K^x\sum_{\vec{k}}\left[e^{-\imath\vec{k}\cdot\vec{a}_1}t^{\dagger}_{A,\vec{k}x}t^{\dagger}_{B,-\vec{k}x} + e^{-\imath\vec{k}\cdot\vec{a}_1}t^{\dagger}_{A,\vec{k}x}t_{B,\vec{k}x} + h.c.\right] \\ + K^y\sum_{\vec{k}}\left[e^{-\imath\vec{k}\cdot\vec{a}_2}t^{\dagger}_{A,\vec{k}y}t^{\dagger}_{B,-\vec{k}y} + e^{-\imath\vec{k}\cdot\vec{a}_2}t^{\dagger}_{A,\vec{k}y}t_{B,\vec{k}y} + h.c.\right]. \qquad (8.9)\end{aligned}$$

In order to diagonalize, let us express the above Hamiltonian as follows:

$$\mathcal{H}_2 = \frac{1}{2}\sum_{\vec{k}\alpha}\Psi^{\dagger}\mathcal{M}_{\alpha}\Psi + \text{constant} \qquad (8.10)$$

where

$$\Psi = \begin{bmatrix} t_{A,\vec{k}\alpha} & t_{B,\vec{k}\alpha} & t^{\dagger}_{A,-\vec{k}\alpha} & t^{\dagger}_{B,-\vec{k}\alpha}\end{bmatrix}^T \qquad (8.11)$$

and

$$\mathcal{M}_x = \begin{pmatrix} J & K^x e^{-\imath\vec{k}\cdot\vec{a}_1} & 0 & K^x e^{-\imath\vec{k}\cdot\vec{a}_1} \\ K^x e^{\imath\vec{k}\cdot\vec{a}_1} & J & K^x e^{\imath\vec{k}\cdot\vec{a}_1} & 0 \\ 0 & K^x e^{-\imath\vec{k}\cdot\vec{a}_1} & J & K^x e^{-\imath\vec{k}\cdot\vec{a}_1} \\ K^x e^{\imath\vec{k}\cdot\vec{a}_1} & 0 & K^x e^{\imath\vec{k}\cdot\vec{a}_1} & J\end{pmatrix}, \qquad (8.12)$$

$$\mathcal{M}_y = \begin{pmatrix} J & K^y e^{-\imath\vec{k}\cdot\vec{a}_2} & 0 & K^y e^{-\imath\vec{k}\cdot\vec{a}_2} \\ K^y e^{\imath\vec{k}\cdot\vec{a}_2} & J & K^y e^{\imath\vec{k}\cdot\vec{a}_2} & 0 \\ 0 & K^y e^{-\imath\vec{k}\cdot\vec{a}_2} & J & K^y e^{-\imath\vec{k}\cdot\vec{a}_2} \\ K^y e^{\imath\vec{k}\cdot\vec{a}_2} & 0 & K^y e^{\imath\vec{k}\cdot\vec{a}_2} & J\end{pmatrix}, \qquad (8.13)$$

$$\mathcal{M}_z = \begin{pmatrix} J & K^z & 0 & K^z \\ K^z & J & K^z & 0 \\ 0 & K^z & J & K^z \\ K^z & 0 & K^z & J\end{pmatrix}. \qquad (8.14)$$

We have to be careful while diagonalizing these matrices. We cannot naively diagonalize the above Hermitian matrices because then the resultant quasiparticles do not obey Bosonic commutation relations (see the discussion in sec. 4.4.2). To obtain the correct Bosonic quasiparticles we must instead diagonalize the non-Hermitian matrix [58, 59]

$$\mathcal{M}'_{\alpha} = \Sigma\mathcal{M}_{\alpha} \qquad (8.15)$$

where

$$\Sigma = \begin{pmatrix} I_{2\times 2} & 0 \\ 0 & -I_{2\times 2}\end{pmatrix} \qquad (8.16)$$

with $I_{2\times 2}$ being the 2 dimensional identity matrix.

Finally, diagonalizing $\mathcal{M}'_{\alpha}$ we have the corresponding eigenvalues as the mode energies

$$\omega_{A,\vec{k}\alpha} = \sqrt{J(J-2K^{\alpha})} \quad \text{and} \quad \omega_{B,\vec{k}\alpha} = \sqrt{J(J+2K^{\alpha})}. \qquad (8.17)$$

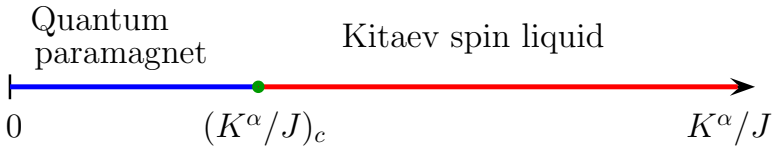

Figure 8.2: Conjectured zero-temperature phase diagram of the bilayer Kitaev model (8.1). Within the harmonic approximation, we find $(K^\alpha/J)_c = 1/2$.

The most important observation here is that the triplon dispersion is independent of the momentum $\vec{k}$. As we increase the value of K^α from zero, energy of one branch monotonically increases while that of the other decreases. Eventually at $K^\alpha_c = J/2$ the energy gap goes to zero thereby suggesting a quantum phase transition. For $K^\alpha > K^\alpha_c$, the energy gap becomes imaginary meaning the quantum paramagnetic phase is unstable. At the harmonic level, the non-dispersive energy modes suggests that there is no magnetic ordering across the quantum critical point. This seems to be in accord with the fact that for $K^\alpha > K^\alpha_c$ we expect a Kitaev spin liquid phase characterized by no symmetry breaking. Can we then say that this non-dispersive energy mode is a sign of spin liquid phase in the $K^\alpha > K^\alpha_c$ region?

Well, while in principle this idea seems to be correct, in practice we have to be very careful. Firstly, unless we can solve the model exactly the dispersion we calculate is not exact. We calculate it to a particular order in perturbation theory. So it might be that the dispersion is flat up to the order we calculate, but has momentum dependence beyond it. One prominent example occurs in the case of Shastry-Sutherland model, wherein the quasiparticle dispersion in the singlet phase is flat up to 5th order in perturbation theory and becomes dispersive only beyond this order [90]. So although our harmonic level dispersion is flat we are not sure about the scenario once the interaction terms are included. Moreover, the Kitaev model does not commute with individual spin components, unlike the Heisenberg model. Hence the use of spin index as a quantum number to label the excitations may not be appropriate. This means that probably the correct excitations in the quantum paramagnetic phase are bound states of two or more triplons. One or all of these may condense at the quantum phase transition. This condensation could then be linked to the gapped vison excitation in the Kitaev spin liquid phase. All this however goes beyond the usual bond-operator theory and we would like to investigate this in future.

8.3 Discussion

Before closing this chapter, we would like to point out that similar analysis can be done for the Kitaev model on a bilayer triangular lattice. In this case, the single layer problem is not exactly solvable as opposed to the Kitaev model on honeycomb lattice and a few numerical studies have already been performed [91, 92]. Using the harmonic level bond-operator theory we can calculate the single-triplon dispersion, and we find that it is dispersive with minima occuring along lines in the Brillioun zone. This

hints towards a spiral ordered phase in the decoupled layer limit. On the triangular lattice bilayer we can also study the Heisenberg model with nearest neighbor and next nearest neighbor AF coupling. Again, using the harmonic level bond-operator theory we easily recover the established magnetically ordered phases. In fact, we can write the corresponding bond-operators in the ordered phase after Hilbert-space rotation. As expected we also find agreement with the spin-wave theory results in the decoupled layer limit. Apart from this, we can also write down bond operators for multi-Q states. In the triangular lattice bilayer, we find that upon inclusion of the zero-point energy, the degeneracy of single-Q and triple-Q states is lifted and the single-Q state is stabilized.

Summary

In chapter 1 we had set the goal to identify a small control parameter and perform systematic calculations in the context of magnetic quantum phase transitions. We chose coupled-dimer magnets, a paradigmatic model to study magnetic quantum phase transitions, as our working model and demonstrated our ideas using it in part I of the thesis. In chapter 2 we saw how phase transitions between different magnetic phases takes place in real material examples which mimic coupled-dimer systems. Importantly, in this chapter, we also reviewed theoretical ideas developed so far to solve coupled-dimer magnets. It then became clear that no analytical method developed so far could consistently describe the entire phase diagram of these systems and we also found the reason behind it, namely the lack of a small control parameter.

We have thus proposed utilizing the limit of large-d, d being the spatial dimension, so that $1/d$ becomes a small parameter. In chapter 3 we have discussed different aspects of the limit $d \to \infty$, which paves the way for an analytic $1/d$ expansion. In particular, the limit $d \to \infty$ in a given model must be implemented with care. Appropriate rescaling of tuning parameter is required to ensure magnetic quantum phase transition even in the large-d limit. One of the important things we learned here is that using the mean-field critical exponents we can identify suitable observables which are analytic even at the critical point. This is a crucial aspect to smoothly connect different phases. This idea, together with identification of $1/d$ as an appropriate small parameter, was not realized before, thus halting analytic calculations across the quantum critical point. Using the example of a hypercubic lattice, we also saw how momentum integrals simplify in the large-d limit. This is one of the central ideas for our work. We thus saw that any Feynman diagram, in the limit $d \to \infty$, can be expressed as a power series in $1/d$. Another technical advantage is that the ground state of the system becomes a simple product state in the large-d limit, owing to the suppression of non-local fluctuations in this limit. This sets up the base to construct the full diagrammatic perturbation theory.

To demonstrate our idea of large-d limit, we chose to generalize the Heisenberg spin-1/2 square-lattice bilayer system (2.2) to a system of coupled-dimers on a hypercube. Based on the ideas discussed in chapter 3 we first introduced the rescaled tuning parameter q (4.4), which is finite even in the limit $d \to \infty$. This model realizes a quantum paramagnetic phase, which does not break any symmetry of the Hamiltonian, and an antiferromagnetically ordered phase, which spontaneously breaks the $SU(2)$ symmetry, connected via a quantum critical point. In chapter 4 we have presented explicit calculations in the quantum paramagnetic phase using the well-known bond-operator theory. We have shown that using $1/d$ as a small parameter we can systematically improve the results obtained from the frequently used leading-order results i.e. within

harmonic approximation. Using diagrammatic perturbation theory we have calculated static and dynamical observables. Importantly, observables have an analytic expansion in $1/d$. However, we find that the quasiparticle lifetime is non-perturbative in the large-d limit and hence does not admit a $1/d$ expansion. Our new method was validated by the fact that perturbation theory in small q in arbitrary d, performed using contiuous unitary-transformations[3], yields exactly the same results as those obtained from our $1/d$ expansion after performing a double expansion in small q. We have also investigated the so called Brueckner theory, which relies on small density of triplon excitations, within our $1/d$ formalism. Remarkably, we could derive our results for the triplon dispersion and hence the phase boundary using this approach. We now understand why the Brueckner approach works so well in the quantum paramagnetic phase; this is because the triplet density scales as $1/d$ in the large-d limit.

Continuing further with our analysis of coupled-dimer magnets using large-d formalism, we discussed the antiferromagnetic phase in chapter 5. Through our calculations it is clear that the systematic $1/d$ expansion can be efficiently used even in the magnetically ordered phases. After appropriate rotation in the Hilbert space we could use all the machinery developed in chapter 4 to perform diagrammatic calculations in the ordered phase. Here again we have calculated static and dynamic observables. Remarkably, using different criteria we obtain the same expression for the phase boundary as derived in chapter 4 and hence we established the internal consistency of our method. Importantly we obtain the gapless Goldstone modes, corresponding to spontaneously broken $SU(2)$ symmetry, including $1/d$ correction beyond the harmonic approximation. This is non-trivial when performing approximate analytic calculations and so this is another success of our method. We have also calculated the dispersion and spectral weight of the amplitude (Higgs) mode. It is known that the amplitude mode can decay into the Goldstone modes and hence detecting it in the dynamic spin susceptibility is difficult. However what we can see is that in the dynamic spin susceptibility dominant contribution to the single-mode spectral weight arises from the Goldstone modes and hence the detection of amplitude mode is difficult even if its decay were absent. Interestingly, we find that in the bond-bond correlation function, the single-mode contribution arises solely from the amplitude mode and hence this is a potential observable to look for in order to detect the amplitude mode. When we talk about magnetically ordered phases we can not ignore the spin-wave theory which has had tremendous success. In our analysis we make contact with the spin-wave theory and find our results in agreement with those obtained from the spin-wave theory in the decoupled-layer limit. Remarkably, in both the phases of the coupled-dimers on a hypercubic lattice, we could prove that the hard-core constraint from the physical Hilbert space is satisfied order by order in $1/d$.

We have thus achieved our goal and have established $1/d$ as a suitable parameter using which the entire phase diagram of coupled-dimer magnets including the quantum critical point can be described consistently. Moreover, the success of our method shows that the bond-operator formalism, originally developed as efficient but uncontrolled mean-field theory, can be cast into a controlled and systematic theory for coupled-dimer magnets. We also found a good agreement with the quantum Monte Carlo

[3]Calculation performed by Kris Coester and Kai P. Schmidt at TU Dortmund.

results[4] in $d = 2$. In this case, our analytical result helped to identify the amplitude (Higgs) mode signal in the bond-bond correlation.

Having dealt with coupled-dimer magnets and established our large-d formalism in part I, we went on show the applicability of $1/d$ expansion technique in the case of the transverse-field Ising model in chapter 7. This shows that the $1/d$ expansion is not just tied to the bond-operator theory and can be independently applied in other situations. In the transverse-field Ising model we again have a quantum paramagnetic phase and a ferromagnetic phase separated by a quantum critical point. However, in this case there is no Goldstone mode, since a discrete symmetry is broken. Here again we first generalized the model to Ising spins on a hypercubic lattice. We then introduced Bosonic particles to depict the reference state and the excited state. We could then borrow all the technical aspects developed in part I to calculate observables. Even in this case our formalism is first of its kind using which the entire phase diagram of the transverse-field Ising model ($d \geq 2$) could be covered consistently.

In chapter 8 we have explored the bilayer Kitaev model on a honeycomb lattice. Here one of the main objectives was to investigate the possibility of looking for signatures of the single layer phases by studying the dimer quantum paramagnetic phase, realized in the strong inter-layer coupling. Within the harmonic level bond-operator theory for the Kitaev model, we saw a flat triplon dispersion as well as a uniform spectral weight associated to it. This is possibly connected to the fact that in the weak inter-layer coupling limit the single layer phase is a Kitaev spin-liquid, which has no magnetic ordering. However the situation is more complicated and quickly goes beyond the scope of this work. Importantly, it seems that the use of bond-operator description in this case may not be valid since the spin is not a good quantum number. Also the phase transition may involve condensation of multiple bound states instead of just a single triplon.

[4]QMC simulation performed by Maximilian Lohöfer and Stefan Wessel at RWTH Aachen.

Outlook

One immediate extension of our method can be made to the case of coupled-dimer magnets in a uniform field. In this case, the triplons are known to form a Bose-Einstein condensate with the order parameter proportional to $\langle S_x + \imath S_y \rangle$. Thus in the BEC phase we have to consider a condensate proportional to $t_x + \imath t_y$, instead of t_z considered in this work. This scenario was previously investigated at the harmonic level [43]. Another possible direction is the investigation of multi particle bound states within the large-d formalism. Usually, condensation of bound states may occur at phase transitions involving two symmetry broken phases whose respective symmetry groups are not subgroup of the other. We envision further applications of the $1/d$ expansion developed here to systems with geometric frustration [93], including cases with non-collinear and incommensurate order. These cases are well within the reach of harmonic approximation of bond-operator theory, and so our $1/d$ expansion can shed light on the quantum corrections in these cases. However, we must point out that the large-d generalization may not be straightforward. The harmonic bond-operator approach has also been applied to systems with quenched disorder [60], and we expect insights into corrections here as well as in similar systems.

An ambitious future goal is to generalize the systematic approach presented here to finite temperatures. Inside the ordered phase, the challenge lies in finding a suitable *temperature-dependent* reference state, with the condensate vanishing as the Néel temperature is approached from below. On the technical side we might also have to think about a different way to implement the constraint from the physical Hilbert space. At zero temperature, the projection operator efficiently separated the physical and unphysical states, and as long as we keep working in the physical sector everything is consistent. However, the evaluation of thermodynamic quantities involves all the states. To be precise, the partition function now involves both physical and unphysical states. It may not be possible to separate out the contributions to an observable coming from the physical and the unphysical states. One way out could be to define thermodynamic averages in an appropriate way only in the physical sector. Actually a similar situation arises in the spin-wave theory using Holstein-Primarkoff transformation. But there with the limit $S \to \infty$ even the physical Hilbert space becomes infinite and so the distinction between physical and unphysical states becomes less important.

Apart from spin systems, the $1/d$ expansion technique could in principle be applied to Bosonic or Fermionic models where the local on-site problem becomes simple in the large-d limit. Recall that our technique uses a product-state ansatz as a reference state and so if the local problem itself is non-trivial then a systematic $1/d$ expansion is not possible. One example of this situation is the single band Hubbard model. It is well known that the dynamical mean-field theory for the single band Hubbard

model becomes exact in the limit $d \to \infty$ but it can not be cast into a systematic $1/d$ expansion for the reason mentioned earlier.

In the context of coupled-dimers, motivated by good agreement with QMC in $2d$, we look forward to QMC results in $d = 3$ where also our analytic results can be easily used. In $3d$, in fact, we expect to observe a signal from the amplitude mode even in the dynamic spin susceptibility. What is also interesting to study is the continuum within the large-d formalism. Especially, the continuum present in the dynamic singlet structure factor, discussed in chapter 6, calls for a more systematic analysis.

Our analysis in chapter 8, motivates interesting directions which are potentially important in studying the signatures of Kitaev spin-liquid. One such possibility is working with the Majorana particles in the dimer quantum paramagnetic phase. Also, a systematic study of the quantum phase transition itself is still open.

We thus conclude this thesis by re-emphasizing our main message that using $1/d$ as a small parameter we can efficiently study the magnetic quantum phase transitions and associated phases. Our method establishes the popular bond-operator theory as a controlled method in the large-d limit.

Appendix A

Coupled Dyson equation

The coupled Dyson's equation in the Nambu matrix representation is given by

$$\mathcal{G} = \left[\mathcal{G}_0^{-1} - \Sigma\right]^{-1} \tag{A.1}$$

where $\mathcal{G}$, $\mathcal{G}_0$ and Σ are matrices given by

$$\mathcal{G} = \begin{pmatrix} \mathcal{G}_N(\vec{k},\omega) & \mathcal{G}_A(\vec{k},\omega) \\ \mathcal{G}_A(\vec{k},-\omega) & \mathcal{G}_N(\vec{k},-\omega) \end{pmatrix}, \tag{A.2}$$

$$\mathcal{G}_0 = \begin{pmatrix} \mathcal{G}_{0N}(\vec{k},\omega) & \mathcal{G}_{0A}(\vec{k},\omega) \\ \mathcal{G}_{0A}(\vec{k},-\omega) & \mathcal{G}_{0N}(\vec{k},-\omega) \end{pmatrix}, \tag{A.3}$$

$$\Sigma = \begin{pmatrix} \Sigma_N(\vec{k},\omega) & \Sigma_A(\vec{k},\omega) \\ \Sigma_A(\vec{k},-\omega) & \Sigma_N(\vec{k},-\omega) \end{pmatrix}. \tag{A.4}$$

In the above expressions $\mathcal{G}_{N(A)}$ stands for normal (anomalous) Green's function, $\mathcal{G}_{0N(A)}$ stands for normal (anomalous) bare Green's function and $\Sigma_{N(A)}$ is the normal (anomalous) self-energy.

In our case, we are using the zero-temperature (or time ordered) Green's function [33], which is the zero-temperature limit of the retarded Green's function, used with the Matsubara frequency. As stated in main text we work in the basis of the Bogoliubov quasiparticles where the bilinear Hamiltonian is diagonal in the harmonic approximation. So our Green's function is defined for τ-particles and all the self-energies are calculated with respect to the vertices in the τ basis.

For clarity, we write down the definitions of the normal and anomalous Green's function with respect to the τ particles. They read as

$$\mathcal{G}_N(\vec{k},t) = -\imath\langle \mathcal{T}_t \tau_{\vec{k}}(t)\tau^\dagger_{\vec{k}}(0)\rangle\,, \tag{A.5}$$

$$\mathcal{G}_A(\vec{k},t) = -\imath\langle \mathcal{T}_t \tau_{\vec{k}}(t)\tau_{-\vec{k}}(0)\rangle\,, \tag{A.6}$$

where t is real time, $\mathcal{T}_t$ is the time-ordering operator and $\langle\ldots\rangle$ is taken with respect to the ground state. When $\langle\ldots\rangle$ is taken with respect to the ground state of the unperturbed Hamiltonian piece, in our case the bilinear Hamiltonian in harmonic approximation, then we obtain the corresponding bare (or unperturbed) Green's function.

In the harmonic approximation, the ground state is just the vacuum of the τ particles and so we have

$$\mathcal{G}_{0N}(\vec{k},\omega) = \left(\omega - \omega_{\vec{k}}\right)^{-1} , \tag{A.7}$$

$$\mathcal{G}_{0A}(\vec{k},\omega) = 0 , \tag{A.8}$$

where $\omega_{\vec{k}}$ is the bare dispersion obtained at the harmonic level. We thus have

$$\mathcal{G}_0 = \begin{pmatrix} \left(\omega - \omega_{\vec{k}}\right)^{-1} & 0 \\ 0 & -\left(\omega + \omega_{\vec{k}}\right)^{-1} \end{pmatrix} . \tag{A.9}$$

Using this and eq. (A.1) we obtain the full propagator

$$\mathcal{G} = \frac{1}{\Xi(\vec{k},\omega)} \begin{pmatrix} \omega + \omega_{\vec{k}} + \Sigma_N(\vec{k},-\omega) & -\Sigma_A(\vec{k},\omega) \\ -\Sigma_A(\vec{k},-\omega) & -\omega + \omega_{\vec{k}} + \Sigma_N(\vec{k},\omega) \end{pmatrix} \tag{A.10}$$

where

$$\Xi(\vec{k},\omega) = \Big(\omega + \omega_{\vec{k}} + \Sigma_N(\vec{k},-\omega)\Big)\Big(\omega - \omega_{\vec{k}} - \Sigma_N(\vec{k},\omega)\Big) + \Sigma_A(\vec{k},\omega)\Sigma_A(\vec{k},-\omega) . \tag{A.11}$$

This then gives us the expression in eq. (4.74). These same details apply in chapters 5 and 7.

Appendix B

Projectors and spin commutation relations

In this appendix, we will present a general discussion on the choice of projection operators P_i, introduced to address the hard-core constraint of triplet operators, as in eq. (2.22). Let us assume that P_i is an arbitrary function of $n_i = \sum_\gamma t^\dagger_{i\gamma} t_{i\gamma}$. For the spin commutation relation we obtain,

$$\begin{aligned}\left[S^\alpha_{im}, S^\beta_{im'}\right] &= \imath \epsilon_{\alpha\beta\gamma} S^\gamma_{im} \delta_{mm'} \\ &+ \frac{(-1)^{m+m'}}{4}\left[t^\dagger_{i\alpha}(P_i^2-1)t_{i\beta} - P_i t^\dagger_{i\alpha} t_{i\beta} P_i - t^\dagger_{i\beta}(P_i^2-1)t_{i\alpha} + P_i t^\dagger_{i\beta} t_{i\alpha} P_i\right].\end{aligned} \tag{B.1}$$

The first line can be easily identified as the standard spin commutator. The second line depends on the choice of the projection operator. Using $P_i = f(n_i)$, these extra terms take the following form:

$$(t^\dagger_{i\alpha} t_{i\beta} - t^\dagger_{i\beta} t_{i\alpha})\left[f^2(n_i - 1) - 1 - f^2(n_i)\right]. \tag{B.2}$$

For any matrix element of $\vec{S}_{im}$ between the physical and the unphysical states to be suppressed, we require $f(0) = 1$ and $f(1) = 0$. This condition automatically ensures that the extra terms (B.2) vanish in the physical Hilbert space. Hence, any function with the property $f(0) = 1$ and $f(1) = 0$ could be chosen as the projection operator, i.e., the choice is not unique.

However, a non-linear function would lead to a more complicated Hamiltonian, and so for practical purposes, $f(x) = 1 - x$ as in eq. (2.22) is most efficient. As already mentioned in chapter 2, the square-root choice is particularly appealing because of its close resemblance to the Holstein-Primakoff representation [75], used in the spin-wave theory. Moreover, the square-root choice delivers exact spin commutation relation both in the physical and the unphysical Hilbert space. However, as already explained, the square-root choice accompanies with a non-convergent series. Interestingly, the Holstein-Primakoff representation works for the spin-wave theory because there $1/S$ controls the square-root expansion. Also, the physical Hilbert space is infinite for $S \to \infty$, unlike our case.

Appendix C

Momentum sums and vertices in chapter 4

C.1 Momentum sums in large d and expectation values

Inside the momentum sums, we frequently need an expansion of the mode energy $\omega_{\vec{k}}$ (4.36) and Bogoliubov coefficients (4.38) in terms of $\gamma_{\vec{k}}$:

$$\begin{aligned}
\frac{\omega_{\vec{k}}}{J} &= 1 + \gamma_{\vec{k}} q - \frac{\gamma_{\vec{k}}^2 q^2}{2} + \frac{\gamma_{\vec{k}}^3 q^3}{2} - \frac{5\gamma_{\vec{k}}^4 q^4}{8} + \mathcal{O}(\gamma_{\vec{k}}^5)\,, \\
v_{\vec{k}}^2 &= \frac{\gamma_{\vec{k}}^2 q^2}{4} - \frac{\gamma_{\vec{k}}^3 q^3}{2} + \frac{15\gamma_{\vec{k}}^4 q^4}{16} + \mathcal{O}(\gamma_{\vec{k}}^5), \\
u_{\vec{k}}^2 &= 1 + v_{\vec{k}}^2, \\
u_{\vec{k}} v_{\vec{k}} &= -\frac{\gamma_{\vec{k}} q}{2} + \frac{\gamma_{\vec{k}}^2 q^2}{2} - \frac{3\gamma_{\vec{k}}^3 q^3}{4} + \frac{5\gamma_{\vec{k}}^4 q^4}{4} + \mathcal{O}(\gamma_{\vec{k}}^5)\,.
\end{aligned} \tag{C.1}$$

We frequently need the following momentum sums:

$$R_1 = \frac{1}{N}\sum_{\vec{k}} u_{\vec{k}} v_{\vec{k}} \quad = \frac{q^2}{4d} + \frac{15q^4}{16d^2} + \mathcal{O}(d^{-3})\,, \tag{C.2}$$

$$R_2 = \frac{1}{N}\sum_{\vec{k}} v_{\vec{k}}^2 \quad = \frac{q^2}{8d} + \frac{45q^4}{64d^2} + \mathcal{O}(d^{-3})\,, \tag{C.3}$$

$$R_3 = \frac{1}{N}\sum_{\vec{k}} \gamma_{\vec{k}} u_{\vec{k}} v_{\vec{k}} = -\frac{q}{4d} - \frac{9q^3}{16d^2} + \mathcal{O}(d^{-3})\,, \tag{C.4}$$

$$R_4 = \frac{1}{N}\sum_{\vec{k}} \gamma_{\vec{k}} v_{\vec{k}}^2 \quad = -\frac{3q^3}{8d^2} + \mathcal{O}(d^{-3})\,. \tag{C.5}$$

These have been evaluated using the momentum summation properties, eqs. (3.6)–(3.9), and the above mentioned expansion in eq. (C.1). The $R_{1\ldots4}$ are related to the

expectation values of the bilinear Hamiltonian (4.24) as follows:

$$\sum_i \langle t^\dagger_{i\alpha} t^\dagger_{i\beta}\rangle = N\delta_{\alpha\beta}R_1\,,\ \sum_i \langle t^\dagger_{i\alpha} t_{i\beta}\rangle = N\delta_{\alpha\beta}R_2,$$
$$\sum_{\langle ij\rangle} \langle t^\dagger_{i\alpha} t^\dagger_{j\beta}\rangle = Nd\delta_{\alpha\beta}R_3\,,\sum_{\langle ij\rangle} \langle t^\dagger_{i\alpha} t_{j\beta}\rangle = Nd\delta_{\alpha\beta}R_4\,. \tag{C.6}$$

However, note that these are only within the harmonic approximation. The full $1/d$ expansion for these expectation values also involve corrections from the interaction terms. This has been calculated in sec. 4.5.5.

Finally, we also need the following higher-order combination of Bogoliubov coefficients:

$$R'_5(\vec{k}) = \frac{1}{N}\sum_{\vec{k}'} u_{\vec{k}'} v_{\vec{k}'} u_{\vec{k}-\vec{k}'} v_{\vec{k}-\vec{k}'} = \frac{\gamma_{\vec{k}} q^2}{8d}\,. \tag{C.7}$$

C.2 Cubic and quartic vertex functions

The cubic vertex functions arising in the asymmetric case, $\kappa \neq 0$, where κ is the asymmetry parameter (4.3), are as follows:

$$\Phi_{31}(123) = -\imath\kappa q J\gamma_{2+3}(u_1u_2v_3 - v_1v_2u_3), \tag{C.8}$$
$$\Phi_{32}(123) = -\imath\kappa q J\gamma_{2-3}(u_1u_2u_3 - v_1v_2v_3), \tag{C.9}$$
$$\Phi_{33}(123) = -\imath\kappa q J\gamma_{2+3}(v_1u_2v_3 - u_1v_2u_3), \tag{C.10}$$
$$\Phi_{34}(123) = -\imath\kappa q J\gamma_{2-3}(u_1v_2v_3 - v_1u_2u_3). \tag{C.11}$$

The quartic vertex functions are:

$$\begin{aligned}\Phi_{41}(1234) = {}& \frac{qJ}{2}\sum_{\alpha,\beta,\alpha\neq\beta}(\gamma_{2+3}u_1v_2u_3v_4 - \gamma_{2+4}u_1u_2v_3v_4)\\ & - qJ\sum_{\alpha,\beta}(\gamma_2 u_1v_2u_3v_4 + \gamma_2 u_1u_2u_3v_4 + \gamma_2 v_1v_2v_3u_4 + \gamma_{2+3+4}u_1v_2u_3v_4)\,, \end{aligned}\tag{C.12}$$

$$\begin{aligned}\Phi_{42}(1234) = {}& \frac{qJ}{2}\sum_{\alpha,\beta,\alpha\neq\beta}(\gamma_{2-4}u_1v_2u_3v_4 + \gamma_{2-4}v_1u_2v_3u_4 - \gamma_{2-4}u_1u_2u_3u_4 - \gamma_{2-4}v_1v_2v_3v_4)\\ & - qJ\sum_{\alpha,\beta}(\gamma_2 u_1v_2u_3v_4 + \gamma_4 v_1u_2v_3u_4 + \gamma_{2-3-4}u_1v_2u_3v_4 + \gamma_{1+2-4}v_1u_2v_3u_4\\ & \quad + \gamma_2 u_1u_2v_3u_4 + \gamma_4 u_1v_2v_3v_4 + \gamma_3 u_1v_2u_3u_4 + \gamma_1 v_1v_2v_3u_4)\,, \end{aligned}\tag{C.13}$$

$$\begin{aligned}\Phi_{43}(1234) = \frac{qJ}{2}\sum_{\alpha,\beta,\alpha\neq\beta}&(\gamma_{2-3}u_1u_2u_3u_4+\gamma_{-3-4}u_1v_2u_3v_4+\gamma_{1+2}v_1u_2v_3u_4+\gamma_{1-4}v_1v_2v_3v_4\\&-\gamma_{2-3}u_1v_2v_3u_4-\gamma_{-3-4}u_1v_2v_3u_4-\gamma_{1+2}u_1v_2v_3u_4-\gamma_{1-4}u_1v_2v_3u_4)\\-qJ\sum_{\alpha,\beta}&(\gamma_3u_1u_2u_3u_4+\gamma_3u_1v_2u_3v_4+\gamma_1v_1u_2v_3u_4+\gamma_1v_1v_2v_3v_4+\gamma_{2-3-4}u_1u_2u_3u_4\\&+\gamma_{2-3-4}u_1v_2u_3v_4+\gamma_{1+2-4}v_1u_2v_3u_4+\gamma_{1+2-4}v_1v_2v_3v_4+\gamma_3u_1u_2v_3u_4\\&+\gamma_3u_1v_2v_3v_4+\gamma_1u_1u_2v_3u_4+\gamma_1u_1v_2v_3v_4+\gamma_1v_1u_2u_3u_4\\&+\gamma_1v_1v_2u_3v_4+\gamma_3v_1u_2u_3u_4+\gamma_3v_1v_2u_3v_4),\end{aligned}\tag{C.14}$$

$$\begin{aligned}\Phi_{44}(1234) = \frac{qJ}{2}\sum_{\alpha,\beta,\alpha\neq\beta}&(\gamma_{2+3}u_1v_2u_3u_4+\gamma_{2-4}u_1v_2v_3v_4+\gamma_{1-4}u_1v_2u_3u_4+\gamma_{1+3}u_1v_2v_3v_4\\&-\gamma_{2+3}u_1u_2v_3u_4-\gamma_{2-4}u_1u_2v_3u_4-\gamma_{2-4}v_1v_2u_3v_4-\gamma_{2+3}v_1v_2u_3v_4)\\-qJ\sum_{\alpha,\beta}&(\gamma_2u_1v_2u_3u_4+\gamma_2u_1v_2v_3v_4+\gamma_4u_1v_2u_3u_4+\gamma_3u_1v_2v_3v_4+\gamma_{2+3-4}u_1v_2u_3u_4\\&+\gamma_{2+3-4}u_1v_2v_3v_4+\gamma_{1+2-4}u_1v_2u_3u_4+\gamma_{1+2+3}u_1v_2v_3v_4+\gamma_2u_1u_2u_3u_4\\&+\gamma_2u_1u_2v_3v_4+\gamma_4u_1v_2u_3v_4+\gamma_3u_1v_2u_3v_4+\gamma_3u_1v_2v_3u_4\\&+\gamma_4u_1v_2v_3u_4+\gamma_2v_1v_2u_3u_4+\gamma_2v_1v_2v_3v_4).\end{aligned}\tag{C.15}$$

Appendix D

Momentum sums and vertices in chapter 5

D.1 Momentum sums and expectation values

Following is the frequently needed expansion of Bogoliubov coefficients (5.34) in terms of $\gamma_{\vec{k}}$

$$u_{\vec{k}a}v_{\vec{k}a} = -\frac{Jq\gamma_{\vec{k}}}{2J_1} + \frac{J^2q^2\gamma_{\vec{k}}^2}{2J_1^2}\frac{1-\lambda_0^2}{1+\lambda_0^2} + \mathcal{O}(\gamma_{\vec{k}}^3)\,, \tag{D.1}$$

$$u_{\vec{k}z}v_{\vec{k}z} = -\frac{Jq\gamma_{\vec{k}}}{2J_2}\left(\frac{1-\lambda_0^2}{1+\lambda_0^2}\right)^2 + \frac{J^2q^2\gamma_{\vec{k}}^2}{2J_2^2}\left(\frac{1-\lambda_0^2}{1+\lambda_0^2}\right)^4 + \mathcal{O}(\gamma_{\vec{k}}^3)\,. \tag{D.2}$$

with J_1 and J_2 defined in eq. (5.32). Similarly, expanding other required combinations in terms of $\gamma_{\vec{k}}$ and using the properties, (3.6)–(3.9), we get the following relevant momentum sums:

$$R_{1a} = \frac{1}{N}\sum_{\vec{k}} u_{\vec{k}a}v_{\vec{k}a} = \frac{J^2q^2}{4J_1^2d}\frac{1-\lambda_0^2}{1+\lambda_0^2} + \mathcal{O}(d^{-2})\,, \tag{D.3}$$

$$R_{2a} = \frac{1}{N}\sum_{\vec{k}} v_{\vec{k}a}^2 = \frac{q^2J^2}{8J_1^2d} + \mathcal{O}(d^{-2})\,, \tag{D.4}$$

$$R_{3a} = \frac{1}{N}\sum_{\vec{k}} \gamma_{\vec{k}}u_{\vec{k}a}v_{\vec{k}a} = -\frac{qJ}{4J_1d} + \mathcal{O}(d^{-2})\,, \tag{D.5}$$

$$R_{4a} = \frac{1}{N}\sum_{\vec{k}} \gamma_{\vec{k}}v_{\vec{k}m}^2 = \mathcal{O}(d^{-2})\,, \tag{D.6}$$

$$R_{1z} = \frac{1}{N}\sum_{\vec{k}} u_{\vec{k}z}v_{\vec{k}z} = \frac{J^2q^2}{4J_2^2 d}\left(\frac{1-\lambda_0^2}{1+\lambda_0^2}\right)^4 + \mathcal{O}(d^{-2})\,, \tag{D.7}$$

$$R_{2z} = \frac{1}{N}\sum_{\vec{k}} v_{\vec{k}z}^2 = \frac{J^2q^2}{8J_2^2 d}\left(\frac{1-\lambda_0^2}{1+\lambda_0^2}\right)^4 + \mathcal{O}(d^{-2})\,, \tag{D.8}$$

$$R_{3z} = \frac{1}{N}\sum_{\vec{k}} \gamma_{\vec{k}}u_{\vec{k}z}v_{\vec{k}z} = -\frac{Jq}{4J_2 d}\left(\frac{1-\lambda_0^2}{1+\lambda_0^2}\right)^2 + \mathcal{O}(d^{-2})\,, \tag{D.9}$$

$$R_{4z} = \frac{1}{N}\sum_{\vec{k}} \gamma_{\vec{k}}v_{\vec{k}z}^2 = \mathcal{O}(d^{-2})\,. \tag{D.10}$$

Note that these expressions are valid for arbitrary h^z, with its value entering via $\lambda_0(h^z)$ according to eq. (5.22).

These $R_{1\ldots4}$ are then related to the expectation values within the harmonic approximation (leading-order bilinear Hamiltonian (5.25)) as follows:

$$\begin{aligned}
&\sum_i \langle t_{i\alpha}^\dagger t_{i\beta}^\dagger\rangle = 3N\delta_{\alpha\beta}R_{1\alpha}\,, \quad \sum_i \langle t_{i\alpha}^\dagger t_{i\beta}\rangle = 3N\delta_{\alpha\beta}R_{2\alpha},\\
&\sum_{\langle ij\rangle} \langle t_{i\alpha}^\dagger t_{j\beta}^\dagger\rangle = 3Nd\delta_{\alpha\beta}R_{3\alpha}\,, \sum_{\langle ij\rangle} \langle t_{i\alpha}^\dagger t_{j\beta}\rangle = 3Nd\delta_{\alpha\beta}R_{4\alpha}\,.
\end{aligned} \tag{D.11}$$

Within the self-energy expressions we also need

$$R'_{az}(\vec{k}) = \frac{1}{N}\sum_{\vec{k}'} u_{\vec{k}'a}v_{\vec{k}'a}u_{(\vec{k}'-\vec{k})z}v_{(\vec{k}'-\vec{k})z} = \frac{J^2\gamma_{\vec{k}}}{32J_1J_2d}\,. \tag{D.12}$$

Similar to chapter 4, the anomalous expectation value $\langle \tilde{t}_{i\alpha}^\dagger \tilde{t}_{i\alpha}^\dagger\rangle$ vanishes upon taking into account $1/d$ corrections, as required by the constraint.

D.2 Hamiltonian coefficients

The coefficients of $\mathcal{H}'_{2c}$, representing the bilinear terms arising from normal ordering of quartic interactions, are as follows:

$$\begin{aligned}
C_{\vec{k}a} &= (u^2_{\vec{k}a} + v^2_{\vec{k}a})qJ\Big[-2\gamma_{\vec{k}}R_{1a} - 6R_{3a} - 6(\gamma_{\vec{k}}R_{2a} + R_{4a})\Lambda - 4(R'_{4a} + 2R_{2a})\frac{\lambda^2}{(1+\lambda^2)^2} \\
&\qquad + R'_{4a} + (R'_{4z} - 2\gamma_{\vec{k}}R_{2z})\Lambda - 2(R_{3z} + R_{4z})\Lambda^2 - 8R_{2z}\frac{\lambda^2}{(1+\lambda^2)^2}\Big] \\
&\quad - 2u_{\vec{k}a}v_{\vec{k}a}qJ\Big[6\gamma_{\vec{k}}R_{2a} + 2R_{4a} + 2(\gamma_{\vec{k}}R_{1a} + R_{3a})\Lambda + 4R'_{3a}\frac{\lambda^2}{(1+\lambda^2)^2} \\
&\qquad + R'_{3a} + 2\gamma_{\vec{k}}R_{2z} + R'_{3z}\Big], \qquad \text{(D.13)} \\
D_{\vec{k}a} &= -(u^2_{\vec{k}a} + v^2_{\vec{k}a})qJ\Big[6\gamma_{\vec{k}}R_{2a} + 2R_{4a} + 2(\gamma_{\vec{k}}R_{1a} + R_{3a})\Lambda + 4R'_{3a}\frac{\lambda^2}{(1+\lambda^2)^2} \\
&\qquad + R'_{3a} + 2\gamma_{\vec{k}}R_{2z} + R'_{3z}\Big] \\
&\quad + 2u_{\vec{k}a}v_{\vec{k}a}qJ\Big[-2\gamma_{\vec{k}}R_{1a} - 6R_{3a} - 6(\gamma_{\vec{k}}R_{2a} + R_{4a})\Lambda - 4(R'_{4a} + 2R_{2a})\frac{\lambda^2}{(1+\lambda^2)^2} \\
&\qquad + R'_{4a} + (R'_{4z} - 2\gamma_{\vec{k}}R_{2z})\Lambda - 2(R_{3z} + R_{4z})\Lambda^2 - 8R_{2z}\frac{\lambda^2}{(1+\lambda^2)^2}\Big], \qquad \text{(D.14)} \\
C_{\vec{k}z} &= -(u^2_{\vec{k}z} + v^2_{\vec{k}z})qJ\Big[(2\gamma_{\vec{k}}R_{1z} + 4R_{3z} + 4R_{4z} + 4\gamma_{\vec{k}}R_{2z})\Lambda^2 + 16(R_{2z} + R'_{4z})\frac{\lambda^2}{(1+\lambda^2)^2} \\
&\qquad + 4R_{3a} + 2(2R_{4a} - R'_{4a})\Lambda + 4\gamma_{\vec{k}}R_{2a}\Lambda^2 + 16R_{2a}\frac{\lambda^2}{(1+\lambda^2)^2}\Big] \\
&\quad - 2u_{\vec{k}z}v_{\vec{k}z}qJ\Big[(4\gamma_{\vec{k}}R_{2z} + 2R_{4z} + 2R_{3z} + 2\gamma_{\vec{k}}R_{1z})v^2 + 16R'_{3z}\frac{\lambda^2}{(1+\lambda^2)^2} \\
&\qquad + 2R'_{3a} + 4\gamma_{\vec{k}}R_{2a}\Lambda^2\Big], \qquad \text{(D.15)} \\
D_{\vec{k}z} &= -(u^2_{\vec{k}z} + v^2_{\vec{k}z})qJ\Big[(4\gamma_{\vec{k}}R_{2z} + 2R_{4z} + 2R_{3z} + 2\gamma_{\vec{k}}R_{1z})\Lambda^2 + 16R'_{3z}\frac{\lambda^2}{(1+\lambda^2)^2} \\
&\qquad + 2R'_{3a} + 4\gamma_{\vec{k}}R_{2a}\Lambda^2\Big] \\
&\quad - 2u_{\vec{k}z}v_{\vec{k}z}qJ\Big[(2\gamma_{\vec{k}}R_{1z} + 4R_{3z} + 4R_{4z} + 4\gamma_{\vec{k}}R_{2z})\Lambda^2 + 16(R_{2z} + R'_{4z})\frac{\lambda^2}{(1+\lambda^2)^2} \\
&\qquad + 4R_{3a} + 2(2R_{4a} - R'_{4a})\Lambda + 4\gamma_{\vec{k}}R_{2a}\Lambda^2 + 16R_{2a}\frac{\lambda^2}{(1+\lambda^2)^2}\Big], \qquad \text{(D.16)}
\end{aligned}$$

where R's are momentum summations of some combination of Bogoliubov coefficients (see Appendix D.1) and we have introduced a shorthand, $\Lambda = \frac{1-\lambda^2}{1+\lambda^2}$. Next, we list the

cubic vertices entering $\mathcal{H}_3'$:

$$\Phi^a_{31} = (J_3\gamma_{2+3} + J_4\gamma_{1+3} + h_{1a}(\lambda, h^z))(u_{1a}u_{2z}v_{3a} + v_{1a}v_{2z}u_{3a})\,, \tag{D.17}$$

$$\Phi^a_{32} = (J_3\gamma_{3-2} + J_4\gamma_{1+3} + h_{1a}(\lambda, h^z))(u_{1a}v_{2z}v_{3a} + v_{1a}u_{2z}u_{3a})\,, \tag{D.18}$$

$$\begin{aligned}\Phi^a_{33} = {}& (J_3\gamma_{2-3} + J_4\gamma_{1-3} + h_{1a}(\lambda, h^z))(u_{1a}u_{2z}u_{3a} + v_{1a}v_{2z}v_{3a}) \\ & + (J_3\gamma_{1+2} + J_4\gamma_{1-3} + h_{1a}(\lambda, h^z))(v_{1a}u_{2z}v_{3a} + u_{1a}v_{2z}u_{3a})\,,\end{aligned} \tag{D.19}$$

$$\Phi^z_{31} = (2J_4\gamma_{2+3} + h_{1a}(\lambda, h^z))(u_{1z}u_{2z}v_{3z} + v_{1z}v_{2z}u_{3z}),\ , \tag{D.20}$$

$$\begin{aligned}\Phi^z_{32} = {}& (2J_4\gamma_{2-3} + h_{1a}(\lambda, h^z))(u_{1z}u_{2z}u_{3z} + u_{1z}v_{2z}v_{3z} + v_{1z}u_{2z}u_{3z} + v_{1z}v_{2z}v_{3z}) \\ & + (2J_4\gamma_{1+2} + h_{1a}(\lambda, h^z))(v_{1z}u_{2z}v_{3z} + u_{1z}v_{2z}u_{3z})\,.\end{aligned} \tag{D.21}$$

The expressions for the quartic vertices are lengthy and tedious to obtain. Since we do not need all of them, we quote the required ones in the following:

$$\begin{aligned}\Phi^z_{41} = {}& -qJ\Lambda^2\gamma_1(u_{1z}u_{2z}u_{3z}v_{4z} + v_{1z}v_{2z}v_{3z}u_{4z}) \\ & - qJ\left(\gamma_4\Lambda^2 + \frac{4\gamma_{2+4}\lambda^2}{(1+\lambda^2)^2}\right)(u_{1z}u_{2z}v_{3z}v_{4z} + v_{1z}v_{2z}u_{3z}u_{4z}),\end{aligned} \tag{D.22}$$

$$\begin{aligned}\Phi^z_{43} = {}& -qJ\Lambda^2\big[\gamma_1(u_{1z}u_{2z}u_{3z}u_{4z} + u_{1z}u_{2z}v_{3z}v_{4z} + u_{1z}v_{2z}u_{3z}v_{4z} + v_{1z}u_{2z}v_{3z}u_{4z} \\ & \qquad + v_{1z}v_{2z}u_{3z}u_{4z} + v_{1z}v_{2z}v_{3z}v_{4z}) + \gamma_4(v_{1z}u_{2z}u_{3z}v_{4z} + u_{1z}v_{2z}v_{3z}u_{4z})\big] \\ & - \frac{qJ}{(1+\lambda^2)^2}\Big[\left(\gamma_4(1-\lambda^2)^2 + 4\gamma_{2-4}\lambda^2\right)(u_{1z}u_{2z}v_{3z}u_{4z} + v_{1z}v_{2z}u_{3z}v_{4z}) \\ & \qquad + \left(\gamma_3(1-\lambda^2)^2 + 4\gamma_{2+3}\lambda^2\right)(u_{1z}u_{2z}v_{3z}u_{4z} + v_{1z}v_{2z}u_{3z}v_{4z}) \\ & \qquad + \left(\gamma_2(1-\lambda^2)^2 + 4\gamma_{2-4}\lambda^2\right)(u_{1z}v_{2z}v_{3z}v_{4z} + v_{1z}u_{2z}u_{3z}u_{4z}) \\ & \qquad + \left(\gamma_1(1-\lambda^2)^2 + 4\gamma_{1+2}\lambda^2\right)(v_{1z}u_{2z}v_{3z}v_{4z} + u_{1z}v_{2z}u_{3z}u_{4z})\Big],\end{aligned} \tag{D.23}$$

$$\begin{aligned}\Phi^{ab}_{41} = {}& -qJ\gamma_{2+3+4}(u_{1a}u_{2a}u_{3b}v_{4b} + v_{1a}v_{2a}v_{3b}u_{4b}) - \frac{2qJ\lambda^2}{(1+\lambda^2)^2}\gamma_{3+4}u_{1a}v_{2a}v_{3b}u_{4b} \\ & - qJ\Lambda\gamma_{2+3+4}(u_{1a}v_{2a}v_{3b}u_{4b} + v_{1a}u_{2a}u_{3b}v_{4b}) \\ & - \frac{qJ}{2}\gamma_{2+4}(u_{1a}u_{2a}v_{3b}v_{4b} - u_{1a}v_{2a}v_{3b}u_{4b})(1-\delta_{ab}),\end{aligned} \tag{D.24}$$

$$\begin{aligned}\Phi^{ab}_{44} = {}& -qJ\big[\gamma_{2+3-4}(u_{1a}u_{2a}u_{3b}u_{4b} + u_{1a}u_{2a}v_{3b}v_{4b} + v_{1a}v_{2a}u_{3b}u_{4b} + v_{1a}v_{2a}v_{3b}v_{4b}) \\ & + \gamma_{1+2-4}(u_{1a}v_{2a}u_{3b}v_{4b} + v_{1a}u_{2a}v_{3b}u_{4b}) + \gamma_{1+2+3}(u_{1a}v_{2a}u_{3b}v_{4b} + v_{1a}u_{2a}v_{3b}u_{4b})\big] \\ & - qJ\Lambda\big[\gamma_{2+3-4}(u_{1a}v_{2a}u_{3b}u_{4b} + u_{1a}v_{2a}v_{3b}v_{4b} + v_{1a}u_{2a}u_{3b}u_{4b} + v_{1a}u_{2a}v_{3b}v_{4b}) \\ & + \gamma_{1+2-4}(v_{1a}u_{2a}u_{3b}u_{4b} + u_{1a}v_{2a}v_{3b}v_{4b}) + \gamma_{1+2+3}(v_{1a}u_{2a}v_{3b}v_{4b} + u_{1a}v_{2a}u_{3b}u_{4b})\big] \\ & - \frac{2qJ\lambda^2}{(1+\lambda^2)^2}\Big[\gamma_{1+2}(v_{1a}u_{2a}u_{3b}u_{4b} + v_{1a}u_{2a}v_{3b}v_{4b}) + \gamma_{3-4}(u_{1a}v_{2a}u_{3b}u_{4b} + u_{1a}v_{2a}v_{3b}v_{4b})\Big] \\ & - \frac{qJ}{2}(1-\delta_{ab})\Big[\gamma_{2-4}(u_{1a}u_{2a}v_{3b}u_{4b} + v_{1a}v_{2a}u_{3b}v_{4b} - v_{1a}u_{2a}u_{3b}u_{4b} - u_{1a}v_{2a}v_{3b}v_{4b}) \\ & + \gamma_{2+3}(u_{1a}u_{2a}v_{3b}u_{4b} + v_{1a}v_{2a}u_{3b}v_{4b} - u_{1a}v_{2a}u_{3b}u_{4b} - v_{1a}u_{2a}v_{3b}v_{4b})\Big].\end{aligned} \tag{D.25}$$

$$\begin{aligned}\Phi_{41}^{az} = -qJ\Bigg[&\gamma_{2+3+4}(u_{1a}u_{2a}u_{3z}v_{4z} + v_{1a}v_{2a}v_{3z}u_{4z}) + \frac{\gamma_{2+4}}{2}(u_{1a}u_{2a}v_{3z}v_{4z} + v_{1a}v_{2a}u_{3z}u_{4z})\\
&+ \Lambda\gamma_{2+3+4}(u_{1a}v_{2a}v_{3z}u_{4z} + v_{1a}u_{2a}u_{3z}v_{4z}) - \Lambda\frac{\gamma_{2+4}}{2}(u_{1a}v_{2a}v_{3z}u_{4z} + v_{1a}u_{2a}u_{3z}v_{4z})\\
&+ \Lambda^2(\gamma_3 u_{1a}v_{2a}u_{3z}u_{4z} + \gamma_3 v_{1a}u_{2a}v_{3z}v_{4z} + \gamma_4 v_{1a}u_{2a}u_{3z}v_{4z} + \gamma_4 u_{1a}v_{2a}v_{3z}u_{4z})\\
&+ \frac{4\lambda^2\gamma_{1+2}}{(1+\lambda^2)^2}(v_{1a}u_{2a}v_{3z}u_{4z} + u_{1a}v_{2a}u_{3z}v_{4z})\Bigg],\end{aligned} \tag{D.26}$$

$$\begin{aligned}\Phi_{45}^{az} = -qJ\Bigg[&\Lambda\gamma_{2+3-4}(u_{1a}v_{2a}u_{3z}u_{4z} + u_{1a}v_{2a}v_{3z}v_{4z} + v_{1a}u_{2a}u_{3z}u_{4z} + v_{1a}u_{2a}v_{3z}v_{4z})\\
&+ \gamma_{2+3-4}(u_{1a}u_{2a}u_{3z}u_{4z} + u_{1a}u_{2a}v_{3z}v_{4z} + v_{1a}v_{2a}u_{3z}u_{4z} + v_{1a}v_{2a}v_{3z}v_{4z})\\
&+ \frac{\gamma_{2-4}}{2}(u_{1a}u_{2a}v_{3z}u_{4z} + v_{1a}v_{2a}u_{3z}v_{4z}) + \frac{\gamma_{2+3}}{2}(u_{1a}u_{2a}v_{3z}u_{4z} + v_{1a}v_{2a}u_{3z}v_{4z})\\
&- \frac{\Lambda}{2}(\gamma_{2+3}u_{1a}v_{2a}u_{3z}u_{4z} + \gamma_{2+3}v_{1a}u_{2a}v_{3z}v_{4z} + \gamma_{2-4}u_{1a}v_{2a}v_{3z}v_{4z} + \gamma_{2-4}v_{1a}u_{2a}u_{3z}u_{4z})\\
&+ \Lambda^2(\gamma_3 u_{1a}v_{2a}u_{3z}v_{4z} + \gamma_3 v_{1a}u_{2a}v_{3z}u_{4z} + \gamma_3 v_{1a}u_{2a}v_{3z}v_{4z} + \gamma_3 u_{1a}v_{2a}u_{3z}u_{4z}\\
&\quad + \gamma_4 u_{1a}v_{2a}u_{3z}v_{4z} + \gamma_4 v_{1a}u_{2a}v_{3z}u_{4z} + \gamma_4 v_{1a}u_{2a}u_{3z}u_{4z} + \gamma_4 u_{1a}v_{2a}v_{3z}v_{4z})\\
&+ \frac{4\lambda^2}{(1+\lambda^2)^2}\gamma_{1+2}(v_{1a}u_{2a}u_{3z}u_{4z} + v_{1a}u_{2a}v_{3z}v_{4z} + u_{1a}v_{2a}u_{3z}u_{4z} + u_{1a}v_{2a}v_{3z}v_{4z})\Bigg],\end{aligned} \tag{D.27}$$

$$\begin{aligned}\Phi_{46}^{az} = -qJ\Bigg[&\Lambda(\gamma_{1+2-4}v_{1z}u_{2z}u_{3a}u_{4a} + \gamma_{1+2-4}u_{1z}v_{2z}v_{3a}v_{4a}\\
&\quad + \gamma_{1+2+3}v_{1z}u_{2z}v_{3a}v_{4a} + \gamma_{1+2+3}u_{1z}v_{2z}u_{3a}u_{4a})\\
&+ (\gamma_{1+2-4}u_{1z}v_{2z}u_{3a}v_{4a} + \gamma_{1+2-4}v_{1z}u_{2z}v_{3a}u_{4a}\\
&\quad + \gamma_{1+2+3}u_{1z}v_{2z}u_{3a}v_{4a} + \gamma_{1+2+3}v_{1z}u_{2z}v_{3a}u_{4a})\\
&+ \frac{\gamma_{2-4}}{2}(v_{1z}v_{2z}u_{3a}v_{4a} + u_{1z}u_{2z}v_{3a}u_{4a}) + \frac{\gamma_{2+3}}{2}(v_{1z}v_{2z}u_{3a}v_{4a} + u_{1z}u_{2z}v_{3a}u_{4a})\\
&- \frac{\Lambda}{2}(\gamma_{2+3}v_{1z}u_{2z}v_{3a}v_{4a} + \gamma_{2+3}u_{1z}v_{2z}u_{3a}u_{4a} + \gamma_{2-4}v_{1z}u_{2z}u_{3a}u_{4a} + \gamma_{2-4}u_{1z}v_{2z}v_{3a}v_{4a})\\
&+ \Lambda^2(\gamma_1 u_{1z}u_{2z}u_{3a}u_{4a} + \gamma_1 u_{1z}u_{2z}v_{3a}v_{4a} + \gamma_1 v_{1z}v_{2z}u_{3a}u_{4a} + \gamma_1 v_{1z}v_{2z}v_{3a}v_{4a}\\
&\quad + \gamma_2 u_{1z}v_{2z}u_{3a}u_{4a} + \gamma_2 u_{1z}v_{2z}v_{3a}v_{4a} + \gamma_2 v_{1z}u_{2z}u_{3a}u_{4a} + \gamma_2 v_{1z}u_{2z}v_{3a}v_{4a})\\
&+ \frac{4\lambda^2}{(1+\lambda^2)^2}\gamma_{3-4}(u_{1z}v_{2z}u_{3a}u_{4a} + u_{1z}v_{2z}v_{3a}v_{4a} + v_{1z}u_{2z}u_{3a}u_{4a} + v_{1z}u_{2z}v_{3a}v_{4a})\Bigg].\end{aligned} \tag{D.28}$$

D.3 Self-energies

In this appendix we present the expressions of the normal self-energies of the $\tilde{\tau}$ particles, needed for determining the mode dispersion to order $1/d$.

The self-energy diagrams involved in the calculation of the transverse modes are shown in fig. D.1. Notice that they are similar to those used in chapter 4 for calculating the triplon dispersion. In this case we have to explicitly distinguish between the transverse mode propagators and the amplitude mode propagator. Evaluation of the frequency integral is straightforward and the enumeration is on the same lines as discussed in chapter 4. After momentum integration we find to order $1/d$:

$$\Sigma^{D.1(a)}(\vec{k},\tilde{\omega}) = A^{(1)}_{\vec{k}a}(u^2_{\vec{k}a}+v^2_{\vec{k}a}) + 2B^{(1)}_{\vec{k}a}u_{\vec{k}a}v_{\vec{k}a} + C_{\vec{k}a}\,, \tag{D.29}$$

$$\begin{aligned}\Sigma^{D.1(b)}(\vec{k},\tilde{\omega}) = \frac{1}{\tilde{\omega}-J_1-J_2}\Bigg[u^2_{\vec{k}a}\Bigg(&\frac{J_3^2+J_4^2-2J_3J_4\gamma_{\vec{k}}}{2d} + 2J_3^2\gamma_{\vec{k}}R'_{3z}(\vec{k}-\vec{Q}) \\ &- 2J_3J_4\gamma_{\vec{k}}R'_{3z}(\vec{Q}) + J_3^2\gamma^2_{\vec{k}}R_{2z}\Bigg) + v^2_{\vec{k}a}J_3^2\gamma^2_{\vec{k}}R_{2a} \\ &+ 2u_{\vec{k}a}v_{\vec{k}a}\Bigg(J_3^2\gamma_{\vec{k}}R_{3a} - 2J_3J_4\gamma_{\vec{k}}R'_{3a}(\vec{k}) + J_3^2\gamma^2_{\vec{k}}R'_{az}(\vec{k}-\vec{Q})\Bigg)\Bigg],\end{aligned} \tag{D.30}$$

$$\begin{aligned}\Sigma^{D.1(c)}(\vec{k},\tilde{\omega}) = -\frac{1}{\tilde{\omega}+J_1+J_2}\Bigg[v^2_{\vec{k}a}\Bigg(&\frac{J_3^2+J_4^2-2J_3J_4\gamma_{\vec{k}}}{2d} + 2J_3^2\gamma_{\vec{k}}R'_{3z}(\vec{k}-\vec{Q}) \\ &- 2J_3J_4\gamma_{\vec{k}}R'_{3z}(\vec{Q}) + J_3^2\gamma^2_{\vec{k}}R_{2z}\Bigg) + u^2_{\vec{k}a}J_3^2\gamma^2_{\vec{k}}R_{2a} \\ &+ 2u_{\vec{k}a}v_{\vec{k}a}\Bigg(J_3^2\gamma_{\vec{k}}R_{3a} - 2J_3J_4\gamma_{\vec{k}}R'_{3a}(\vec{k}) + J_3^2\gamma^2_{\vec{k}}R'_{az}(\vec{k}-\vec{Q})\Bigg)\Bigg],\end{aligned} \tag{D.31}$$

$$\Sigma^{D.1(d)}(\vec{k},\tilde{\omega}) = \Sigma^{D.1(e)}(\vec{k},\tilde{\omega}) = -\frac{\gamma_{\vec{k}}qJ^2R_{3a}}{2J_1}\left[u^2_{\vec{k}a}+v^2_{\vec{k}a}+2u_{\vec{k}a}v_{\vec{k}a}\Lambda_0\right], \tag{D.32}$$

$$\begin{aligned}\Sigma^{D.1(f)}(\vec{k},\tilde{\omega}) = \frac{q^2J^2}{\tilde{\omega}-J_1-2J_2}\Bigg[u^2_{\vec{k}a}\Bigg(&\frac{\Lambda_0^4}{2d} + \gamma^2_{\vec{k}}R_{2z}\Lambda_0^2 + 2\gamma_{\vec{k}}R_{3z}\Lambda_0^3\Bigg) + v^2_{\vec{k}a}\gamma^2_{\vec{k}}R_{2z} \\ &+ 2u_{\vec{k}a}v_{\vec{k}a}\Bigg(\gamma^2_{\vec{k}}R_{2z}\Lambda_0 + \gamma_{\vec{k}}R_{3z}\Lambda_0^2\Bigg)\Bigg],\end{aligned} \tag{D.33}$$

$$\begin{aligned}\Sigma^{D.1(g)}(\vec{k},\tilde{\omega}) = -\frac{q^2J^2}{\tilde{\omega}+J_1+2J_2}\Bigg[v^2_{\vec{k}a}\Bigg(&\frac{\Lambda_0^4}{2d} + \gamma^2_{\vec{k}}R_{2z}\Lambda_0^2 + 2\gamma_{\vec{k}}R_{3z}\Lambda_0^3\Bigg) + u^2_{\vec{k}a}\gamma^2_{\vec{k}}R_{2z} \\ &+ 2u_{\vec{k}a}v_{\vec{k}a}\Bigg(\gamma^2_{\vec{k}}R_{2z}\Lambda_0 + \gamma_{\vec{k}}R_{3z}\Lambda_0^2\Bigg)\Bigg],\end{aligned} \tag{D.34}$$

$$\begin{aligned}\Sigma^{D.1(h)}(\vec{k},\tilde{\omega}) = \frac{q^2J^2}{\tilde{\omega}-3J_1}\Bigg[u^2_{\vec{k}a}\Bigg(&3\gamma^2_{\vec{k}}R_{2a}\Lambda_0^2 + 6\gamma_{\vec{k}}R_{3a}\Lambda_0 + \frac{3}{2d}\Bigg) + 3v^2_{\vec{k}a}\gamma^2_{\vec{k}}R_{2a} \\ &+ 2u_{\vec{k}a}v_{\vec{k}a}\Bigg(3\gamma^2_{\vec{k}}R_{2a}\Lambda_0 + 3\gamma_{\vec{k}}R_{3a}\Bigg)\Bigg],\end{aligned} \tag{D.35}$$

$$\begin{aligned}\Sigma^{D.1(i)}(\vec{k},\tilde{\omega}) = -\frac{q^2J^2}{\tilde{\omega}+3J_1}\Bigg[v^2_{\vec{k}a}\Bigg(&3\gamma^2_{\vec{k}}R_{2a}\Lambda_0^2 + 6\gamma_{\vec{k}}R_{3a}\Lambda_0 + \frac{3}{2d}\Bigg) + 3u^2_{\vec{k}a}\gamma^2_{\vec{k}}R_{2a} \\ &+ 2u_{\vec{k}a}v_{\vec{k}a}\Bigg(3\gamma^2_{\vec{k}}R_{2a}\Lambda_0 + 3\gamma_{\vec{k}}R_{3a}\Bigg)\Bigg],\end{aligned} \tag{D.36}$$

with abbreviations $\Lambda_0 = \frac{1-\lambda_0^2}{1+\lambda_0^2}$, J_1 and J_2 from eq. (5.32) and J_3 and J_4 from eq. (5.45). To order $1/d$, it is sufficient to evaluate the above self-energy (and thus J_3 and J_4) at $\lambda = \lambda_0$. The only exception is the first two terms of $\Sigma^{D.1(a)}$. These arise from $\mathcal{H}'_{2b}$ which requires the $1/d$ expansion of λ.

Similarly, we can deal with the amplitude mode. The corresponding Feynman diagrams are shown in fig. D.2. After frequency and momentum integration we are left with the expressions:

$$\Sigma^{D.2(a)}(\vec{k},\tilde{\omega}) = A_{1\vec{k}z}(u_{\vec{k}z}^2 + v_{\vec{k}z}^2) + 2B_{1\vec{k}z}u_{\vec{k}z}v_{\vec{k}z} + C_{\vec{k}z}, \tag{D.37}$$

$$\Sigma^{D.2(b)}(\vec{k},\tilde{\omega}) = \frac{4J_4^2}{\tilde{\omega}-2J_2}\Bigg[R_{2z}\gamma_{\vec{k}}^2(1-\gamma_{\vec{k}})(u_{\vec{k}z}+v_{\vec{k}z})^2 + \frac{u_{\vec{k}z}^2}{2d}(1-\gamma_{\vec{k}}) + 2R_{3z}\gamma_{\vec{k}}(u_{\vec{k}z}^2 + u_{\vec{k}z}v_{\vec{k}z}) - 2\gamma_{\vec{k}}R'_{3z}(\vec{k})(u_{\vec{k}z}^2 + u_{\vec{k}z}v_{\vec{k}z})\Bigg], \tag{D.38}$$

$$\Sigma^{D.2(c)}(\vec{k},\tilde{\omega}) = -\frac{4J_4^2}{\tilde{\omega}+2J_2}\Bigg[R_{2z}\gamma_{\vec{k}}^2(1-\gamma_{\vec{k}})(u_{\vec{k}z}+v_{\vec{k}z})^2 + \frac{v_{\vec{k}z}^2}{2d}(1-\gamma_{\vec{k}}) + 2R_{3z}\gamma_{\vec{k}}(v_{\vec{k}z}^2 + u_{\vec{k}z}v_{\vec{k}z}) - 2\gamma_{\vec{k}}R'_{3z}(\vec{k})(v_{\vec{k}z}^2 + u_{\vec{k}z}v_{\vec{k}z})\Bigg], \tag{D.39}$$

$$\Sigma^{D.2(d)}(\vec{k},\tilde{\omega}) = \frac{2J_4^2\gamma_{\vec{k}}^2}{\tilde{\omega}-2J_1}(1-\gamma_{\vec{k}})(u_{\vec{k}z}+v_{\vec{k}z})^2R_{2a}, \tag{D.40}$$

$$\Sigma^{D.2(e)}(\vec{k},\tilde{\omega}) = -\frac{2J_4^2\gamma_{\vec{k}}^2}{\tilde{\omega}+2J_1}(1-\gamma_{\vec{k}})(u_{\vec{k}z}+v_{\vec{k}z})^2R_{2a}, \tag{D.41}$$

$$\Sigma^{D.2(f)}(\vec{k},\tilde{\omega}) = \Sigma^{D.2(g)}(\vec{k},\tilde{\omega}) = -\frac{q^2J^2}{J_2}\Lambda_0^4\gamma_{\vec{k}}R_{3z}(u_{\vec{k}z}+v_{\vec{k}z})^2, \tag{D.42}$$

$$\Sigma^{D.2(h)}(\vec{k},\tilde{\omega}) = \frac{2q^2J^2}{\tilde{\omega}-J_2-2J_1}\left[\frac{u_{\vec{k}z}^2}{2d} + 2\gamma_{\vec{k}}R_{3a}\Lambda_0^2(u_{\vec{k}z}^2+u_{\vec{k}z}v_{\vec{k}z}) + \gamma_{\vec{k}}^2R_{2a}\Lambda_0^4(u_{\vec{k}z}+v_{\vec{k}z})^2\right], \tag{D.43}$$

$$\Sigma^{D.2(i)}(\vec{k},\tilde{\omega}) = -\frac{2q^2J^2}{\tilde{\omega}+J_2+2J_1}\left[\frac{v_{\vec{k}z}^2}{2d} + 2\gamma_{\vec{k}}R_{3a}\Lambda_0^2(v_{\vec{k}z}^2+u_{\vec{k}z}v_{\vec{k}z}) + \gamma_{\vec{k}}^2R_{2a}\Lambda_0^4(u_{\vec{k}z}+v_{\vec{k}z})^2\right], \tag{D.44}$$

$$\Sigma^{D.2(j)}(\vec{k},\tilde{\omega}) = \frac{2q^2J^2}{\tilde{\omega}-3J_2}\Lambda_0^4\left[\gamma_{\vec{k}}^2R_{2z}(u_{\vec{k}z}+v_{\vec{k}z})^2 + \frac{u_{\vec{k}z}^2}{2d} + 2\gamma_{\vec{k}}R_{3z}(u_{\vec{k}z}^2+u_{\vec{k}z}v_{\vec{k}z})\right], \tag{D.45}$$

$$\Sigma^{D.2(k)}(\vec{k},\tilde{\omega}) = -\frac{2q^2J^2}{\tilde{\omega}+3J_2}\Lambda_0^4\left[\gamma_{\vec{k}}^2R_{2z}(u_{\vec{k}z}+v_{\vec{k}z})^2 + \frac{v_{\vec{k}z}^2}{2d} + 2\gamma_{\vec{k}}R_{3z}(v_{\vec{k}z}^2+u_{\vec{k}z}v_{\vec{k}z})\right]. \tag{D.46}$$

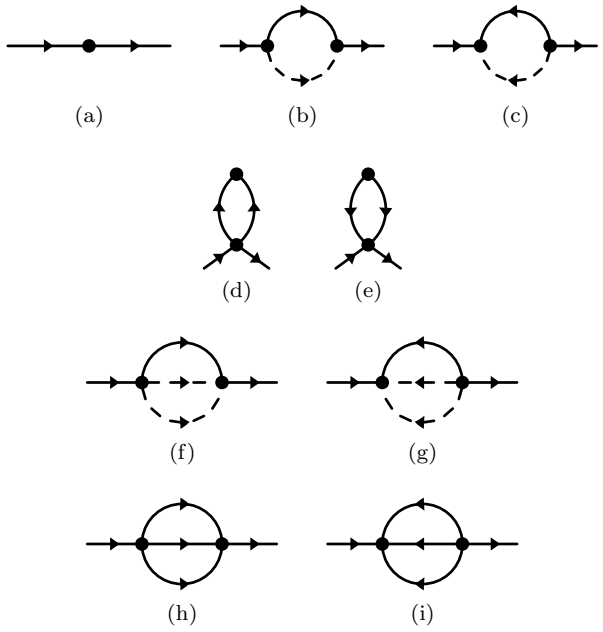

Figure D.1: Normal self-energy diagrams contributing to the order $1/d$ calculation of transverse mode dispersion. Solid (dashed) lines correspond to $\tilde{\tau}_{xy}$ ($\tilde{\tau}_z$) propagators. The bilinear vertex stands for $\mathcal{H}'_{2b} + \mathcal{H}'_{2c}$, while the cubic (quartic) vertices represents $\mathcal{H}'_3$ ($\mathcal{H}'_4$). This figure is taken from ref. [70].

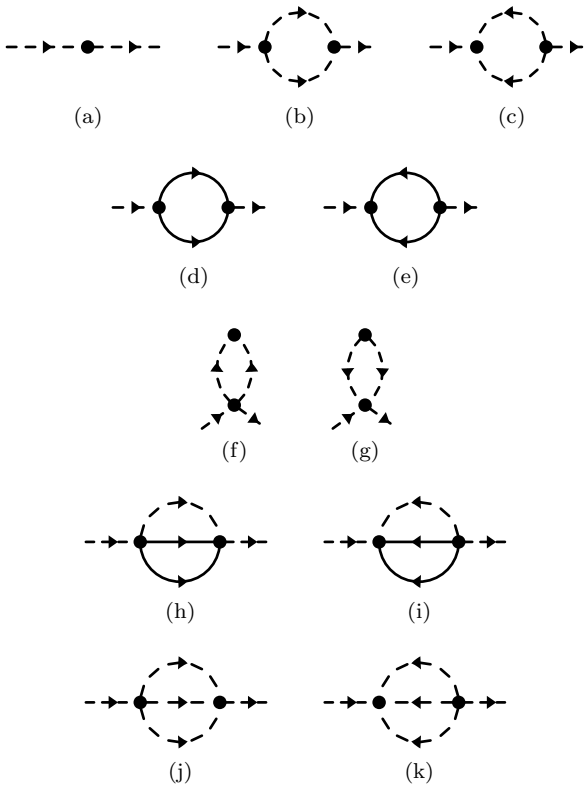

Figure D.2: Feynman diagrams corresponding to the normal self-energy contributs to the longitudinal mode dispersion up to order $1/d$. The notation is same as in Fig. D.1. This figure is taken from ref. [70].

Bibliography

[1] P. W. Anderson, "More is different," *Science*, vol. 177, no. 4047, 1972.

[2] L. Balents, "Spin liquids in frustrated magnets," *Nature*, vol. 464, pp. 199–208, 2010.

[3] C. Castelnovo, R. Moessner, and S. L. Sondhi, "Magnetic monopoles in spin ice," *Nature*, vol. 451, pp. 42–45, 2008.

[4] K. G. Wilson, "The renormalization group: Critical phenomena and the Kondo problem," *Rev. Mod. Phys.*, vol. 47, no. 773, 1975.

[5] N. Goldenfeld, *Lectures on Phase Transitions and the Renormalization Group*. Addison-Wesley Publishing Company, 1992.

[6] S. Sachdev, *Quantum Phase Transitions*. Cambridge University Press, Cambridge, UK, 2nd ed., 2011.

[7] A. Altland and B. Simons, *Condensed matter field theory*. Cambridge University Press, Cambridge, UK, 2010.

[8] M. Vojta, "Quantum phase transitions," *Rep. Prog. Phys.*, vol. 66, pp. 2069–2110, 2003.

[9] M. Vojta, "Thermal and quantum phase transitions." Lectures given at the Les Houches Doctoral Training School in Statistical Physics, 2015.

[10] N. D. Mermin and H. Wagner, "Absence of ferromagnetism or antiferromagnetism in one- or two-dimensional isotropic Heisenberg models," *Phys. Rev. Lett.*, vol. 17, no. 1133, 1966.

[11] H. von Löhneysen, A. Rosch, M. Vojta, and P. Wölfle, "Fermi-liquid instabilities at magnetic quantum phase transitions," *Rev. Mod. Phys.*, vol. 79, no. 1015, 2007.

[12] P. Merchant, B. Normand, K. W. Krämer, M. Boehm, D. F. McMorrow, and C. Rüegg, "Quantum and classical criticality in a dimerized quantum antiferromagnet," *Nature Physics*, vol. 10, pp. 373–379, 2014.

[13] B. Bruognolo, A. Weichselbaum, C. Guo, J. von Delft, I. Schneider, and M. Vojta, "Two-bath spin-boson model: Phase diagram and critical properties," *Phys. Rev. B*, vol. 90, no. 245130, 2014.

[14] J. Goldstone, A. Salam, and S. Weinberg, "Broken symmetries," *Phys. Rev.*, vol. 127, no. 965, 1962.

[15] T. Brauner, "Spontaneous symmetry breaking and nambu-goldstone bosons in quantum many-body systems," *Symmetry*, vol. 2, pp. 609–657, 2010.

[16] D. Pekker and C. M. Varma, "Amplitude/higgs modes in condensed matter physics," *Annu. Rev. Condens. Matter Phys.*, vol. 6, pp. 269–297, 2015.

[17] M. Greiter, "Is electromagnetic gauge invariance spontaneously violated in superconductors?," *Annals of Physics*, vol. 319, pp. 217–249, 2005.

[18] P. W. Anderson, "Plasmons, gauge invariance, and mass," *Phys. Rev.*, vol. 130, no. 439, 1963.

[19] Z. Nussinov and J. van den Brink, "Compass models: Theory and physical motivations," *Rev. Mod. Phys.*, vol. 87, no. 1, 2015.

[20] A. Kitaev, "Anyons in an exactly solved model and beyond," *Annals of Physics*, vol. 321, pp. 2–111, 2006.

[21] J. Chaloupka, G. Jackeli, and G. Khaliullin, "Kitaev-Heisenberg model on a honeycomb lattice: Possible exotic phases in Iridium Oxides A_2IrO_3," *Phys. Rev. Lett.*, vol. 105, no. 027204, 2010.

[22] J. Knolle, D. L. Kovrizhin, J. T. Chalker, and R. Moessner, "Dynamics of a two-dimensional quantum spin liquid: Signatures of emergent Majorana fermions and fluxes," *Phys. Rev. Lett.*, vol. 112, no. 207203, 2014.

[23] J. Knolle, G.-W. Chern, D. L. Kovrizhin, R. Moessner, and N. B. Perkins, "Raman scattering signatures of Kitaev spin liquids in A_2IrO_3," *Phys. Rev. Lett.*, vol. 113, no. 187201, 2014.

[24] Y. Singh, Y. Tokiwa, J. Dong, and P. Gegenwart, "Spin liquid close to a quantum critical point in $Na_4Ir_3O_8$," *Phys. Rev. B*, vol. 88, no. 220413 (R), 2013.

[25] S. H. Chun *et al.*, "Direct evidence for dominant bond-directional interactions in a honeycomb lattice Iridate Na_2IrO_3," *Nature Physics*, vol. 11, pp. 462–466, 2015.

[26] I. Rousochatzakis, J. Reuther, R. Thomale, S. Rachel, and N. B. Perkins, "Phase diagram and quantum order by disorder in the Kitaev $K_1 - K_2$ honeycomb magnet." arXiv:1506.09185, 2015.

[27] S. Rachel, L. Fritz, and M. Vojta, "Landau levels of Majorana fermions in a spin liquid." arXiv:1509.01246.

[28] C. Rüegg *et al.*, "Quantum magnets under pressure: Controlling elementary excitations in $TlCuCl_3$," *Phys. Rev. Lett.*, vol. 100, no. 205701, 2008.

[29] C. Rüegg *et al.*, "Pressure-induced quantum phase transition in the spin-liquid $TlCuCl_3$," *Phys. Rev. Lett.*, vol. 93, no. 257201, 2004.

[30] T. Giamarchi, C. Rüegg, and O. Tchernyshyov, "Bose-Einstein condensation in magnetic insulators," *Nature Physics*, vol. 4, pp. 198–204, 2008.

[31] S. Mühlbauer *et al.*, "Skyrmion lattice in a chiral magnet," *Science*, vol. 323, no. 5916, 2009.

[32] T. Senthil, A. Vishwanath, L. Balents, S. Sachdev, and M. P. A. Fisher, "Deconfined quantum critical points," *Science*, vol. 303, no. 5663, 2004.

[33] G. D. Mahan, *Many-particle physics*. New York: Kluwer Academic Plenum Publications, 3rd ed., 2000.

[34] S. Chakravarty, B. I. Halperin, , and D. R. Nelson, "Low-temperature behavior of two-dimensional quantum antiferromagnets," *Phys. Rev. Lett.*, vol. 60, no. 1057, 1988.

[35] T. Siegrist *et al.*, "Crystal structure of the high-t_c superconductor $Ba_2YCu_3O_{9-\delta}$," *Phys. Rev. B*, vol. 35, pp. 7137–7139, 1989.

[36] J. M. Tranquada *et al.*, "Neutron scattering study of magnetic excitations in $YBa_2Cu_3O_{6+x}$," *Phys. Rev. B*, vol. 40, pp. 4503–4516, 1989.

[37] J. Otimaa, R. R. P. Singh, and Z. Weihong, "Quantum spin ladders at $T = 0$ and at high temperatures studied by series expansions," *Phys. Rev. B*, vol. 54, pp. 1009–1018, 1996.

[38] Y. Sassago *et al.*, "Temperature-dependent spin gap and singlet ground state in $BaCuSi_2O_6$," *Phys. Rev. B*, vol. 55, no. 8357, 1997.

[39] J. Otsuki and Y. Kuramoto, "Dynamical mean-field theory for quantum spin systems: Test of solutions for magnetically ordered states," *Phys. Rev. B*, vol. 88, no. 024427, 2013.

[40] S. Sachdev and R. N. Bhatt, "Bond-operator representation of quantum spins: Mean-field theory of frustrated quantum Heisenberg antiferromagnets," *Phys. Rev. B*, vol. 41, no. 9323, 1990.

[41] V. N. Kotov, O. Sushkov, Z. Weihong, and J. Oitmaa, "Novel approach to description of spin-liquid phases in low-dimensional quantum antiferromagnets," *Phys. Rev. Lett.*, vol. 80, no. 5790, 1998.

[42] A. Collins, C. J. Hamer, and Z. Weihong, "Modified triplet-wave expansion method applied to the alternating Heisenberg chain," *Phys. Rev. B*, vol. 74, no. 144414, 2006.

[43] T. Sommer, M. Vojta, and K. W. Becker, "Magnetic properties and spin waves of bilayer magnets in a uniform field," *Eur. Phys. J. B*, vol. 23, no. 329, 2001.

[44] R. Ganesh, S. V. Isakov, and A. Paramekanti, "Néel to dimer transition in spin-S antiferromagnets: Comparing bond operator theory with quantum Monte Carlo simulations for bilayer Heisenberg models," *Phys. Rev. B*, vol. 84, no. 214412, 2011.

[45] V. N. Kotov, J. Otimaa, O. P. Sushkov, and Z. Weihong, "Low-energy singlet and triplet excitations in the spin-liquid phase of the two-dimensional J_1-J_2 model," *Phys. Rev. B*, vol. 60, no. 14613, 1999.

[46] M. Vojta unpublished.

[47] N. W. Ashcroft and N. D. Mermin, *Solid state physics*. Brooks Cole, 1st ed., 1976.

[48] K. Yosida, *Theory of Magnetism*. Springer, 2nd ed., 1998.

[49] A. V. Chubukov and D. K. Morr, "Phase transition, longitudinal spin fluctuations, and scaling in a two-layer antiferromagnet," *Phys. Rev. B*, vol. 52, pp. 3521–3532, 1995.

[50] Z. Weihong, "Various series expansions for the bilayer $S =$ Heisenberg antiferromagnet," *Phys. Rev. B*, vol. 55, no. 12267, 1997.

[51] C. J. Hamer, J. Oitmaa, , and Z. Weihong, "Restoration of symmetry in the spectrum of the bilayer Heisenberg antiferromagnet," *Phys. Rev. B*, vol. 85, no. 014432, 2012.

[52] J. Otimaa, C. J. Hamer, and Z. Weihong, *Series expansion methods for strongly interacting lattice models*. Cambridge University Press, Cambridge, UK, 2006.

[53] W. Metzner and D. Vollhardt, "Correlated lattice Fermions in $d = \infty$ dimensions," *Phys. Rev. Lett.*, vol. 62, no. 324, 1989.

[54] A. Georges, G. Kotliar, W. Krauth, and M. J. Rozenberg, "Dynamical mean-field theory of strongly correlated Fermion systems and the limit of infinite dimensions," *Rev. Mod. Phys.*, vol. 68, no. 13, 1996.

[55] D. G. Joshi, K. Coester, K. P. Schmidt, and M. Vojta, "Nonlinear bond-operator theory and $1/d$ expansion for coupled-dimer magnets. I. Paramagnetic phase," *Phys. Rev. B*, vol. 91, no. 094404, 2015.

[56] A. Kolezhuk and S. Sachdev, "Magnon decay in gapped quantum spin systems," *Phys. Rev. Lett.*, vol. 96, no. 087203, 2006.

[57] M. E. Zhitomirsky, "Decay of quasiparticles in quantum spin liquids," *Phys. Rev. B*, vol. 73, no. 100404(R), 2006.

[58] S. Wessel and I. Milat, "Quantum fluctuations and excitations in antiferromagnetic quasicrystals," *Phys. Rev. B*, vol. 71, no. 104427, 2005.

[59] E. R. Mucciolo, A. H. C. Neto, and C. Chamon, "Excitations and quantum fluctuations in site-diluted two-dimensional antiferromagnets," *Phys. Rev. B*, vol. 69, no. 214424, 2004.

[60] M. Vojta, "Excitation spectra of disordered dimer magnets near quantum criticality," *Phys. Rev. Lett.*, vol. 111, no. 097202, 2013.

[61] A. Collins and C. J. Hamer, "Two-particle bound states and one-particle structure factor in a Heisenberg bilayer system," *Phys. Rev. B*, vol. 78, no. 054419, 2008.

[62] L. Wang, K. S. D. Beach, and A. W. Sandvik, "High-precision finite-size scaling analysis of the quantum-critical point of $S = 1/2$ Heisenberg antiferromagnetic bilayers," *Phys. Rev. B*, vol. 73, no. 014431, 2006.

[63] Y. Q. Qin, B. Normand, A. W. Sandvik, and Z. Y. Meng, "Multiplicative logarithmic corrections to quantum criticality in three-dimensional dimerized antiferromagnets." arXiv:1506.06073.

[64] C. Knetter and G. S. Uhrig, "Perturbation theory by flow equations: dimerized and frustrated $S = 1/2$ chain," *Eur. Phys. J. B*, vol. 13, no. 209, 2000.

[65] C. Knetter, K. P. Schmidt, and G. S. Uhrig, "The structure of operators in effective particle-conserving models," *J. Phys. A: Math. Gen.*, vol. 36, no. 7889, 2003.

[66] K. Coester, D. G. Joshi, M. Vojta, and K. P. Schmidt unpublished.

[67] V. N. Kotov, O. P. Sushkov, and R. Eder, "Excitation spectrum of the $S = 1/2$ quantum spin ladder with frustration: Elementary quasiparticles and many-particle bound states," *Phys. Rev. B*, vol. 59, no. 6266, 1999.

[68] S. Wenzel, L. Bogacz, and W. Janke, "Evidence for an unconventional universality class from a two-dimensional dimerized quantum Heisenberg model," *Phys. Rev. Lett.*, vol. 101, no. 127202, 2008.

[69] L. Fritz, R. L. Doretto, S. Wessel, S. Wenzel, S. Burdin, , and M. Vojta, "Cubic interactions and quantum criticality in dimerized antiferromagnets," *Phys. Rev. B*, vol. 83, no. 174416, 2011.

[70] D. G. Joshi and M. Vojta, "Nonlinear bond-operator theory and $1/d$ expansion for coupled-dimer magnets. II. Antiferromagnetic phase and quantum phase transition," *Phys. Rev. B*, vol. 91, no. 094405, 2015.

[71] K. Hida, "Quantum disordered state without frustration in the double layer Heisenberg antiferromagnet – Dimer expansion and projector Monte Carlo study," *J. Phys. Soc. Jpn.*, vol. 61, no. 1013, 1992.

[72] T. Coletta, N. Laflorencie, and F. Mila, "Semiclassical approach to ground-state properties of hard-core bosons in two dimensions," *Phys. Rev. B*, vol. 85, no. 104421, 2012.

[73] D. Podolsky, A. Auerbach, and D. P. Arovas, "Visibility of the amplitude (Higgs) mode in condensed matter," *Phys. Rev. B*, vol. 84, no. 174522, 2011.

[74] S. Sachdev, "Exotic phases and quantum phase transitions: model systems and experiments." preprint arXiv:0901.4103.

[75] J. Holstein and N. Primakoff, "Field dependence of the intrinsic domain magnetization of a ferromagnet," *Phys. Rev.*, vol. 58, no. 1098, 1940.

[76] C. J. Hamer, Z. Weihong, and P. Arndt, "Third-order spin-wave theory for the Heisenberg antiferromagnet," *Phys. Rev. B*, vol. 46, no. 6276, 1992.

[77] M. Lohöfer, T. Coletta, D. G. Joshi, F. F. Assaad, M. Vojta, S. Wessel, and F. Mila, "Dynamical structure factors and excitation modes of the bilayer Heisenberg model." arXiv:1508.07816.

[78] S. Gazit, D. Podolsky, and A. Auerbach, "Fate of the Higgs mode near quantum criticality," *Phys. Rev. Lett.*, vol. 110, no. 140401, 2013.

[79] S. A. Weidinger and W. Zwerger, "Higgs mode and magnon interactions in $2d$ quantum antiferromagnets from Raman scattering," *Eur. Phys. J. B*, vol. 88, no. 237, 2015.

[80] D. Podolsky and S. Sachdev, "Spectral functions of the Higgs mode near two-dimensional quantum critical points," *Phys. Rev. B*, vol. 86, no. 054508, 2012.

[81] E. Ising, "Contributions to the theory of ferromagnetism," 1924.

[82] L. Onsager, "Crystal statistics. I. A two-dimensional model with an order-disorder transition," *Phys. Rev.*, vol. 65, pp. 117–149, 1944.

[83] D. Bitko, T. F. Rosenbaum, and G. Aeppli, "Quantum critical behavior for a model magnet," *Phys. Rev. Lett.*, vol. 77, no. 940, 1996.

[84] R. Coldea *et al.*, "Quantum criticality in an Ising chain: Experimental evidence for emergent E_8 symmetry," *Science*, vol. 327, pp. 177–180, 2010.

[85] Z. Weihong, J. Otimaa, and C. J. Hamer, "Series expansions for the $3d$ transverse Ising model at $T = 0$," *J. Phys. A: Math. Gen.*, vol. 27, no. 5425, 1994.

[86] M. Polini, F. Guinea, M. Lewenstein, H. C. Manoharan, and V. Pellegrini, "Artificial graphene as a tunable Dirac material," *Nature Nanotech.*, vol. 8, pp. 625–633, 2013.

[87] F. L. Pedrocchi, S. Chesi, and D. Loss, "Physical solutions of the Kitaev honeycomb model," *Phys. Rev. B*, vol. 84, no. 165414, 2011.

[88] F. Zschocke and M. Vojta, "Physical states and finite-size effects in Kitaev's honeycomb model: Bond disorder, spin excitations, and NMR lineshape," *Phys. Rev. B*, vol. 92, no. 014403, 2015.

[89] H.-D. Chen and Z. Nussinov, "Exact results of the Kitaev model on a hexagonal lattice: spin states, string and brane correlators, and anyonic excitations," *J. Phys. A: Math. Theor.*, vol. 41, no. 075001, 2008.

[90] S. Miyahara and K. Ueda, "Exact dimer ground state of the two dimensional Heisenberg spin system $SrCu_2(BO_3)_2$," *Phys. Rev. Lett.*, vol. 82, no. 3701, 1999.

[91] I. Kimchi and A. Vishwanath, "Kitaev-Heisenberg models for iridates on the triangular, hyperkagome, kagome, fcc, and pyrochlore lattices," *Phys. Rev. B*, vol. 89, no. 014414, 2014.

[92] G. Jackeli and A. Avella, "Quantum order by disorder in the Kitaev model on a triangular lattice," *Phys. Rev. B*, vol. 92, no. 184416, 2015.

[93] E. C. Samulon *et al.*, "Asymmetric quintuplet condensation in the frustrated $S = 1$ spin dimer compound $Ba_3Mn_2O_8$," *Phys. Rev. Lett.*, vol. 103, no. 047202, 2009.

Publications

Part I of this thesis is based on the following publications:

- D. G. Joshi, K. Coester, K. P. Schmidt and M. Vojta; Nonlinear bond-operator theory and $1/d$ expansion for coupled-dimer magnets. I. Paramagnetic phase; Phys. Rev. B **91**, 094404 (2015).
- D. G. Joshi and M. Vojta; Nonlinear bond-operator theory and $1/d$ expansion for coupled-dimer magnets. II. Antiferromagnetic phase and quantum phase transition; Phys. Rev. B **91**, 094405 (2015).
- M. Lohöfer, T. Coletta, D. G. Joshi, F. F. Assaad, M. Vojta, S. Wessel and F. Mila; Dynamical structure factors and excitation modes of the bilayer Heisenberg model; Phys. Rev. B **92**, 245137 (2015).

Chapters in part II of the thesis are unpublished. This thesis does not contain the work from the following publication:

- M. Laubach, D. G. Joshi, J. Reuther, R. Thomale, M. Vojta and S. Rachel; Quantum disordered insulating phase in the frustrated cubic-lattice Hubbard model; Phys. Rev. B *Rapid Comm.* **93**, 041106(R) (2016).

Acknowledgment

I feel fortunate to have Prof. Dr. Matthias Vojta as my doctoral thesis advisor. He is not only a brilliant scientist but also a wonderful person. He is an immense source of knowledge. It was a great learning experience, and a privilege to work with him throughout these three years. I am thankful to him for numerous enlightening discussions, for answering my silliest questions, and for a continuous support. Talking to him has always been very encouraging, especially during my non-productive period. It meant a lot to me, and it is beyond words to express my gratitude towards him. Apart from my main PhD project, he led me to explore many small ideas, which has helped me broaden my knowledge in condensed matter physics. Under his supervision, I enjoyed a lot of freedom, and he let me work at my own pace. He has been almost an ideal supervisor that I had envisioned before the start of my PhD.

After I leave Dresden, I am surely going to miss my weekly meetings with Prof. Vojta. Apart from our scheduled meeting, he was very approachable and always available for discussion. I hope that I will have the opportunity to keep working with him in future. I am also thankful to him for his helpful career advice, as well as for improving my presentation skills. I express my sincere thanks to him for reading the previous drafts of this thesis, which has led to a much improved current version. I also greatly acknowledge his help at various levels at the beginning of my stay in Dresden.

During my PhD, it was my privilege to collaborate with Kris Coester, Kai Schmidt, Manuel Laubach, Johannes Reuther, Ronny Thomale, Stephan Rachel, Maximillian Lohöfer, Tommaso Coletta, Fakher Assaad, Stefan Wessel, and Frederic Mila. I owe a big thanks to all of them. In particular, I greatly acknowledge many useful discussions with Kai Schmidt, Stephan Rachel, and Stefan Wessel. I hope that in future I will have some more opportunities to collaborate with them.

I immensely thank the International Max Planck Research School (IMPRS), because of which I got an opportunity to work with Prof. Vojta. I greatly benefited from the structured PhD program of IMPRS. I also acknowledge the support from the German-Israeli Foundation, the Helmholtz Virtual Institute, and the DFG SFB 1143.

My entire stay during the PhD was an amazing experience, thanks to the wonderful members of the Theoretical Solid State Physics group, as well as those from the Condensed Matter Theory group lead by Prof. Carsten Timm. I take this opportunity to thank the present and past members: Dietmar Lehmann, Pier Paolo Baruselli, Lukas Janssen, Tobias Meng, Stephan Rachel, Alexia Rod, Eugen Wolf, Fabian Zschocke, Mark Steudtner, Oleksiy Kashuba, Paolo Michetti, Maxim Breitkreiz, Chris Koschenz, Tim Ludwig, Andrey Bolotnikov, Christoph Berke, Kevin Seja, Jacob Schmiedt, Stefan Rex, Philip Brydon, Alex Lau, Alex Wollny, Johannes Mierau and Eric Andrade. I apologize to whom I might have forgotten to thank. I had a great time with many

of them, whether it was hiking, boating, cycling, visiting Christmas markets, watching movies or playing board games. In particular, I am thankful to Fabian, Jacob, and Tim for making me feel so comfortable in Dresden and at the Institute, within no time. I will cherish the memories of so many interesting coffee breaks and the corresponding discussions at the Institute. I am also thankful to some of the people from the neighboring Institutes for a good time in Dresden. In particular, I thank: Sujit, Krishanu, Sthitadhi, Deepjyoti, Olga, Sreejith, Ajeesh, and Ricardo. I also thank all the members of the Institut für Theoretische Physik. Particularly, I greatly acknowledge the help from Martin Richter, one of the former members of the Institute, during my initial period in Dresden.

Apart from fun and entertainment, I had numerous physics discussions with many of the group members. During my first year, I greatly benefited from discussions with Jacob, and I am very thankful to him. I am grateful to Tobias, whom I have bugged with stupid questions on countless occasions. I thank him for his encouragement, helpful discussions, many useful advices, and a helpful feedback on the initial draft of the thesis. I am also grateful to Stephan Rachel for many fruitful discussions. It was also a pleasure discussing physics with Alexia, Mark, and Chris.

Without the colossal help from Frau Gudrun Latus, my stay in Dresden would have been very difficult. I simply have no words to express my gratitude towards her. I owe her a huge thanks for her help on countless occasions. I take this opportunity to also thank Frau Tatjana Schoffer.

The Welcome Center of TU Dresden has played a great role in making my PhD tenure memorable. Through their cultural events, I got an opportunity to explore many parts of Germany, and learned several things. It was simply a great experience! I thank all the members of the Welcome Center, and in particular, Maike, Maria, Nicole, and Claudia. I hope the Welcome Center gets even bigger and better.

I was extremely delighted to find a Cricket club in Dresden. It was one of the things which quickly made me feel like home in Dresden. I will cherish the memories of many matches and tournaments. It is pleasure to thank the fellow teammates: Chintan, Rahul, Guru, Sami, Anni, Uddi, Hardik, Siva, Francis, and many others. I also wish to thank all my relatives, friends, and well wishers in India. I greatly appreciate their encouragement. Especially, I wish to thank Mohit, Piyush, and Shadab for some great and relaxing vacations.

Last but not the least, I express my thanks and regards, to my parents and my sister. Without their encouragement, blessings, and support I could not have achieved anything.

Erklärung

Hiermit versichere ich, dass ich die vorliegende Arbeit ohne unzulässige Hilfe Dritter und ohne Benutzung anderer als der angegebenen Hilfsmittel angefertigt habe. Die aus fremden Quellen direkt oder indirekt übernommenen Gedanken sind als solche kenntlich gemacht. Die Arbeit wurde bisher weder im Inland noch im Ausland in gleicher oder ähnlicher Form einer andered Prüfungsbehörde vorgelegt. Diese Dissertation wurde am Institut für Theoretische Physik der Technischen Universität Dresden unter Betreuung von Herrn Prof. Dr. Matthias Vojta angefertigt. Ich erkenne die Promotionsordnung der Fakultät Mathematik und Naturwissenschaften der Technischen Universität Dresden vom 23.02.2011 an.